University of Rostock
Mathematisch-Naturwissenschaftliche Fakultät
Leibniz-Institut für Katalyse e. V.
Spezielle (metall)organische Synthesen und Katalysen

Homogeneous carbonylations of renewable methyl pentenoates and other unusual olefins

This thesis has been submitted in fulfilment
of the requirements for the degree of
Doctor of Philosophy (Ph.D.) in Chemistry
at the University of Rostock

Stephan Behrens
***19.05.1992 in Bremen**

Rostock,10.03.2020

https://doi.org/10.18453/rosdok_id00002655

This work was conducted at the Leibniz-Institute for Catalysis e. V. at the University of Rostock under the supervision of Prof. Dr. rer. nat. Armin Börner beginning from October 2016 to September 2019.

Reviewer 1: Prof. Dr. rer. nat. Armin Börner
Universität Rostock
Mathematisch-Naturwissenschaftliche Fakultät
Institut für Chemie

Reviewer 2: Prof. Dr. habil. Anna M. Trzeciak
University of Wroclaw
Faculty of Chemistry

Year of submission: 2019

Year of defense: 2020

Abstract

This thesis is dedicated to the catalytic conversion of the different isomers of methyl pentenoate as bio renewable resource that can be produced from lignocellulosic biomass. The first part focuses on the rhodium catalysed hydroformylation reaction and the synthesis of formyl substituted pentanoic acid methyl ester, especially methyl 5-formylpentanoate, which can act as platform chemicals for the synthesis of different monomers for polyamide and polyester synthesis. For this purpose, several ligands have been tested and the reaction conditions have been optimised for the most promising systems. The second part deals with the synthesis of dimethyl adipate from methyl pentenoates via the palladium catalysed alkoxycarbonylation reaction, utilising new bidentate pyridyl-substituted diphosphine and comparing them to the well-known palladium BuPox catalyst. Mechanistic investigations have also been conducted to identify relevant catalytic species as well as the resting state of the catalysts used. The final part of the thesis regarding methyl pentenoates describe experiments and results obtained in the rhodium catalysed hydroaminomethylation for the synthesis of amines. Employing several amines as well as aqueous ammonia, the aim was to find a catalytic system that selectively generates methyl 6-aminocaproate. Also, some research has been conducted for the rhodium catalysed hydroformylation of 1,2,4-trivinylcyclohexane to synthesise the corresponding trialdehyde, which could be an interesting monomer for polymer industry. From the corresponding alkoxycarbonylation product, a new tridentate phosphite was synthesised that was also tested in the hydroformylation of methyl pentenoates.

Zusammenfassung

Die Verwendung der verschiedenen Isomere des Pentensäuremethylesters als erneuerbarer Rohstoff - gewinnbar aus Lignocellulose - in homogenen Carbonylierungsreaktionen war Gegenstand dieser Arbeit. Zunächst wurde die Rh-katalysierte Hydroformylierung als Syntheseroute zu den entsprechenden Formyl-substituierten Pentansäuremethylester untersucht. Das Hauptaugenmerk lag hierbei auf der selektiven Synthese von 5-Formylpentanäuremethylester, welches als Ausgangsstoff für die Herstellung verschiedener Monomere für Polyamide und Polester dienen kann. Zu diesem Zweck wurde eine Vielzahl von Phosphin- und Phosphit-Liganden getestet und die vielversprechendsten Systeme hinsichtlich der Reaktionsbedingungen optimiert. Des Weiteren wurde die Synthese von Adipinsäuredimethylester über die Pd-katalysierte Methoxycarbonylierung untersucht, wobei neuartige bidentate Pyridyl-substituierte Diphosphin-Liganden getestet und mit dem literaturbekannten Palladium-BuPox-Katalysator verglichen. Zu diesem Zweck wurden außerdem spektroskopische Untersuchung zur Charakterisierung der mechanistisch relevanten Spezies durchgeführt. Schließlich wurden die Pentensäuremethylester in der Rh-katalysierten Hydroaminomethylierung zur Synthese der entsprechenden primären Amine eingesetzt. Das Ziel war ein Katalysatorsystem, das selektiv 6-Aminocapronsäuremethylester erzeugt. Hierfür wurden einige sekundäre Amine getestet. Des Weiteren wurde die Rh-katalysierte Hydroformylierung von 1,2,4-Trivinylcyclohexan zur Synthese des entsprechenden Trialdehyds durchgeführt, welches ein interessantes Monomer in der Polymersynthese darstellen könnte. Außerdem wurde aus dem hydrierten Hydroxycarbonylierungsprodukt ein Triphosphit hergestellt, welches als neuartiger tridentater Ligand in der Hydroformylierung von Pentensäuremethylestern und anderer Olefine eingesetzt wurde.

Statement of authorship

I hereby declare that the work presented in this thesis is original and carried out by myself only with the help of the stated sources and devices. I further declare that this thesis has not been submitted, either wholly or in part, to any academic institution for the award of any other degree or qualifications.

Rostock, 09.10.2019

Stephan Behrens

Acknowledgements

I want to take this opportunity to express my deepest gratitude to everyone who helped and supported me during three years of doctoral studies. Without them, I would not be where I am today.

First and foremost, I would like to thank Prof. Dr. Armin Börner for offering me the opportunity to conduct my doctoral studies in a high quality - and somewhat familial - work group. His kind and patient personality as well as his in depth insight into chemistry provided the guidance and motivation I needed to keep spirits high and push through the home stretch.

I also want to thank my dear colleagues that made my time in the work group an overall pleasurable experience, on a professional as well as personal level. A special shout out is due for Dr. Christoph Kubis, Matthias Koenig and Peter Kucmierczyk. The joint projects and discussions we had where inspiring and highly motivating.

My appreciation also goes to Dr. Wolfgang Baumann for his help in specially requested NMR experiments. Without his dedication in this matter, large parts of this work would not have been possible. Dr. Christine Fischer and her colleagues for the swift GC-FID-, GC/MS-measurements as well as general mass spectrometry. Their advice was invaluable to my work.

Last but not least, I want to thank my family for their patience and sacrifices they had to made for enabling me to follow my dreams, constantly encouraging me along the way. As well as my friends, who helped me keep a clear mind by providing distraction, motivation as well as recreation in turbulent times. For that, I am immeasurably grateful.

Table of contents

List of figures

List of tables

List of abbreviations

2-EtDMS	2-Ethyldimethyl succinate
5-FMP	Methyl 5-formylpentenoate
2-MeDMG	Dimethyl 2-Methylglutarate
Acc	Acceptor
Acn	Acetonitrile
BASF	Badische Anilin- und Soda-Fabrik
C	Conversion
Dest	destilled
DMA	Dimethyl adipate
Don	Donor
DTBPP	1,3-Bis(di-*tert*-butyl)phosphinopropane
DTBPX	1,2-Bis[(di-*tert*-butyl)phosphino]-*o*-xylene
Eq	Equivalent
Fig	Figure
GC	Gas chromatography
h	hour
HAM	Hydroaminomethylation
HMDA	Hexamethylenediamine
HP-IR	High pressure infrared
HP-NMR	High pressure nuclear magnetic resonance
IR	Infrared
M2P	Methyl pent-2-enoate
M3P	Methyl pent-3-enoate
M4P	Methyl pent-4-enoate

Min	minute
MS	Mass spectroscopy
MV	Methyl valerate
NMR	Nuclear magnetic resonance
p	Pressure
PTSA	*p*-Toluenesulfonic acid
rpm	rounds per minute
S	Selectivity
T	Temperature
t (parameter)	Time
t (unit)	Ton
Tab	Table
Tf	Triflate
TfOH	Trifluoromethanesulfonic acid
THOPCH	1,2,4-Tris(3-hydroxypropyl)cyclohexane
TPP	Triphenylphosphine
TPPTS	Triphenylphosphine trisulfonate
TsOH	see PTSA
Ts	Tosylate, see PTSA
TVCH	1,2,4-Trivinylcyclohexane
UCC	Union Carbide Cooperation
VE	Valence electron
Y	Yield

1 Introduction

1.1 Renewable resources as alternative substrates in hitherto mineral oil dependent processes for the synthesis of bulk chemicals

In the last decades the consciousness for environmental protection and the depletability of fossil fuels grew in the general public. These topics now dominate many of the current political debates. The two main reasons for this will be explained in the following.

The amount of mineral oil left in known and accessible reserves is thought to be about 448 Gt (2017). This number contains conventional as well as unconventional deposits. The adjective "conventional" is used for deposits that are easily accessible with established technologies. Consequently the extraction of the oil is cheap and the obtainable profit therefore higher. On the other hand, the extraction of oil is more complicated for unconventional deposits, which demands more expensive technologies. The reason for this lies in the local geological circumstances and physicochemical properties of the oil (e. g. viscosity, etc.), that vary for every deposit. In 2016, the amount of mineral oil extracted was 4374 Mt. Together with the already build-up reserves, it is obvious that there won't be any shortages regarding this resource for the next decades. Nonetheless the ever increasing demand (4387 Mt in 2016) will be harder to satisfy by the extraction that is more or less working to capacity. Therefore the economic impact will be observable much sooner than the full depletion of the resource. [1]

The other reason is the fear of climate change. To counter this, a multitude of new technologies are developed that have the aim to either physically store CO_2 or make it available - or rather: more reactive - in synthetic processes. Aside from these efforts, it is also necessary to decrease or even stop the emission of CO_2 to halt the progression of climate change and limit the repercussions to a manageable extent. For this, the use of fossil fuels has to be renounced. Instead, renewable resources should be utilised in energy production and chemical industry, together with the implementation of CO_2 "consuming" processes.

1.1.1 Known processes

Whilst a broad spectrum of processes, that are based around bio-renewable resources and deliver an equally broad spectrum of platform chemicals for the synthesis of bulk and fine chemicals, is already known, not many processes are applied in the industry. This is due to the poor economic feasibility of most of these processes, since most renewable resources are more chemically complex compared to fossil fuels. This complexity leads to various problems regarding catalyst performance

and poisoning, the amount of product work up and substrate pre-treatment required, and the acquisition cost of the feedstock. [2,3]

A prime example is lignocellulose, which is an inedible waste product of the agricultural industry and amounts to almost 70 % of the agriculturally produced biomass. Compared to fossil fuels it contains a significantly higher amount of oxygen and is far more functionalised. Lignocellulose consists of three major compounds: Cellulose, hemicellulose and lignin. Cellulose and hemicellulose are both polysaccharides and consist either solely of β-1,4-glycosidically polymerised D-glucose (cellulose) or different monosaccharides like D-xylose or D-arabinose (hemicellulose). Lignin on the other hand is a more or less structurally random polymer consisting mainly of coumaryl, coniferyl and synapyl alcohols. [4] Until today, this complexity is the reason why the conversion of lignocellulosic biomass is too energy and resource intensive to be economically viable. [2, 3] Additionally the utilised catalysts are prone to poisoning and the selectivity for the formation of certain products of interest is fairly low. Nonetheless, since the 1990's significant improvements and developments have been made. Today, processes for conversion of lignocellulose include: Pyrolysis for the formation of "bio oils" and "green" syngas, enzymatic catalytic conversion *ex vivo* and *in vivo*, and the chemo catalytic conversion of lignocellulose. [5,6]

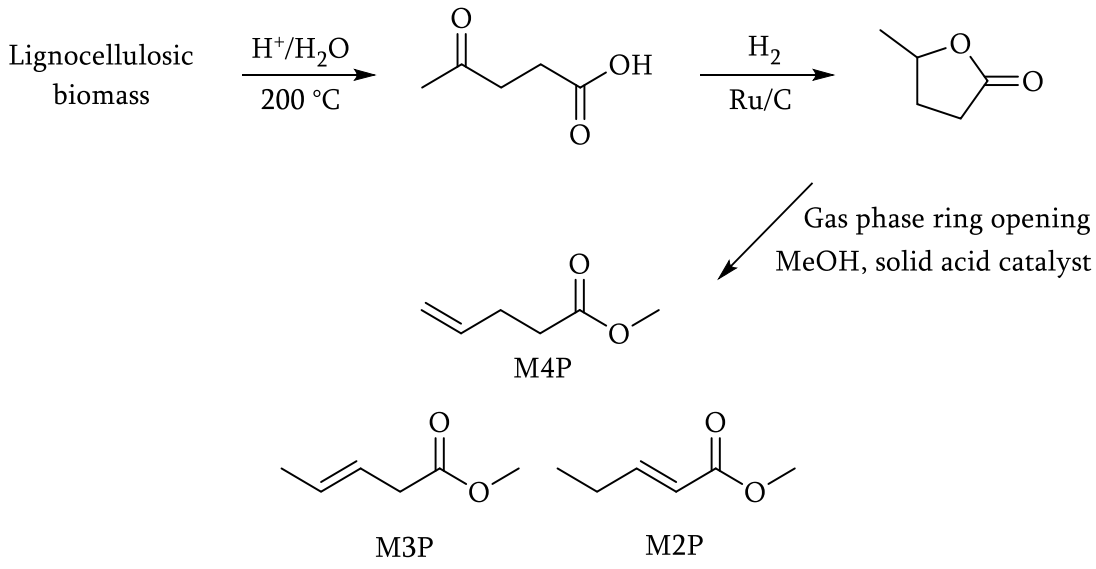

Fig. 1: Route for the synthesis of isomeric methyl pentenoates from lignocellulosic biomass.

All these processes lead to a large variety of so called platform chemicals that can be used to manufacture other industrially interesting products. These platform chemicals include for example 5-hydroxomethylfurfural or levulinic acid, while the latter can also be formed by conversion of the former in acidic aqueous media. [3,7,8,9]

For this work, levulinic acid is the relevant product of the valorisation of lignocellulosic biomass, since it serves as a platform chemical for the synthesis of pentenoic acid esters. The synthesis can be realised by heterogeneously catalysed hydrogenation of levulinic acid by Ru/C, which forms γ-valerolactone (GVL), followed by an acid catalysed ring opening reaction. This reaction is performed heterogeneously with a solid acid catalyst, while the substrate and other reactants are in the gas phase. This reaction leads to the free isomeric pentenoic acid. In contrast, if methanol is present, the reaction leads to an isomeric mixture of methyl pentenoates (M4P, M3P and M2P), making it easier to separate the products from GVL. [9]

1.2 Scope of this work

As described further above, it is of great public interest to produce industrially relevant chemicals from renewables. Therefore the aim of this work was the application of bio sourced methyl pentenoates in industrially relevant homogeneously catalysed carbonylation and carboxylation reactions for the synthesis of adipic acid derivatives that can be used for polyamide and polyester production.

1.2.1 Hydroformylation of isomeric methyl pentenoates

The synthesis of 5-formylpentanoic acid (5-FPA) or a mixture of the corresponding branched aldehydes, from pentenoic acid derivatives was frequently investigated in the last decades. In several cases the corresponding methyl esters were used, resulting formyl methylpentanoates are abbreviated as FMPs. In general, three isomeric pentenoic acids having the double in 2-, 3- and 4-position exist. However, until today research hasn't been successful to find an economic hydroformylation process capable of generating 5-formylvaleric acid and its esters, respectively, with a regioselectivity greater than 95 % from this feedstock. In 1981, BASF SE claimed a patent that described a process that gave the corresponding methyl ester with *n*-regioselectivities of 70 %. [10] For that aim

cobalt carbonyl complexes were employed at 120 °C and 200 bar syngas and isomeric methyl pentenoates as substrates. The latter were generated by alkoxycarbonylation of 1,3-butadiene. The same company improved in 1988 on that concept, by patenting new cobalt catalysts and additionally the utilisation of phosphine modified Rh(I)-carbonyl complexes in the hydroformylation. Predominantly, tertiary phosphines, such as triphenylphosphine (TPP) and its derivatives were used. Regarding the cobalt catalysts, the reaction temperature was lowered to 100 °C and the pressure to 130 bar syngas and simultaneously achieving a regioselectivity of nearly 69 %. Experiments with rhodium catalysts were mentioned, but not detailed. [11] In another patent application in 1992 BASF described the utilisation of rhodium catalysts modified with bidentate diphosphites. The reaction conditions were much milder than in the previously reported processes with the temperature being set at 100 °C and the pressure at only 5 bar syngas. The ligand with the best performance was a BIPHEPHOS-derived bis(dioxaphosphepine) that was able to convert 95.5 % of the substrate into the desired product with a *n*-regioselectivity of 76.7 % regarding the linear aldehyde. (Fig. 2)

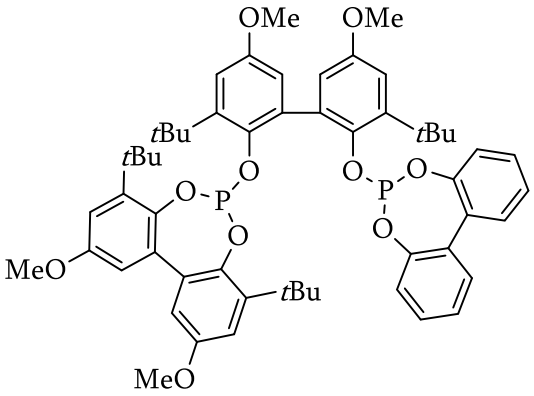

Fig. 2: Bidentate phosphite ligand utilised by BASF in 1993.

In another experiment, a TPP modified rhodium complex was used under the same reaction conditions. This led to conversions of only 34 % in the same timeframe as the bisphosphite modified catalyst reported above. The *n*-regioselectivity only amounted to 8.8 %. [12] Du Pont also showed interest in the manufacturing of 5-FMP. For this purpose they submitted their first patent in 1995. Herein a process was claimed that improved upon the approaches of the BASF, that utilised a diphosphite modified Rh(I)-catalyst. A formally tetradentate ligand depicted in Fig. 3 showed the

most promise. The corresponding catalyst was able to convert 54.2 % of the substrate within 27 h into the desired aldehydes with *n*-regioselectivity of about 80 % regarding 5-FMP and the optimal reaction condition being 90 °C and 10 bar syngas. The main drawback of this process is the significantly lower catalyst activity compared to preceding processes. [13] In 2003, experiments with bidentate phosphoroamidites were also conducted.

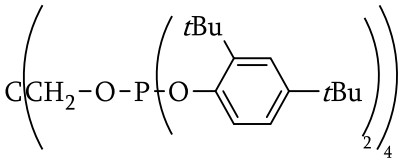

Fig. 3: Phosphite ligand, 1993, DuPont.

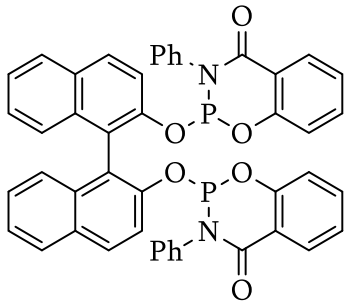

Fig. 4: Amidite, BASF, 2003

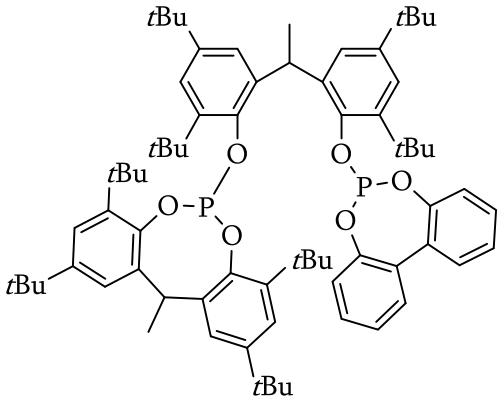

Fig. 5: Nonsymmetric diphosphite, Tsai et. al, 2000.

It was found that if a salicylanilide based phosphoroamidite with a BINOL-backbone was employed, as shown in Fig. 4, regioselectivities of nearly 85 % regarding 5-FMP at a conversion of 80 % after 2 h at 100 °C and 10 bar were possible. [14] Also Tsai et al. took benefit from the general stability of bisphosphites by using relatively cheap starting materials. These nonsymmetric bidentate ligands were successfully employed in the hydroformylation of pentenoic acid esters, of

which the best results were yielded by the ligand described in Fig. 5. The catalyst modified with this ligand was able to produce 5-FMP with *n*-regioselectivity of 78 % by converting 82 % of the substrate into the desired aldehydes. The reaction temperature was 100 °C and the syngas pressure at about 6 bars. [15] De Vries et al. were able to achieve the best results until today by using a 2-phasic solvent system (toluene/water, 1:1), with the catalyst system in the aqueous phase and the substrate and reaction products in the organic phase. The water solubility of the catalyst was achieved by modification with the trisulphonated triphenylphosphine analogue trisodium triphenylphosphine-3,3′,3″-trisulphonate (TPPTS). With this system they were able to achieve 92 % selectivity towards 5-FMP with a conversion of only 15.4 % over night. The reaction was conducted at 100 °C and 10 bar syngas. Comparing these findings to the results obtainable by TPP-modified rhodium catalysts in neat toluene at the same reaction conditions, it can be shown that even though the catalyst activity is low (15.4 % vs. 100 %), the *n*-regioselectivity is by far superior (92 % vs. 19.7 %), making this process far more interesting for industrial application. [16]

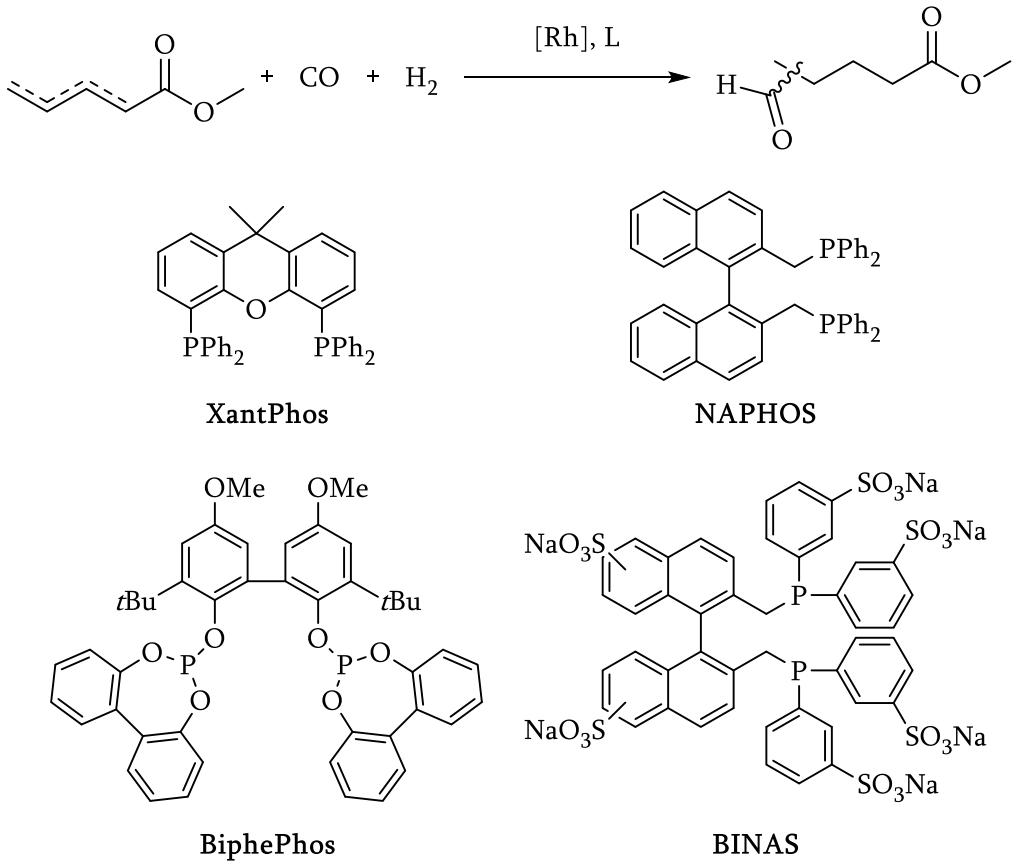

Fig. 6: Ligands used in the rhodium catalysed hydroformylation of methyl pentenoates in preceding research.

M4P M3P

Fig. 7: Substrates of interest.

Substrate	*Ligand*	*Conversion [%]*	*Yield [%]*	*Selectivity[c] [%]*
M4P	Xantphos [a]	95.6	90.7	91.7
	BIPHEPHOS[a]	99.6	95.7	87.2
	BINAS [b]	90.9	83.6	98.2
	NAPHOS [a]	94.8	90.5	95.5
M3P	Xantphos [a]	63.0	59.7	66.6
	BIPHEPHOS [a]	79.8	8.3	55.8
	BINAS [b]	75.2	67.4	70.5
	NAPHOS [a]	89.1	47.2	60.2
Mixture (M4P:M3P, 9:1)	Xantphos [a]	46.7	44.1	83.0
	BINAS [b]	33.3	28.5	69.0
	NAPHOS [a]	79.7	67.5	53.0

Table 1: Preceding results. [17] (a) Homogeneous approach in toluene. T = 100 °C, p = 5 bar, CO/H_2 = 1, Rh:L:substrate = 1:4:1000, c_{Rh} = 100 ppm, t = 20 h. (b) Two-phasic approach with toluene/water (1:1). T = 110 °C, p = 10 bar, CO/H_2 = 1, Rh:L:substrate = 1:4:1000, c_{Rh} = 100 ppm, t = 20 h. (c) Ratio of the amount of n-aldehyde to the total amount of product aldehydes.

The aim of this work consequently was the synthesis of 5-FMP via the Rh(I)-catalysed hydroformylation of isomeric mixtures of methyl pentenoates with regioselectivities greater than 90 % regarding the *l*-aldehyde. A part of this was already part of my master thesis, in which I found promising catalyst systems, comprised of Rh(I)-species modified with BINAS (2-phasic approach), BIPHEPHOS, NAPHOS and Xantphos. [17] Further candidates where modified with tris(2,4-di-*tert.*-butylphenyl)phosphite (Alkanox) and triphenyl phosphite. A summary of the best results is shown in Table 1 and the results have been patented. [18]

In this work I focused on the optimisation of the hydroformylation with the BINAS-modified catalyst, as well as its recirculation, as well as the optimisation of the catalysis with the BIPHEPHOS-modified system. Furthermore methyl 2-pentenoate was tested as a substrate and its behaviour in the substrate hydrogenation was studied.

1.2.2 Alkoxycarbonylation of a mixture of isomeric methyl pentenoates

The synthesis of adipic acid esters starting from the corresponding pentenoic acid esters is known since 1983. [19] BASF was interested in a process that produces adipic acid monoesters in the highest possible purity. This was achieved by the hydroformylation of pentenoic acid esters and a consecutive oxidation of the generated semi aldehyde with molecular oxygen. The catalyst in use was a TPP-modified palladium species that was able to generate the product in a yield of 70 %.

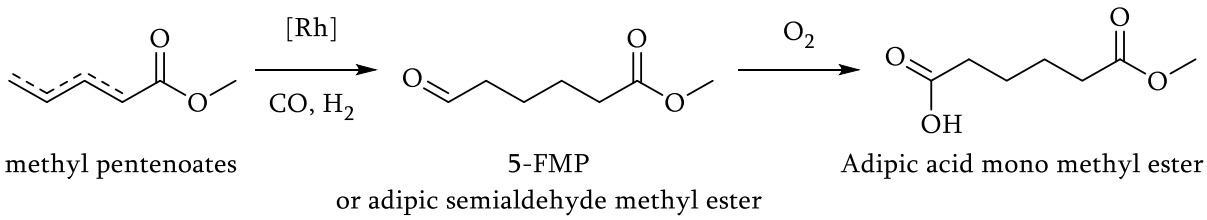

Fig. 8: Scheme for the synthesis of adipic acid monoesters as described in [19].

In 1986 DuPont patented a process that described a two-step approach for the conversion of butadiene. [20] Herein the pentenoates was generated via the hydroformylation of butadiene. Subsequent alkoxycarbonylation provided the desired product, which was generated in an overall yield of 66 %. The catalyst precursor in use was $RhCl_3$.

In another patent from the year 1988 BASF described the synthesis of adipic acid via a three-step route. The first step employed a cobalt catalyst that was used in the hydroformylation of methyl pentenoates. In the second step the resulting methyl adipate semi aldehyde was oxidized with molecular oxygen to form the adipic acid mono ester, followed by hydrolysis in a strongly acidic medium to yield the free dicarboxylic acid. [21]

Another way to selectively form adipic acid and its esters was described by DuPont in 1993. [22] Differing from previous patents an iridium catalyst as well as a bimetallic Rh/Ir-catalyst was used. With these systems, dicarboxylic acids could be produced in yields of up to 97.5 % with a selectiv-

ity of 88.5 % regarding adipic acid, starting from pentenoic acid esters. In 1994 γ-valerolactone was added to the substrate scope in another patent. [23][24]

As shown, the synthesis of adipic acid from pentenoic acid and its derivatives was performed exclusively via hydroesterification. The first alkoxycarbonylation of this substrate was reported in 1995 by DuPont. [25] The reaction conditions were chosen similarly like other alkoxycarbonylations. The reaction temperatures were in the range of 90 – 140 °C and the pressure about 60 bar CO. The ligands that were used for modification of the catalyst were bidentate metallocene compounds. In the best case the substrate in use, methyl 3-pentenoate (M3P), was converted into dimethyl adipate with a selectivity of 76 % and a conversion of 89 %.

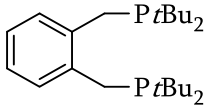

Fig. 9: Bidentate diphosphine DTBPX.

An example for an alkoxycarbonylation of pentenoic acid esters with a DTPBX-modified (BuPox) palladium catalyst was made by BASF and DuPont in 2002. Here, high yields and conversion were achieved, though the *l/b*-ratios were fairly low (only about 70 % regarding the dimethyl adipate). [26]

Furthermore Jiménez-Rodriguez et al. showed that by employing a DTBPX-modified catalyst already described above, reaction temperatures as low as 50 °C were possible without significantly impacting the activity of the catalyst. Full conversion was achieved after 3 h with quantitative yield of the dimethyl adipate. [27]

An example of a hydroxycarbonylation reaction patented by Shell is the conversion of 3-pentanoic acid catalysed by DTBPX and DTBPP-palladium catalysts in water as solvent. With this system it was possible to obtain adipic acid with a selectivity of 99 % and conversions of 90 %. [28]

In 2012 de Vries *et al.* investigated the synthesis of methyl pentenoates starting from γ-valerolactone and the methoxycarbonylation to form dimethyl adipate. The most successful system was able to convert the whole amount of substrate within an hour nearly quantitatively into dimethyl adipate. The reaction was conducted at 75 °C and 20 bar CO-pressure. Furthermore, influence of water on the catalytic process was studied. They were able to show that water has inhibitory properties, which lead to lower conversion and overall lower catalyst activities.

The regioselectivity is also impacted, as well as the chemoselectivity since the presence of water enables the hydroxycarbonylation as a competing mechanism. [29]

Loe *et al.* were able to synthesize and test new ligands that structurally resembled the well-known DTBPX ligand (see Fig. 10). [30] With these new ligands, it was possible to achieve high *l*/*b*-ratios, though the catalyst activities were significantly lower than those of catalysts used in prior publications.

Fig. 10: DTBPX derivative (left) and an anthracene analogue. (right)

In 2017 Nobbs *et al.* introduced a new BuPox-type ligand, where the di-*tert.*-butylphenyl units were replaced with the six membered 2,2‘,6,6,‘-tetramethyl-4-oxophosphinan-1-yl moiety. With a natural bite angle of about 100° and the phosphacycle units that are new for this kind of catalyst, the authors expected superior properties compared to DTBPX. Employing this ligand in the palladium catalysed methoxycarbonylation of methyl pentenoates, it was indeed possible to achieve higher catalyst activities (93 % in 4 h) than for the state of the art BuPox-systems and comparable *l*/*b*-ratios. This improvement was explained by the higher electrophilicity of the BPX-modified palladium compared to the DTBPX-modified species, which leads to a stronger bonding a faster deprotonation of MeOH to the acyl-palladium species as rate determining step. Therefore the methanolysis is favoured. The comparable regioselectivity is due to the comparable steric bulk around the catalytic centre with both ligands. The same work group also conducted mechanistic studies on this system, also with the help of quantum chemical methods. It was shown that the mechanism at hand is the most probable candidate and explains activity and regioselectivity with the energetically more favourable transition states for the formation of the adipate. Furthermore evidence was given, that the substrate acts as a sort of inhibitor since it is able to form chelates via coordination of the ester group, thus blocking critical coordination sites necessary for key steps inside the catalytic cycle. Also, this behaviour apparently has an impact on the regioselectivity of the reaction. [31,32] Further patents starting from 2003 are summarized under citation [33].

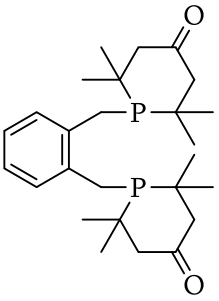

Fig. 11: BPX ligand.

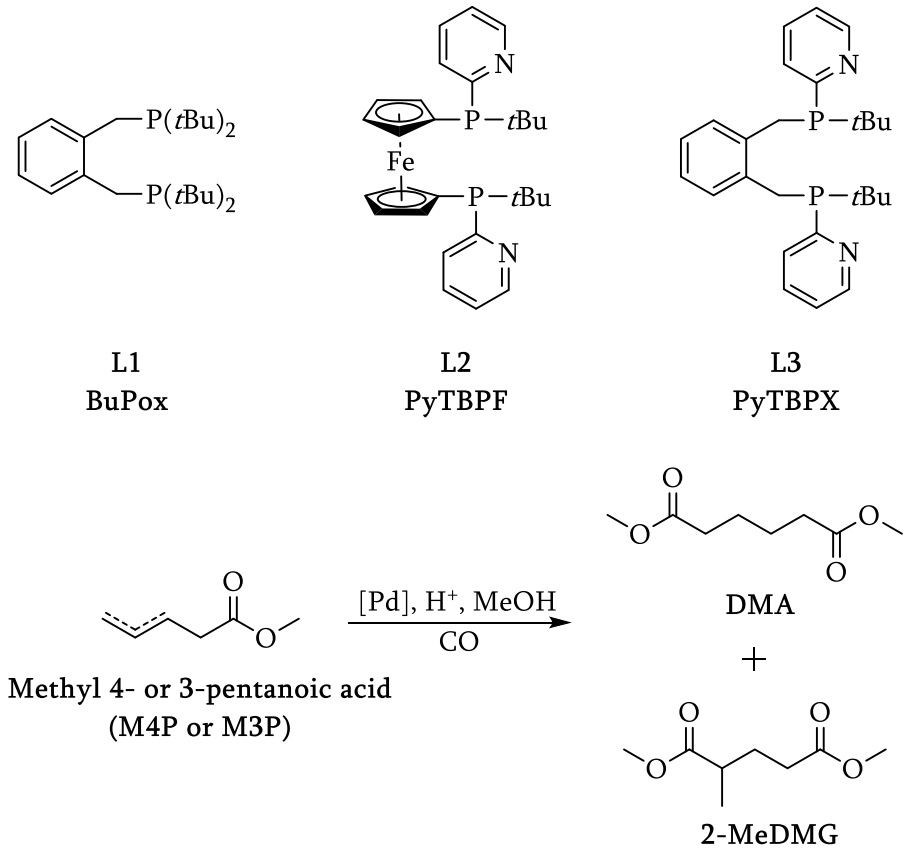

Fig. 12: Utilised ligands and reaction scheme of the palladium catalysed alkoxycarbonylation of methyl pentenoates to give dimethyl adipate (DMA) Dimethyl 2-methylglutarat (2-MeDMG) or Dimethyl 2-Ethylsuccinat (2-EtDMS).

To further improve existing processes, the scope of this work also contains investigations on the methoxycarbonylation of methyl pentenoates to synthesize dimethyl adipate with focus on high conversions and selectivities. For this purpose, highly efficient ligands (PyTBPF and PyTBPX, see Fig. 12) have been employed. These ligands were originally developed by Evonik in cooperation

with Leibniz Institute of Catalysis Rostock (LIKAT) for utilisation in the alkoxycarbonylation of ethylene. [91]

1.2.3 Hydroaminomethylation of isomeric methyl pentenoates

The rhodium catalysed hydroaminomethylation of isomeric pentenoates is one possibility to synthesize 6-aminocaproic acid esters and ε-caprolactam that has yet to catch attention. The usual methods to sustainably synthesize polyamide precursors are limited to biosynthetic processes starting from pimelates [34], carbohydrates [35], methanol [36], and 5-FMP. [37] Processes for the production of 6-aminocaproic acid are well known, though they don't start directly from pentenoic acid derivatives. Usual substrates are 5-FMP [38] and 3-pentennitrile. [39]

The direct synthesis of ε-caprolactame can be realised via transition metal catalysed reductive amination of 5-FMP with high chemoselectivities (yields of up to 84.4 %), [40] or via the thermal cyclisation of 6-aminocaproates or 6-aminocapronitrile. [41]

The most commonly applied synthetic route for ε-caprolactam starts from cyclohexanol, which can be produced from mineral oil via multiple steps. [42] Cyclohexanone is converted to cyclohexanone oxime by reacting it with bis(hydroxylammonium)sulfate. Then, the oxime is subjected to a Beckmann type rearrangement that leads directly to the desired lactam. This process will be described with more detail in the following.

Another aim of this work was the application of the rhodium catalysed hydroaminomethylation reaction to synthesize aminocaproic acid derivatives directly from methyl pentenoates. [43]

1.3 Possible applications of 5-formylpentenoates, adipates and 6-aminocaproates

The three main products of the reactions described above, methyl 5-formylpentenoate, dimethyl adipate and methyl 6-aminocaproate, are compounds that are already established starting materials in the chemical industry. Their main use lies in the polymer chemistry as monomers for polyamide and polyester synthesis. Here 5-FMP can act as platform chemical for the synthesis of ε-caprolactame (or 6-aminocaproates), ε-caprolactone (or 6-hydroxocaproates), hexamethylenediamine and adipic acid.

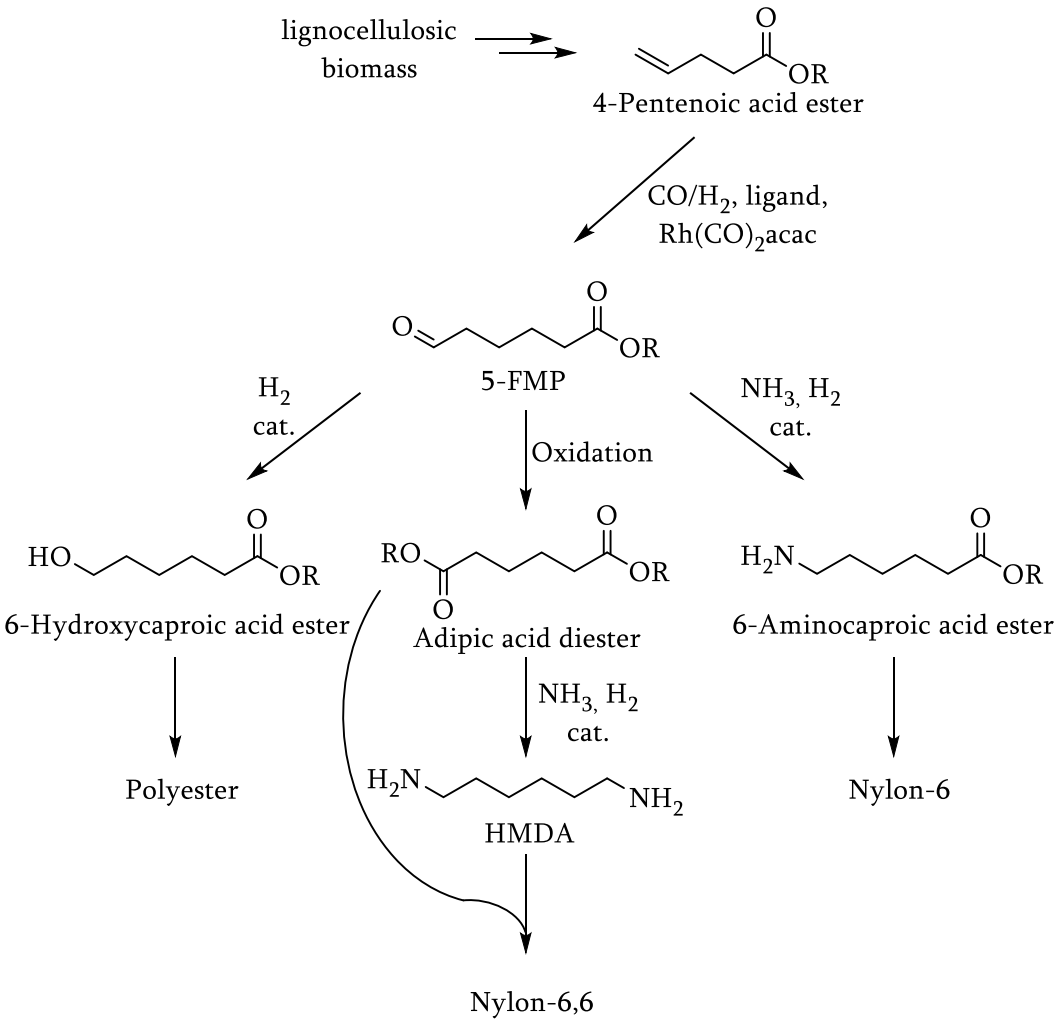

Fig. 13: Alternative synthetic routes towards monomers of polyamides. The synthesis of the pentenoic acid derivatives can be realised starting from lignocellulosic resources via levulinic acid and γ-valerolactone as intermediates.

The reductive amination of 5-FMP /5-FPA is a process known since 1954. [44] In the patent at hand ammonia and molecular hydrogen was used in the presence of Raney-Ni to convert 5-FMP into the corresponding 6-aminocaproic acid ester with yields of up to 70 %. In 1987, BASF claimed a process that was built on the previously mentioned patent and was able to make major improvements. The reaction conditions were significantly milder and the yields were raised to 90 % of 6-aminocaproate and even 3.3 % of ε-caprolactam. For this purpose, a heterogeneous mixed phase catalyst comprised of nickel oxide and aluminium oxide was used in a set up for continuous production. [45] In 1990, further improvements were made in regard by changing the catalyst to aluminium oxide supported ruthenium. This modification improved the space time yields to 88 %

per hour. [46] In 1997, DuPont also discovered a process for the utilisation of a mixture of isomeric FPA's. Sadly, there were no remarks on the procedure and result of the patented process. [47] An improved process was patented in 1998, wherein 6-aminocaproic acid was synthesized by hydroformylation of 3-pentenoic acid and subsequent imine formation with ammonia in a single batch. The catalyst used was a Rh(I)-species modified with a diphosphite strongly related to BiphePhos (Fig. 14). In a second step, the resulting aqueous phase was subjected to a hydrogenation reaction by addition to a mixture comprised of Raney-Ni and aqueous ammonia. The overall yield of caprolactam and valeric acid ester was 17 % and 79 %. [48]

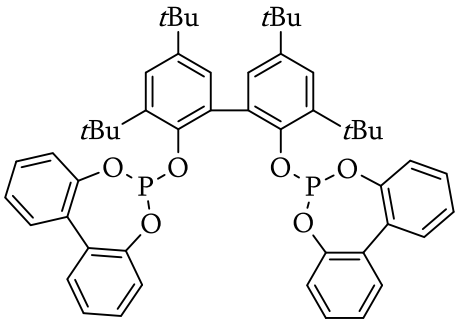

Fig. 14: BiphePhos analogue diphosphite. The methoxy groups in para-position have been replaced by tBu groups.

In the same year another process was published that was heterogeneously catalysed by supported ruthenium. The best results were obtained with a titanium oxide support, which was able to convert the usual substrates into the desired products with yields of about 97 %. [49] Another patent described the use of ruthenium supported on a mixed phase of titanium oxide and silicon oxide. The reaction was carried out in a continuous set up. Under these conditions 5-FPA was completely converted and a yield of 90.5 % of the lactam and 5.8 % of the 6-aminocaproic acid was realised. [50] This process was further improved by Pestman and Van Lieshout in 2000. [51] They used ruthenium supported on titanium oxide as a heterogeneous catalyst. Additionally, the catalyst was doped with nickel. This modification led to a yield of 99.8 % caprolactam and 6-aminocaproic acid, in both batch and continuous processes.

Furthermore, 5-FMP can be oxidised to form adipic acid derivatives. [52] An example of a complete synthetic route from levulinic acid towards adipic acid via γ-valerolactone was described by DSM in 2012. [53] Levulinic acid is obtainable by acid catalysed hydrolysis of lignocellulosic biomass and therefore a "green" compound. In 1988, BASF has discovered a process for the oxidation

of 5-FMP, where 5-FMP was prepared from M3P via hydroformylation. The product was purified via distillation and then treated batch wise with molecular oxygen for a long time. [54] After full conversion the reaction yielded 95 % of adipic acid monoester. The free dicarboxylic acid was obtained after simple acid catalysed hydrolysis of the ester with simultaneous destillative separation of the liberated methanol.

The reductive amination of adipic acid to form hexamethylenediamine (HMDA) is known since the 1970's and was realised by heterogeneous catalysis with aluminium oxide supported ruthenium in the presence of ammonia or an amine, favourably HMDA. The resulting product mixture in the autoclave contained differing amounts of HMDA, ε-caprolactam and polymeric residues. In 1972, two other processes were described in patents, in which cobalt and iron catalysts were tested. [55,56,57] The Fe catalysts showed an overall better selectivity than the cobalt systems regarding the HMDA formation.

Furthermore the possibility of reducing 5-FPA towards 6-hydroxycaproic acid exists as a way to produce monomers for polyester synthesis. Alternatively, it can be directly hydrogenated to form 1,6-hexanediol, which was patented by Esso in 1996. [58] As catalyst PtO_2 was used which was able to fully convert 5-FMP with high selectivity into the desired product. Another process utilised nickel catalysts, which lead to a lower chemoselectivity due to harsher reaction conditions than for the platinum catalysed reaction. [59] This problem was tackled by using Raney-Ni as hydrogenating catalyst, which enabled lower reaction condition than before. [60] Additionally, the reaction could be conducted continuously as well as batch wise. An interesting publication from Kobayashi *et al.* described a selective reduction of 5-FPA by tetrabutylammonium fluoride as catalyst and polymethylhydrosiloxane as reductant. The reaction temperature was set to -70 °C at which 5-FMP was fully converted into methyl 6-hydroxyhexanoate. [61] Another process with comparable results was developed by Lorca *et al.*, where BINOL-modified Zr-catalysts was utilised for the selective reduction of aldehydes. [62] BASF improved the batch wise hydrogenation of 5-FMP by Raney-Ni. [63] The yield of methyl 6-hydroxycaproate was raised to 91 %. The synthesis 6-hydroxycaproic acid from the side products of the industrially applied cyclohexane oxidation and the reduction of these side products directly into 1,6-hexanediol was performed successfully. [64,65]

Alternatively, the same products can be synthesised by reduction of adipic acid and its esters. For this purpose, Morikawa *et al.* synthesised and tested different Raney catalysts. [66] In most cases, mixtures of 6-hydroxycaproic acid and 1,6-hexanediol were obtained. A research group of BASF developed a new process in order to minimise the amount of undesired dimeric and oligomeric side products. [67] For this aim, hydrogenation of the substrate was realised in the presence of a Cu catalyst under harsh reaction conditions, employing a continuous set up. The reactor output was purified via distillation and the desired products isolated.

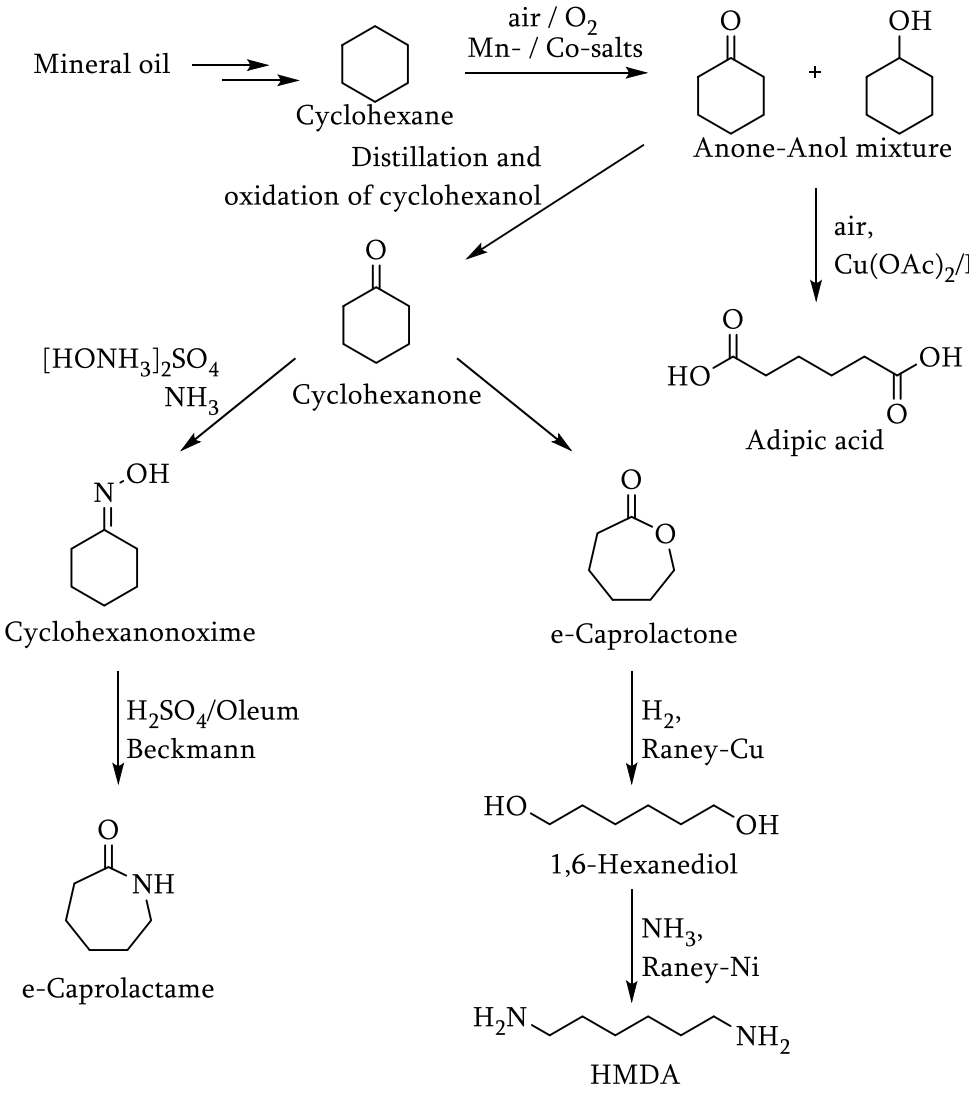

Fig. 15: Traditional synthetic routes for monomers of polyamides.

The residue of the distillation was recycled into the reactor and subjected to another reaction cycle after addition of fresh substrate. For each cycle the composition of the product fraction was comparable. A process where nearly all of dimethyl adipate is converted into the corresponding diol used a catalyst mixture containing CuO, ZnO and Al_2O_3 for the hydrogenation step. [68]

All of the mentioned products are currently synthesised by employing crude oil dependent processes. A brief overview will be given in the following.

Adipic acid is accessible through the oxidative cleavage of cyclohexane. This two-step process starts from the incomplete oxidation of cyclohexane by air with manganese and cobalt salts, e. g. relevant acetates, as catalysts. Here a mixture of cyclohexanol and cyclohexanone is produced that is used in the second step after purification by distillation. The second reaction step is also an oxidation that can either be conducted by reaction of the cyclohexanol/cyclohexanone mixture with nitric acid and ammonium metavanadate or by reacting it with Cu and Mn acetate and air. With this method the production capacity was at about 2.3 Mt per year in 1996.

HMDA is almost exclusively synthesized via the hydrogenation of the corresponding dinitrile, called adiponitrile. Another possible route was found by Celanese in 1981 that also starts from cyclohexanone. This route is comprised of the oxidation of that ketone towards caprolactone and the subsequent hydrogenation with Raney-Cu to form 1,6-hexanediol. Finally, the amination of this product with ammonia and Raney-Ni leads to the final product HMDA. With this, a production of 30 kt HMDA per year is possible.

ε-Caprolactam is industrially synthesized from cyclohexanone. Via this production pathway, the cyclohexanone is first reacted with hydroxylammonium sulphate to form cyclohexanone oxime. The addition of ammonia to this step is critical to keep the pH at roughly 7. This is also the main drawback of this reaction, because huge quantities of the waste product ammonium sulphate are formed, which renders the process less economic. In the final step the oxime is converted into the desired caprolactam via a Beckmann rearrangement reaction with concentrated sulphuric acid or oleum. [69]

Another possibility for the formation of ε-caprolactam is the use of 6-oxohexanoic acid and its esters (5-FMP or 5-FPA) as starting material. The conversion into the lactam can be realised via the reductive amination of these substrates to directly form 6-aminocaproic acid. Alternatively the

utilisation for the synthesis of monomers for other polyamides or -esters is also possible. For example HMDA can be formed via oxidation of 5-FVA to give adipic acid and subsequent reductive amination. (see Fig. 3) Another possibility is the synthesis of 6-hydroxycaproic acid via hydrogenation of 5-FPA for the production of polyesters.

ε-Caprolactam serves as starting material for the manufacturing of Nylon-6, a polyamide that was first synthesized by P. Schlack in 1938 and sold under the trade name Perlon™ in Germany. This invention was directly inspired by the work of W. H. Carothers, who synthesized the first polyamide Nylon-6,6 via polycondensation of hexamethylenediamine (HMDA) and adipic acid in 1935. At the beginning of this century the global production capacity was about 6 Mt per year. The main use for these polyamides is the production of synthetic fibres and thermoplastics.

Monomers	Polymers
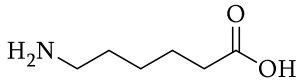 6-Aminocaproic acid 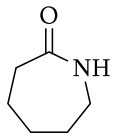 ε-Caprolactone	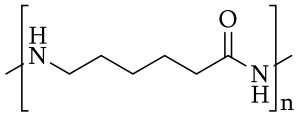 Polycaprolactam (Nylon-6)
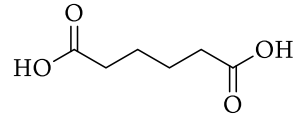 Adipic acid 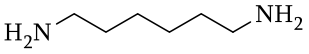 Hexamethylenediamine (HMDA)	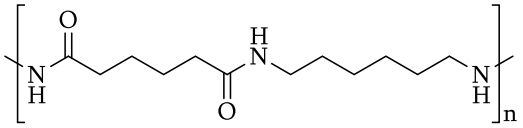 Poly(*N,N*-hexamethyleneadipic diamide) (Nylon-6,6)

Table 2: Two polyamides and their monomers.

In principal, polyamides are synthesised via the polycondensation of two different monomers (AA/BB polyamides, Nylon-6,6) or only one monomer (AB polyamides, Nylon-6). (see Table 2) Of course, other compositions of different monomers are also possible. Industrial scale polycondensations for the formation of AA/BB type polyamides are usually carried out in the melt of the respective "nylon salt" (e.g., $[Z\text{-}(NH_3)_2]^{2+}[Z'\text{-}(COO)_2]^{2-}$) at 200-300 °C and nitrogen pressures of up to 30 bar. Since water is used in the process as internal heat transfer agent, these high pressures are nec-

essary to keep the water from evaporating from the raw polymeric mixture. Typically the pressure is released stepwise during the process to lower the water content and favour the polycondensation. When 80 – 90 % of monomer is converted, the reaction is continued at temperatures above the melting point of the polymer and under vacuum. This last step can also be performed in solid state at temperatures below the melting point. AB type polyamides are usually manufactured from their corresponding cyclolactams. For Nylon-6 the reaction is carried out in water at temperatures of about 260 °C and the reaction itself can be considered as a 2-step reaction *in situ*, beginning with the hydrolytic ring opening to form 6-aminocaproic acid. This step is either followed by the direct addition of the lactam to the growing chain or the condensation of two 6-aminocaproic acid molecules. Which of the two possibilities for the last step is favoured strongly depends on the water content in the reaction mixture. At lower water content, the addition of the lactam is favoured. Otherwise the condensation of the aliphatic amino acids is the main reaction pathway. If lower molecular weights are desired, small amounts of monofunctionalized compounds, e. g. acetic acid, can be added to act as chain-terminating agents. [70]

2 Theoretical principles

2.1 Hydroformylation

The hydroformylation (or "oxo synthesis") is a reaction, where an alkene reacts with carbon monoxide and molecular hydrogen via transition metal catalysis to form aldehydes.

This reaction type was discovered by accident in 1938 by Otto Roelen, who worked for Ruhrchemie at that time. Originally, Roelen worked on a way to refeed ethylene, which is an undesired side product of the Fischer-Tropsch synthesis, together with ammonia into the reactor. [71] Much to his surprise, he found the imine of propanal as side product in the resulting product mixture and he concluded that somehow another reaction mechanism than the Fischer-Tropsch mechanism must be involved. [72] In the same year Roelen patented his findings and in 1940 the first plant was built by Ruhrchemie, that was able to produce in a 15 kt scale long chained alcohols from the corresponding olefins with cobalt catalysts. This plant was completed in cooperation with IG Farben AG during the Second World War. However, the plant was never put into operation. [73,74] Until the late 70's, cobalt catalysts were state of the art and not much research was conducted on new catalysts. This changed with the research of Wilkinson, who investigated the effect of P-ligand modified rhodium compounds on the hydroformylation reaction, and Shell, which investigated the effect of phosphines on the cobalt catalysts. This marked the starting point of the development of highly efficient and selective catalysts for the oxo process. Industrially applied processes derived from this research are described in the following. The "low pressure oxo process", or in short LPO process, is a kind of rhodium catalysed hydroformylation that was first implemented by many different companies (such as UCC, Celanese, Mitsubishi, BASF, etc.) in 1976. [75] In this process, the catalyst remains in the reactor and the reaction products are separated via thermal work up procedures. Improvements were made in 1984, which resulted in the so called Rhône/Poulenc process. This method employs a 2-phasic solvent system, where one phase is aqueous and the other organic. The basic idea is that the catalyst in use is water soluble and therefore remains in the aqueous phase. The products and the substrates, which are usually lipophilic, stay in the organic phase and consequently can be easily separated from the catalyst by simple phase separation. Then, the catalyst solution can be refed into the reactor, together with fresh substrate solution. In this way, the catalyst is not subjected to the thermal strain caused by the distillation step of the LPO processes.

2.1.1 Influence of the transition metal

Many transition metals are active in the hydroformylation reaction. A simple and rough classification regarding their relative activity can be made as shown:

Rh >> Co > Ir > Ru > Os > Pt > Pd > Tc > Mn > Fe > Re

rhodium is by far the most active metal, almost 1000 times more active than corresponding cobalt catalysts. This is the reason for the much milder reaction condition and lower catalyst loadings that can be found for rhodium catalysed hydroformylation reaction compared to those used in cobalt catalysed reactions. (see Table 3) The main drawback of rhodium is its price, since it is quite expensive compared to cobalt. [76] The other metals are usually of academic interest only, because of their low activity and are not part of this work.

Metal Reaction conditions	Rh	Co
c_{kat} [g/kg]	10^-2 – 10^-1	1 – 10
Temperature [°C]	80 - 140	< 200
Pressure [bar]	< 50	< 200

Table 3: General reaction conditions for the hydroformylation reaction comparing rhodium and cobalt catalysts.

2.1.2 Mechanism of the rhodium catalysed hydroformylation

The mechanism of the rhodium catalysed hydroformylation can vary drastically depending on the catalyst system. In this work only those mechanisms in action for unmodified and P-ligand modified rhodium catalysts are reviewed.

2.1.2.1 Unmodified rhodium catalysts

The rhodium catalysed hydroformylation with unmodified rhodium catalysts usually starts with the formation of the catalytically active species by addition of the rhodium precursor without ligand under catalytic conditions. The generally accepted catalytic cycle is shown in Fig. 16.

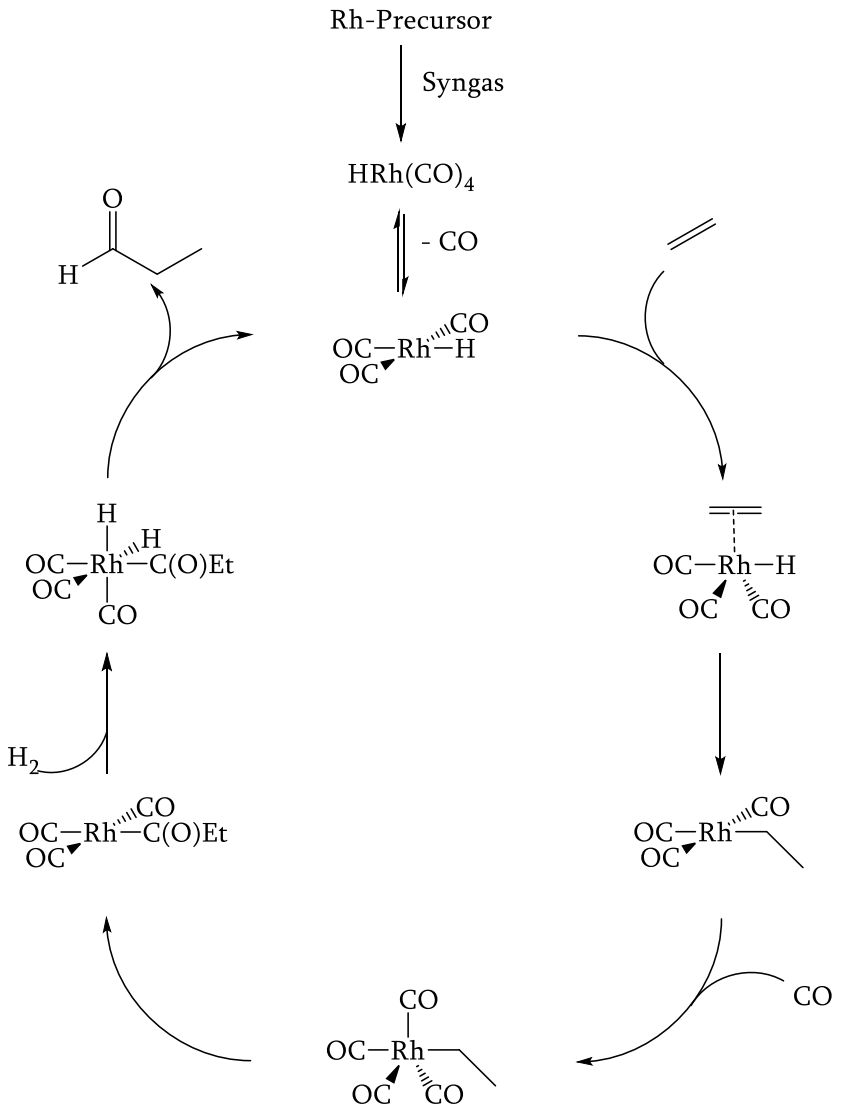

Fig. 16: Mechanism of the hydroformylation with unmodified Rh(I) complexes.

Under catalytic conditions, the precursor is converted into the dimeric $Rh_2(CO)_8$ complex via addition of CO. Oxidative addition of molecular hydrogen and dissociation of one CO ligand leads to the formation of the catalytically active complex $RhH(CO)_3$, a quadratic planar 16 VE-species. The olefinic substrate is now coordinated via the double bond to a free coordination site at the apical position that leads to a change of the coordination geometry. The now trigonal bipyramidal 18 VE-complex then undergoes an insertion reaction of the olefin into the rhodium H bond to form the quadratic planar alkyl species (16 VE). Coordination of a CO ligand and subsequent insertion into the rhodium alkyl bond forms the acyl complex. Oxidative addition of molecular hydrogen and subsequent reductive elimination liberates the product aldehyde and regenerates the catalytically active species.

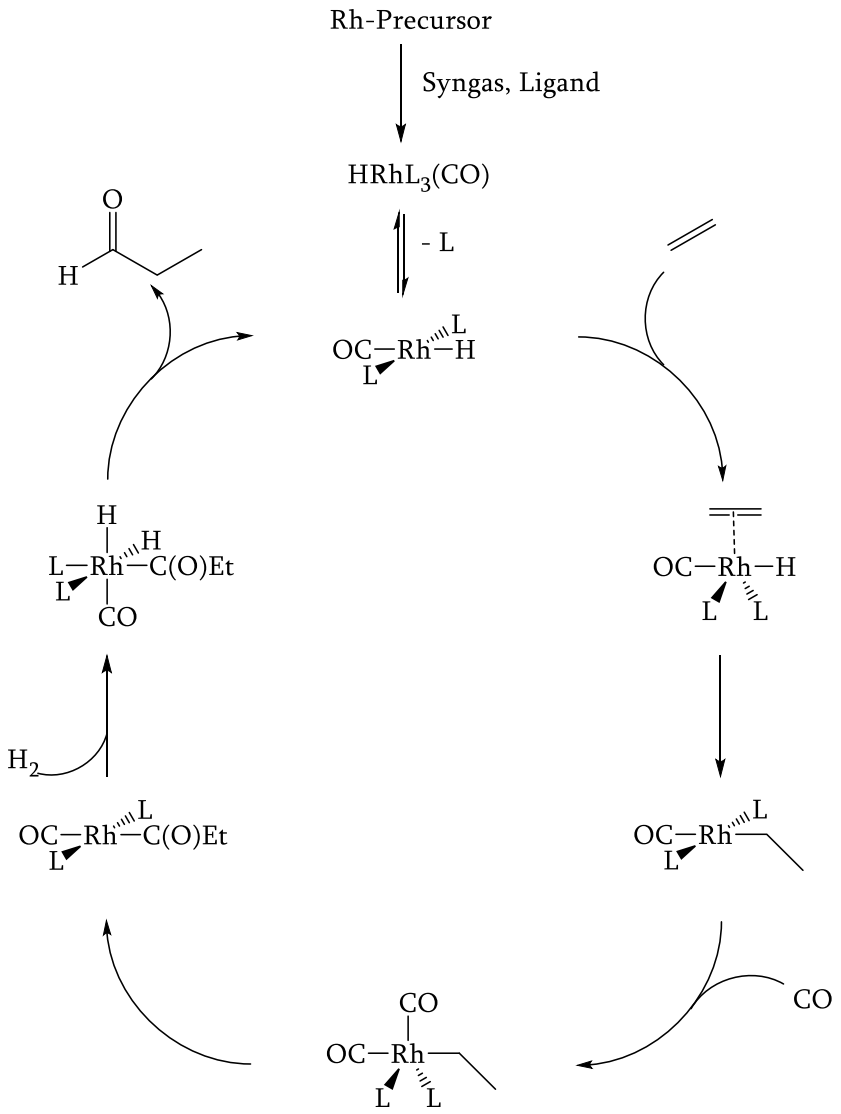

Fig. 17: Ligand modified hydroformylation.

2.1.2.2 P-Ligand modified rhodium catalysts

The mechanism of the P-ligand modified rhodium catalysed hydroformylation differs greatly from the unmodified catalysis and depends on the steric and electronic properties of the ligand in use. The mechanism that was proposed by Wilkinson is applicable for PPh_3-modified rhodium catalysts. It commences with the formation of the catalytically active species from the catalyst precursor by dissociation of a PPh_3 ligand, forming the quadratic planar 16 VE complex $RhH(CO)(PPh_3)_2$. The two TPP ligands coordinate in a *trans* fashion. This step is followed by the coordination of the olefin via the double bond and the subsequent insertion of the olefin in the Rh-H bond.

After CO addition, the CO ligand in *cis* position to the olefin inserts into the M-C bond. Consecutive oxidative addition of H_2 and reductive elimination leads to the liberation of the product aldehyde and the regeneration of the catalytically active species. [77]

As already described above, the mechanism shown in Fig. 17 is only applicable for the use of TPP. When TPP is replaced with the phosphite Alkanox - the IUPAC name is tris(2,4-di-*tert.*-butylphenyl)phosphite – the most obvious difference is that because of its steric properties only one P-ligand coordinates to the metal centre. This leads to the favoured formation of the highly catalytically active species $[(L)RhH(CO)_3]$.

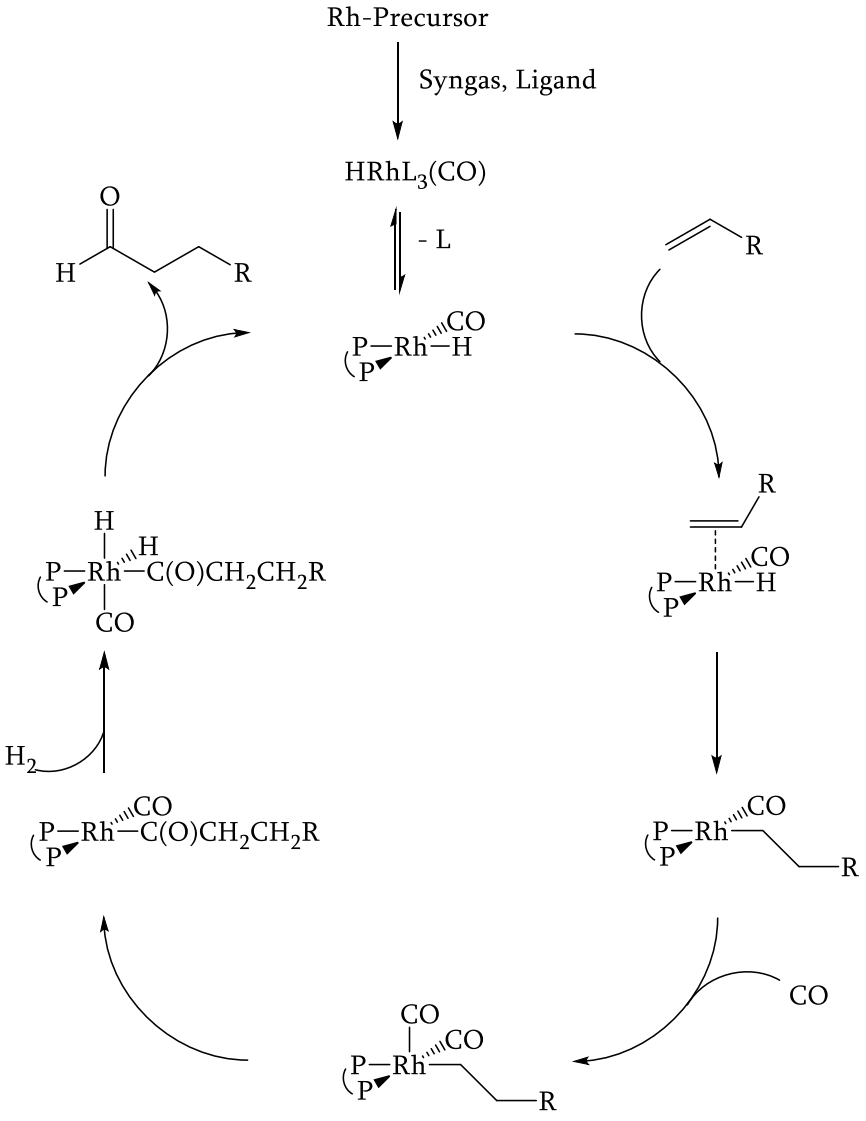

Fig. 18: Rhodium catalysed hydroformylation with a diphosphine modified catalyst.

Another effect is the favoured, albeit undesired, cluster formation at low L:Rh ratios, that leads to rhodium black formation and therefore catalyst deactivation. This problem can be tackled by addition of large excesses of the ligand (usually ca. L:Rh ratio of 200), effectively suppressing cluster formation and shifting the equilibria from the clusters towards the catalytically active species. Especially this property is characteristic for sterically demanding monophosphites with *t*Bu-moieties in *ortho* position. The mechanism for the rhodium catalysed hydroformylation with bidentate ligands differs with regard to the coordination of the phosphorus. In case the distance between the two P atoms in the ligand is short enough, they are forced to coordinate in a *cis* fashion. Depending on the ligand, this can be the reason for the typical increase in regioselectivity for substituted olefins with regard to the linear aldehyde if a bidentate ligand is used, since the steric bulk of the ligand forces the substrate into a coordination, where the sterically most demanding side of the olefin points away from the ligand, thus increasing the probability of a more selective olefin insertion into the Rh-H bond. (see Fig. 18)

There are different ways to quantify the steric demand that a coordinating ligand owns in a transition metal complex. One of them is Tolman's cone angle θ. [78] It was introduced, because the coordinating behaviour of ligands in Ni(0) complexes could not be explained by their electronic properties alone. [79] In case of symmetric P-ligands of the type PR_3, the cone angle is defined as twice the angle that is created between the M-P bond and the outer Van-der-Waals radii of the outer substituents of the ligand. (see Fig. 19) For asymmetric ligands of the type $PR^1R^2R^3$ an approximated equation exists for the minimisation of the sum of the half angles θ_i (see equation *(1)* & Fig. 19) created between the M-P bond and the outer Van-der-Waals radii of the different substituents. [78,80]

$$\Theta = \frac{2}{3}\sum_{i=1}^{3}\frac{\theta_i}{2} \qquad (1)$$

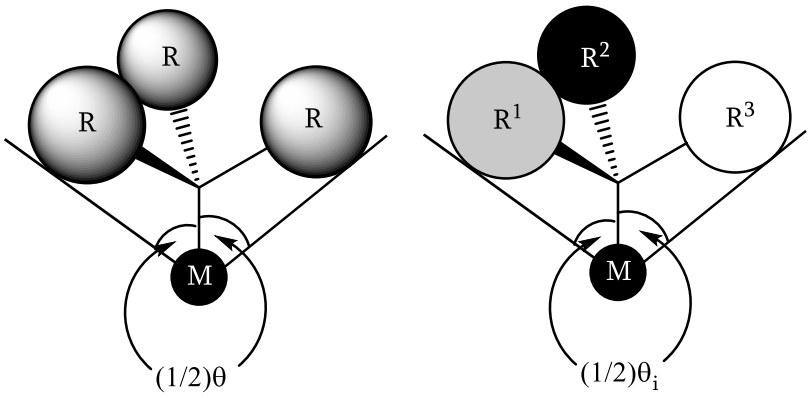

Fig. 19: Tolman's cone angle for symmetric (left) and asymmetric ligands (right).

Nonetheless, the model of Tolman's cone angle has to be treated with caution, because it is solely based on the space filling model of the considered complex. In real systems, observable differences in the cone angle can occur due to steric and electronic interactions inside the complex, thus leading to different coordination behaviours than predicted by the theoretically determined value.

For bidentate ligands, the corresponding angle for the quantification of the steric bulk is called "natural bite angle" α. Casey and Whiteker were the first to describe this bite angle as the theoretically determined P-M-P angle inside the chelate complex. For the calculation, some simplifications are assumed: For one, the influence of the electronic properties of the metal as well as the influence of other ligands inside the considered complex is disregarded. Furthermore, a set P-M bond distance is picked that can be derived from crystallographic data retrieved from structurally similar complexes. Typically, this distance is assumed to be 2.3 Å for rhodium complexes. In the literature, a bite angle is generally given as an interval that takes the flexibility of the ligand into account. The boundaries of the interval are calculated in such a way that the energetic difference compared to the natural bite angle is less than 3 kcal*mol^{-1}. [81]

2.2 Alkoxycarbonylation

The alkoxycarbonylation is described as the synthesis of esters from olefins or alkynes, carbon monoxide and an alcohol. This reaction type is related to the hydroxycarbonylation reaction that uses water instead of alcohols to form the corresponding carboxylic acids or even lactones. (see Fig. 20)

2.2.1 Mechanism of the palladium catalysed alkoxycarbonylation

For the palladium catalysed methoxycarbonylation (alkoxycarbonylation with methanol) of ethylene towards methyl propionate two mechanism have been suggested by Drent *et al.* [82] (see Fig. 20:) Because of reaction intermediates which could not be detected, they assumed that either only one catalytic cycle is active during the reaction or two catalytic cycles independently take place at the same time. The hydride cycle **A** starts from a quadratic planar 16 VE palladium hydride species that is generated starting from the employed catalyst precursor. In the next step the olefin coordinates and inserts into the Pd-H bond to form the corresponding quadratic planar 16 VE alkyl complex. Similar to the hydroformylation, this step determines the regioselectivity of the reaction. After CO coordination and insertion into the palladium alkyl bond, the acyl species is formed. Via alcoholysis, which usually is the rate determining step, the product is liberated and the hydride species regenerated. [83]

The alkoxy cycle **B** starts from an alkoxy complex as the catalytically active species generated from the precursor. CO coordinates and inserts into the M-O bond to form a palladium alkoxycarbonyl species. In the subsequent step, the olefin coordinates and inserts into the M-CO bond to form an alkyl complex. Oxidative addition of the alcohol and reductive elimination liberates the product and regenerates the catalytically active species. The reaction intermediates were isolated and characterised by Liu *et al.* [84]

Because of the mechanistic investigations carried out until today, it is assumed that the hydride cycle is more relevant for most alkoxycarbonylation reactions. [85] Of course, this strongly depends on the applied catalyst system, as well as additives.

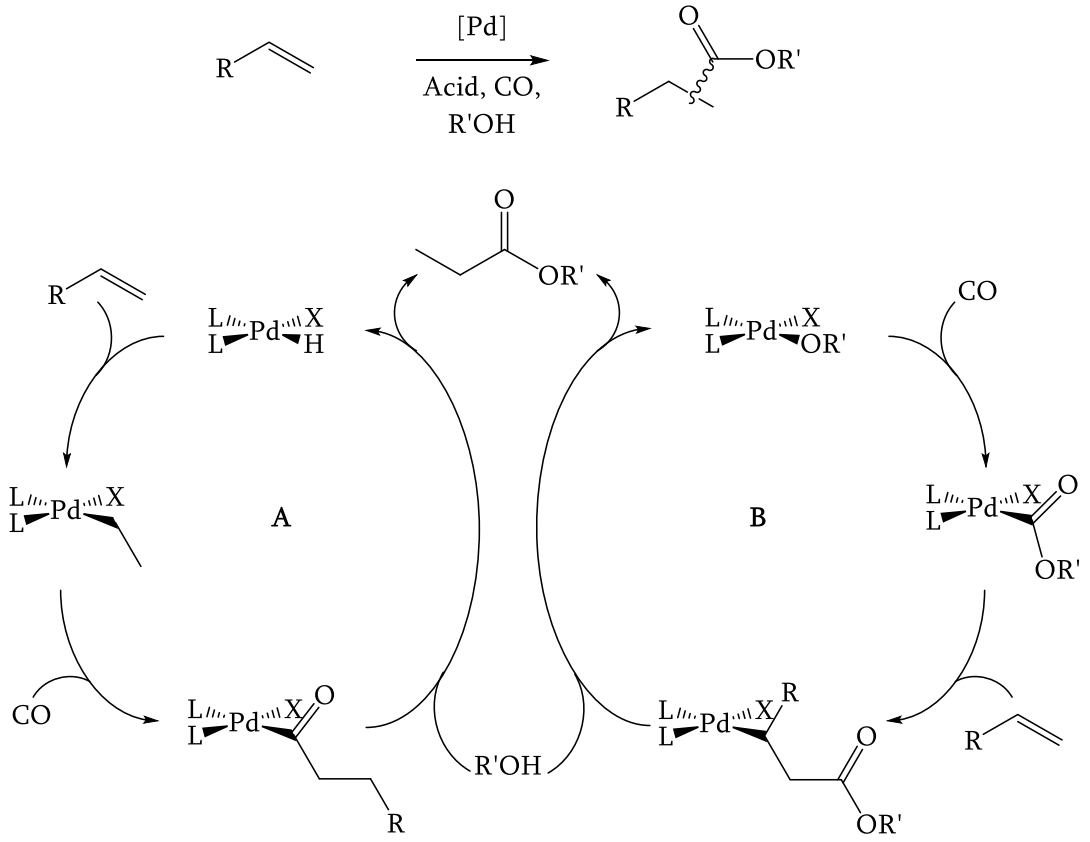

*Fig. 20: Mechanisms of the alkoxycarbonylation. (**A**) Hydride cycle. (**B**) Alkoxy cycle.*

2.3 Hydroaminomethylation

The hydroaminomethylation (in the following abbreviated as HAM) is defined as the reaction of olefins with syngas and primary or secondary amines or ammonia to form the corresponding saturated amines, elongated by one CH_2 group. The whole reaction can be divided into three steps:

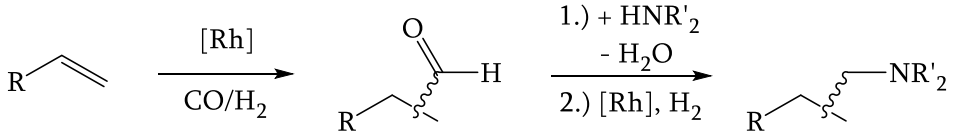

Fig. 21: Reaction scheme of the hydroaminomethylation.

(1) Hydroformylation of the olefin

(2) Imine formation and formation of water

(3) Hydrogenation of the imine to form the amine.

Because of the possibility to clearly separate these steps into the hydroformylation, imination and hydrogenation step, catalysed by the same catalyst, the reaction can be classified as tandem catalysis. [86,87a] Typical reaction conditions are temperatures of 90 – 130 °C and pressures of 30 – 60 bars of syngas.

2.3.1 Mechanisms

The hydroformylation mechanism was already reviewed in 2.1.2. For the enamine hydrogenation, two mechanisms can be assumed. Which one of the mechanism is active, depends on whether the catalytically active species is cationic or neutral. In case of a neutral species, the catalytic cycle starts with the oxidative addition of molecular hydrogen. The substrate coordinates via its double bond and inserts into the M-H bond to form the corresponding alkyl complex. Product formation occurs by reductive elimination of the alkyl moiety with the remaining hydride ligand simultaneously regenerating the starting complex.

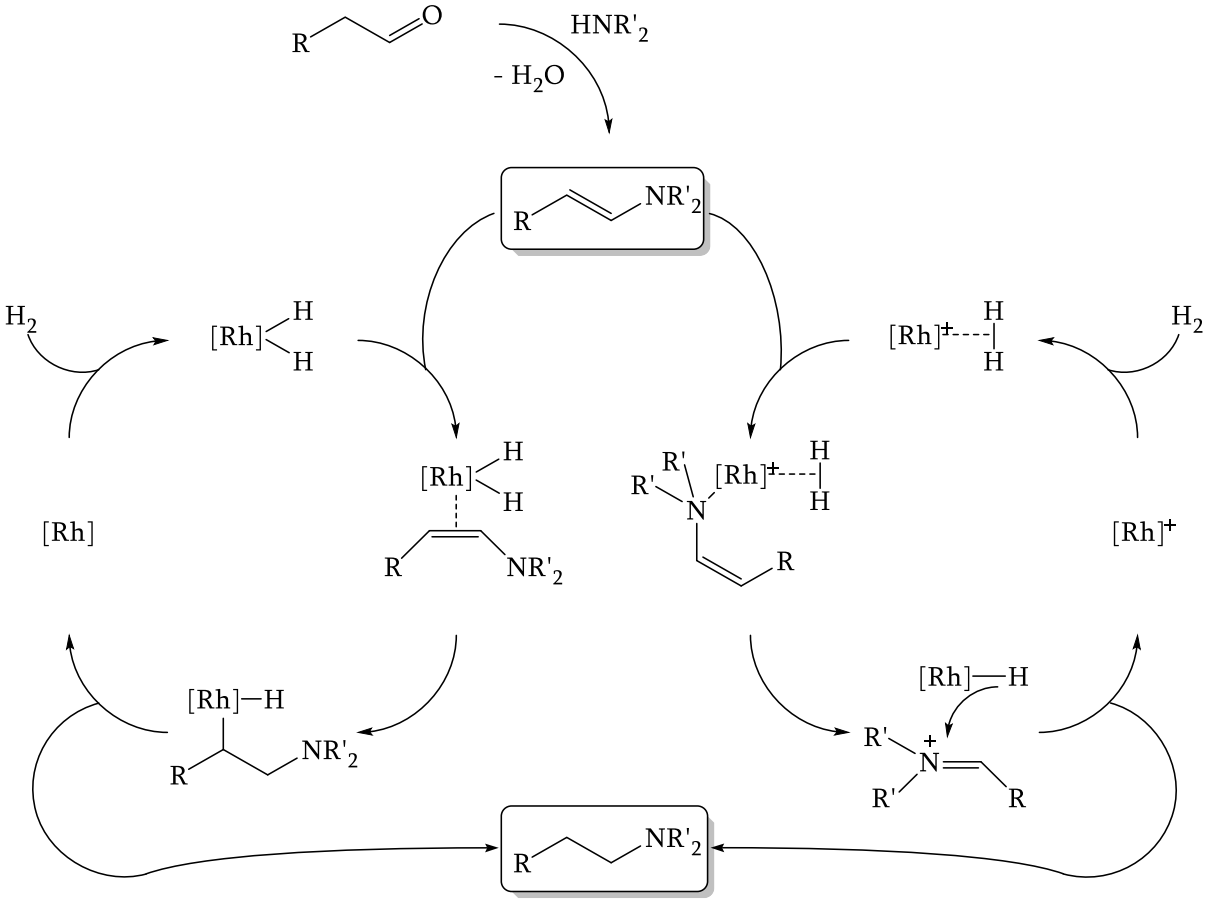

*Fig. 22: Mechanisms of the enamine hydrogenation. **Left**: Catalysis with neutral rhodium complexes. **Right**: Catalysis with cationic rhodium complexes.*

If the catalytically active species is cationic in nature, oxidative addition of hydrogen cannot occur. Instead, the starting complex forms together with hydrogen a σ-complex. After coordination of the enamine via the lone pair of the nitrogen, a concerted transfer of a proton to the enamine occurs, the imine forms and a neutral hydride complex is generated, which is able to hydrogenate the formed imine. [87]

Hydroaminomethylation operates with unmodified as well as ligand modified catalysts. Efficient catalyst precursor are Rh_2O_3, $[Ru_3(CO)_{12}]$ as well as $[Rh(\mu\text{-}Cl)_2(COD)_2]$, because of their ability to selectively form the catalytically active species under reaction conditions. [87a,88]

3 General Part

3.1 Hydroformylation of isomeric methyl pentenoates

3.1.1 Rhodium catalysed hydroformylation of methyl 3-pentenoate and methyl 4-pentenoate with different ligands

The synthesis of 5-FMP from methyl pentenoates via the rhodium catalysed hydroformylation was first tested using different catalytic systems. These systems were generated from the catalyst precursor $Rh(CO)_2acac$ and different ligands. The Rh:L ratio was picked with literature known standard values in mind. The utilised ligands are shown in *Fig. 23*.

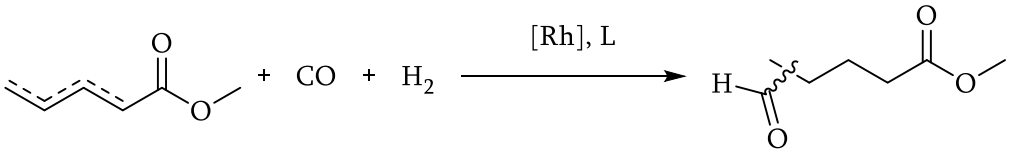

Monodentate: PAr_3 $P(OAr')_3$

Ar = Ph (**TPP**), 3-sulphonatophenyl (**TPPTS**)
Ar' = Ph (**Triphenylphosphite**),
2,4-di-*tert.*-butylphenyl (**Alkanox**)

Bidentate:

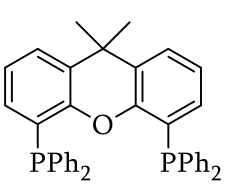

XantPhos

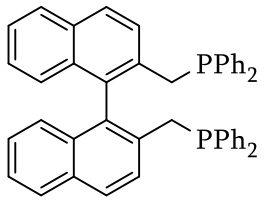

NAPHOS

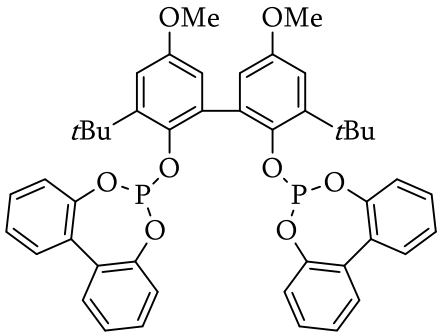

BiphePhos

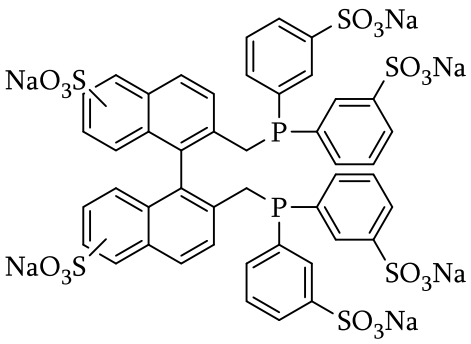

BINAS

Fig. 23: Rhodium catalysed hydroformylation of methyl pentenoates.

Ligand	Rh:L:M4P:M3P	Conversion [%]	Yield [%]	Selectivity [%]
TPP	1:150:1000:0	95.3	93.4	72.1
	1:20:0:1000	18.4	14.2	42.2
	1:150:900:100	18.8	16.1	11.0
Alkanox	1:20:1000:0	100	69.3	45.8
	1:20:0:1000	98.2	59.9	48.5
Triphenylphosphit	1:20:1000:0	79.4	74.9	71.0
	1:20:0:1000	72.1	44.7	50.1
XantPhos	1:4:1000:0	95.6	90.7	91.7
	1:4:0:1000	63.0	59.7	49.8
	1:4:900:100	46.7	44.1	83.0
NaPhos	1:4:1000:0	94.8	90.5	95.5
	1:4:0:1000	89.1	60.2	47.2
	1:4:900:100	79.7	67.5	53.0
BiphePhos	1:4:1000:0	99.6	68.8	87.2
	1:4:0:1000	79.8	8.3	55.8
	1:4:900:100	100	94.2	97.7

Table 4: Results of preliminary experiments on the hydroformylation of a mixture of M4P and M3P. (a) Homogeneous approach in toluene. T = 100 °C, p = 5 bar, CO/H_2 = 1, Rh:L:substrate = 1:4:1000, c_{Rh} = 100 ppm, t = 20 h. (b) Two phasic approach with toluene/water (1:1). T = 110 °C, p = 10 bar, CO/H_2 = 1, Rh:L:substrate = 1:4:1000, c_{Rh} = 100 ppm, t = 20 h.

The ligands TPPTS and BINAS were used in a biphasic approach (comparable to the Rhône-Poulenc processes) to make the catalyst more water-soluble so it remains in the aqueous phase.

The improvement of the water-solubility is achieved by the introduction of sulfonyl moieties into the ligands. These experiments were already part of my master thesis.[17]

3.1.1.1 Homogeneous catalysis

The Results of the homogeneously catalysed approach of the conversion of methyl 3- and methyl 4-pentenoate towards 5-formylvalerate are shown in Table 4. It comes with no surprise that the reactions with methyl 4-pentenoate perform better than the corresponding reactions with methyl 3-pentenoate. The reason for this is the higher reactivity of terminal alkenes due to lower steric hindrance (Keuleman's rule [89]) and lesser stabilisation through hyperconjugation. Generally, when an internal methyl pentenoates is used, it is advised to choose a catalyst known for its isomerisation capabilities since this will partly convert the internal olefin to the terminal one thus increasing the regioselectivity of the reaction. At the same time the isomerisation attitude can be the main drawback of these catalysts, because methyl 2-pentenoate can also be formed. Methyl 2-pentenoate is the most stable of the constitutional isomers since it represents an α,β-unsaturated carboxylic acid. The reactivity of methyl 2-pentenoate in the hydroformylation reaction is described in section 3.1.2. Out of the monodentate ligands, TPP was the most effective because of its superior performance regarding chemo- and stereoselectivity in the hydroformylation of M4P. In comparison the utilisation of Alkanox led to a catalyst that is significantly more active even at low Rh:L-ratios, though it has a higher hydrogenation activity and lower regioselectivity. Unsurprisingly, the hydroformylation of M3P was generally less chemoselective and regioselective, especially when a catalyst with low isomerising tendency was used. Here the Results of Alkanox were similar to those for the corresponding reaction with M4P. Looking at the results of the catalysis employing bidentate ligands, they performed significantly superior regarding overall chemo- and regioselectivity than the monodentate modified catalysts. Here the best results were achieved with a BiphePhos-modified catalyst, even for a mixture of M4P and M3P. (see Table 4, last entry)

3.1.2 Hydroformylation of methyl 2-pentenoate

3.1.2.1 Homogeneous catalysis

The hydroformylation of methyl 2-pentenoate (M2P) was screened with NaPhos, XantPhos and BiphePhos under non optimised reaction conditions. The results are summarised in Table 5. As shown, the main reaction path for this substrate is the hydrogenation that leads to the formation

of methyl valerate. The desired aldehyde is effectively a side product that was formed with low regioselectivities with regard to the *l*-aldehyde. Since the methyl 2-pentenoate is the substrate with the most steric demand compared to its isomers and also the most stable – since it is an α,β-unsaturated carboxylic acid ester – it comes with no surprise that it was only converted at a very low rate (Keuleman's rule) and with low regioselectivity (low isomerisation tendency because of the conjugated double bond).

Ligand	*C[a] [%]*	*Y[b] [%]*	*S[c] [%]*
Xantphos	23.3	1.2	53.6
NAPHOS	46.8	9.7	33.6

*Table 5: Results of the experiments regarding the homogeneous hydroformylation of M2P. T = 100 °C, p = 15 bar, t = 20 h, c_{Rh} = 0.286 µmol*mL^{-1}, Rh:L:M2P 1:4:1000. See section 4.2.1. (a) Conversion of substrate. (b) Yield of aldehydes. (c) Regioselectivity of the reaction as the ratio of the amount 5-FMP to the amount of all aldehydes in the product mixture.*

Ligand	*C[a] [%]*	*Y[b] [%]*	*S[c] [%]*
TPPTS	94.2	<1	38.7
BINAS	13.4	2.7	76.1

*Table 6: Results of the two phase hydroformylation of M2P. T = 110 °C, p = 20 bar, t = 20 h, c_{Rh} = 0.286 µmol*mL^{-1}, Rh:L:M2P 1:4:1000. (a) Conversion of substrate. (b) Yield of aldehydes. (c) Regioselectivity of the reaction as the ratio of the amount 5-FMP to the amount of all aldehydes in the product mixture.*

3.1.2.1 Two phase catalysis

The two phase hydroformylation of methyl 2-pentenoate with BINAS and TPPTS delivered comparable results as in the homogeneous process. The hydrogenation of the substrate was equally favoured and the regioselectivity regarding the *l*-aldehyde comparably low with the exception of the catalysis with BINAS. Here, even though only a small amount of aldehyde was formed, the regioselectivity was at about 76 % of the linear aldehyde. The results are shown in Table 6.

3.1.3 Comparison of different stirring techniques with regard to conversion, yield and *n*-regioselectivity of the hydroformylation of methyl 3-pentenoate

The availability of different stirring techniques for autoclaves, which are able to strongly influence the performance of a catalytic reaction by improving mass transfer in between different phases, led us to compare the results of the hydroformylation of methyl 3-pentenoate above, where a simple magnetic stirring bar was used, with those where we utilised a gas entrainment impeller. For two phase catalysis, mass transfer is a rather demanding issue since it occurs between three phases: gas, organic and aqueous phase. Consequently, the catalytic performance is worse, the less the reaction medium is dispersed. This can be countered by employing a gas entrainment impeller that is able to suck gas from the gas phase into the liquid phase at high speed (ca. 1000 rpm), leading to high dispersion of the reaction mixture as well as high concentration of dissolved gas. The results in Table 7 were obtained with non-optimised reaction conditions. As can be seen, the usage of a gas entrainment impeller is favourable with regard to overall catalytic activity, though chemo- and regioselectivity are significantly lower. The lower chemoselectivity is caused by higher H_2 concentration in the liquid phases that leads to higher concentration of the hydrogenated substrate methyl valerate.

Gas entrainment impeller	*C[a] [%]*	*Y[b] [%]*	*S[c] [%]*
Yes	57.8	47.5	46.3
No	38.6	35.5	65.6

*Table 7: Comparison of the two phase hydroformylation of methyl 3-pentenoate with and without gas entrainment impeller. Reaction conditions: Rh:L:M3P => 1:4:1000, c_{Rh} = 0.286 µmol*mL^{-1}, t = 20 h, T = 110°C, p = 15 bar. (a) Conversion of substrate. (b) Yield of aldehydes. (c) Regioselectivity of the reaction as the ratio of the amount 5-FMP to the amount of all aldehydes in the product mixture.*

3.1.4 Optimisation of reaction conditions for the hydroformylation of a mixture of isomeric methyl pentenoates with a BINAS-modified Rh(I)-catalyst

The optimisation of the reaction conditions was conducted for the hydroformylation of a 9:1 mixture of M4P and M3P with a BINAS-modified rhodium catalyst in a two phase approach. For this, the pressure was varied first and then the temperature. The results are summarised in Table 8. The

best conditions were at T = 100 °C and p = 50 bar, where the substrate was converted almost quantitatively with a yield of 95 % of the aldehydes. 5-FMP was formed with a regioselectivity of 88 %. The most common side product was methyl valerate.

Nr.	*1*	*2*	*3*	*4*	*5*	*6*	*7*	*8*	*9*	*10*
T [°C]	110	110	110	110	110	80	90	100	110	120
p [bar]	10	20	30	40	50	50	50	50	50	50
C[a] [%]	38.6	49.8	84.1	>99.0	>99.0	>99.0	>99.0	>99.0	>99.0	99.2
Y[b] [%]	35.5	42.9	74.3	93.7	89.4	97.2	96.5	95.4	92.3	93.9
S[c] [%]	65.6	55.3	49.3	48.3	57.0	67.9	84.2	88.1	77.3	87.2

*Table 8: Results of the optimisation experiments for the hydroformylation of a mixture of M4P and M3P with the BINAS modified rhodium catalyst in the two phase approach. Reaction conditions: Rh:L:M4P:M3P => 1:4:900:100, c_{Rh} = 0.286 µmol*mL^{-1}, t = 3 h. (a) Conversion of substrate. (b) Yield of aldehydes. (c) Regioselectivity of the reaction as the ratio of the amount 5-FMP to the amount of all aldehydes in the product mixture.*

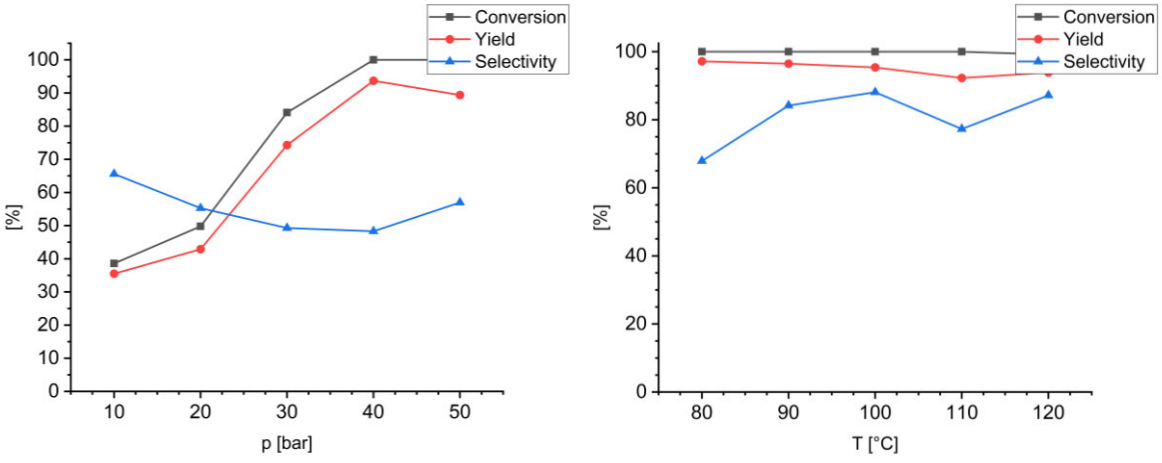

Fig. 24: Graphical representation of the results from Table 8. ***Left:*** *Variation of pressure at 110 °C.* ***Right:*** *Variation of temperature at 50 bars.*

Nr.	*1*	*2*	*3*	*4*	*5*	*6*	*7*	*8*	*9*	*10*
T [°C]	100	100	100	100	100	80	90	100	110	120
p [bar]	10	15	20	30	40	15	15	15	15	15
C^a [%]	>99.0	>99.0	>99.0	>99.0	>99.0	>99.0	98.6	>99.0	>99.0	>99.0
Y^b [%]	94.2	94.7	95.4	95.8	96.3	96.5	94.6	94.5	94.2	92.9
S^c [%]	97.7	97.2	84.8	90.5	87.8	81.7	97.8	97.6	97.4	97.3

*Table 9: Results of the optimisation experiments for the hydroformylation of a mixture of M4P and M3P with the BiphePhos modified rhodium catalyst in the homogeneous approach. Reaction conditions: Rh:L:M4P:M3P => 1:4:900:100, c_{Rh} = 0.286 µmol*mL^{-1}, t = 3 h. (a) Conversion of substrate. (b) Yield of aldehydes. (c) Regioselectivity of the reaction as the ratio of the amount 5-FMP to the amount of all aldehydes in the product mixture.*

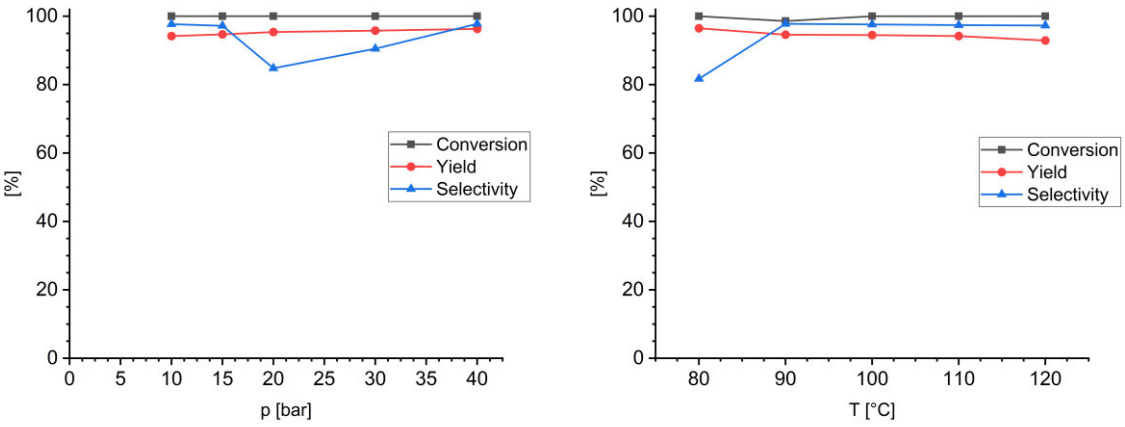

Fig. 25: Graphical representation of the results from Table 9. ***Left:*** *Variation of pressure at 100 °C.* ***Right:*** *Variation of temperature at 15 bars.*

3.1.5 Recycling of the BINAS-modified Rh(I)-catalyst in the hydroformylation of methyl pentenoates

The recycling of the BINAS modified rhodium catalyst for the two phase catalysis was investigated. Since the catalyst remains in the aqueous phase because of its water solubility and the substrate in the organic phase, simple phase separation is enough to recover the catalyst, which can be reused for consecutive reactions. As shown in Table 10, the regioselectivity of the reaction drastically decreased after the first run and the aldehyde yield was higher. This change in catalyst performance shows that the catalyst was subjected to irreversible changes, maybe even to decomposition. To investigate on this, the leaching of rhodium and phosphorus into the organic phase was quantified via ICP-OES. The samples were prepared by acidic fusion with concentrated nitric acid at 200 °C in a pressure tube to destroy all organic compounds. The results show that heavy leaching of rhodium occured into the organic phase in addition to rhodium black formation. This supports the impression that the catalyst quickly decomposed after the first run and that heterogeneous catalysis with rhodium nano particles took over for the following runs. This also explains the similarity of these results to those for the catalysis with "naked" Rh, realised by not adding any ligand to the reaction mixture.

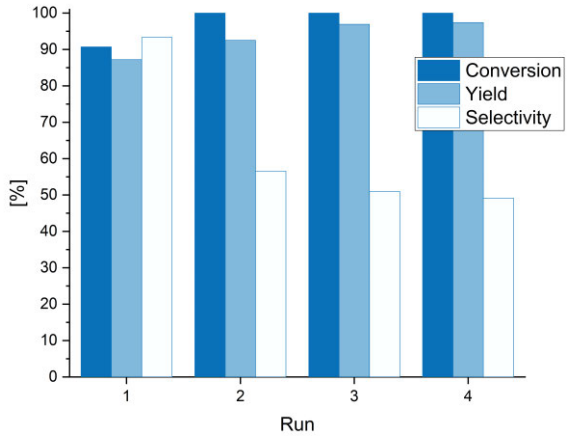

Run	C[a] [%]	Y[b] [%]	S[c] [%]
1	90.7	87.2	93.3
2	>99	92.5	56.6
3	>99	96.9	51.0
4	>99	97.4	49.1

Table 10: Results of the recycling of the BINAS modified Rh(I) catalyst in the two phasic hydroformylation of methyl pentenoates. Reaction conditions per run: T = 110 °C, p = 20 bar, t = 18 h, n_{Rh} = 1.43 µmol, n_{Ligand} = 5.72 µmol, n_{M4P} = 1.43 mmol, $V_{toluene}$ = 2.5 mL, V_{H2O} = 2.5 mL. (a) Conversion of substrate. (b) Yield of aldehydes. (c) Regioselectivity of the reaction as the ratio of the amount 5-FMP to the amount of all aldehydes in the product mixture.

3.1.6 Mechanistic and kinetic investigations

3.1.6.1 Isomerisation of methyl pentenoates catalysed by the precatalyst under inert conditions

For the investigations on the rhodium catalysed isomerisation of methyl pentenoates as side reaction besides the hydroformylation reaction the behaviour of the complex [Rh(L)acac] towards methyl 4-pentenoate was observed. For this a solution of the precursor and 4 equivalents of BiphePhos in dry toluene was prepared under argon atmosphere and heated to 100 °C. Then an exact amount of substrate was added. Stirring commenced at 100 °C for 2 hours and every 15 minutes a sample was taken for GC analysis. The isomeric substrate composition was quantified and the results are summarised in Table 11.

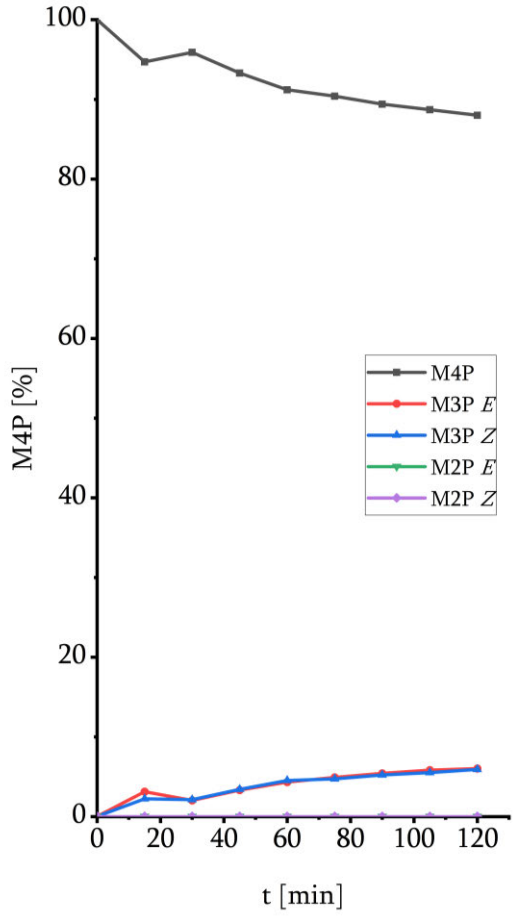

t [min]	M4P [%]	M3P [%]		M2P [%]	
		E	*Z*	*E*	*Z*
0	100	-	-	-	-
15	94.7	3.1	2.2	-	-
30	95.9	2.0	2.1	-	-
45	93.3	3.3	3.4	-	-
60	91.2	4.3	4.5	-	-
75	90.4	4.9	4.7	-	-
90	89.4	5.4	5.2	-	-
105	88.7	5.8	5.5	-	-
120	88.0	6.0	5.9	-	-

*Table 11: Results of the investigation on the isomerisation reaction of methyl pentenoates catalysed by $Rh(CO)_2acac$. Reaction conditions: Rh:L:M4P => 1:4:1000, c_{Rh} = 0.286 µmol*mL^{-1}, t = 3 h, T = 100 °C.*

The results show that the complex [Rh(BiphePhos)acac] is active in isomerisation of the substrate, though it only isomerises the substrate slowly. This has to be kept in mind for further investigations on the isomerisation of the substrate under catalytic condition since substrate addition after catalyst preforming cannot always be realised. Furthermore it was surprising that methyl 2-pentenoate was not detected, albeit it is thermodynamically more stable in comparison to the other isomers because of its conjugated double bond. Consequently the position of the double bond was only shifted by one position.

3.1.7 Summary

As was the aim of this work, methyl pentenoates were successfully employed in the rhodium catalysed hydroformylation for the synthesis of methyl 5-formylpentenoate. The best results were achieved with a BiphePhos-modified Rh(I) catalyst generated *in situ* from BiphePhos and $Rh(CO)_2acac$. With this catalytic system, high conversions (100 % within 3 hours of the reaction) of the pentenoates into the desired product, high chemoselectivities (only about 5 % of by-products, mainly methyl valerate) and high *n*-regioselectivities (about 98 %, with regard to 5-FMP) were achievable. The 2-phasic approach was not quite as successful, even though the BINAS-modified catalyst performed relatively well (full conversion within 3 h, high chemoselectivity with 5.5 % of by-products formed and good *n*-regioselectivity of about 88 %). In this case, the main problem lied in the recyclability of the catalyst. The performed experiments showed a rather fast decomposition of the catalyst after the first run, observable by heavy leaching of rhodium into the organic phase and cluster formation and subsequent precipitation of rhodium black.

Since the reactions were performed batch wise and the substrates were in the presence of the precatalyst before starting the hydroformylation, experiments were conducted to observe the isomerising influence of the precatalyst on the substrates. Luckily, the isomerisation ability of the precatalyst is negligible and, starting from M4P, only low amounts of isomers are formed.

3.2 Alkoxycarbonylation of isomeric methyl pentenoates

3.2.1 Methods

The methoxycarbonylation of an isomeric mixture of methyl pentenoates was investigated. As catalysts, diphosphine- and diphosphite-modified palladium complexes were utilised. As ligands BuPox (or DTBPX), PyTBPF and PyTBPX were selected. The last two ligands were developed at LIKAT by the work group of Prof. Beller in cooperation with Evonik. As promoter and proton source methanesulfonic acid was employed. The ratio of the compounds in use (Pd:ligand:$MeSO_3H$:M4P:M3P) was 1:4:10:900:100. Autoclaves were prepared as described in 3.1.

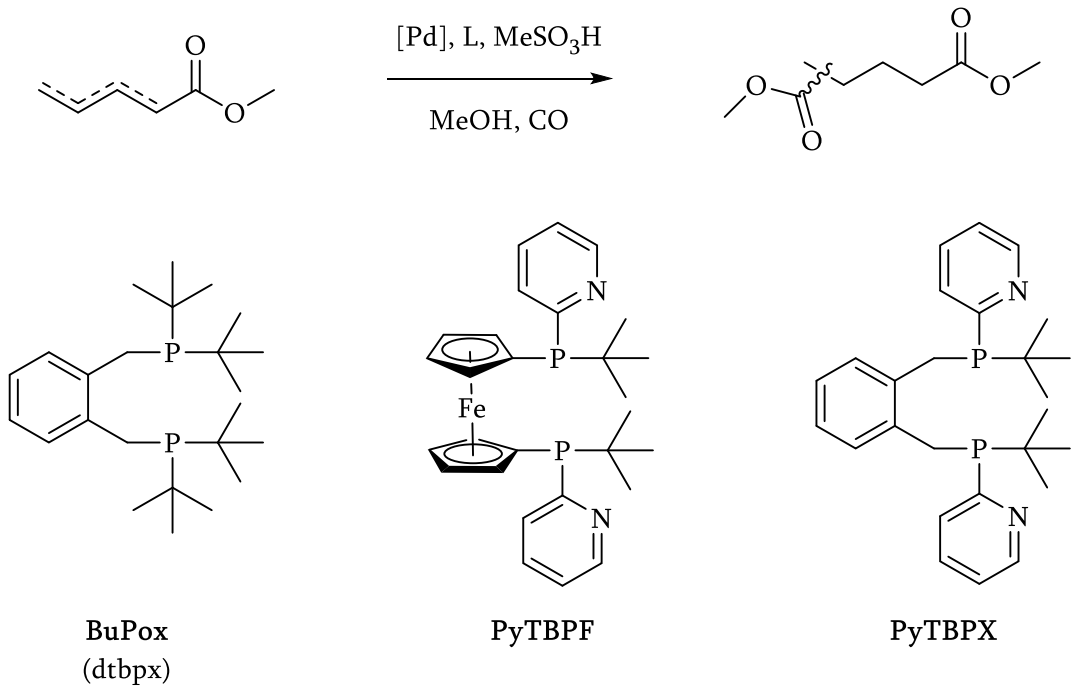

Fig. 26: Reaction scheme and ligands for the methoxycarbonylation of methyl pentenoates towards dimethyl adipate.

3.2.2 Preliminary experiments

The reaction conditions were constant for all preliminary tests with a set temperature of 100 °C and a pressure of 20 bar of CO gas. As Brønsted acid methane sulfonic acid was used. The Pd:L:$MeSO_3H$:M4P:M4P ratio was 1:4:10:900:100. The palladium concentration was 100 ppm based on the mole fraction. After 20 h the reaction was stopped and the crudes were analysed via GC/FID. The conversion was calculated as the amount of converted substrate and the yield is the amount of diester based on the amount of remaining substrate, side products and products.

Ligand	m_{M4P} *[mg]*	m_{M3P} *[mg]*	m_{Ligand} *[mg]*	V_{MeOH} *[mL]*	*Conversion [%]*	*Yield [%]*	n-*Regiosel. [%]*
BuPox	146.5	16.5	2.5	5	16.4	16.4	99.9
PyTBPF	145.7	17.9	3.1	5	86.6	86.6	85.1
PyTBPX	172.0	35.5	2.5	5	77.4	77.4	86.8

Table 12: Results of the preliminary experiments for the alkoxycarbonylation of isomeric methyl pentenoates. Reaction conditions: Pd:L:$MeSO_3H$:M4P:M3P => 1:4:10:900:1000, c_{Pd} = 0.286 µmolmL^{-1}, t = 20 h, T = 100 °C, p_{CO} = 20 bar. Solvent: MeOH*

The *n*-regioselectivity was calculated as the amount of formed dimethyl adipate based on the total amount of diester present in the product mixture. The preliminary results are shown in Table 12.

When BuPox was used as a ligand, only 16.4 % of the olefin was converted after 20 h. Side reactions could not be observed; only diesters were observed. Additionally the only isomer formed was dimethyl adipate. By switching to PyTBPX as ligand, the activity of the catalytic system was drastically higher than in comparison to the BuPox-modified system. Since the only difference between these two ligands was the substitution of a *t*Bu group with a pyridyl group on each P centre, this can be seen as the reason of the increased activity. The conversion was 77.4 % after 20 h and side products were not observed, so the yield of the diesters was also 77.4 %. Dimethyl adipate was formed with an *n*-regioselectivity of 86.8 % and therefore was much lower than for the process with the BuPox system.

Utilisation of PyTBPF led to an even more active catalyst that converts 86.6 % of substrate within 20 h fully into the corresponding diesters. Side products were not detected. The *n*-regioselectivity was at 85.1 % regarding dimethyl adipate.

Nr.	*1*	*2*	*3*	*4*	*5*	*6*	*7*	*8*	*9*	*10*
T [°C]	100	100	100	100	100	80	90	100	110	120
p [bar]	10	20	30	40	50	20	20	20	20	20
C[a] [%]	93.9	97.4	96.3	96.0	94.7	93.7	97.9	98.6	100	100
Y_{DMA} [b] [%]	80.7	82.5	81.6	80.3	78.8	81.0	84.4	85.0	85.7	84.9
$Y_{2\text{-MeDMG}}$ [b] [%]	11.2	12.7	12.6	13.4	13.6	10.7	11.4	11.7	12.5	13.4
$Y_{2\text{-EtDMS}}$ [b] [%]	1.9	2.1	2.1	2.3	2.3	2.0	2.1	1.8	1.8	1.8
S[c] [%]	86.0	84.7	84.7	83.7	83.2	86.5	86.2	86.2	85.7	84.9

*Table 13: Optimisation of the alkoxycarbonylation reaction of methyl pentenoates employing a PyTBPF modified catalyst. Reaction conditions: Pd:L:MeSO₃H:M4P:M3P => 1:4:10:900:1000, c_{Pd} = 0.286 µmol*mL^{-1}, t = 20 h. Solvent: MeOH. (a) Conversion of substrate. (b) Yield of diesters. (c) Regioselectivity of the reaction as the ratio of the amount DMA to the amount of all diesters in the product mixture.*

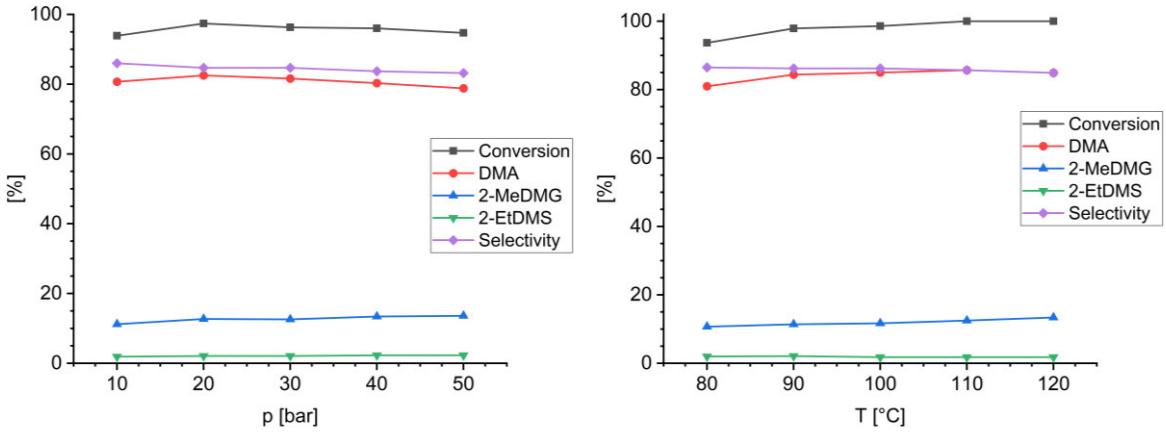

Fig. 27: Graphical representation of the results from Table 13. ***Left:*** *Variation of pressure at 100 °C.* ***Right:*** *Variation of temperature at 20 bar.*

Nr.	*1*	*2*	*3*	*4*	*5*	*6*	*7*	*8*	*9*	*10*
T [°C]	100	100	100	100	100	80	90	100	110	120
p [bar]	10	20	30	40	50	10	10	10	10	10
C[a] [%]	100	100	100	98.3	83.5	100	100	100	90.5	77.0
Y_{DMA}[b] [%]	83.8	82.9	82.4	80.2	75.8	79.3	80.4	81.5	73.7	62.3
$Y_{2\text{-MeDMG}}$[b] [%]	13.7	14.6	15.1	15.4	15.0	15.9	15.9	15.5	14.2	12.1
$Y_{2\text{-EtDMS}}$[b] [%]	2.4	2.5	2.5	2.7	2.6	4.0	3.7	3.0	2.6	2.1
S[c] [%]	83.8	82.9	82.4	81.6	81.2	79.9	80.4	81.5	81.4	81.6

*Table 14: Optimisation of the alkoxycarbonylation reaction of methyl pentenoates employing a PyTBPX modified catalyst. Reaction conditions: Pd:L:MeSO₃H:M4P:M3P => 1:4:10:900:1000, c_{Pd} = 0.286 µmol*mL^{-1}, t = 20 h, T = 100 °C, p_{CO} = 20 bar. Solvent: MeOH. (a) Conversion of substrate. (b) Yield of diesters. (c) Regioselectivity of the reaction as the ratio of the amount DMA to the amount of all diesters in the product mixture.*

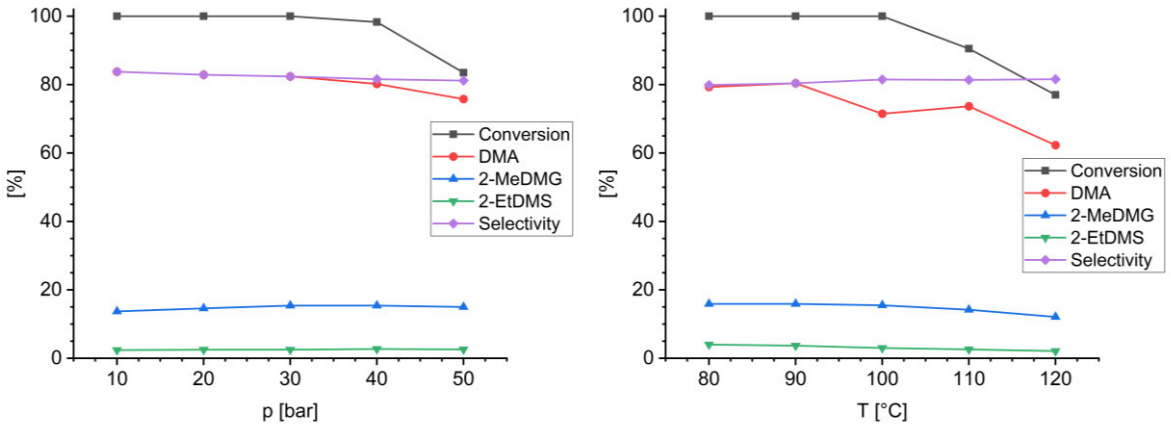

Fig. 28: Graphical representation of the results from Table 14. ***Left:*** *Variation of pressure at 100 °C.* ***Right:*** *Variation of temperature at 10 bar.*

3.2.3 Optimisation of reaction conditions

3.2.3.1 With PyTBPF as ligand

The reaction conditions were optimised systematically over the course of multiple experiments in the same fashion as already established for the hydroformylation: First, the pressure was varied and then the temperature. The results are shown in Table 13. Variation of the CO pressure does not seem to have a significant effect on the catalytic performance apart from a slight decrease in *n*-regioselectivity. In contrast, the temperature has a greater influence. By increasing the temperature, more substrate was converted into the final products, however the *n*-regioselectivity decreased. Additionally, the catalyst seems to at least partially decompose at temperatures higher than 120 °C, since significant amounts of palladium black were formed. Therefore, the optimal reaction conditions are at 100 °C and 20 bar for the PyTBPF-modified catalyst.

3.2.3.1 With PyTBPX as ligand

The optimisation of the reaction conditions of the methoxycarbonylation of isomeric methyl pentenoates with a PyTBPX-modified palladium catalyst was performed as described in section 3.2.3.1. The results are shown in Table 14.

First the pressure was varied and the temperature kept constant. At high CO pressures, inhibition of the catalysis occurred, as indicated by low substrate conversions. This was expected, since high CO pressures lead to the more favoured formation of complexes with multiple carbonyl ligands that may block important coordination sites. The *n*-regioselectivity was only slightly impacted. Variation of the reaction temperature showed that conversions are significantly lower at high temperatures, which is explainable by catalyst decomposition. Here, the *n*-regioselectivity was only slightly impacted as well. Based on these results, the optimised reaction conditions for the methoxycarbonylation with the PyTBPX-modified catalyst are at 100 °C and 10 bar.

3.2.4 Mechanistic investigations

3.2.4.1 Identification of catalytically relevant species

Spectroscopic and mechanistic investigations on the methoxycarbonylation of ethylene as model reaction with PyTBPF and PyTBPX have been conducted in the course of this work to experimentally prove that the hydride mechanism as described by Eastham *et al.* is the prevalent mechanism. [90] First, full NMR-spectroscopic characterisation of the postulated resting state as found by Dong *et al.* and its synthetic predecessors was performed, starting with the free ligands PyTBPF and PyTBPX.

These ligands are shown on p. 11 in Fig. 12. PyTBPF is a ligand with a ferrocenyl backbone and a *t*Bu- and pyridyl-moiety on each P-centre. PyTBPX has an *o*-xylene backbone and the same substituents on the P centres as PyTBPF. As one can clearly see, PyTBPX is derived from DTBPX (BuPox). These two ligands produce extraordinarily active catalyst species in the palladium catalysed methoxycarbonylation reaction of ethylene.

3.2.4.1.1 Resting state

As resting state of the palladium catalyst modified with PyTBPF and PyTBPX, a complex of the type [Pd(P∩P)X]X was expected, where X is a halide, a pseudo halide or a weakly coordinating anion and one coordination site is occupied by one of the pyridyl substituents. (see Fig. 29) This structure was isolated by Dong *et al.* and verified via X-ray crystallography for the complex modified with PyTBPF. The full synthetic route is shown in Fig. 33. [97] For the complexes of the type Pd(P∩P)dba and [Pd(P∩P)X]X spectroscopic investigations were conducted during this work to deliver experimental evidence for this resting state and other catalytically relevant species.

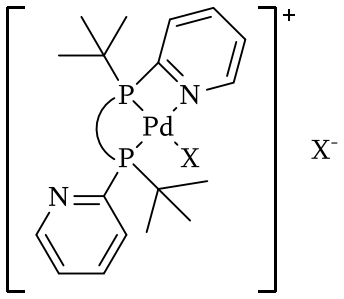

Fig. 29: Expected resting state Pd(P∩P)X]X. X = halide, pseudo halide.

Free ligands L2 and L3

As illustrated in Fig. 30, the ^{31}P-NMR show for each ligand a singlet at 6.95 ppm (PyTBPF) and 7.83 ppm (PyTBPX). These signals are in the expected range for phosphines. Therefore, both compounds either are symmetric molecules or the two possible diastereomers are interconverted faster than the NMR-timescale. For a summary of the ^{1}H NMR spectra, see A.2.3.4..

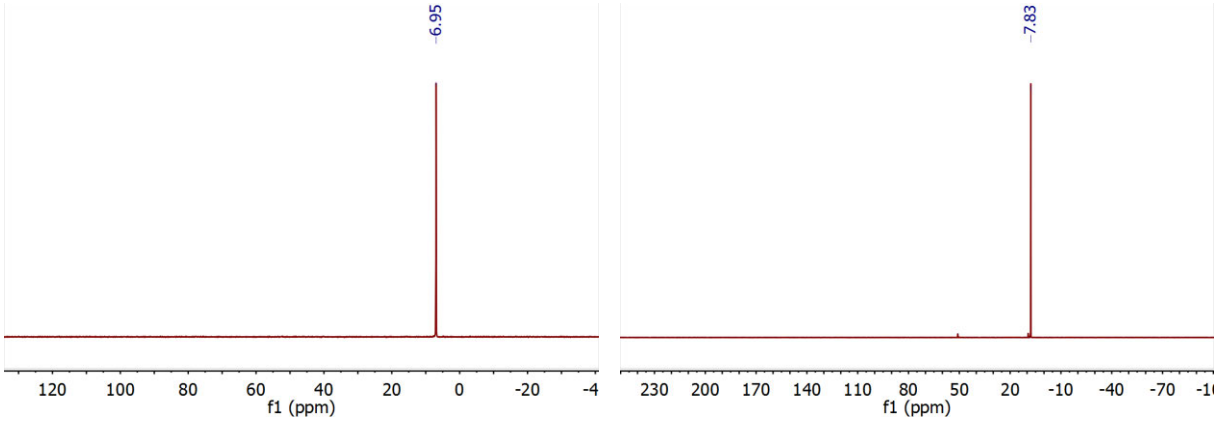

*Fig. 30: ^{31}P NMR spectra of PyTBPF (**left**) and PyTBPX (**right**) in CD_2Cl_2 at rt.*

Protonation of the diphosphines L2 and L3

The behaviour of PyTBPF and PyTBPX in protic media was investigated. For this purpose, solutions of the respective diphosphine and an organic acid (e. g. trifluoromethanesulfonic acid) were prepared and analysed by NMR spectroscopy. In relation to the diphosphine, the amount of acid added was the same as in the subsequent catalysis. The corresponding ^{31}P-NMR spectra showed no significant difference in comparison to the spectra of the diphosphines, so no P-protonation occurred. If P-protonation had occurred, a P-H-coupling should have been observable as a doublet. Instead, the pyridyl groups were protonated, which was observable in the ^{1}H-spectra by a broad band in the range of roughly 8.75 – 9.25 ppm for both ligands. The ^{31}P-signals underwent a slight low field shift. For L2, pTSA was also investigated since it was used in the IR spectroscopic investigations. For 5 equivalents of pTSA, the ^{31}P NMR spectrum was the same as for the experiments with TfOH.

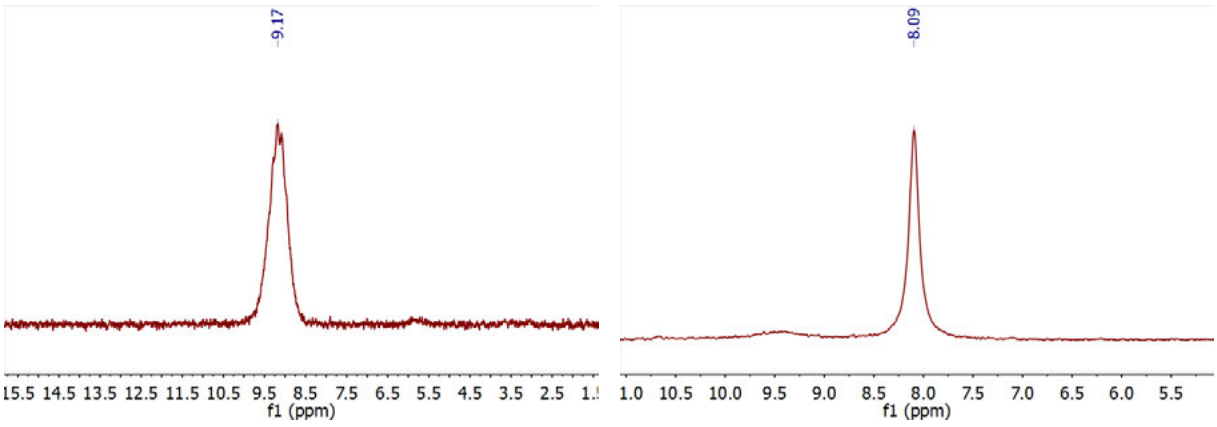

*Fig. 31: ^{31}P NMR spectra of the protonation experiments of PyTBPF (**left**) and PyTBPX (**right**) in CD_2Cl_2 at rt.*

To investigate the influence of higher amounts of acid, L2 was subjected to 20 eq. of TfOH and pTSA. For TfOH, immediate decomposition of the diphosphine was observed. For pTSA the signal in the ^{31}P NMR spectrum is shifted to lower field, indicating deshielding of the P centres. No P-H-coupling was observed. A possible explanation of the very low basicity of the phosphorus could be the protonation of the pyridyl moieties, indicated by a very broad signal in the ^{1}H NMR. The N-protonation leads to a positive charge at the nitrogen, which is stabilised by delocalisation in the π-electronic system of the aromatic ring. The lone pair of the phosphorus also participates, effectively lowering the electron density at the P centre and consequently its basicity.

To support this explanation, the protonation of BuPox led to a different result. Here the P centre was protonated as observed in the corresponding proton coupled ^{31}P NMR spectrum with a P,H coupling constant of $^{1}J_{P,H}$ = 454 Hz. The corresponding signal in the ^{1}H NMR is at 5.9 ppm and showed the same coupling constant of $^{1}J_{H,P}$ = 454 Hz. Additionally, a coupling constant of $^{3}J_{H,H}$ = 5.7 Hz was observed, indicating the coupling with the methylene protons of the xylene backbone. (see Fig. 32) For more detailed spectra and the spectrum of the BuPox ligand see A.2.3.4.

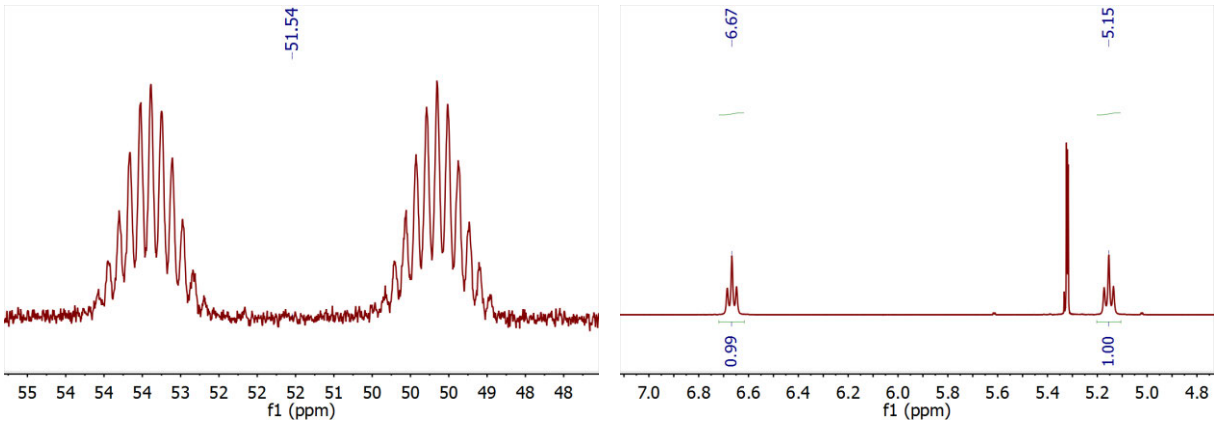

*Fig. 32: ^{31}P NMR (**left**) and part of the ^{1}H NMR (**right**) of the protonated DTBPX (BuPox). The signal at 5.32 ppm in the ^{1}H NMR is assignable to CD_2Cl_2.*

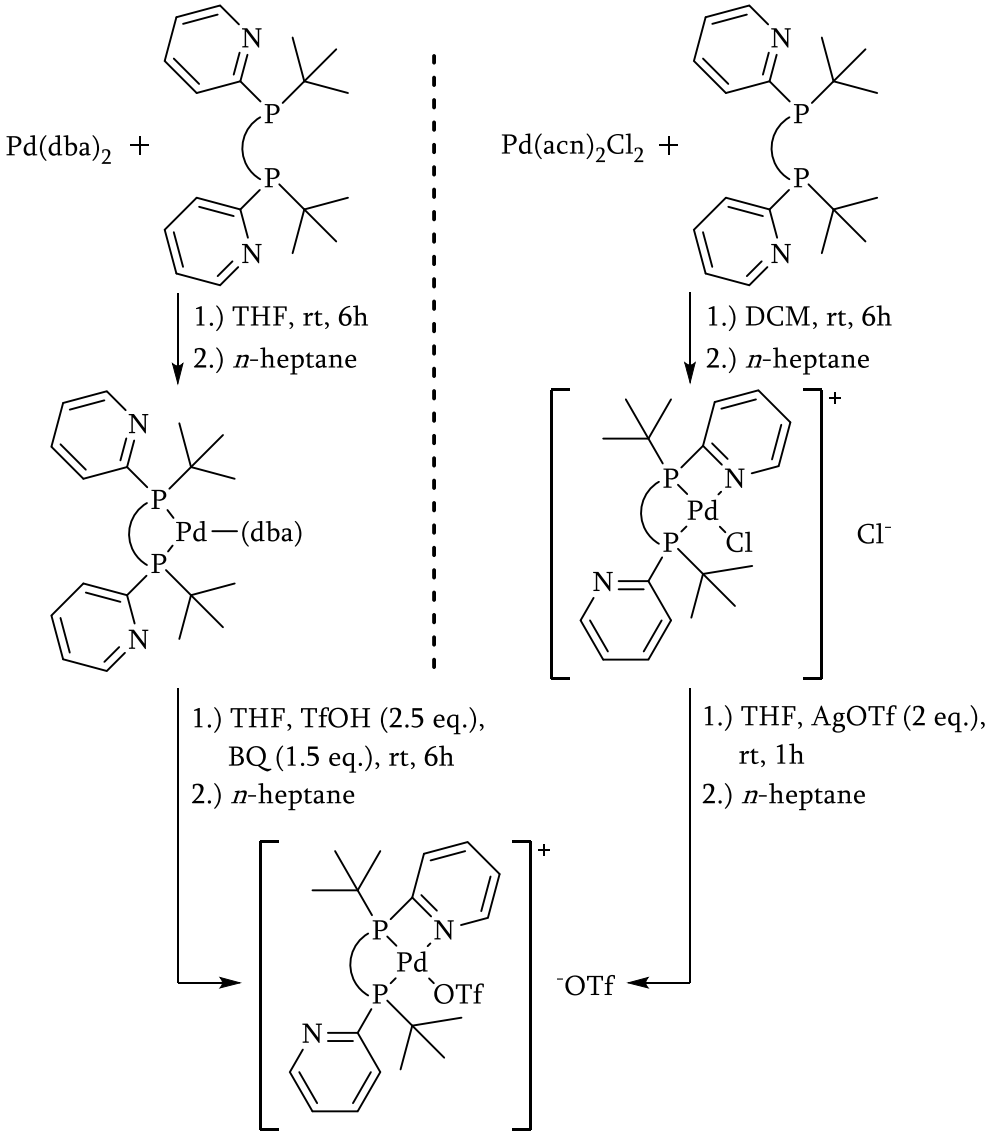

Fig. 33: Synthetic pathways for the synthesis of [Pd(L)OTf]OTf.

[Pd(L2)OTf]OTf and [Pd(L3)OTf]OTf

Two synthetic pathways have been tested for the complexes of the type [Pd(L)OTf]OTf.

The first pathway starts from the corresponding Pd^0(L)dba complexes. These dba complexes are reacted with benzoquinone as oxidiser and trifluoromethanesulfonic acid to form a dark red complex for PyTBPF and a pale yellow complex with PyTBPX. (see section 4.3.3.3)

The second synthetic route is Brønsted acid free and realised in two steps: For the first step, $Pd(L)Cl_2$ is synthesized via a ligand exchange of acetonitrile in $Pd(acn)_2Cl_2$ with the corresponding diphosphine. For PyTBPX, single crystals could be obtained and analysed via X-ray crystallography. The crystal structure shows that the ligand is coordinating in a *cis*-fashion regarding the two P centres. Additionally one pyridyl substituent is coordinating via the nitrogen atom and the last coordination site is occupied by one chloride. The second chloride is somewhere in the outer sphere of the complex acting as a counter ion, since the resulting distorted quadratic planar complex is cationic and needs it to be stabilised. The second step is comprised of a salt metathesis between the dichloro complex and silver(I) triflate. The driving force of this reaction is the precipitation of AgCl, effectively exchanging the chlorido ligands with triflate. Here, single crystals were also obtained for the complex containing PyTBPX. The crystal structure of [Pd(PyTBPF)OTf]OTf has already been published. [91] Via both synthetic pathways, the same product for both ligands was formed, as indicated by the ^1H and ^{31}P NMR spectra. The main product can be described as an asymmetric complex as shown in Fig. 34. In these complexes the ligands coordinate via the phosphorus atoms in a *cis*-fashion to the metal centre. Additionally one of the pyridyl moieties is bound to the metal centre, leading to two magnetically and chemically inequivalent P centres. This situation is expressed by the two doublets in the ^{31}P NMR spectra. (see Fig. 35, for a more detailed presentation of the spectra, see A.2.3.3) The suggested structure is also supported by X-ray crystallography of single crystals obtained from recrystallization of [Pd(PyTBPF)OTf]OTf (see A.2.3.3) and [Pd(PyTBPX)OTf]OTf (this work, see Fig. 36). As typical for Pd(II) 16 VE complexes, the overall coordination geometry is distorted quadratic planar. The 7 membered ring formed by the coordination of the ligand to the palladium centre adopts a boat confirmation.

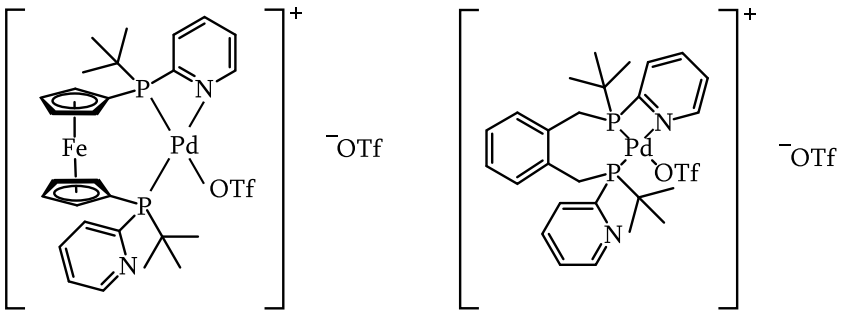

Fig. 34: [Pd(PyTBPF)OTf]OTf (left) and [Pd(PyTBPX)OTf]OTf. (right)

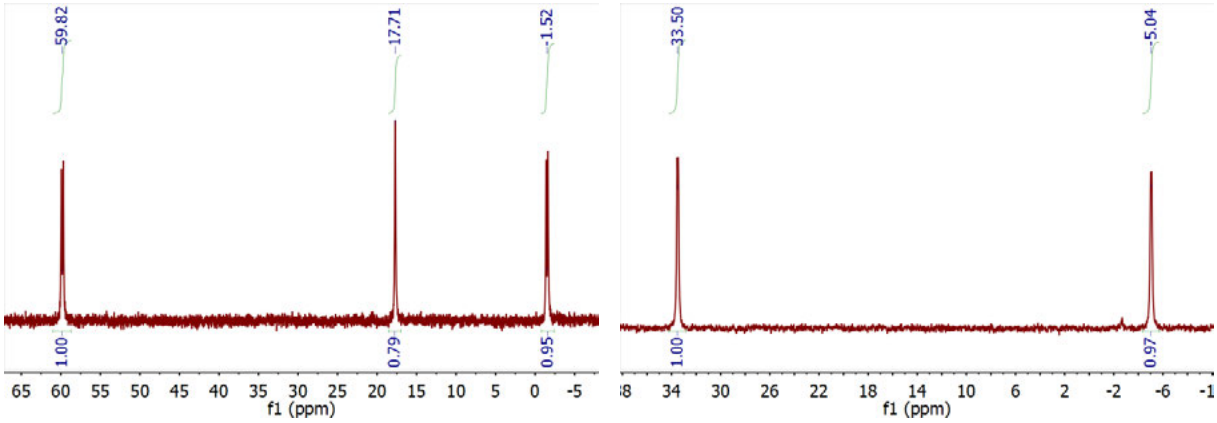

*Fig. 35: [31]P NMR of [Pd(PyTBPF)OTf]OTf (**left**) and [Pd(PyTBPX)OTf]OTf (**right**).*

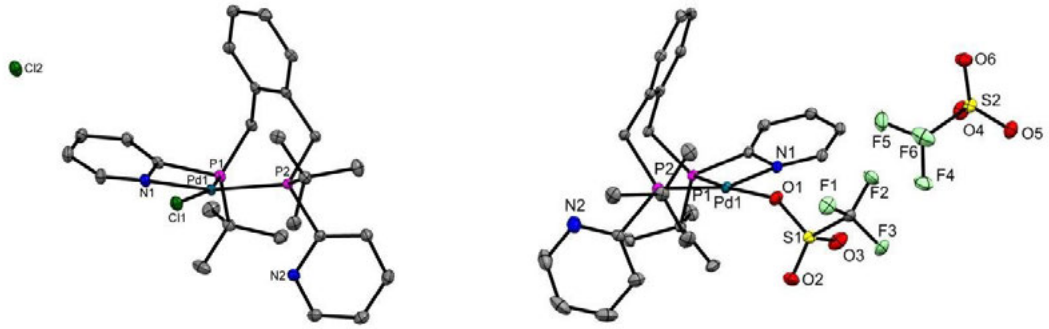

*Fig. 36: Crystal structures. [Pd(PyTBPX)Cl]Cl (**left**): P1-Pd1-P2 93.635(13)°, P1-Pd1-N1 69.92(3)°, P1-Pd1 2.2207(3) Å, P2-Pd1 2.2707(4) Å, N1-Pd1 2.1319(11) Å. [Pd(PyTBPX)OTf]OTf (**right**): P1-Pd1-P2 95.53(2)°, N1-Pd1-P1 69.39(5), P1-Pd1-2.2481(5) Å, P2-Pd1 2.2644(6) Å, N1-Pd1-P1 69.39(5) Å. The detailed crystal structure data can be reviewed in A.2.3.3. Solvent molecules have been omitted for clarity.*

Furthermore, these complexes express a certain dynamic in solution, where one pyridyl unit substitutes the other at the metal centre. At room temperature, this process seems to be slower than the NMR timescale, which is why a twofold set of signals can be seen in the ^{1}H NMR spectra. With the help of ^{1}H NOESY NMR, this exchange process was made visible by choosing a short spin evolution time showing the correlation of spin systems that are part of a chemical exchange process. (see A.2.3.5) Because of this equilibrium, room temperature ^{15}N NMR experiments of these compounds failed, since the signals were expected to be too broad to be visible in the final spectrum.

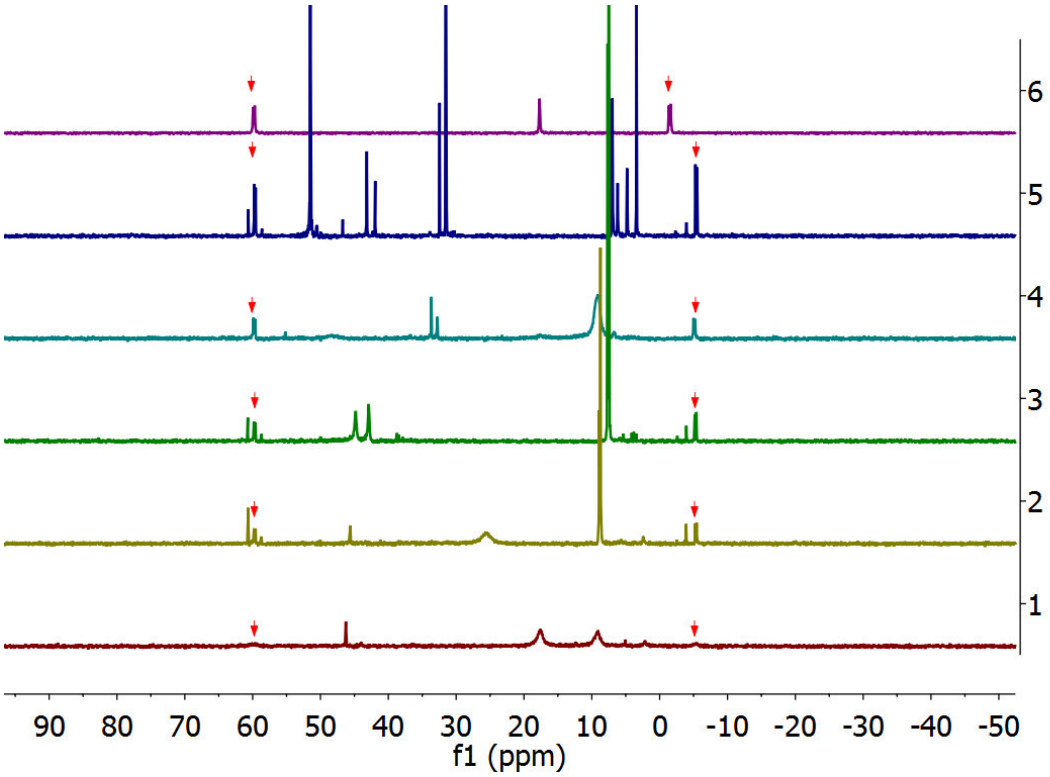

Fig. 37: ^{31}P-NMR spectra of different in situ experiments starting from different palladium precursors and PyTBPF as ligand. Precursors: (1)$Pd_2(dba)_3$, (2) $Pd(OAc)_2$, (3) $Pd(dba)_2$, (4) $PdCl_2$, (5) $Pd(acac)_2$. The isolated complex [Pd(PyTBPF)OTf]OTf is depicted in spectrum 6 and has been marked with red arrows.

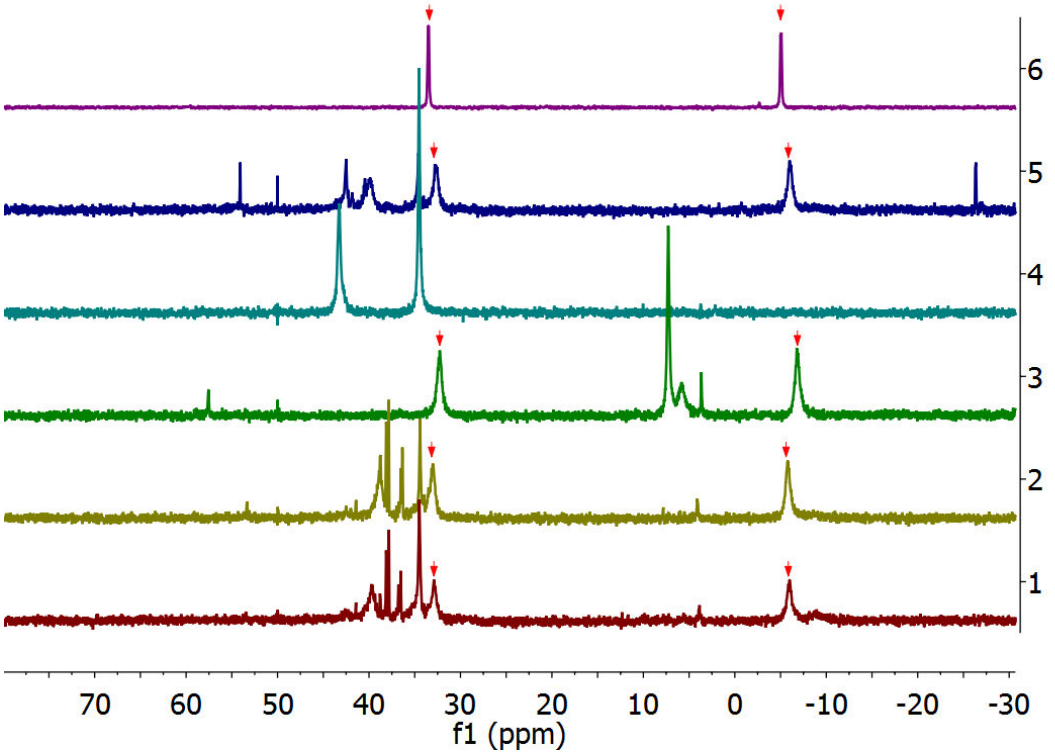

Fig. 38: ^{31}P-NMR spectra of different in situ experiments starting from different palladium precursors and PyTBPX as ligand. Precursors: (1)Pd(dba)$_2$, (2) Pd$_2$(dba)$_3$, (3) Pd(acac)$_2$, (4) PdCl$_2$, (5) Pd(OAc)$_2$. The isolated complex [Pd(PyTBPX)OTf]OTf is depicted in spectrum 6 and has been marked with red arrows.

In situ Synthesis of [Pd(L2)OTf]OTf and [Pd(L3)OTf]OTf with different palladium precursors

The *in situ* synthesis of the expected resting state was conducted with different palladium catalyst precursors, being Pd(OAc)$_2$, Pd(acac)$_2$, Pd(dba)$_2$, Pd$_2$(dba)$_3$ and PdCl$_2$. The synthesis was conducted by dissolution of the precursor, the ligand and 5 eq. of benzoquinone in the desired NMR solvent and addition of a solution of 7 eq. TfOH. The results are depicted in Fig. 37 (PyTBPF) and Fig. 38 (PyTBPX). As can be seen, most *in situ* formations led to the expected resting state with varying amounts of side products.

3.2.4.1.2 Hydride complex [Pd(L∩L)(X)H]X

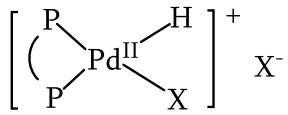

Fig. 39: Hydride species. X = solv., OTf, OTs. Instead of X, a coordination of a pyridyl substituent is also possible.

To observe the hydride species, *in situ* experiments were NMR spectroscopically analysed giving special attention to the relevant chemical shifts. The *in situ* experiments were realised as described further above with deuterated methanol as NMR solvent.

The NMR spectra for the preparation with PyTBPF gave evidence, that the main component is the expected resting state [Pd(PyTBPF)OTf]OTf, as indicated by the main signals in the ^{31}P NMR spectrum at 59.8 ppm and -1.5 ppm. In the ^{1}H NMR spectrum the resonance from the NMR solvent overlaps with the Cp-H signals. Apart from that, all the relevant signals from the resting state are present and no hydride signal was observed.

The experiment with PyTBPX showed comparable results, with the difference, that the resting state was formed more selectively. Here, no hydride signal was observed either.

When the experiment was repeated with BuPox, the hydride was quite easy to obtain following the same synthetic method as described for the other complexes. In the ^{1}H NMR spectrum, the hydride complex expressed a distinct signal at -10.75 ppm. The signal is split into a doublet of doublets with coupling constants of $^{2}J_{H,P}$ = 182.36 Hz and 22.58 Hz. This corresponds to an asymmetric complex shown in Fig. 39, where the two P centres coordinate in a *cis* fashion and the hydride in a *trans* position with regard to one phosphorus and *cis* with regard to the other. The last coordination side is either occupied by a solvent molecule, the anion of the acid or one pyridyl substituent. The ^{31}P NMR spectrum showed a complex set of signals. Two of these signals were assigned to the hydride complex: one doublet at 75.1 ppm and the other at 23.9 ppm with a coupling constant of $^{2}J_{P,P}$ = 17.4 Hz, which is within the characteristic range of two *cis* coordinating P centres.

These results support the calculations published by Dong *et al.* (see [91]) Assuming the hydride mechanism proposed by Eastham *et al.* is the predominant mechanism for the catalysis with PyTBPF and PyTBPX as it is for BuPox, the results shown above are not surprising. Since the hydride species is not energetically favoured in comparison to the N-protonated species, we do not observe signals assignable to hydrides.

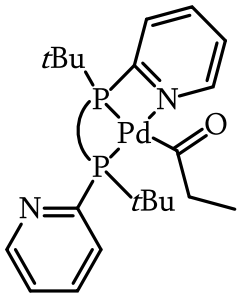

Fig. 40: Expected acyl species for the catalysts modified with PyTBPF and PyTBPX.

3.2.4.1.3 Acyl species

Acyl complexes can typically be observed via IR spectroscopy because of the characteristic C=O vibrational frequency at about 1690 cm^{-1}. To observe this species for the PyTBPF and PyTBPX modified systems, a solution of the catalyst was prepared by dissolution of the [Pd(L)dba] species in a solvent in a Schlenk flask and addition of 7 eq. of pTSA. After a few minutes of stirring the solution was transferred into a stainless steel autoclave connected to a FT/IR spectrometer. Then the mixture was heated to the desired temperature and 10 bar of ethylene was added. After 1 hour of stirring 10 bar of CO are added and the mixture was stirred for another hour. For every step FT/IR measurements are being made to monitor changes of the reaction mixture. All reactions were conducted at room temperature.

The first experiments were conducted in THF as an aprotic solvent to stop the reaction at the acyl complex. (see Fig. 41) In theory a strong band should grow in the area of 1690 cm^{-1}, because the acyl complex is thermodynamically more stable than the other intermediates. For the PyTBPF-modified catalyst evolution of a small vibrational band at 1692 cm^{-1} takes place, indicating the acyl formation, though in much smaller quantities than expected. Other bands formed after addition of ethylene are at 1740 cm^{-1}, which can be assigned to an aldehyde group, and another at 2338 cm^{-1}

that has yet to be assigned. The reaction was stopped after 130 min. Replacement of the solvent by methanol resulted in immediate product formation. But we were not able to observe the acyl complex. Therefore, a more bulky alcohol (*t*-amyl alcohol) was used. (see Fig. 42) This way, small amounts of an acyl species were detected in addition to a species indicated by a vibrational band at 1717 cm^{-1} assignable to an ester group. For the PyTBPX-modified catalyst, the experiments were conducted in the same way. First, the reaction was conducted in THF. (see Fig. 43) During the reaction neither acyl formation nor by-product formation could be observed. The only additional band formed was the one at 2337 cm^{-1}. Changing the solvent to *t*-amyl alcohol did not lead to acyl formation either, the only products formed, contained ester and carbonyl-groups. (see Fig. 44) It is conceivable that a polyketone was formed. More experiments have to be conducted in that regard in the future.

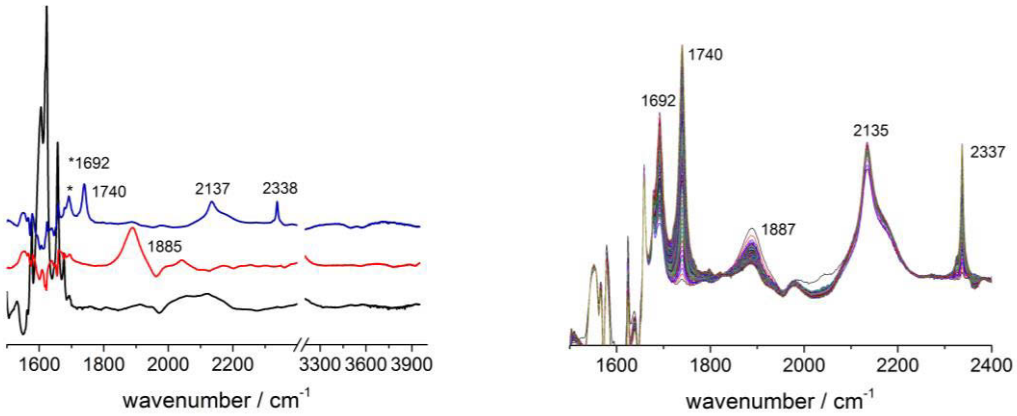

Fig. 41: In situ FT/IR-experiments with [Pd(PyTBPF)OTs]OTs in THF. Left: catalyst spectrum (black), catalyst spectrum after addition of ethylene (red), spectrum after addition of CO and 130 min of reaction time (blue). Right: Evolution of the measured spectra after addition of CO.

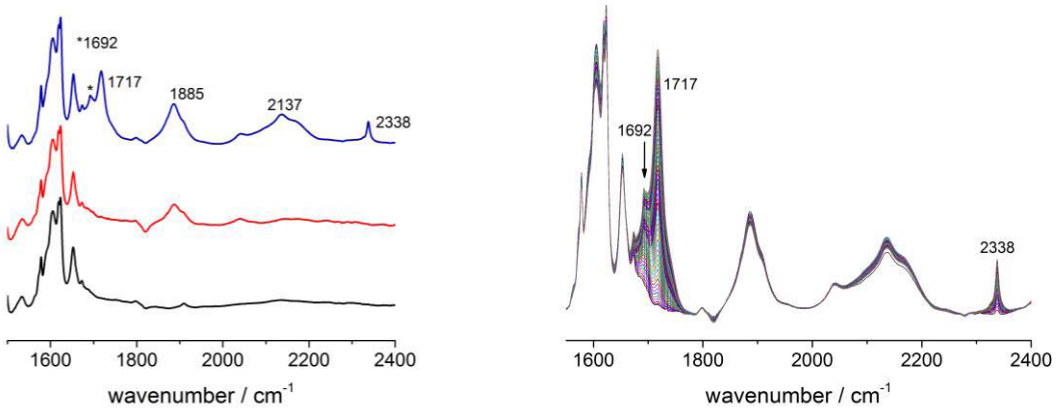

Fig. 42: In situ FT/IR-experiments with [Pd(PyTBPF)OTs]OTs in t-amyl alcohol. Left: catalyst spectrum (black), catalyst spectrum after addition of ethylene (red), spectrum after addition of CO and 90 min of reaction time (blue). Right: Evolution of the measured spectra after addition of CO.

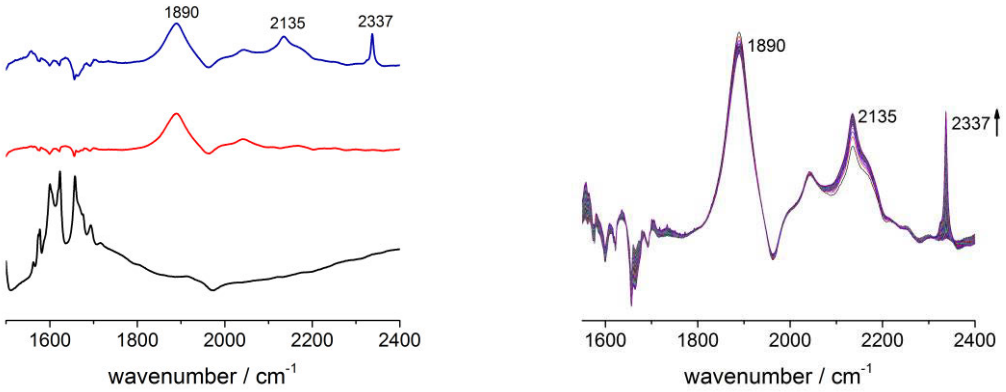

Fig. 43: In situ FT/IR-experiments with [Pd(PyTBPX)OTs]OTs in THF. Left: catalyst spectrum (black), catalyst spectrum after addition of ethylene (red), spectrum after addition of CO and 130 min of reaction time (blue). Right: Evolution of the measured spectra after addition of CO.

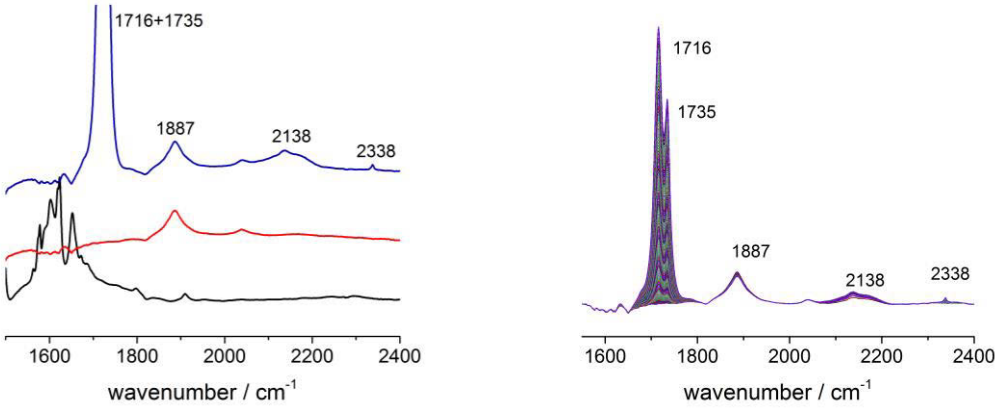

Fig. 44: In situ FT/IR-experiments with [Pd(PyTBPX)OTs]OTs in t-amyl alcohol. Left: catalyst spectrum (black), catalyst spectrum after addition of ethylene (red), spectrum after addition of CO and 90 min of reaction time (blue). Right: Evolution of the measured spectra after addition of CO.

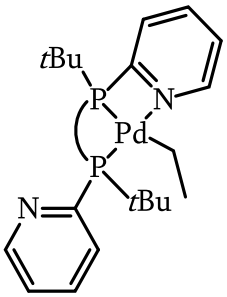

Fig. 45: Expected alkylated species, modified with PyTBPX and PyTBPF.

3.2.4.1.4 Alkyl species

The alkyl species can possibly be observed via HP-NMR spectroscopy. For this reason the catalyst solution was prepared under inert atmosphere in a Schlenk flask by dissolving Pd(L)dba in methanol, adding *p*TSA and stirring for a few minutes. A sample of the solution was collected and analysed. Then, the solution was transferred into a sapphire NMR tube and charged with 50 bar of ethylene.

The resulting NMR spectra were compared before and after addition of ethylene to visualise changes in the composition of the catalyst solution. By comparing the ^{1}H-NMR spectra for each complex before and after addition of ethylene, one can see that there was no change, apart from the CH_2-signal of ethylene. The same conclusion can be drawn from the ^{13}C-NMR spectra. The

^{31}P-NMR spectra reveal, that the main species present in the solution is the suspected resting state [Pd(L)OTs]OTs. In conclusion, no alkyl-species was observed. The calculation conducted by Dong *et al.* support this observation since the calculated energetic difference between the alkyl species and the resting state is only about 4 kJ*(molK)$^{-1}$, leading to fast equilibria between these two species. Low temperature NMR could circumvent this by "freezing" the thermodynamically more stable alkyl species and thus inhibit the back reaction towards the resting state. This already has been successfully realised for the corresponding BuPox complexes by Eastham *et al.* [90]

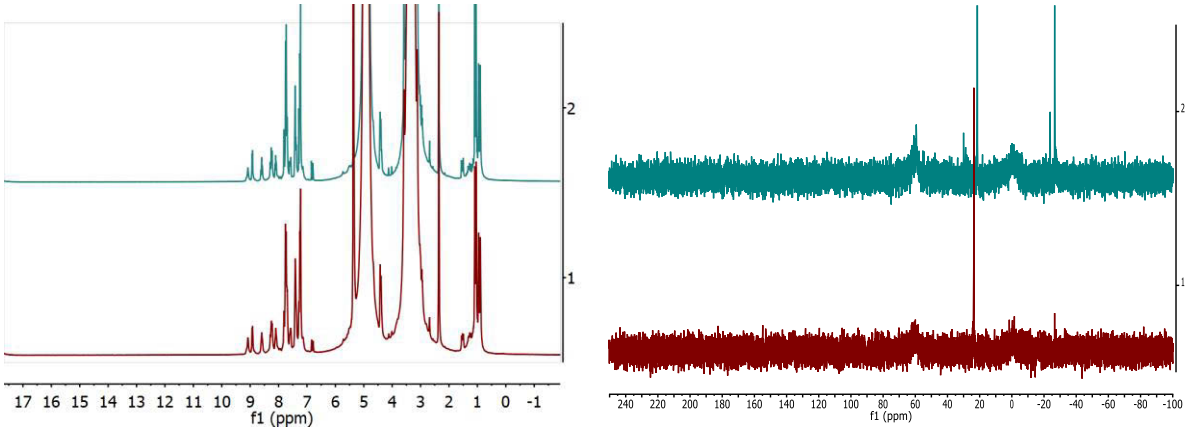

Fig. 46: ^{1}H NMR (left) and ^{31}P NMR (right) of [Pd(PyTBPF)OTf]OTf before (top) and after (bottom) addition of ethylene (50 bar).

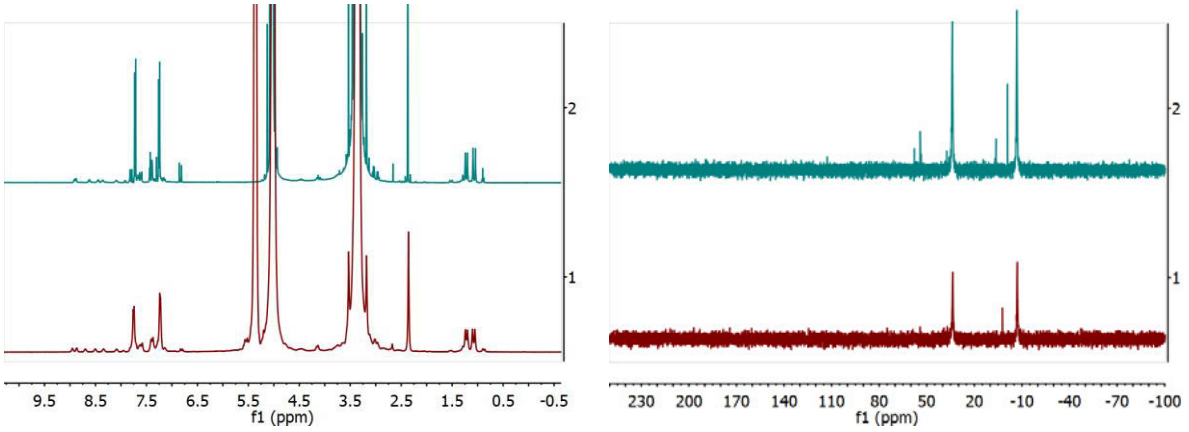

Fig. 47: ^{1}H NMR (left) and ^{31}P NMR (right) of [Pd(PyTBPX)OTf]OTf before (top) and after (bottom) addition of ethylene (50 bar).

3.2.5 Summary

The methoxycarbonylation reaction was successfully applied for the conversion of methyl pentenoates into dimethyl adipate. Utilising the two diphosphine ligands PyTBPF and PyTBPX, highly active catalysts were generated, in comparison to the corresponding BuPox-modified catalyst, that were able to fully convert the product into dimethyl adipate and its isomers (*n*-regioselectivity of 85 % with regard to dimethyl adipate) with excellent chemoselectivities (no side reactions).

Since the mechanistic investigations on the superior catalytic activity of the PyTBPF- and PyTBPX-modified catalysts over the BuPox-modified catalyst lacked experimental evidence, spectroscopic investigations were also conducted with ethylene as model substrate. During these investigations it was proven that the complex of the type [Pd(L)OTf]OTf with one coordinated pyridyl substituent is indeed the resting state as suspected by Dong *et al.* [91] Furthermore, the calculations performed by Dong *et al.* showed that a hydride species should not be observable because it is more energetically unstable than the corresponding N-protonated species. This is also supported by the NMR spectroscopic investigations under conditions at which hydride species usually form. Alkyl and acyl species have yet to be identified and are in the focus of ongoing experiments.

3.3 Hydroaminomethylation of isomeric methyl pentenoates

3.3.1 Methods

The rhodium catalysed hydroaminomethylation (HAM) of methyl pentenoates for the synthesis of 6-aminocaproates was investigated too. As secondary amines pyrrolidine, piperidine and aqueous dimethylamine were screened in preliminary experiments with BiphePhos. Because of their favourable initial results, piperidine and aq. dimethylamine were then used in further studies, which also employed XantPhos and the BiphePhos analogue SK-35. Reaction conditions were optimised for the BiphePhos modified catalyst. Additionally the hydroaminomethylation with aqueous ammonia was tested.

3.3.2 Results and discussion

In the following table, the reaction conditions and results of the corresponding reactions are shown. Each reaction was conducted at 100 °C and 20 bar of syngas. The concentration of the employed rhodium catalyst was 100 ppm with regard to the mole fraction. The L:Rh ratio was 4 and 1600 equivalents of amine, 900 equivalents of methyl 4-pentenoate and 100 equivalents of methyl 3-pentenoates have been used. The results are shown in Table 15.

Methyl 4-pentenoate

Ligand	Amine	C_{Subst}[a] [%]	Y_{Amine}[b] [%]	$Y_{Enamine}$[b] [%]	S_{chemo}[c] [%]	S_{regio}[d] [%]
Biphephos	Pyrrolidin	98.3	19.3	13.8	34.6	-
	Piperidin	100	94.8	0	94.8	20.0
	DMA (aq., 40 w.-%)	97.9	93.3	0	95.4	64.7

*Table 15: Preliminary results of the hydroaminomethylation of M4P employing a BiphePhos modified rhodium catalyst. Reaction conditions: Rh:L:Amine:M4P:M3P => 1:4:1600:900:1000, c_{Rh} = 0.286 µmol*mL^{-1}, t = 20 h, T = 100 °C, p = 20 bar. (a) Conversion of substrate. (b) Yields. (c) Chemoselectivity regarding HAM. (d) Regioselectivity of the reaction as the ratio of the amount 5-FMP to the amount of all aldehydes formed..*

The results of the HAM of methyl 4-pentenoate give evidence that the catalysis strongly depends on the basicity of the secondary amine. When pyrrolidine was used, the substrate was almost fully converted, however the resulting product mixture was comprised of a multitude of products. Besides methyl 6-pyrrolidylcaproate and its corresponding enamine, large quantities of the *iso*-product, methyl valerate, aldol condensation products and amides were present.

When piperidine was used instead, the reaction was much more selective. The reaction yielded 95 % of the desired amine with an *n*-regioselectivity of about 20 %. With an aqueous solution of dimethylamine, the corresponding methyl 6-(*N*,*N*-dimethylamino)caproate was formed with a regioselectivity of 64.7 %.

Mixture of methyl 4-pentenoate and methyl 3-pentenoate

Ligand	Amine	C_{Subst}[a] [%]	Y_{Amin}[b] [%]	$Y_{Enamine}$[b] [%]	S_{chemo}[c] [%]	S_{regio}[d] [%]
Biphephos	Piperidine	100	83.5	0	83.5	67.6
	Dimethylamine (aq., 40 w.-%)	100	84.4	0	84.4	61.3
Xantphos	Piperidine	60.9	54.4	0	89.3	83.6
Bupox	Piperidine	85.4	79.4	0	92.9	58.2
SK-35	Piperidine	94.4	31.6	12.1	46.3	69.0
	Dimethylamine (aq., 40 w.-%)	100	96.4	0	96.4	65.3

*Table 16: Hydroaminomethylation of a mixture of methyl pentenoates employing different ligands. Reaction conditions: Rh:L:Amine:M4P:M3P => 1:4:1600:900:1000, c_{Rh} = 0.286 µmol*mL^{-1}, t = 20 h, T = 100 °C, p = 20 bar. (a) Conversion of substrate. (b) Yields. (c) Chemoselectivity regarding HAM. (d) Regioselectivity of the reaction as the ratio of the amount 5-FMP to the amount of all aldehydes in the product mixture.*

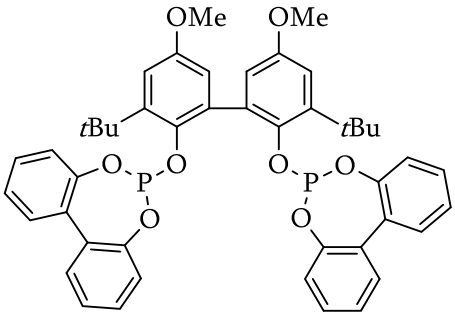

Biphephos

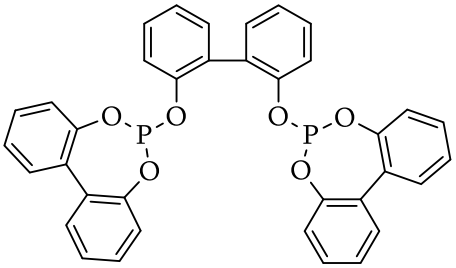

SK-35

*Fig. 48: BiphePhos (**left**) and SK-35 (**right**)*

The same reactions were conducted with a 9:1 mixture of methyl 4-pentenoate (M4P) and methyl 3-pentenoate (M3P). The BiphePhos-modified rhodium catalyst delivered similar Results of piperidine and aqueous dimethylamine. When SK-35 was used, the reaction with piperidine led to inferior chemoselectivity, but similar *n*-regioselectivity. Surprisingly, the catalyst performance was better for the reaction with aqueous dimethylamine compared to the same reaction with the BiphePhos-modified catalyst.

Optimisation of reaction conditions

The reaction conditions were optimised for the hydroaminomethylation with the BiphePhos-modified catalyst and piperidine. For the optimisation itself, the reaction parameters were systematically varied, starting with the pressure. The results are shown in Table 17.

Aqueous ammonia in the HAM of isomeric methyl pentenoates

Ligand	Amine	C_{Subst}[a] [%]	Y_{Amin}[b] [%]	$Y_{Enamine}$[b] [%]	$S_{primär}$[c] [%]	$S_{sek.}$[c] [%]	$S_{tert.}$[c] [%]
Biphephos	NH_3 (aq., 28 w.-%)	100	86.6	0	31.5	27.9	40.5

Table 17: rhodium catalysed hydroaminomethylation of M4P and M3P in toluene with aqueous NH_3 (28 w-%) at 110 °C and 20 bar (syngas). The reaction was left running for 20 h. c_{Rh} = 100 ppm. Rh:L:M4P:M3P 1:4:900:100. (a) Conversion of substrate. (b) Yields. (c) Chemoselectivity regarding primary, secondary and tertiary amine.

Since the industrially scaled synthesis of primary amines from olefins and ammonia is of huge interest for the polymer industry, the utilisation of an aqueous solution of ammonia was tested in the HAM of isomeric methyl pentenoates too. As expected, besides the desired product methyl 6-aminocaproate, the corresponding secondary and tertiary amines were formed. Furthermore, significant side product formation regarding hydrogenation and aldol condensation has occurred, with an overall yield of 13.3 %. Because of the poor selectivity regarding the amine formation, further investigations on the hydroaminomethylation with aqueous ammonia have been halted.

3.3.3 Summary

The hydroaminomethylation of methyl pentenoates was investigated with focus on the formation of tertiary amines from secondary amines. The most promising results were achieved with a XantPhos-modified catalyst and piperidine as secondary amine. Even though conversion were low (only about 60 % in 20 h), chemoselectivity (10 % of by-product formation) and *n*-regioselectivity (about 84 % with regard to the terminal amine) were satisfactory. The experiments with aq. ammonia were not successful, since the chemoselectivity towards the primary amine (32 %) was disappointing.

3.4 Hydroformylation of unusual substrates

3.4.1 Trivinylcyclohexane

3.4.1.1 Background

The hydroformylation of 1,2,4-trivinylcyclohexane and the resulting trialdehydes have not been described yet. 1,2,4-Trivinylcyclohexane was first mentioned in the literature in 1960. [92] The compound can be synthesised by leading 1,5,9-cyclododecatrien over a palladium catalyst at 400 – 600 °C. The yield of TVCH was 90 % and it was comprised of stereoisomers of every configuration. In 2013, a process was claimed in a patent that was aimed at the enrichment of certain configurational isomers. [93] To achieve this enrichment, an isomeric mixture of trivinylcyclohexane was subjected to thermal treatment that results in enrichment of the (*all-R*)- or the (*all-S*)-isomer. Rectification can be used to further purify the products. So far, the available applications for 1,2,4-trivinylcyclohexane are various hydrosilylation and hydroesterification processes. [94,95]

The aim of this work was to establish a new process regarding the hydroformylation of 1,2,4-trivinylcyclohexane to synthesize 1,2,4-tris(oxopropyl)cyclohexane. For this, diphosphine- and diphosphite-modified rhodium catalysts will be utilised, particularly Xantphos- and BiphePhos-modified catalysts.

Name of isomers	Structure
(1*S*,2*R*,4*R*)-1,2,4-Trivinylcyclohexan	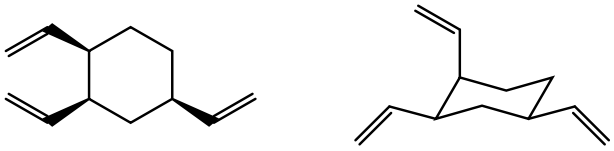
(1*S*,2*S*,4*R*)-1,2,4-Trivinylcyclohexan	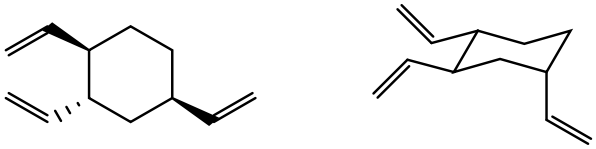
(1*R*,2*R*,4*R*)-1,2,4-Trivinylcyclohexan	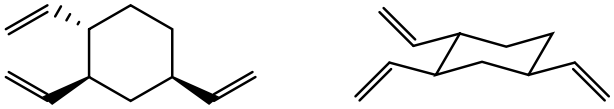
(1*S*,2*R*,4*S*)-1,2,4-Trivinylcyclohexan	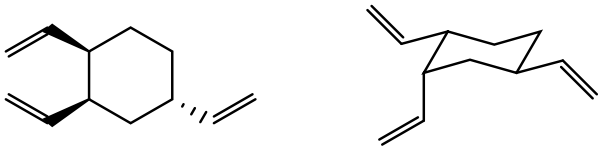

Table 18: Configurational isomers of 1,2,4-trivinylcyclohexane. Only diastereomers are shown.

3.4.1.2 Results and discussion

3.4.1.2.1 Hydroformylation of 1,2,4-trivinylcyclohexane

The synthesis of 1,2,4-tris(3-oxopropyl)cyclohexane commences with 1,2,4-trivinylcyclohexane and was realised by rhodium catalysed hydroformylation. The reaction conditions are shown in section 4.5.1 and the results in Table 19. The difficulty of this process lies in the existence of different configurational isomers that are poorly separable. The amount of possible stereoisomers is 2^n, where n defines the number of stereocentres within the molecule. With that in mind, the number of possible stereoisomers for TVCH is 8. The amount of spectroscopically differentiable diastereomers can be calculated with (2n-2), which amounts to 4 with n = 3. Assuming full conversion of the substrate to the trialdehyde, the situation gets more complex depending on the regioselectivity of the reaction. If the reaction proceeds ideally, meaning *all-l*, no additional stereocentres are introduced and the number of isomers in the product mixture stays the same. The other extreme are the *all-b* products. In this case three more stereocentres are introduced, leading to a total amount of 64 stereoisomers, comprised of 32 diastereomeric pairs. Therefore, the complexity depends strongly on the regioselectivity of the hydroformylation reaction. Comparison of the GC/MS data of the product mixtures revealed that the chemoselectivity towards the aldehydes is favourable, since no hydrogenation product was found. The BiphePhos-modified rhodium catalyst is superior to the XantPhos-modified one, because of its significantly higher activity and the higher yields of trialdehyde. The only side products with a yield of 20 % were the corresponding dialdehydes. The regioselectivity of the reaction was assessed by means of the corresponding ^{13}C-DEPT-NMR spectra. (see Fig. 49) As shown in the spectra, a fourfold signal set with a fitting number of CH-, CH_2- and CH_3-groups is visible, which is expected for a mixture of 4 diastereomeric pairs of the *all-l*-trialdehyde.

Ligand	Rh:L:TVCH	T [°C]	p [bar]	t [h]	C_{TVCH}[a] [%]	$Y_{Trialdehyde}$[b] [%]
BiphePhos	1:4:1000	100	20	4	100	80.0
XantPhos	1:4:1000	100	20	20	98	5.7

*Table 19: Hydroformylation of TVCH. Reaction conditions: Rh:L:TVCH => 1:4:1000, c_{Rh} = 0.286 µmol*mL^{-1}, t = 20 h, T = 100 °C, p = 20 bar. (a) Conversion of substrate. (b) Yield.*

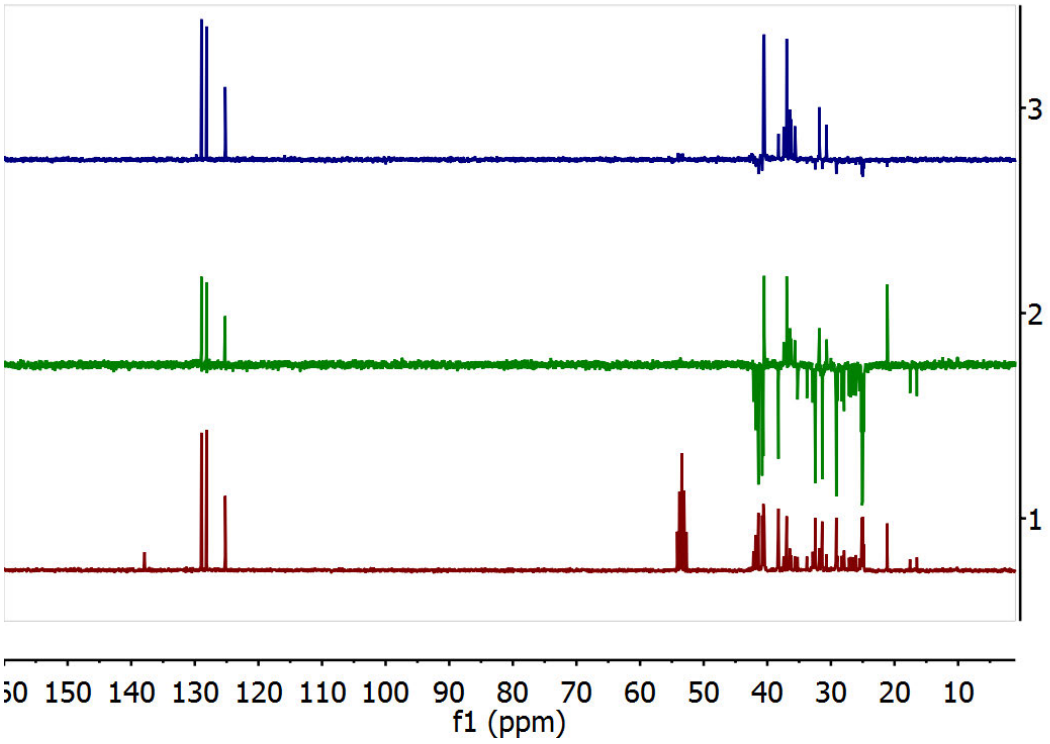

*Fig. 49: NMR spectra of the product mixture from the hydroformylation of TVCH. (**1**) ^{13}C NMR (**2**) ^{13}C DEPT-135 (**3**) ^{13}C DEPT-90.*

3.4.1.2.2 Synthesis of a triphosphite derived from 1,2,4-tris(3-hydroxopropyl)cyclohexane and its performance as ligand in rhodium catalysed hydroformylations

Starting from 1,2,4-tris(3-hydroxopropyl)cyclohexane, the triphosphite **SB111** was synthesized. (see Fig. 59) THOPCH is available by hydroesterification of 1,2,4-trivinylcyclohexane and subsequent hydrogenation. **SB111** has 2,4-di-*tert.*-butylphenyl substituents on each P centre. The synthesis of the phosphite was realised by dropwise addition of a solution of the corresponding phosphorochloridite to a solution of THOPCH and 6 eq. of NEt_3 in THF at 0 °C. This led to the esterification towards the phosphite with the formation of insoluble triethylammonium chloride as colourless side product that was filtered off. After solvent removal, the slightly yellowish and oily raw product was purified via column chromatography (CH_2Cl_2:CyH:NEt_3 => 9:90:1) to give the pure products as a colourless foam. **SB111** yielded 80 %. The corresponding ^{31}P NMR spectra of the purified product shows multiple signals in the range of 125 to 130 ppm (see A.4.1.2.2), which is in the expected range for diphosphites. The different signal stem from four diastereomers with three inequivalent P centres each. Additionally, the ^{1}H NMR spectra show no OH-signals, so the product can be considered as pure, not taking the different isomers into account. Mass spectrometry confirms that the product is comprised only of the desired species. (see section 4.5.1.2.2)

The ligand was tested in the rhodium catalysed hydroformylation. Substrates, reaction conditions and results are shown in Table 20.

Substrate	SB111		
	Conversion [%]	Yield [%]	Selectivity [%]
Oct-1-ene	82	82	93
Oct-2-ene	24	23	51
n-Octene (tech. mix.)	16	15	50
M4P	100	96	90
M3P	100	79	30
M4P/M3P (9:1)	83	81	76
TVCH	97	71	-

Table 20: Results of the rhodium catalysed hydroformylation of different substrate with SB111 and SB118 modified rhodium catalysts. Reaction parameters: T = 100 °C; p = 20 bar; CO:H_2 1:1; Rh:L:Substrate 1:4:1000; t = 20 h, c_{Rh} = 100 ppm.

4 Experimental part

4.1 General remarks

Solvents were purified and dried via standard methods prior to experiments, except toluene, methanol and THF. [96] These were dried via a solvent purification system and used without further treatment.

Deionised water for the two phase catalysis was degassed prior to the experiments by passing dry argon through it for 20 minutes and then multiple evacuations and ventilations with dry argon.

NMR spectra were recorded with the spectrometers Bruker AV 400, AV 300 and Fourier 300 at room temperature. Solvent signals were used as internal standards for field locking purposes. The signals were assigned with the help of the pure substance spectra. A full characterisation of the product mixture via ^{1}H NMR was not possible, since most signals in the range of methoxy-, CH_3-, CH_2- and CH-groups overlap. Apart from that, the signals in the range of 9 – 10 ppm assignable to aldehyde-protons could be used to quantify the regioselectivity of the reaction. The signal at higher frequencies coupling to a triplet is assignable to the *n*-aldehyde. The *b*-aldehydes show up as doublets at lower shifts.

Gas chromatograms were recorded with a Hewlett Packard Agilent GC HP6890 and 7890A, both fitted with FI detectors. As columns, 30m HP5 35/10-8-280/5 and 60m Agilent DB-WAX 122-7062 were used. For quantification of the substrates, methyl valerate, 5-FMP, dimethyl adipate and dimethyl 2-methylglutarate, calibrations have been made to calculate conversions and yields. As internal standard tetradecane and benzaldehyde were procured from Sigma Aldrich.

The analysis of the experiments for the catalyst leaching in the two phase hydroformylation was made via ICP-OES. The apparatus in use is a Varian/Agilent 715-ES.

Catalytic experiments without a gas entrainment impeller were conducted in a autoclave of the type HEL ChemSan II, which allows 8 simultaneously conducted reactions with automatic temperature and pressure stabilisation and recording of the gas consumption.

Catalytic experiments with gas entrainment impellers were performed in an autoclave of the type Parr Compact autoclaves (series 5500).

4.2 Hydroformylation of isomeric methyl pentenoates

4.2.1 Hydroformylation of methyl 2-pentenoate

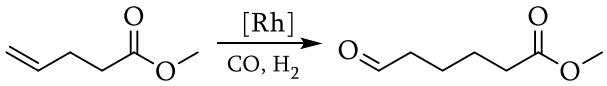

Fig. 50: Reaction scheme of the hydroformylation of methyl pentenoates. Only the 1-aldehyde is shown.

Homogeneous catalysis: To prepare the reaction solutions, a 10 mL-Schlenk tube was prepared for each reaction. The desired amount of ligand was weighed in and dissolved in 5 mL of toluene. After this, a previously prepared stock solution of $Rh(CO)_2acac$ (c_{Rh} = 0.012 mmol*mL^{-1}) in toluene was added. The resulting solution was mixed thoroughly and then methyl 2-pentenoate was added.

Two phase catalysis: To prepare the reaction solutions, a 10 mL Schlenk tube was prepared for each reaction. The ligand was weighed in and dissolved in 2.5 mL of deionised and degassed water. Then, the $Rh(CO)_2acac$ stock solution was added and the solution carefully mixed. Finally 2.5 mL of toluene was added to the solution to form a two phase system. Methyl 2-pentenoate is added. The resulting two phasic mixture has been used for the catalytic experiments.

The autoclaves were flushed with inert gas and the reaction solution transferred via syringes. The reactor vessels were closed and flushed 4 times with argon and 5 times with syngas. Then, the syngas pressure was set to the reaction pressure and the reaction mixture heated to reaction temperature. The reaction was stirred at constant temperature and pressure for 20 h. Afterwards, the autoclaves were cooled down to less than 40 °C and ventilated. The autoclaves were flushed with argon at least 5 times. Afterwards samples were collected for analytical means. The results are shown in Table 5 and Table 6 and the corresponding gas chromatograms are shown in A.1.1.

4.2.2 Comparison of different stirring techniques with regard to conversion, yield and n-regioselectivity in the rhodium catalysed hydroformylation of methyl 3-pentenoate

24.2 mg (0.01144 mmol) of BINAS was weighed into a prepared 25 mL-Schlenk tube and dissolved in 5 mL deionised and degassed water. A $Rh(CO)_2acac$ stock solution (0.237 mL, c_{Rh} = 0.012 $mmol*mL^{-1}$) was introduced and the resulting mixture was stirred for a few minutes. Afterwards, 5 mL toluene was added, resulting in a two phasic solvent system. Finally methyl 3-pentenoate (0.325 g, 0.45 mL, 2.8474 mmol) was added.

The autoclave was flushed with argon, the prepared reaction mixture was transferred and the reactor vessel closed. The closed autoclave was flushed four additional times with argon and then three times with syngas. The reactor was pressurised with 10 bar syngas and heated to 110 °C, while stirring the reaction solution (500 rpm). When the final reaction conditions are reached, the stirring velocity was raised to 1100 rpm (with gas entrainment impeller) or 900 rpm (without gas entrainment impeller). The reaction was stirred for 20 h, while the temperature was kept constant. After cool down, the autoclave was depressurised and flushed with argon at least 5 times. After that, the autoclave has been opened and samples have been prepared for analytical purposes. The results are shown in Table 7. (Detailed experimental data are shown in A.1.2)

4.2.3 Optimisation of reaction conditions for the two-phasic hydroformylation of methyl pentenoates with a BINAS-modified Rh(I)-catalyst

The optimisation experiments started with variation of the reaction pressure. For this purpose, five identical reaction solutions are prepared and subjected to the hydroformylation at 110 °C and 10, 20, 30, 40 and 50 bar of syngas. The optimisation of the reaction temperature was performed similarly. Five reaction solutions were subjected to the hydroformylation reaction at 80, 90, 100, 110 and 120 °C and the previously optimised reaction pressure.

The preparation of the reaction solutions, the preparation of the autoclave and the realisation of the experiments were performed as described in section 4.2.1 for the two phase catalysis. To simplify the protocol, 12.5 mL of the aqueous and organic phase were separately prepared. Then, 2.5 mL of each solution was transferred to each autoclave, which was sufficient for five batches. For

the aqueous precatalyst solution, the ligand and the precursor were dissolved in deionised and degassed water. The substrate was dissolved in toluene. The results are shown in Table 8. (Detailed experimental data are shown in A.1.3)

4.2.4 Optimisation of reaction conditions for the homogeneous hydroformylation of methyl pentenoates with a BiphePhos-modified Rh(I)-catalyst

The optimisation experiments started with variation of the reaction pressure. Five identical reaction solutions were prepared and subjected to the hydroformylation at 110 °C and 10, 20, 30, 40 and 50 bar of syngas. The optimisation of the reaction temperature was achieved in a similar fashion. Five reaction solutions were subjected to the hydroformylation reaction at 80, 90, 100, 110 and 120 °C and the previously optimised reaction pressure.

The preparation of the reaction solutions, the preparation of the autoclave and the reaction were carried out as described in section 4.2.1 for the homogeneous version. To simplify the procedure, 25 mL of the reaction mixture has been prepared. Then, 5 mL of the solution are transferred to each autoclave, which is sufficient for 5 batches. For this purpose, BiphePhos (22.5 mg, 0.02860 mmol) was weighed into a 50 mL-Schlenk tube and dissolved in 25 mL of toluene. The precursor stock solution (0.590 mL, c_{Rh} = 0.012 mmol*mL^{-1}) was added and the resulting mixture stirred for a few minutes. Finally the substrates methyl 4-pentenoate (0.733 g, 6.40665 mmol, 0.79 mL) and methyl 3-pentenoate (0.083 g, 0.71185 mmol, 0.09 mL) were introduced. The results are shown in Table 9. (Detailed experimental data are shown in A.1.4)

4.2.5 Recycling of the BINAS-modified Rh(I)-catalyst in the two-phasic hydroformylation of methyl pentenoates

The preparation of the reaction mixture was realised as described in section 4.2.1 for the two phase catalysis. For the recycling experiments, a mixture of the isomeric substrates methyl 4-pentenoate and methyl 3-pentenoate was employed with a molar ratio of 9:1. For this purpose, methyl 4- pentenoates (0.147 g, 1.28133 mmol) and methyl 3-pentenoate (0.016 g, 0.14237 mmol) were introduced into the previously prepared catalyst solution, consisting of BINAS (12.12 mg, 0.00572 mmol), catalyst precursor (0.368 mg, 0.00143 mmol), 2.5 mL pure toluene and 2.5 mL of

deionised and degassed water. The reaction mixture was transferred into the autoclave, which was subsequently closed and flushed four times with argon and five times with syngas. The reaction was left stirring for 20 h at 100 °C and 50 bar of syngas. After cool down, the organic phase was collected via phase separation and sampled for analytical purposes. After taking a sample of 0.5 mL for ICP-OES, the aqueous phase was refed into the autoclave, fresh organic substrate solution was added and the reaction was started again. This was repeated four times. The results are shown in Table 10. (Detailed experimental data are shown in A.1.5)

4.2.5.1 Comparison between BINAS-modified and unmodified Rh(I)-catalyst

The preparation of the reaction mixture followed the procedure described in section 4.2.1 for the two phase catalysis without the addition of ligand. As substrate mixture, M4P (0.147 g, 1.28133 mmol, 0.158 mL) and M3P (0.016 g, 0.14237 mmol, 0.018 mL) in a 9:1 ratio were used. The substrate mixture was introduced into the previously prepared reaction mixture consisting of $Rh(CO)_2acac$ (0.368 mg, 0.00143 mmol), 2.5 mL of toluene and 2.5 mL of deionised water and transferred into the autoclave. Then the autoclave was closed and flushed with argon and subsequently with syngas. Then the autoclave was brought to a reaction temperature of 100 °C and pressurised to 50 bar of syngas. Stirring commenced for 20 h. After cool down, samples were collected and analysed.

4.2.5.2 Sample preparation ICP-OES

0.5 mL of each phase was collected from the crude mixture and the solvent evaporated under vacuum at 60 °C. Both residues were subjected to acidic fusion with a nitrating acid mixture (conc. HNO_3 (65 %) + conc. H_2SO_4 (94-96 %); 1:1) in a pressure tube at 200 °C. The temperature was kept constant over the course of 8 h to destroy any organic compounds and transform them into inorganic and water-soluble material. The acidic fusions were left to cool overnight and then diluted with deionised water to 50 mL. The resulting solutions were analysed by ICP-OES.

4.2.6 Isomerisation in the presence of the precatalyst [Rh(BIPHEPHOS)(acac)]

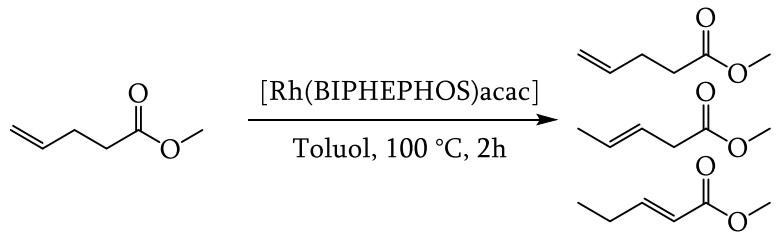

Fig. 51: Isomerisation of M3P with a BiphePhos modified catalyst.

5.4 mg (6.86 µmol) of BiphePhos was dissolved in 5.5 mL of dry toluene. Subsequently, 0.24 mL of a $Rh(CO)_2acac$ stock solution (c_{Rh} = 7.15 µmol*mL^{-1}, 1.72 µmol, toluene) was added and the mixture stirred for a few minutes. Then, M4P (0.212 g, 0.227 mL, 1.72 mmol) was weighed in. The resulting solution was mixed and a sample (0.3 mL) was taken for GC analytic purposes. The remaining reaction mixture was heated to 100 °C and stirred for 2 h. Every 15 min, a sample (0.3 mL) was collected and analysed via GC-FID. Every sample was diluted with toluene to a final volume of 1 mL. (Detailed experimental data are shown in A.1.6.1.1)

4.3 Alkoxycarbonylation of isomeric methyl pentenoates

4.3.1 Preliminary experiments

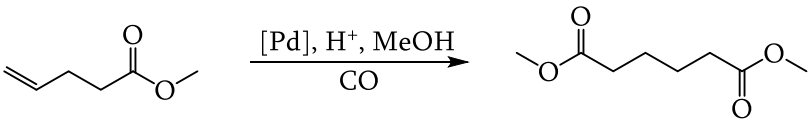

Fig. 52: Reaction scheme of the alkoxycarbonylation of methyl pentenoates. Only one regioisomer of the possible products is shown.

First, a stock solution of $Pd(OAc)_2$ and methanesulfonic acid was prepared. For this, $Pd(OAc)_2$ (10 mg, 0.04455 mmol) was weighed into a 25 mL-Schlenk tube and dissolved in 10 mL of dry MeOH. The final palladium concentration should be c_{Pd} = 0.00446 mmol*mL^{-1}. The stock solution for methanesulfonic acid was prepared by filling 10 mL of dry MeOH into another Schlenk tube and consecutively adding $MeSO_3H$ (13.7 mg, 0.143 mmol, 9.3 µL) with a microliter syringe. With these stock solutions it was easier to add both components to the reaction mixtures.

The ligand (0.00572 mmol) was weighed into a Schlenk tube and dissolved in 3.5 mL of dry MeOH. Then 0.321 mL of the previously prepared $Pd(OAc)_2$ solution, M4P (0.147 g, 1.28133 mmol, 0.158 mL) and M3P (0.017 g, 0.14237 mmol, 0.018 mL) was added. Finally, 1 mL of the $MeSO_3H$ stock solution was added and the resulting solution diluted (with dry MeOH) to receive a final volume of 5 mL. This reaction mixture was transferred into the autoclave and the autoclave was then flushed with argon and CO. The reaction mixture was heated to 100 °C and pressurised to 40 bar with CO. Temperature and pressure were kept constant for 20 h. After cool down, the apparatus was vented and flushed with Argon. The crude was sampled and analysed via GC/MS and GC-FID. The results are shown in Table 12. (Detailed experimental data are shown in A.2.1)

4.3.2 Optimisation of the reaction conditions for the catalysis with PyTBPF and PyTBPX as ligands

4.3.2.1 Diphosphine PyTBPF

The ligand (14.7 mg, 28.60 µmol) and $Pd(OAc)_2$ were weighed into a Schlenk tube and dissolved in 25 mL of dry MeOH. The resulting solution was mixed thoroughly. M4P (0.7325 g, 0.790 mL, 7.40665 mmol) and M3P (0.0834 g, 0.090 mL, 0.71185 mmol) were added, as well as $MeSO_3H$ (5 µL, 0.0072 mmol). The resulting solution was stirred for a few minutes. The reaction solution was spread evenly between 5 autoclaves (5 mL each). The optimisation was performed similarly to section 4.2.4, where one reaction parameter was varied for a set of experiments, starting with the pressure and finishing with the temperature. The reaction was finished after 3 h and the crude was sampled for GC analytical purposes. The results and the optimised parameters are shown in Table 13 (see section 3.2.3.1) (Detailed experimental data are shown in A.2.2.1)

4.3.2.2 Diphosphine PyTBPX

The ligand (12.5 mg, 28.60 µmol) and $Pd(OAc)_2$ were weighed into a Schlenk tube and dissolved in 25 mL of dry MeOH. The resulting solution was mixed thoroughly. M4P (0.7325 g, 0.790 mL, 7.40665 mmol) and M3P (0.0834 g, 0.090 mL, 0.71185 mmol) were added, as well as $MeSO_3H$ (5 µL, 0.0072 mmol). The resulting solution was stirred for a few minutes. The reaction solution was spread evenly between 5 autoclaves (5 mL each). The optimisation was conducted similarly to section 4.2.4, where one reaction parameter was varied for a set of experiments, starting with the

pressure and finishing with the temperature. The reaction was finished after 3 h and the crude was sampled for GC analytical purposes. The results and the optimised parameters are shown in Table 14 (see section 3.2.3.1) (Detailed experimental data are shown in A.2.2.2)

4.3.3 Characterisation and structural investigation of the catalysts in use

4.3.3.1 Synthesis of Pd(PyTBPF)dba and Pd(PyTBPX)dba

The synthesis was performed successfully according to the literature procedure for the synthesis of Pd(BuPox)dba. [97] For this, the ligand (0.4 mmol) and $Pd_2(dba)_3$ (0.2 mmol) were weighed into a Schlenk flask under inert atmosphere and dissolved in 20 mL of dry THF, while getting stirred. Stirring commenced for 6 h at room temperature, during which a colour change from deep violet to yellowish orange occurred. Afterwards, the solvent was reduced to 1 mL *in vacuo* and then diluted with 5 mL of dry *n*-heptane. Precipitation of the product set in. The suspension was stirred for another hour and then reduced to 1 mL and again diluted with 5 mL of heptane. The orange precipitate was filtered off via a Schlenk frit and washed with heptane. The solid was dried *in vacuo* overnight and was used without further purification. Yield: 80 % (for Pd(PyTBPF)dba); 77 % (for Pd(PyTBPX)dba). (Detailed experimental data are shown in A.2.3.1)

4.3.3.2 Synthesis of [Pd(PyTBPF)Cl]Cl and [Pd(PyTBPX)Cl]Cl

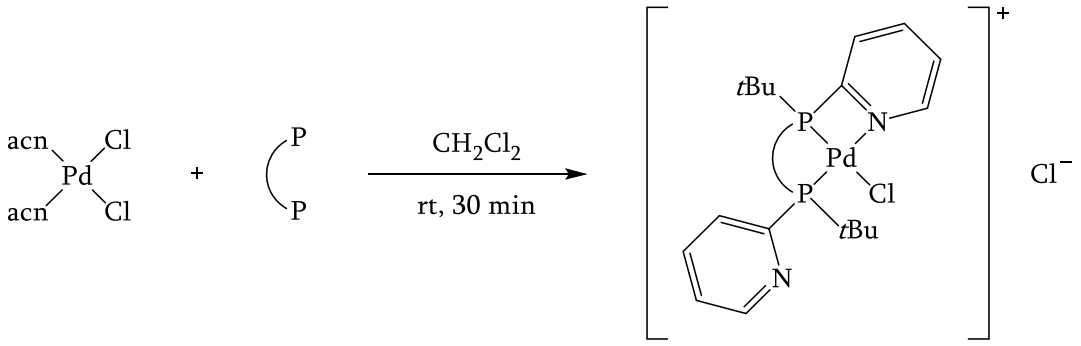

Fig. 53: Reaction scheme of the synthesis of [Pd(P-P)Cl]Cl.

As Pd(II)-precursor $Pd(acn)_2Cl_2$ was used, because of its better solubility in organic solvents. It can be easily synthesised. For this reason, $PdCl_2$ (0.5 g, 1.93 mmol) was weighed into a Schlenk flask and dissolved in 10 mL of dry acetonitrile. The solution was stirred at 80 °C for 4 h. After cooling to room temperature, the solvent was removed *in vacuo* and the yellow residue was dried *in vacuo* at 50 °C overnight. The product was used without further purification.

$Pd(acn)_2(Cl)_2$ (51.8 mg, 0.2 mmol) and the ligand (0.2 mmol) were weighed into a Schlenk flask and dissolved in 5 mL of dry THF. The resulting solution was stirred for 30 min and then evaporated until 1 mL was left. Then 5 mL of dry diethylether were added, precipitating a yellow solid. The solid was filtered off and washed with dry diethylether. Drying in vacuo resulted in a yellow powder comprised of the complex Pd(L)Cl2. Crystals suitable for X-ray crystallography were produced by dissolution in dry methanol, addition of a small amount of heptane and slow evaporation over multiple days in the refrigerator. Yield: 105.1 mg, 76 % ([Pd(PyTBPF)Cl]Cl); 82.2 mg, 67 % ([Pd(PyTBPX)Cl]Cl) (Detailed experimental data are shown in A.2.3.2)

4.3.3.3 Synthesis of [Pd(PyTBPF)OTf]OTf and [Pd(PyTBPX)OTf]OTf starting from Pd(PyTBPF)dba and Pd(PyTBPX)dba

The procedure was realised according to the literature procedure of Dong *et al.* [97c] The synthesis started from the corresponding dba-complexes. The dba-complexes (0.18 mmol) were weighed into a Schlenk flask together with benzoquinone (21.6 mg, 0.2 mmol) and dissolved in 5 mL of abs. dichloromethane. Trifluoromethanesulfonic acid (34.3 µL, 0.59 mmol) was added dropwise. The

resulting solution was stirred for 15 min at ambient temperature and then evaporated *in vacuo* until 2 mL were left. The solution was diluted with 6 mL of abs. Diethylether to precipitate the product. (Dark red for [Pd(PyTBPF)OTf]OTf, pale yellow for [Pd(PyTBPX)OTf]OTf) The resulting suspensions were filtered and the solids were washed with abs. diethylether and dried *in vacuo* overnight. Yields: 54 % ([Pd(PyTBPF)OTf]OTf); 50 % ([Pd(PyTBPX)OTf]OTf). (Detailed experimental data are shown in A.2.3.5.

4.3.3.4 H^+-free synthesis of [Pd(PyTBPF)OTf]OTf and [Pd(PyTBPX)OTf]OTf starting from [Pd(PyTBPF)Cl]Cl and [Pd(PyTBPX)Cl]Cl

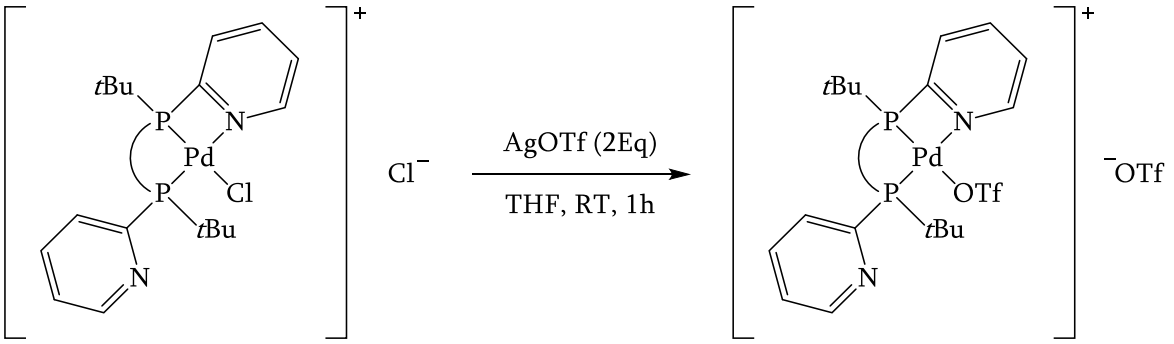

Fig. 54: Reaction scheme of the synthesis of [Pd(P-P)OTf]OTf starting from the corresponding dichloro complexes.

$Pd(L)(Cl)_2$ was weighed into a Schlenk flask and dissolved in 2.5 mL of dry THF. Another solution was prepared by dissolving 2 Eq. of AgOTf in dry THF. The AgOTf solution was added dropwise while stirring at room temperature. The yellow solution almost immediately changed its colour while precipitation of AgCl occured (to dark red for PyTBPF, pale yellow for PyTBPX). Stirring was commenced for 1 h. After that, the AgCl was filtered off and washed with dry THF. The filtrate was reduced *in vacuo* to 1 mL and diluted with 5 mL of dry heptane to precipitate the product. The resulting suspension was stirred for 1 h. The solid was filtered off, washed with dry heptane and dried *in vacuo* overnight. Yields: 88.2 % ([Pd(PyTBPF)OTf]OTf); 79.3 % ([Pd(PyTBPX)OTf]OTf). (Detailed experimental data are shown in A.2.3.3)

4.3.3.5 NMR-spectroscopic characterisation of the ligand PyTBPF and PyTBPX

The ligand (0.03 mmol) was weighed into a Schlenk flask under inert atmosphere and dissolved in 1 mL of a deuterated solvent. The solution is transferred into a Young NMR tube and analysed by NMR spectroscopy. The results are discussed in section 3.2.4. (Detailed experimental data are shown in A.2.3.4)

4.3.3.5.1 Protonation of the ligands with trifluoromethanesulfonic acid

A stock solution of trifluoromethanesulfonic acid in dry CD_2Cl_2 was prepared with a concentration of c_{TfOH} = 120 mmol*L^{-1}. The ligand (0.03 mmol) was dissolved in 0.5 mL of dry CD_2Cl_2. While stirring, 0.5 mL of the stock solution was added dropwise. The resulting solution was transferred into a Young NMR tube and analysed via NMR spectroscopy. The results are discussed in section 3.2.4. (Detailed experimental data are shown in A.2.3.4.1)

4.3.3.6 NMR-spectroscopic characterisation of the complexes Pd(L)dba and [Pd(L)OTf]OTf

The complexes (0.03 mmol) were weighed into a Schlenk flask and dissolved in 1 mL of a deuterated solvent. The solutions were then transferred into a Young NMR tube and analysed via NMR spectroscopy. (Detailed experimental data are shown in A.2.3.5)

4.3.3.7 In situ synthesis of the suspected resting states [Pd(L)OTf]OTf or [Pd(L)OTs]OTs starting from different precursors

Ligand (0.06 mmol) and precursor (0.03 mmol, In case of Pd_2dba_3, 0.015 mmol are used) were weighed into a Schlenk flask and dissolved in 0.5 mL of a deuterated solvent. When a Pd(0) precursor was used, benzoquinone (0.15 mmol) was added as an oxidising agent. The solution was stirred for a few minutes. Afterwards, 0.5 mL of a solution of the acid in use (0.21 mmol) and the deuterated solvent was added. The resulting solution was stirred for another 5 minutes and finally transferred into a Young NMR tube. The sample was then NMR spectroscopically analysed. The results, weighings, solvents and precursors are shown in section A.2.3.6.

4.3.3.8 In situ-IR experiments for the identification of a palladium acyl species

4.3.3.8.1 General procedure for the *in situ*-IR experiments

A FT/IR spectrometer fitted with a flow cell with CaF_2 windows that is connected to a 10 mL stainless steel autoclave via heated capillaries and a micro gear pump was used for the *in situ* IR experiments. At first, background spectra of the solvent in use were recorded. After this, the autoclave was emptied and the previously prepared reaction solution was added. Then, the reaction solution was heated to the desired temperature and the system was pressurised until the desired pressure was reached. IR spectra were measured over the course of the entire experiment.

4.3.3.8.2 Sample preparation

(a) Ligand (0.3 mmol) and $Pd(dba)_2$ (86 mg, 0.15 mmol) were weighed into a Schlenk flask and dissolved in 2.5 mL of a dry solvent. In another Schlenk flask, dry *p*TSA (129.0 mg, 0.75 mmol) was dissolved in 2.5 mL of the same dry solvent. The acid was added to the palladium ligand solution and the mixture was stirred for a few minutes. The resulting catalyst solution was transferred into the 10 mL autoclave. The reaction itself was conducted at room temperature and at first with 10 bar ethylene for 2 h. After these 2 h, 10 bar of CO were added, resulting in a final overall pressure of 20 bar. The reaction mixture was stirred for another 2 h while recording the IR spectra.

(b) Pd(L)dba (0.15 mmol) and *p*TSA (129.0 mg, 0.75 mmol) were weighed into a Schlenk tube and dissolved in 5 mL of a dry solvent. The final palladium concentration was at c_{Pd} = 30 mmol*L^{-1}. The resulting solution was transferred into the 10 mL autoclave and the *in situ* spectroscopic measurements were conducted as described in section (a).

4.3.3.9 In situ-HP NMR for the identification of a palladium alkyl species

4.3.3.9.1 General procedure for the NMR experiments

For the HP NMR experiments, a NMR tube made from sapphire glass with a length of 10 cm, a diameter of 0.5 cm and a wall thickness of 1 mm, which can withstand pressure of up to 300 bar, was utilised. The filled tube was sealed pressure-tight and pressurised with the desired gases until the target pressure was reached. The sample was then inserted into the spectrometer (Bruker AV300 or AV400) via a chain. The measurement is performed without rotation of the sample.

4.3.3.9.2 Sample preparation

The reaction solutions were prepared as described in section 4.3.3.7, transferred into a 10 mL autoclave and pressurised with ethane until the target pressure was reached. At room temperature, the sample was stirred for 2 h and then transferred into the sapphire glass tube.

4.4 Hydroaminomethylation of methyl pentenoates

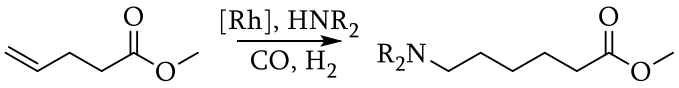

Fig. 55: Reaction scheme of the HAM of methyl pentenoates. Only the linear product is shown.

In a Schlenk flask the ligand was weighed in and dissolved in 4 mL of dry toluene. Afterwards, 0.12 mL of a $Rh(CO)_2acac$ stock solution in toluene (c_{Rh} = 0.012 mmol*mL^{-1}) was added. The resulting solution was stirred for a few minutes. Then methyl 3-pentenoate, methyl 4-pentenoate and the amine were added. The reaction solution was transferred to an autoclave, which was subsequently flushed with Argon and with syngas. Then, the autoclave was heated and pressurised to the desired reaction conditions. The reaction was left stirring at constant temperature and pressure for 20 h and the product mixture was sampled and analysed afterwards. The results were shown in Table 15. The weighings and reaction conditions were shown in section A.3.

4.5 Hydroformylation of unusual substrates

4.5.1 Hydroformylation of 1,2,4-trivinylcyclohexane

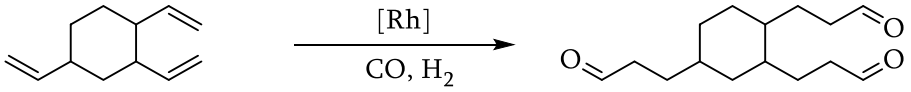

Fig. 56: Reaction scheme of the hydroformylation of 1,2,4-trivinylcyclohexane.

The ligand (0.00572 mmol) was weighed into a Schlenk flask and dissolved in 5 mL of dry toluene. Afterwards, 0.12 mL of a $Rh(CO)_2acac$ stock solution in toluene (c_{Rh} = 0.012 mmol*mL^{-1}) was added and the resulting mixture was stirred for a few minutes. 1,2,4-Trivinylcyclohexane (0.232 g, 1.43 mmol, 0.28 mL) was weighed into the Schlenk flask and the resulting mixture was transferred into an autoclave. The autoclave was flushed with Ar and syngas and subsequently heated and pressurised to the desired reaction conditions. The reaction was conducted for 20 h and the resulting product mixture was analysed via GC and NMR. The results are shown in Table 19 and the corresponding reaction conditions and weighings are shown in section A.4.1.

4.5.1.1 Rhodium catalysed hydroaminomethylation of 1,2,4-trivinylcyclohexane

To a solution of ligand (0.00572 mmol) in 5 mL of dry toluene 0.12 mL of a $Rh(CO)_2acac$ stock solution in toluene (c_{Rh} = 0.012 mmol*mL^{-1}) was added and then well mixed. 1,2,4-TVCH (0.232 g, 1.43 mmol, 0.28 mL) and the amine were weighed into the same Schlenk flask. The resulting solution was again stirred for a few minutes and then transferred into the autoclave. The autoclave was prepared as described above. The catalysis was conducted at 100 °C and a syngas pressure of 20 bar. (Detailed experimental data are shown in A.4.1.1)

4.5.1.2 Synthesis of a triphosphite derived from 1,2,4-tris(3-hydroxopropyl)cyclohexane

4.5.1.2.1 Synthesis of bis(2,4-di-tert-butylphenyl)phosphorochloridite [98]

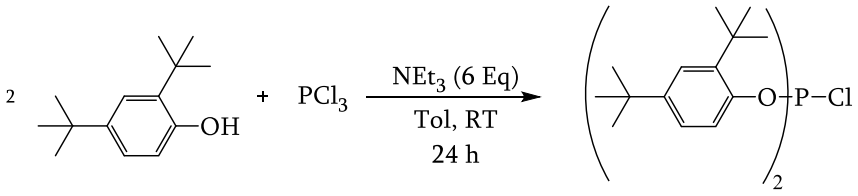

Fig. 57: Reaction scheme of the synthesis of bis(2,4-di-tert.-butylphenyl)phosphorochloridite.

A 500 mL Schlenk flask was fitted with a dropping funnel, heated out and flushed with Argon. 2,4-Di-*tert.*-butylphenol (10 g, 48.46840 mmol) was added to the flask, dissolved in 250 mL of dry toluene and mixed with NEt_3 (14.7 g, 20.2 mL, 145.40520 mmol). The solution was cooled down to 0°C while stirring. Simultaneously, the dropping funnel was charged with a solution of PCl_3 (3.328 g, 2.12 mL, 24.23420 mmol) in 50 mL of dry toluene. Afterwards, the PCl_3 solution was added dropwise at 0 °C within 15 minutes. After complete addition, the dropping funnel was rinsed with dry toluene and the reaction mixture was allowed to warm up to room temperature. Stirring commenced for another 24 h. During this time a white precipitate formed that was filtered off and washed with dry toluene. The solvent of the yellowish filtrate was removed *in vacuo*. The remaining yellow oil was dried at 50 °C *in vacuo* overnight and was used without further purification. Yield: 11.28 g (97.6 %). Purity: 90 % determined by quantitative NMR. ^{31}P NMR (122 MHz, CD_2Cl_2) δ 160.9. ^{1}H NMR (300 MHz, CD_2Cl_2) δ 7.50 (d, J = 2.5 Hz, 2H, 3-Ar-H), 7.37 (dd, $^{3}J_{H,H}$ = 8.4 Hz, $^{5}J_{H,H}$ = 1.4 Hz, 2H, 6-Ar-H), 7.27 (dd, $^{3}J_{H,H}$ = 8.4 Hz, $^{4}J_{H,H}$ = 2.5 Hz, 2H, 5-Ar-H), 1.49 (s, 18H, tBu-H), 1.38 (s, 18H, tBu-H).

For further usage, the raw product was dissolved in 20 mL of dry THF (c = 0.68669 mmol*mL^{-1}). (Detailed experimental data are shown in A.4.1.2.1)

4.5.1.2.2 Synthesis of the triphosphites starting from 1,2,4-tris(3-hydroxopropyl)cyclohexane

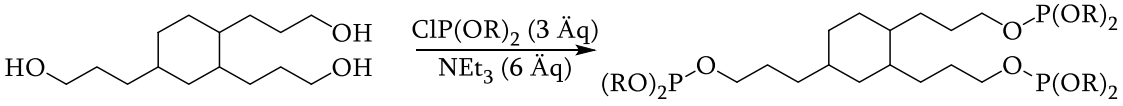

Fig. 58: General reaction scheme of the synthesis of triphosphites from THOPCH.

The synthesis of the triphosphite was started by charging a Schlenk flask with 1,2,4-tris(3-hydroxypropyl)cyclohexane, dissolving it in dry THF and adding NEt_3. The resulting solution was cooled down to 0 °C. Then the previously prepared solution of the phosphorochloridite in THF was added dropwise to the stirred reaction mixture. Simultaneously a white precipitate was formed. After complete addition of the chloridite, the reaction mixture was allowed to warm up to room temperature and stirred for another 24 h. The precipitate was filtered off and washed with dry THF. The solvent of the filtrate was removed *in vacuo*, resulting in yellowish foam. The raw product was purified via column chromatography. (Detailed experimental data are shown in A.4.1.2.2)

Synthesis of 1,2,4-tris(3-((bis(2,4-di-tert-butylphenyl)phosphanyl)oxy)propyl)cyclohexane

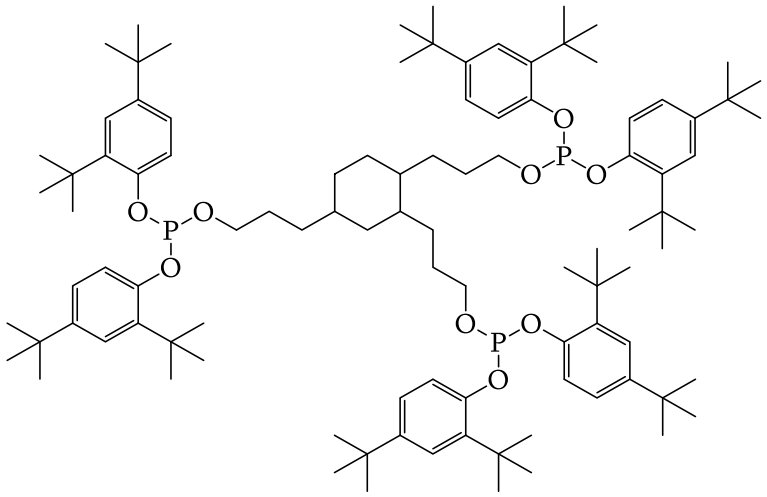

*Fig. 59: Structural formula of **SB111**.*

The synthesis of this substance is realised as described above.

- Weighings:

THOPCH	0.43 g	-	1.66504 mmol
NET_3	1.01 g	1.4 mL	9.99024 mmol
Bis(2,4-di-*tert*-butylphenyl)-phosphorochloridite	1.25 g		4.99512 mmol

The work up was conducted via column chromatography with dry silica gel as the stationary phase. As eluent mixture, a mixture of *n*-heptane, dichloromethane and NEt_3 was used. (Hep:DCM:NEt_3 90:9:1) The product containing fraction was collected and the solvent removed *in vacuo* resulting in colourless foam. The product was dried *in vacuo* at 50 °C for 5 h. Yield: 0.4892 g (80 %). Purity: 100 % determined via quantitative ^{31}P NMR and GC-MS. ^{31}P NMR (122 MHz, CD_2Cl_2) δ 126.94 (m). ^{1}H NMR (300 MHz, CD_2Cl_2) δ 7.39 (m, 6H,), 7.13 (m, 12H,), 4.10 (m, 6H, R-CH_2-O-R), 1.8 - 0.4 (m, 21H), 1.43 (m, 54H, tBu-H), 1.3 (m, 54 H, tBu-H). ^{13}C NMR (75 MHz, CD_2Cl_2) δ 149.5 (C), 145.2 (C), 138.7 (C), 124.4 (CH), 123.5 (CH), 118.0 (CH), 63.4 (CH_2), 41.0 (CH), 40.9 (CH), 38.8 (CH_2), 37.1 (CH), 35.0 (C), 34.3(C), 33.4(CH_2), 31.9 (CH_2), 31.7 (CH_2), 31.3 (CH_3), 29.9 (CH_3), 29.3 (CH_2), 29.2(CH_2), 29.0 (CH_2), 28.0 (CH_2), 27.9(CH_2), 22.7 (CH_2). E.A. calculated for $C_{99}H_{153}O_9P_3$: C, 75.25; H, 9.76; P, 5.88. Found: C, 75.33: H, 9.74; P, 5.88. (Detailed experimental data are shown in A.4.1.2)

4.5.1.2.3 Trial of the synthesised triphosphite **SB111** in the rhodium catalysed hydroformylation

To test the synthesised triphosphite in the rhodium catalysed hydroformylation, it was weighed into a Schlenk flask and dissolved in 5 mL of dry toluene. 0.2 mL of a $Rh(CO)_2acac$ stock solution in toluene (c_{Rh} = 7.15 µmol*mL^{-1}) was added and the resulting solution was well mixed. The olefin (1.43 mmol) was added and the reaction mixture is transferred into an autoclave. The catalysis was performed at 100 °C and 20 bar of syngas. After 3 h, the reaction mixture was allowed to cool down and the autoclave was vented. The crude was collected and sampled for analytical purposes. The results are shown in Table 20. (Detailed experimental data are shown in A.4.1.2.3)

5 Summary

To conclude, the catalytic conversion of pentenoic acid esters regarding the hydroformylation and alkoxycarbonylation reaction, was successfully improved during this work. Regarding the rhodium catalysed hydroformylation, now methyl 5-formylpentenoate can be synthesised with high regioselectivity and only little side product formation. The main side product methyl valerate stems from the hydrogenation of the substrate. Other side reactions, such as aldol condensations could not be observed. Of course the chemo- and regioselectivities strongly depend on the substrate isomer in use. Generally speaking, the overall catalytic performance got worse, the further away the double bond was from the terminal end of the chain. Consequently, the hydroformylation of methyl 2-pentenoate, being the most stable of the three isomers, was converted into the corresponding semi aldehyde only in marginal amounts and methyl valerate was the main product. In accordance with Keuleman's rule, the best results were achieved with the terminal olefin methyl 4-pentenoate. If a substrate mixture of methyl 3- and methyl 4-pentenoate was used, the catalytic performance was slightly worse in contrast to the reactions with the pure substrates.

The alkoxycarbonylation of methyl pentenoates with highly efficient alkoxycarbonylation catalysts that are modified with pyridyl-substituted diphosphines was equally successful. Compared to the corresponding BuPox-modified catalyst, the investigated PyTBPF and PyTBPX-modified catalyst were significantly more active albeit less regioselective. Where the BuPox-modified catalyst almost exclusively forms the linear dimethyl adipate, the PyTBPX and PyTBPF modified catalysts also form the corresponding "branched" dicarboxylic acid esters dimethyl 2-methylglutarate and dimethyl 3-ethylsuccinate. We conclude that the pyridyl-substituents of the ligand have a significant influence on the catalytic performance. Therefore, we decided to gain more insight into the catalytically relevant species. The resting state of the catalyst as postulated by Dong *et al.* [91] is supported by our research and is comprised of the ligand coordinating to the metal in a *cis*-fashion with regard to its P centres as well as one coordinating pyridyl group. The last coordination site is occupied by either one anion of the employed acid, or a solvent molecule. Species relevant to the established mechanisms for the alkoxycarbonylation [90], like a hydride-, alkyl- or acyl-species could not be observed, indicating a different reaction pathway than originally assumed. More research has to be conducted in this regard. Looking at the hydroaminomethylation of methyl pentenoates, problems that are typical for this kind of reaction arose.

Since the hydroaminomethylation of methyl pentenoates using aqueous ammonia was not viable because of low selectivities regarding the formation of primary amines, only the hydroaminomethylation with secondary amines delivered promising results. Sadly, the comparably good results were overshadowed by the fact, that industrial interests lie in the formation of primary amines, so that this type of reaction was not further investigated.

The rhodium catalysed hydroformylation of an isomeric mixture 1,2,4-trivinylcyclohexane was performed successfully. While the different configurational isomers could not be separated, the resulting product mixtures consisted of about 80 % of linear trialdehyde. The remaining 20 % could be assigned to different dialdehydes.

The hydroformylation of methyl pentenoates with the triphosphite **SB111** delivered only mediocre results. Similar results were obtained with other substrates.

6 Bibliography

[1] Bundesanstalt für Geowissenschaften und Rohstoffe, *BGR Energiestudie 2017 – Daten und Entwicklungen der deutschen und globalen Energieversorgung* **2017**.

[2] J.-P. Lange, Catalysis for Biorefineries: What Industry Needs? in *Nanotechnology in Catalysis: Applications in the Chemical Industry, Energy Development, and Environment Protection*, 1 edition, Wiley-VCH, **2017**, volume 1, chapter 24, p. 585 pp.

[3] R. Palkovits, *Chem. Ing. Tech.* **2018**, *90*, 1699 – 1708.

[4] A. M. Ruppert, K. Weinberg, R. Palkovits, *Angew. Chem. Int. Ed.* **2012**, *51*, 2564 – 2601.

[5] M. Stöcker, *Angew. Chem. Int. Ed.*, **2008**, *47*, 9200 – 9211.

[6] T. W. Walker, A. H. Motagamwala, J. A. Dumesic, G. W. Huber, *J. Catal.* **2019**, *369*, 518 – 525.

[7] (a) G. W. Huber, A. Corma, *Angew. Chem. Int. Ed.* **2007**, *46*, 7184 – 7201; (b) J. Zakzeski, P. C. A. Bruijnincx, A. L. Jongerius, B. M. Weckhuysen, *Chem. Rev.* **2010**, *110*, 3552 – 3599; (c) J.-P. Lange, E. Van Der Heide, J. van Buijtenen, R. Price, *ChemSusChem* **2012**, *5*, 150 – 166; (d) M. J. Climent, A. Corma, S. Iborra, *Green chem.* **2014**, *16*, 516 – 547; (e) I. Delidovich, K. Leonhard, R. Palkovits, *Energy Environ. Sci.* **2014**, *7*, 2803 – 2830; (f) R. Rinaldi, R. Jastrzebski, M. T. Clough, J. Ralph, M. Kennema, P. C. A. Bruijninx, B. M. Weckhuysen, *Angew. Chem. Int. Ed.* **2016**, *55*, 8164 – 8215; (g) W. Leitner, J. Klankermayer, S. Pischinger, H. Pitsch, K. Kohse-Höinghausen, *Angew. Chem. Int. Ed.* **2017**, *56*, 5412 – 5452.

[8] C. O. Tuck, E. Pérez, I. T. Horváth, R. A. Sheldon, M. Poliakoff, *Science* **2012**, *337*, 695 – 699.

[9] J. G. de Vries, *Chem. Rev.* **2016**, *16*, 2787 – 2800.

[10] R. Kummer (BASF AG), *EP0031100*, **1980**.

[11] R. Kummer, F. Merger, W. Bertleff, R. Fischer (BASF AG), *EP0295551A2*, **1988**.

[12] M. Roeper, P. M. Lorz, D. Koeffer (BASF AG), *US5264616*, **1993**.

[13] C. B. Hansen, J. G. de Vries (DSM N. V., E.I. du Pont de Nemours and Company), *WO95/18089*, **1995**.

[14] P. M. Burke, J. M. Garner, W. Tam (E. I. du Pont de Nemours and Company), *US6664427B1*, **2003**.

[15] J.-C. Tsai, H.-H. Tai, T.-T. Su, B.-P. Wang (Industrial Technology Research Institute), *US6017843*, **2000**.

[16] R. F. M. J. Parton, M. C. C. Janssen, B. Engendahl, J. G. de Vries (DSM IP Assets B.V.), *WO2014/111446A1*, **2014**.

[17] S. Behrens (**2016**), *Hydroformylierung von Pentensäuremethylestern* (Unpublished master's thesis), University of Rostock, Rostock, Germany.

[18] S. Behrens, G. M. Torres, A. Boerner, R. Franke, D. Selent (Evonik Degussa GmbH), *US2018290957*, **2018**.

[19] H.-W. Schneider, W. Richter, W. Disteldorf, R. Kummer (BASF AG), *DE3325372A1*, **1983**.

[20] P. M. Burke (E. I. du Pont de Nemours and Company), *EP0188209A2*, **1986**.

[21] R. Kummer, F. Merger, W. Bertleff, R. Fischer (BASF AG), *EP0295551A2*, **1988**.

[22] E. M. Atadan (E.I. du Pont de Nemours and Company), *US5218144*, **1993**.

[23] E. M. Atadan (E. I. du Pont de Nemours and Company), *US5292944*, **1994**.

[24] H. S. Bruner, S. L. Lane, B. E. Murphree (E. I. du Pont de Nemours and Company), *US5710325*, **1998**.

[25] O. E. Sielcken (DSM N.V.), *EP0662467A1*, **1995**.

[26] (a) M. Slany, M. Schäfer, M. Röper (BASF AG), *WO02/46143A1*, **2002**; (b) E. Bunel, D. Clark (E. I. Du Pont de Nemours and Company), *WO02/48094A1*, **2002**.

[27] C. Jiménez-Rodriguez, G. R. Eastham, D. J. Cole-Hamilton, *Inorg. Chem. Commun.* **2005**, *8*, 878-887.

[28] E. Drent, R. Van Ginkel, W. W. Jager (Shell Internationale Research Maatschappij B.V.), *WO2004/103942A1*, **2004**.

[29] J. G. de Vries, N. Sereinig, E. W. M. van de Vondervoort, M. C. C. Janssen (DSM IP Assets B. V.), *WO2012/131027A1*, **2012**.

[30] C. H. Low, J. D. Nobbs, M. van Meurs, L. P. Stubbs, E. Drent, S. Aitipamula, M. H. L. Pung, *Organometallics* **2015**, *34*, 4281-4292.

[31] J. D. Nobbs, C. H. Low, L. P. Stubbs, C. Wang, E. Drent, M. van Meurs, *Organometallics* **2017**, *36*, 391-398.

[32] L. Zhao, B. Pudasaini, A. Genest, J. D. Nobbs, C. H. Low, L. P. Stubbs, M. van Meurs, N. Rösch, *ACS Catal.* **2017**, *7*, 7070-7080.

[33] (a) E. Bunel, D. Clark (E. I. du Pont de Nemours and Company), *US20030105348A1*, **2003**; (b) E. Drent, R. Van Ginkel, W. W. Jager (Shell international Research Maatschappij B. V.), *WO2004/103942*, **2004**; (c) E. Drent, R. Ernst, W. W. Jager, C. A. Krom (Shell Internationale Research Maatschappij), *WO2006/084892A2*, **2006**; (d) J. A. M. Van Broekhoven, E. Drent, R. Ernst, W. W. Jager, C. A. Krom (Shell Internationale Research Maatschappij), *WO2006/084889A1*, **2006**; (e) A. M. C. F. Castelijns, M. C. C. Janssen, H. W. L. M. Vaessen (DSM IP Assets B. V.), *EP2537840A1*, **2012**; (f) J. R. Peterson, C. M. Yost, J. Wu (Thesis Chemistry, LLC), *US2013/0116424A1*, **2013**; (g) R. F. M. J. Parton, M. C. C. Janssen, B. Engendahl, J. G. de Vries (DSM IP Assets B. V.), *WO2014/111446A1*, **2014**.

[34] (a) M. K. Lau (Bioamber Inc.), *WO2014/031724A1*, **2014**; (b) M. K. Lau (Bioamber Inc.), *US2015/0203879A1*, **2015**; (c) P. C. Raemakers-Franken, M. Schürmann, A. C. Trefzer, S. M. A. de Wildeman (DSM IP Assets B.V.), *WO2009/113855A2*, **2009**; (d) S. C. H. Turk, M. Schürmann, A. C. Trefzer, P. C. Raemakers-Franken, H. H. Menke (DSM IP Assets B.V.), *WO2012/031911A2*, **2012**. (e) S. C. H. Turk, M. Schürmann, A. C. Trefzer, P. C. Raemakers-Franken, H. H. Menke (DSM IP Assets B.V.), *US2013/0237698A1*, **2013**.

[35] M. J. Burk, A. P. Burgard, R. E. Osterhout, P. Pharkya (Genomatica Inc.), *WO2010/129936A1*, **2010**.

[36] (a) A. P. Burgard, R. E. Osterhout, S. J. van Dien, C. Tracewell, P. Pharkya, S. Andrae (Genomatica Inc.), *WO2014/099725A1*, **2014**; (b) A. P. Burgard, R. E. Osterhout, S. J. van Dien, C. Tracewell, P. Pharkya, S. Andrae (Genomatica Inc.), *US2015/0329885A1*, **2015**. (c) R. E. Osterhout, A. P. Burgard, P. Pharkya, S. Andrae (Genomatica Inc.), *WO/2015084633A1*, **2015**.

[37] P. C. Raemakers-Franken, M. Schurmann, A. C. Trefzer, S. M. A de Wildeman (DSM IP Assets B.V.), *US8673599B2*, **2014**.

[38] F. Merger, R. Fischer, W. Harder, C.-U. Priester, U. Vagt (BASF AG), *DE3843792A1*, **1990.**

[39] E. E. Bunel, T. A. Koch, R. Ozer, S. K. Sengupta (E.I. du Pont de Nemours and Company), *US6365770B1*, **2002**.

[40] (a) F. Merger, R. Fischer, W. Harder, C.-U. Priester, U. Vagt (BASF AG), *DE3843791A1*, **1990**; (b) H. F. W. Wolters, S. L. Lane, W. Buijs, F. E. Edward, N. F. Haasen (DSM N.V., E.I. du Pont de Nemours and Company), *EP0729943A2*, **1996**; (c) W. Buijs, H. F. W. Wolters (DSM N.V., E.I. du Pont de Nemours and Company), *EP0729944A2*, **1996**; (d) H. F. W. Wolters, S. L. Lane, W. Buijs, N. F. Haasen, F. E. Herkes (DSM N.V., E.I. du Pont de Nemours and Company), *US5700934*, **1997**; (e) H. F. W. Wolters, S. L. Lane, W. Buijs, F. E. Herkes, N. F. Haasen (DSM N.V., E.I. du Pont de Nemours and Company), *US5717089*, **1998**; (f) R. P. M. Guit, W. Buijs (DSM N.V., E.I. du Pont de Nemours and Company), *WO98/09944*,**1998**.

[41] (a) F. Merger, R. Fischer, C.-U. Priester (BASF AG), *DE3843793A1*, **1990**; (b) E. Fuchs, T. Witzel (BASF AG), *DE4422610A1*, **1996**; (c) J. Ritz, E. Fuchs, G. Volt, G. Achhammer, R. Fischer (BASF AG), *US5693793*, **1997**; (d) W. Buijs, H. F. W. Wolters, R. P. M. Guit, F. P. W. Agterberg (DSM N.V.), *WO98/37063*, **1998**; (e) R. P. M. Guit, S. L. Lane (DSM N.V., E.I. du Pont de Nemours and Company), *WO99/42440*, **1999**. (f) F. Ohlbach, A. Ansmann, R.-H. Fischer, J.-P. Melder (BASF AG), *WO01/96294A1*, **2001**.

[42] K. Weissermel, H.-J. Arpe, *Industrielle Organische Chemie*, 5. Ausgabe, Wiley-VCH, Weinheim, **1998**, p. 509.

[43] (a) I. Nobuo, H. Motoyuki, O. Takashi, W. Natuko, W. Toshiyasu (Mitsubishi Gas Chemical Co.) *DE3040432A1* **1981**; (b) H.-W. Schneider, R. Kummer, D. Zimmerling (BASF AG) *EP0157311A2* **1985**; (c) W. Holderich, H. Aichinger, F. Naeumann, R. Fischer (BASF AG) *EP0266689B1* **1992**.

[44] R. H. Hasek (Eastman Kodak Co.), *US2777873*, **1957**.

[45] H. M. Hutmacher, F. J. Broecker, F. Merger, R. Fischer, U. Vagt, H. W. Schneider, W. Richter (BASF AG), *DE3602378A1*, **1987**.

[46] F. Merger, R. Fischer, W. Harder, C. U. Priester, U. Vagt (BASF AG), *DE3843792A1*, **1990**.

[47] I. Toth, O. J. Gelling, R. P. M. Guit, A. J. F. Simons, S. H. Niemann (DSM N.V., E.I. du Pont de Nemours and Company), *WO9702228A1*, **1997**.

[48] T. C. Eisenschmid, J. R. Briggs, D. L. Packett, K. D. Olson, J. M. Maher (Union Carbide Plastic), *WO9846565A1*, **1998**.

[49] F. E. Herkes, R. Pestman, J. A. F. Boogers (DSM N.V., E.I. du Pont de Nemours and Company), *WO9835938A1*, **1998**.

[50] S.-J. Chu, H.-Y. Hsu, C.-T. Lin, K.-C. Lai, J. H. Tsai (Industrial Technology Research Institute, Acelon Chemicals & Fiber Corporation), *US5977356A*, **1999**.

[51] R. Pestman, L. H. W. M. Van Lieshout (DSM N.V.), *EP0984002A1*, **2000**.

[52] (a) P. M. Burke (E.I. du Pont de Nemours and Company), *EP0188209A2*, **1986**; (b) R. Maerkl, W. Bertleff, H. J. Wilfinger, G. Schuch, W. Harder, G. Kuehn, P. Panitz (BASF AG), *EP0301450A1*, **1989**; (c) H. S. Jr. Bruner (E.I. du Pont de Nemours and Company), *WO9216476A2*, **1992**; (d) E. M. Atadan (E.I. du Pont de Nemours and Company), *US5218144A*, **1993**; (e) E. M. Atadan, J. H. S. Bruner (E.I. du Pont de Nemours and Company), *US5292944A*, **1994**; (f) G. Protzmann, G. Luft (DSM N.V.), *WO9933779A1*, **1999**; (g) M. Slany, M. Schaefer, M. Roeper (BASF AG), *WO2002046143A1*, **2002**; (h) E. E. Bunel, D. A. Clark, *US20030105348A1*, **2003**; (i) E. Drent, R. Van Ginkel, W. W. Jager (Shell Int. Research), *WO2004103942A1*, **2004**; (j) J. G. De Vries, N. Sereinig, E. W. M. Van de Vondervoort, M. C. C. Janssen (DSM IP Assests B.V.), *WO2012131028A1*, **2012**.

[53] A. M. C. F. Castelijns, M. C. C. Janssen, H. W. L. M. Vaessen (DSM IP Assests B.V.), *EP2537840A1*, **2012**.

[54] R. Kummer, F. Merger, W. Bertleff, R. Fischer (BASF AG), *EP0295551A2*, **1988**.

[55] A. Lambert, G. H. Lang (ICI Ltd.), *GB1178389*, **1970**.

[56] J. R. B. Boocock, F. T. Flood, B. J. Kershaw (DuPont Canada), *CA907059*, **1972**.

[57] J. R. B. Boocock, R. J. Paquin, D. B. Kelly (DuPont Canada), *CA907060*, **1972**.

[58] J. B. Zachry, C. L. Aldridge, B. Rouge (Exxon Research Engineering Co.), *US3253018*, **1966**.

[59] J. B. Zachry, C. L. Aldridge (Exxon Research Engineering Co.), *US3189619*, **1965**.

[60] W. Richter, W. Harder, R. Fischer, U. Vagt (BASF AG), *DE3823695A1*, **1990**.

[61] Y. Kobayashi, E. Takahisa, M. Nakano, K. Watantani, *Tetrahedron* **1997,** *53*, 1627-1634.

[62] M. Lorca, D. Kuhn, M. Kurosu, *Tetrahedron Lett.* **2001,** *42*, 6243-6246.

[63] A. Modi, R.-H. Fischer, T. Krug, T. Sirch (BASF AG), *DE10316658A1*, **2004**.

[64] R. Pinkos, T. Sirch, G.-D. Tebben, R.-H. Fischer (BASF SE), *WO2009100989A2*, **2009**.

[65] (a) O. Abillard, G.-D. Tebben, R. Pinkos, T. Wabnitz (BASF SE), *WO2010063659A2*, **2010**; (b) R. Pinkos, D. Breuninger, G.-D. Tebben (BASF SE), *WO2010115798A2*, **2010**; (c) R. Pinkos, D. Breuninger, G.-D. Tebben (BASF SE), *WO2010115738A1*, **2010**.

[66] K. Morikawa, S. Hirayama, Y. Ishimura, Y. Suyama, T. Nozawa, H. Monzen, M. Miura, K. Marumo, T. Naito (Showa Denko KK), *EP0724908A1*, **1996**.

[67] R. Fischer, R. Pinkos, F. Stein (BASF AG), *DE19750532A1*, **1999**.

[68] P. Yuan, Z. Liu, T. Hu, H. Sun, S. Liu, *React. Kinet. Mech. Catal.* **2010,** *100*, 427-439.

[69] K. Weissermel, H.-J. Arpe, *Industrielle Organische Chemie*, 5. Ausgabe, Wiley-VCH, Weinheim, **1998**, p. 509.

[70] (a) H.-G. Elias, *Macromolecules - Volume 2: Industrial Polymers and Syntheses*, Wiley-VCH, Weinheim, **2007**, 456 – 470; (b) A. J. Peacock, A. Calhoun, *Polymer Chemistry – Properties and Applications*, Carl Hanser Verlag, München, **2006**, 339 – 344.

[71] M. Rasch, *Technikgeschichte* **1987**, *54*, 104.

[72] G. D. Frey, *J. Organomet. Chem.* **2014**, *754*, 5.

[73] O. Roelen (Chem. Verwertungsges. Oberhausen GmbH), *GP849548*, **1938**.

[74] J. Hibbel, E. Wiebus, B. Cornils, *Chemie Ingenieur Technik* **2013**, *85*, 1853-1871.

[75] M. Beller, B. Cornils, C. D. Frohning, C. W. Kohlpaintner, *J. Mol. Catal. A* **1995**, *104*, 17.

[76] (a) R. Franke, D. Selent, A. Börner, *Chem. Rev.* **2012**, *112*, 5675–5732; (b) K. D. Wiese, D. Obst, *Top. Organomet. Chem.* **2006**, *18*, 1-33.

[77] D. Evans, J. A. Osborn, G. Wilkinson, *J. Chem. Soc.* **1968**, *0*, 3133-3142.

[78] C. A. Tolman, *Chem. Rev.* **1977**, *77*, 313-348.

[79] C. A. Tolman, *J. Am. Chem. Soc.* **1970**, *92*, 2956-2965.

[80] C. A. Tolman, *J. Am. Chem. Soc.* **1974**, *96*, 53-60.

[81] C. P. Casey, G. T. Whiteker, *Isr. J. Chem.* **1990**, *30*, 299-304.

[82] E. Drent, P. H. M. Budzelaar, *Chem. Rev.* **1996**, *96*, 663-681.

[83] G. Cavinato, L. Toniolo, *J. Organomet. Chem.* **1990**, 187-195.

[84] J. Liu, B. T. Heaton, J. A. Iggo, R. Whyman, *Angew. Chem. Int. Ed.* **2004**, *43*, 90-94.

[85] (a) A. Brennführer, H. Neumann, M. Beller, *ChemCatChem* **2009**, 1, 28-41; (b) I. del Río, C. Claver, P. W. N. M. van Leeuwen *Eur. J. Inorg. Chem.* **2001**, 2719-2738; (c) E. Drent, P. H. M. Budzelaar, *J. Org. Chem.* **2000**, *593-594*, 211-225.

[86] (a) A. Börner, R. Franke, *Hydroformylation: Fundamentals, Processes, and Applications in Organic Synthesis*, Wiley-VCH, Weinheim, **2016**, 464-490. (b) D. E. Fogg, E. N. Dos Santos, *Coord. Chem. Rev.* **2004**, *248*, 2365-2379. (c) J.-C. Wasilke, S. J. Obrey, R. T. Baker, G. C. Bazan, *Chem. Rev.* **2005**, *105*, 1001-1020.

[87] (a) P. Kalck, M. Urrutigoïty, *Chem. Rev.* **2018**, *118*, 3833-3861; (b) A. Fabrello, A. Bachelier, M. Urrutigoïty, P. Kalck, *Coord. Chem. Rev.* **2010**, *254*, 273-287.

[88] (a) A. F. M. Iqbal, *Helv. Chim. Acta* **1971**, *54*, 1440-1445; (b) J. F. Knifton, D. C Alexander, *Isr. J. Chem.* **1986**, *27*, 255-261; (c) A. Schmidt, M. Marchetti, P. Eilbracht, *Tetrahedron* **2004**, *60*, 11487-11492.

[89] A. I. M. Keulemans, A. Kwantes, Th. Van Bavel, *Recl. Trav. Chim. Pays-Bas* **1948**, *67*, 298-308.

[90] G. R. Eastham, B. T. Heaton, J. A. Iggo, R. P. Tooze, R. Whyman, S. Zacchini, *Chem. Commun.* **2000**, 609-610.

[91] K. Dong, R. Sang, Z. Wei, J. Liu, R. Dühren, A. Spannenberg, H. Jiao, H. Neumann, R. Jackstell, R. Franke, M. Beller, *Chem. Sci.* **2018**, *9*, 2510-2516.

[92] G. Wilke, *Angew. Chem.* **1963**, *1*, 10-20.

[93] R. W. Cruse, V. Khare, J. Kowalski, W. Stanczyk (Momentive Performance Mat. Inc.), *US20130018212A1*, **2013**.

[94] W. Schroeder, T. Keil (Huels Chemische Werke AG), *EP0495175A2*, **1992**.

[95] A. M. Allgeier, C. P. Lenges, R. Shapiro, W. Tam, *US20040122252A1*, **2004**.

[96] D. D. Perrin, W. L. F. Amarego in *Purification of Laboratory Chemicals*, Pergamon Press, Oxford, **1988**.

[97] (a) W. Clegg, M. R. J. Elsegood, G. R. Eastham, R. P. Tooze, X. Lan Wang and K. Whiston, *Chem. Commun.* **1999**, 1877-1878; (b) C. J. Rodriguez, D. F. Foster, G. R. Eastham and D. J. Cole-Hamilton, *Chem. Commun.* **2004**, 1720-1721; (c) K. Dong, R. Sang, Z. Wei, J. Liu, R. Dühren, A. Spannenberg, H. Jiao, H. Neumann, R. Jackstell, R. Franke, M. Beller, *Chem. Sci.* **2018**, 9, 2510 – 2516.

[98] K. M. Dyballa, R. Franke, C. Weilbeer, D. Selent, A. Börner (Evonik Degussa GmbH), *US2017/158723A1*, **2017**.

A. Appendix

A.1. Hydroformylation of isomeric methyl pentenoates

A.1.1. Hydroformylation of methyl 2-pentenoate

Table 5, Entry 1

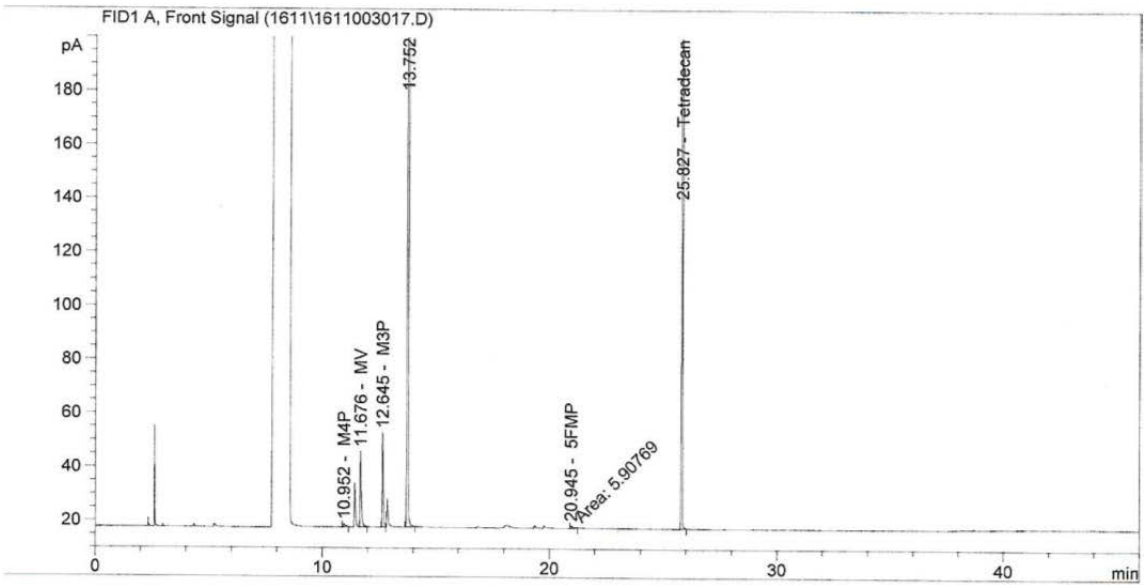

Appendix Fig. 1: Gas chromatogram (GC-FID) of Table 5, Entry 1.

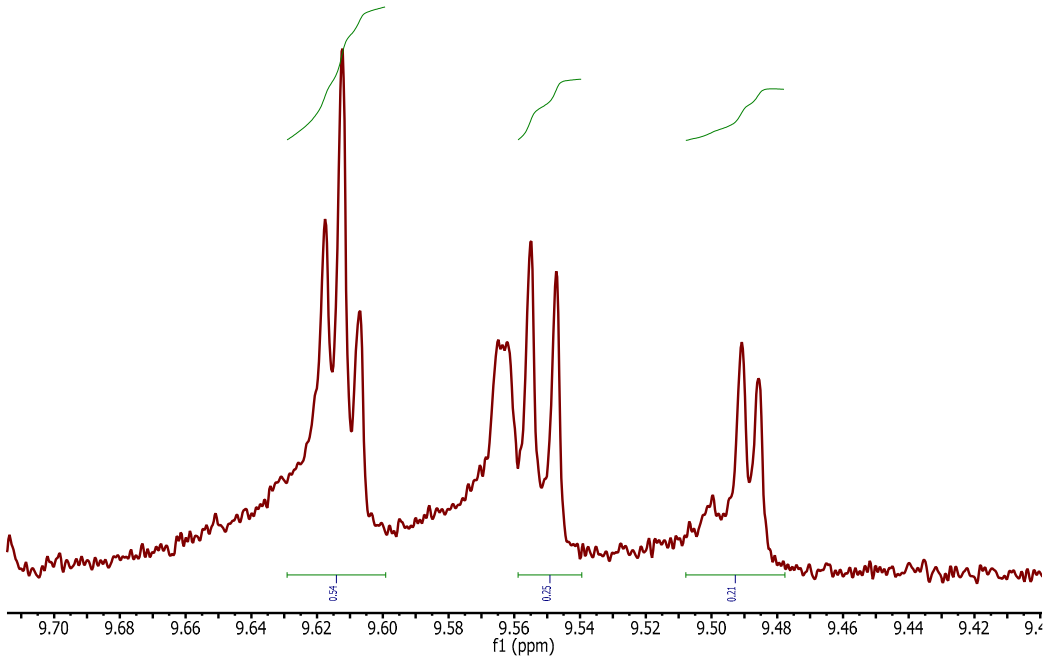

Appendix Fig. 2: ^{1}H NMR in CD_2Cl_2 at rt of the product mixture. Corresponds to Table 5, Entry 1.

Substance	Retention time [min]	Area
Methyl valerate	11.676	109.02589
Methyl 4-pentenoate	10.952	6.68779
Methyl 3-pentenoate	12.645	115.64047
Methyl 2-pentenoate	13.752	255.04566
Methyl 5-formylvalerate	20.945	5.90769

Table 5, Entry 2

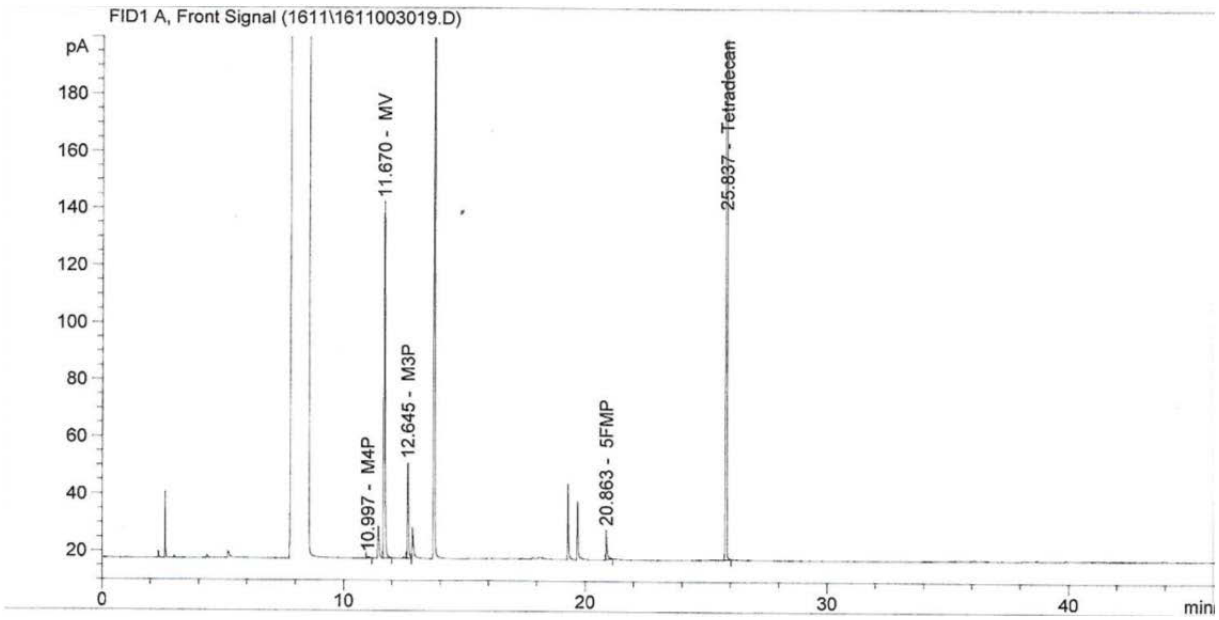

Appendix Fig. 3: Gas chromatogram (GC-FID) of Table 5, Entry 2.

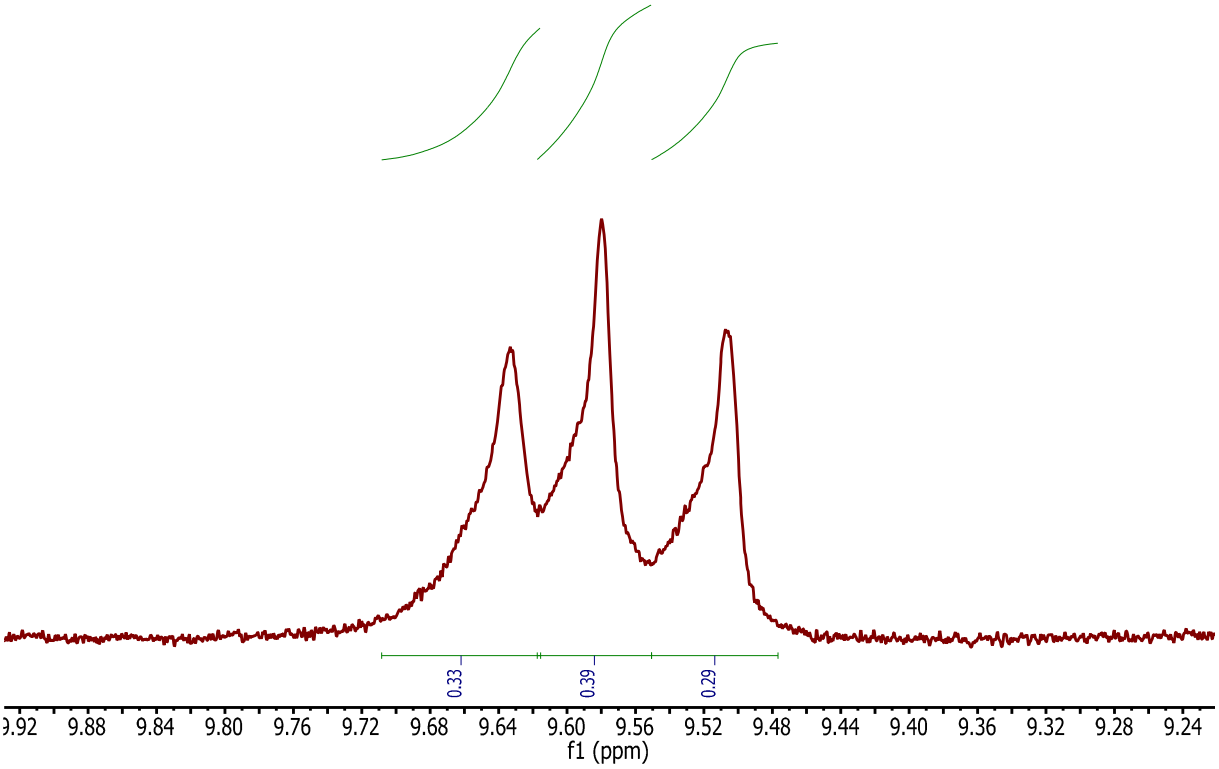

Appendix Fig. 4: ^{1}H NMR in CD2Cl2 at rt of the product mixture. Corresponds to Table 5, Entry 2.

Substance	Retention time [min]	Area
Methyl valerate	11.676	446.92996
Methyl 4-pentenoate	10.952	3.07325
Methyl 3-pentenoate	12.645	108.39088
Methyl 2-pentenoate	13.752	
Methyl 5-formylvalerate	20.945	32.81614

Table 6, Entry 1

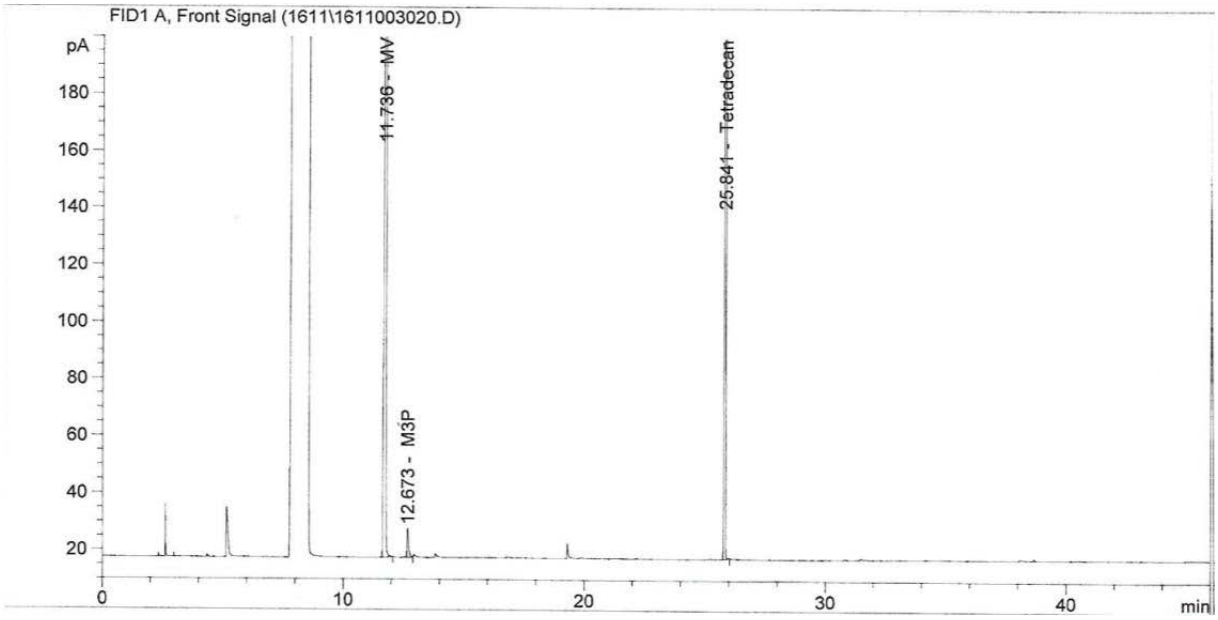

Appendix Fig. 5: Gas chromatogram (GC-FID) of Table 6, Entry 1.

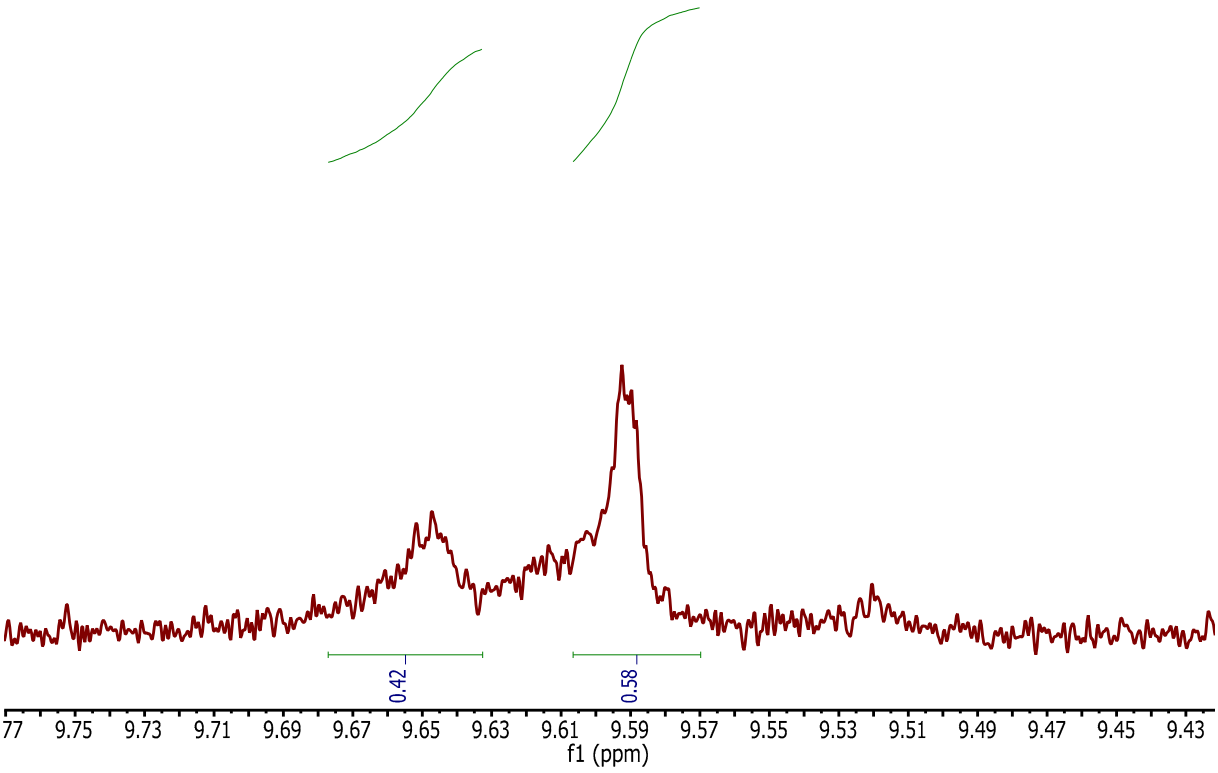

Appendix Fig. 6: ^{1}H NMR in CD2Cl2 at rt of the product mixture. Corresponds to Table 6, Entry 1.

Substance	Retention time [min]	Area
Methyl valerate	11.7	2219.26978
Methyl 4-pentenoate	11.0	-
Methyl 3-pentenoate	12.6	37.94210
Methyl 2-pentenoate	13.8	-
Methyl 5-formylvalerate	20.9	-

Table 6, Entry 2

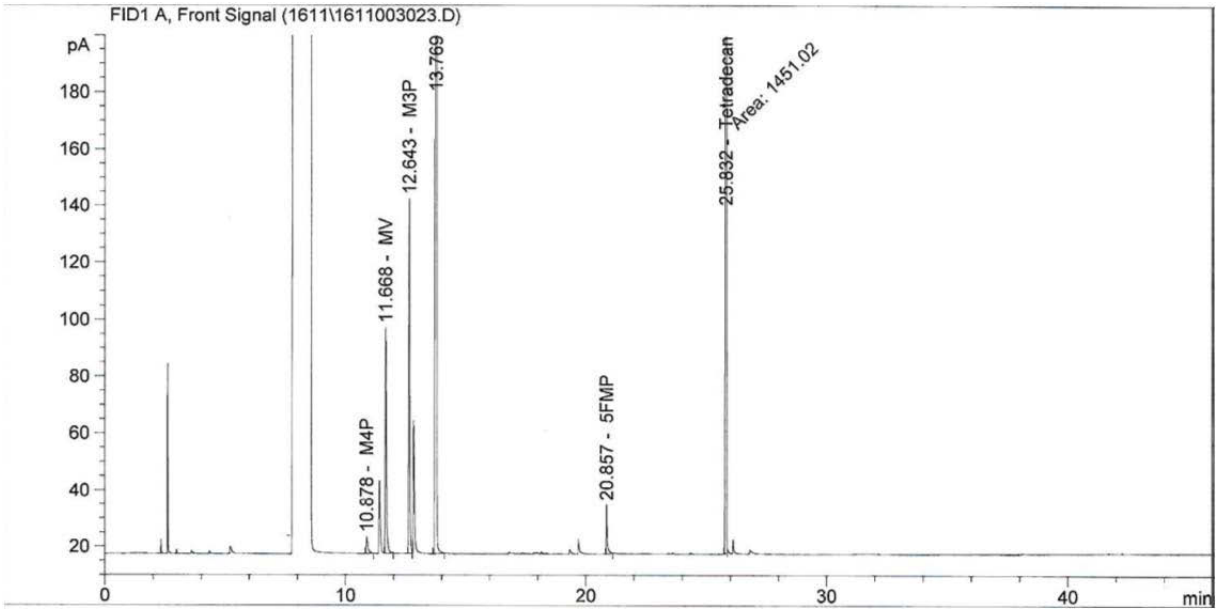

Appendix Fig. 7: Gas chromatogram (GC-FID) of Table 6, Entry .

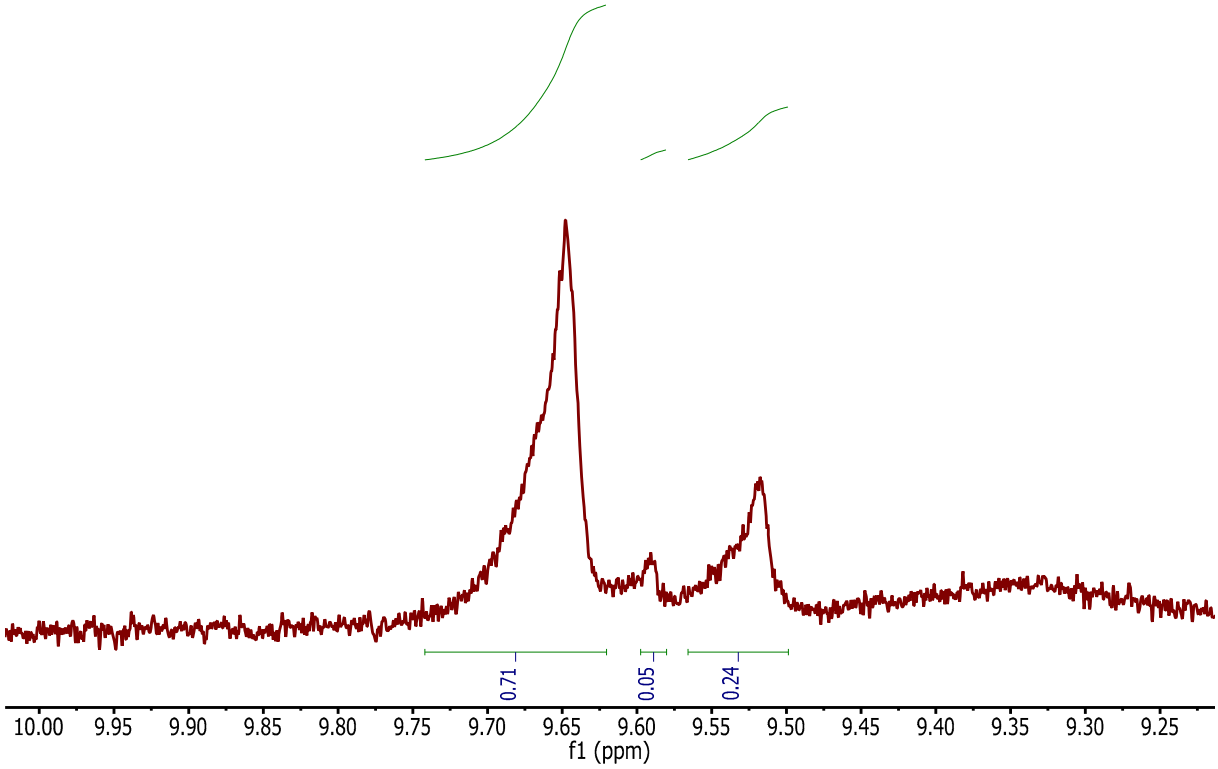

Appendix Fig. 8: 1H NMR in CD2Cl2 at rt of the product mixture. Corresponds to Table 6, Entry 2.

Substance	Retention time [min]	Area
Methyl valerate	11.7	290.42569
Methyl 4-pentenoate	10.9	28.40268
Methyl 3-pentenoate	12.6	389.72668
Methyl 2-pentenoate	13.7	
Methyl 5-formylvalerate	20.9	49.54668

A.1.2. Comparison of different stirring techniques with regard to conversion, yield and *n*-regioselectivity in the Rh catalysed hydroformylation of methyl 3-pentenoate

Table 7, Entry 1

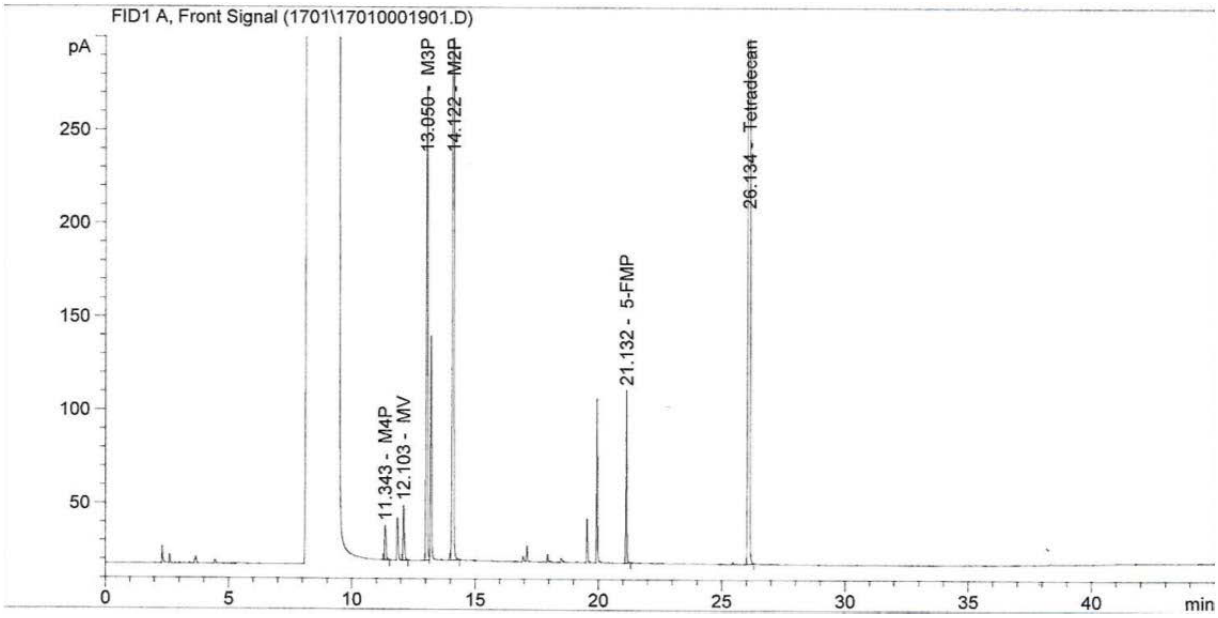

Appendix Fig. 9: Gas chromatogram (GC-FID) of Table 7, Entry 1.

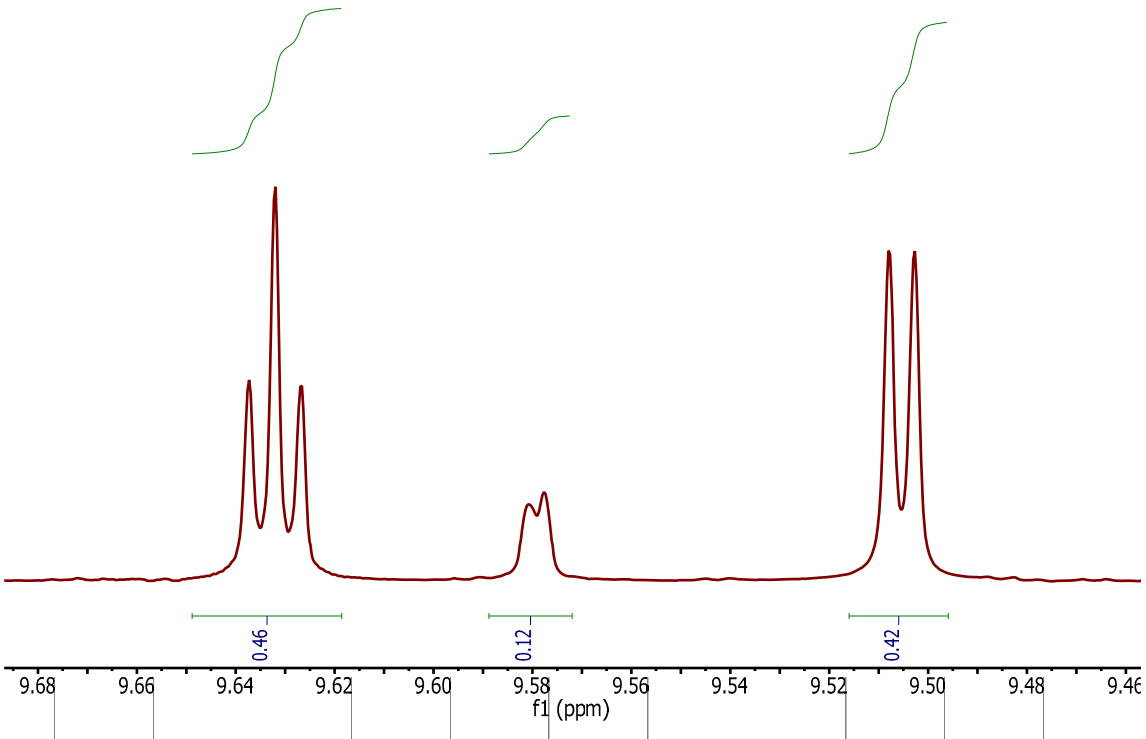

Appendix Fig. 10: ^{1}H NMR in CD2Cl2 at rt of the product mixture. Corresponds to Table 7, Entry 1.

Substance	Retention time [min]	Area
Methyl valerate	12.1	105.93140
Methyl 4-pentenoate	11.3	70.70728
Methyl 3-pentenoate	13.1	892.05621
Methyl 2-pentenoate	14.1	1817.72937
Methyl 5-formylvalerate	21.1	207.36900

Table 7, Entry 2

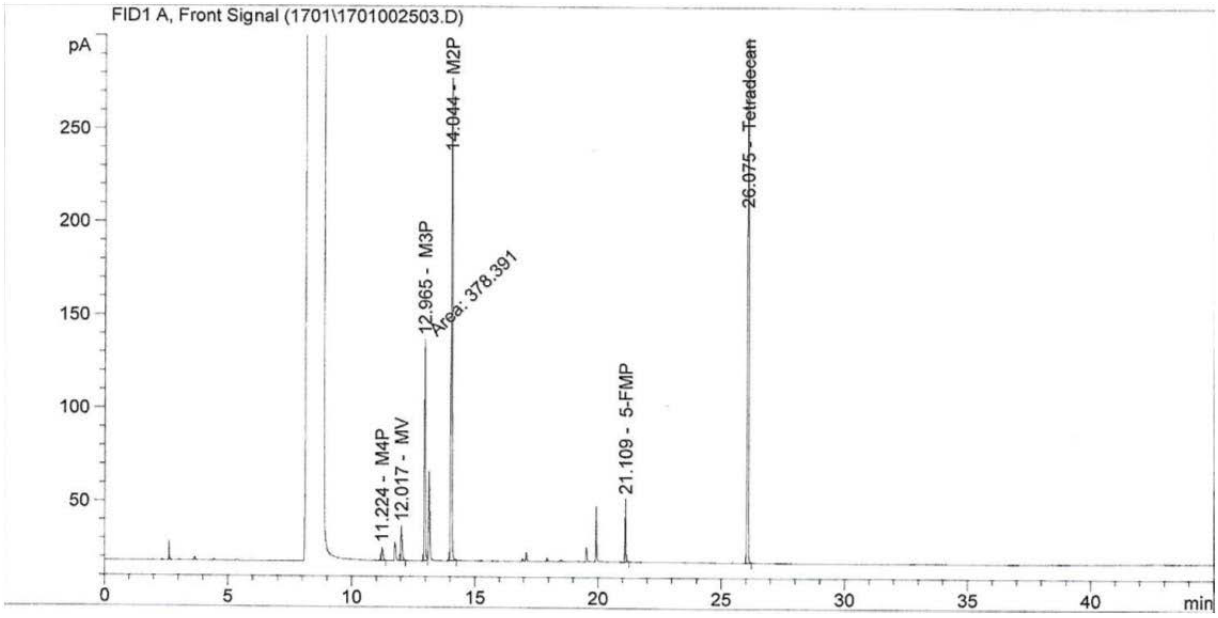

Appendix Fig. 11: Gas chromatogram (GC-FID) of Table 7, Entry 2.

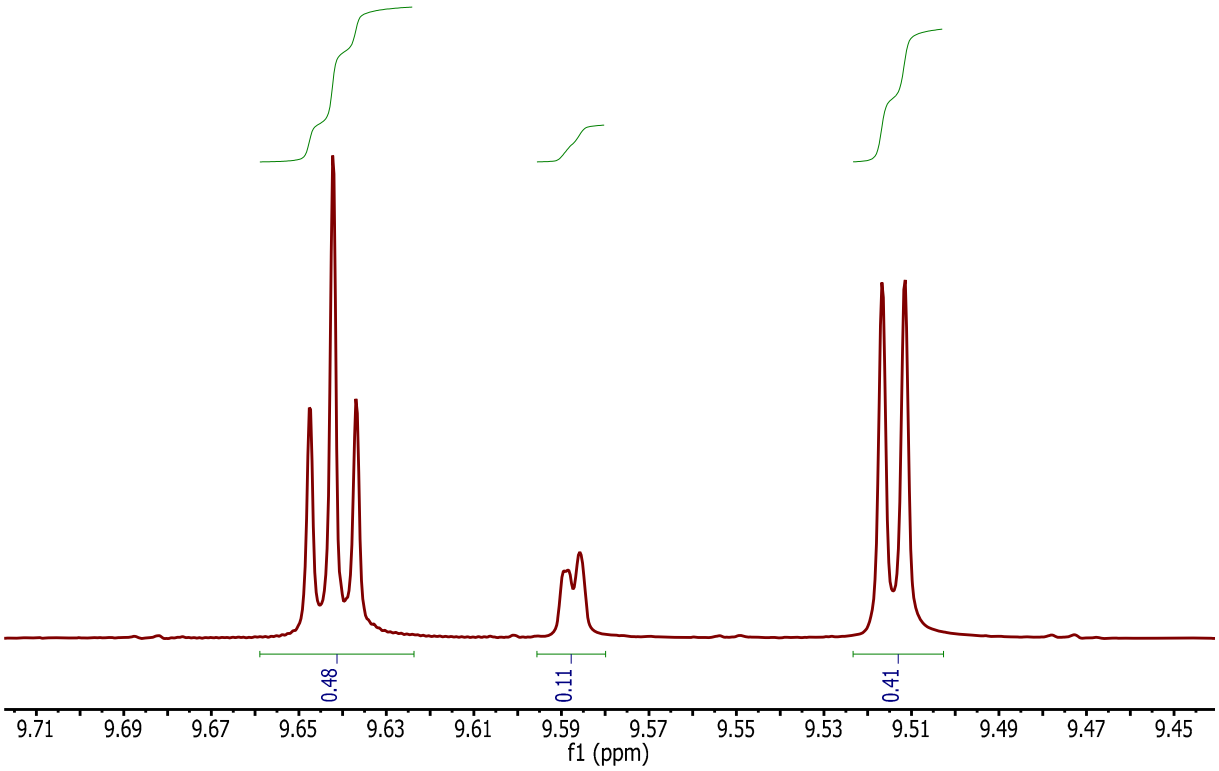

Appendix Fig. 12: ^{1}H NMR in CD2Cl2 at rt of the product mixture. Corresponds to Table 7, Entry 2.

Substance	Retention time [min]	Area
Methyl valerate	12.0	67.49003
Methyl 4-pentenoate	11.2	28.77292
Methyl 3-pentenoate	13.0	378.39148
Methyl 2-pentenoate	14.0	827.43396
Methyl 5-formylvalerate	21.1	73.36356

A.1.3. Optimisation of reaction conditions for the two phasic hydroformylation of methyl pentenoates with a BINAS-modified Rh(I)-catalyst

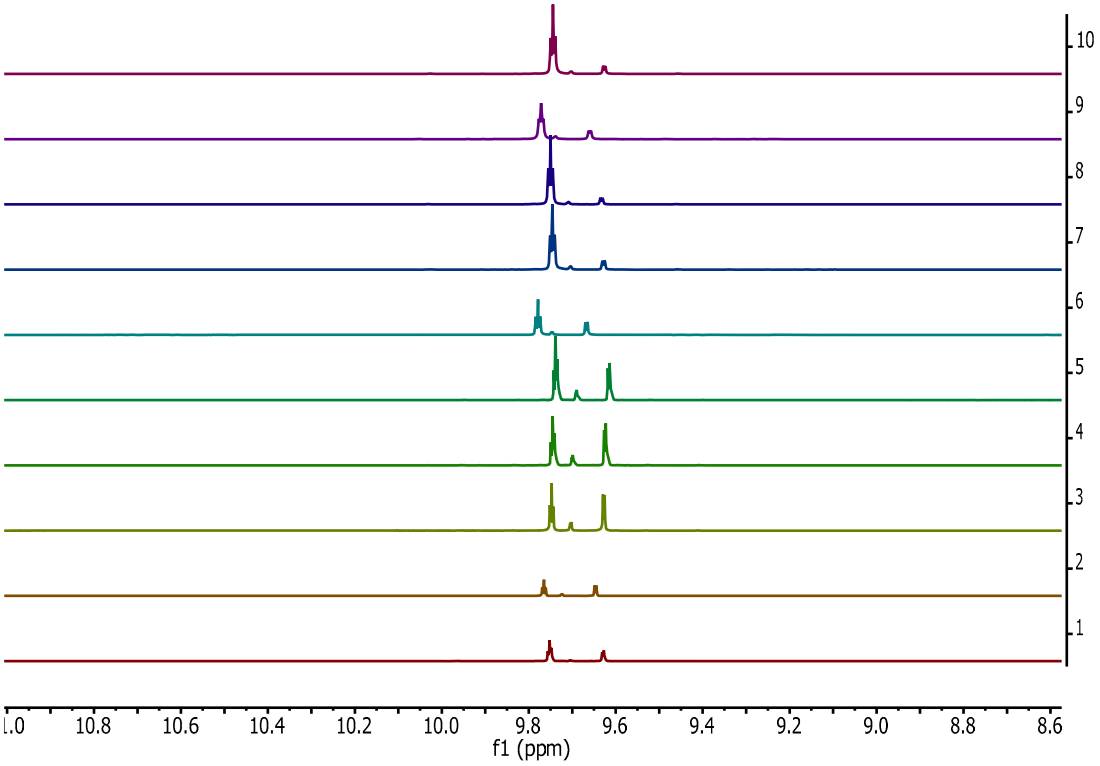

Appendix Fig. 13: Stacked ^{1}H NMR spectra of the product mixtures of table 8

Table 8, Entry 1

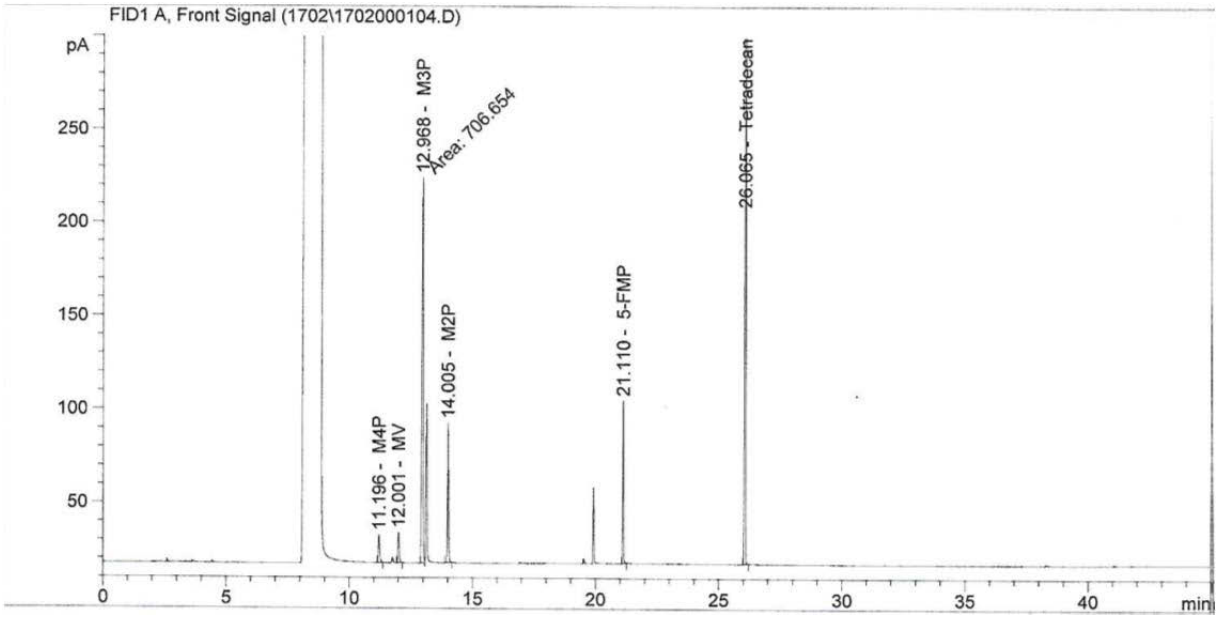

Appendix Fig. 14: Gas chromatogram (GC-FID) of Table 8, Entry 1.

Substance	Retention time [min]	Area
Methyl valerate	12.0	58.27884
Methyl 4-pentenoate	11.2	59.03115
Methyl 3-pentenoate	13.0	706.65350
Methyl 2-pentenoate	14.0	216.00923
Methyl 5-formylvalerate	21.1	190.38226

Table 8, Entry 2

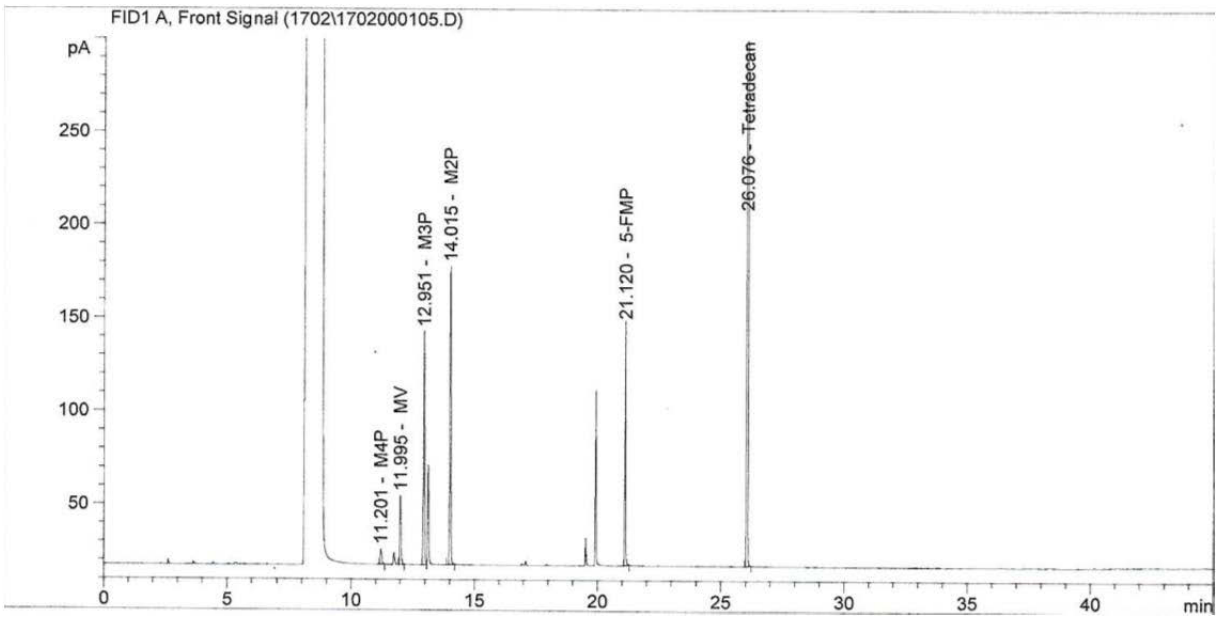

Appendix Fig. 15: Gas chromatogram (GC-FID) of Table 8, Entry 2.

Substance	Retention time [min]	Area
Methyl valerate	12.0	133.52547
Methyl 4-pentenoate	11.2	33.59358
Methyl 3-pentenoate	13.0	402.23978
Methyl 2-pentenoate	14.0	479.52673
Methyl 5-formylvalerate	21.1	316.08783

Table 8, Entry 3

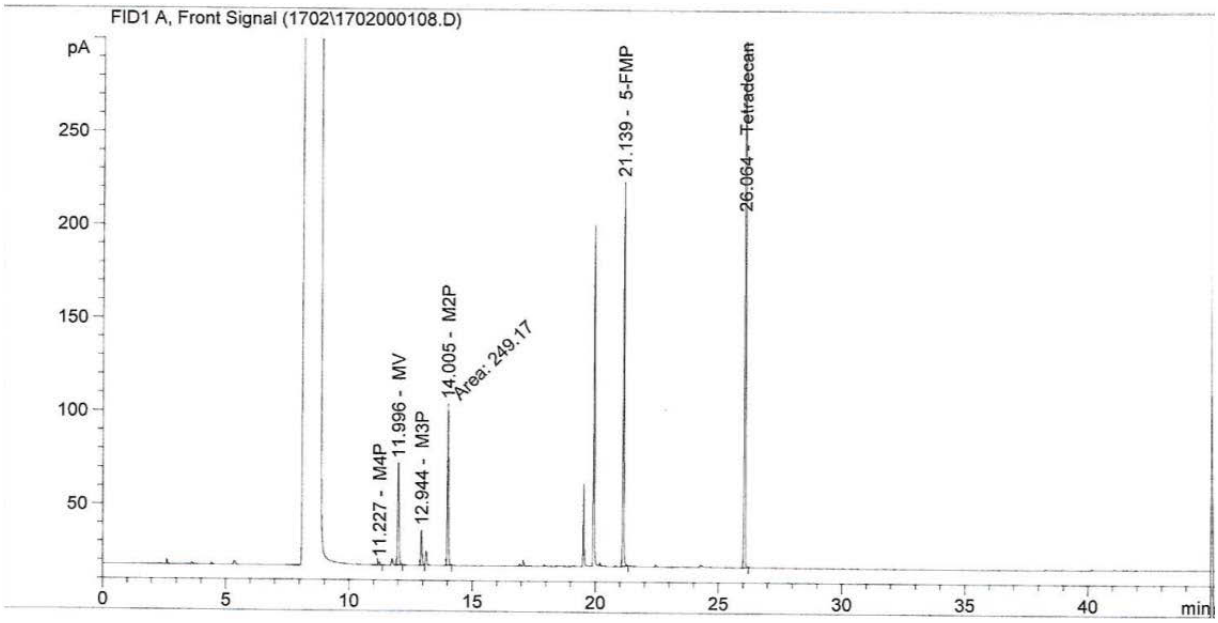

Appendix Fig. 16: Gas chromatogram (GC-FID) of Table 8, Entry 3.

Substance	Retention time [min]	Area
Methyl valerate	12.0	197.12291
Methyl 4-pentenoate	11.2	5.98382
Methyl 3-pentenoate	13.0	62.36082
Methyl 2-pentenoate	14.0	249.17021
Methyl 5-formylvalerate	21.1	564.46179

Table 8, Entry 4

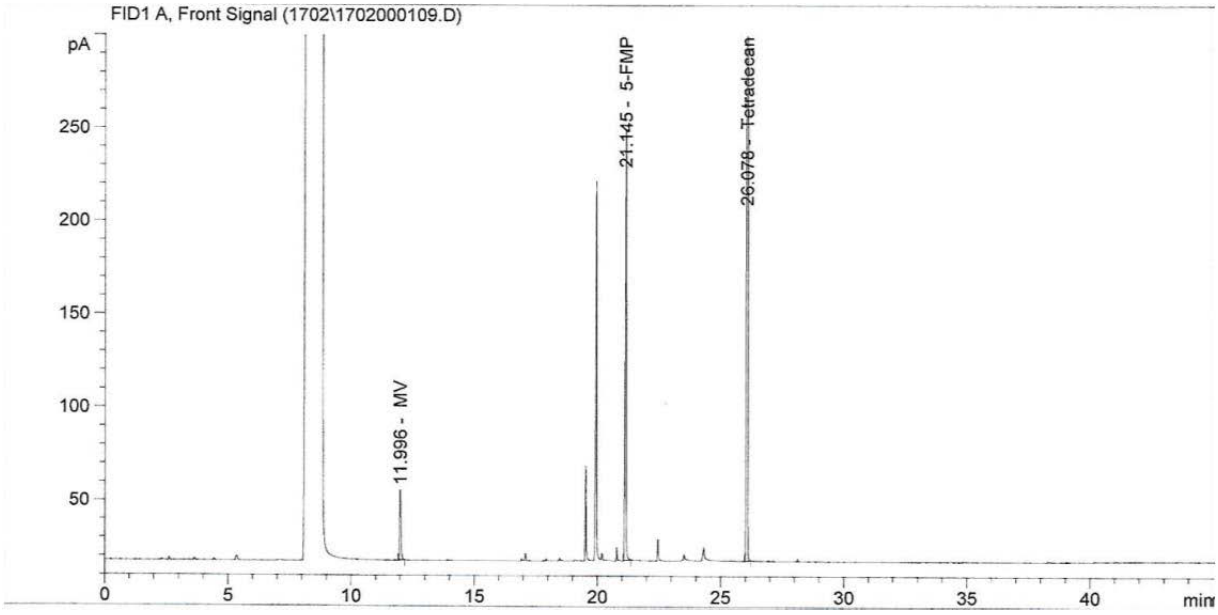

Appendix Fig. 17: Gas chromatogram (GC-FID) of Table 8, Entry 4.

Substance	Retention time [min]	Area
Methyl valerate	12.0	137.68823
Methyl 4-pentenoate	11.2	-
Methyl 3-pentenoate	13.0	-
Methyl 2-pentenoate	14.0	-
Methyl 5-formylvalerate	21.1	669.33496

Table 8, Entry 5

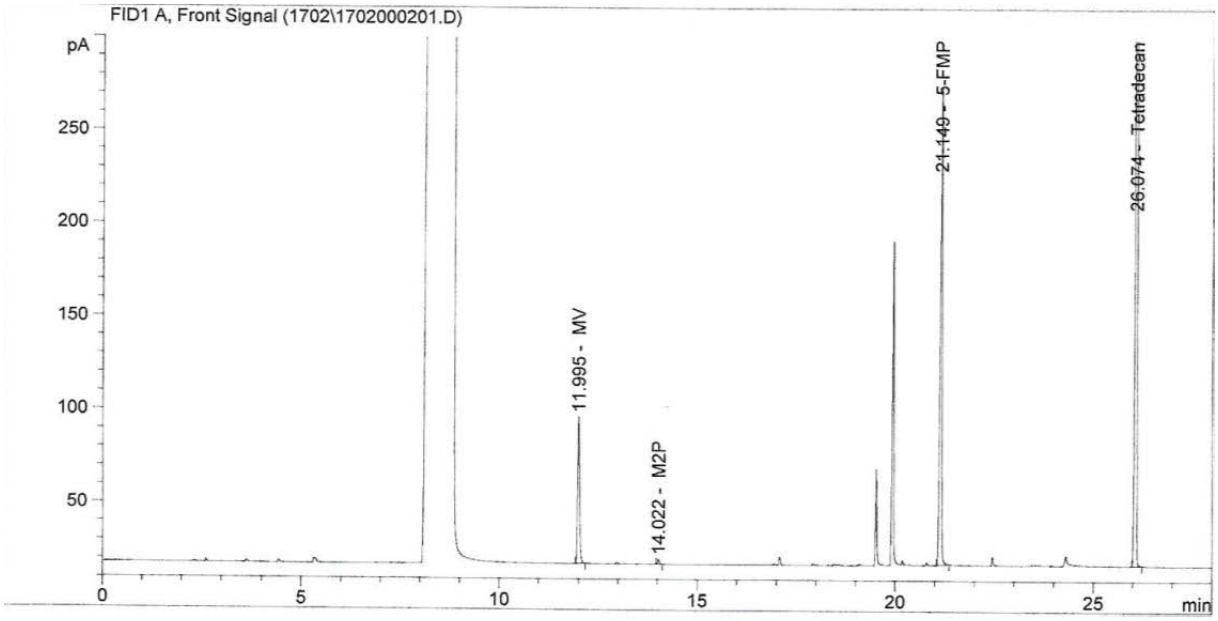

Appendix Fig. 18: Gas chromatogram (GC-FID) of Table 8, Entry 5.

Substance	Retention time [min]	Area
Methyl valerate	12.0	281.97568
Methyl 4-pentenoate	11.2	-
Methyl 3-pentenoate	13.0	-
Methyl 2-pentenoate	14.0	7.22884
Methyl 5-formylvalerate	21.1	784.04321

Table 8, Entry 6

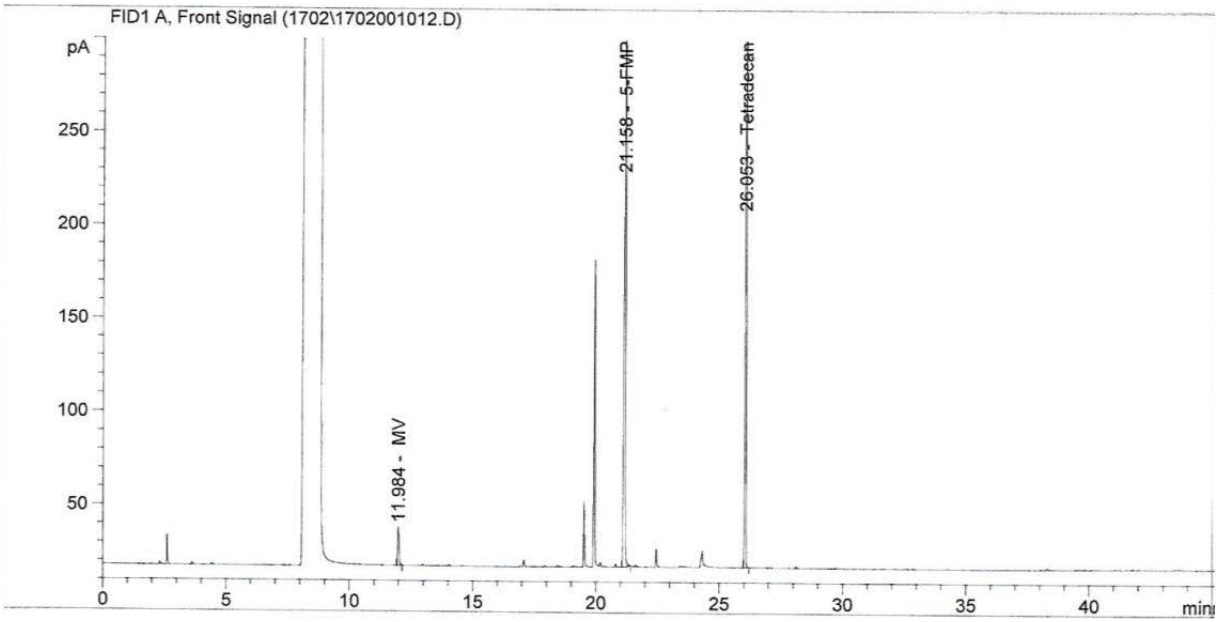

Appendix Fig. 19: Gas chromatogram (GC-FID) of Table 8, Entry 6.

Substance	Retention time [min]	Area
Methyl valerate	12.0	74.31973
Methyl 4-pentenoate	11.2	-
Methyl 3-pentenoate	13.0	-
Methyl 2-pentenoate	14.0	-
Methyl 5-formylvalerate	21.1	1139.89893

Table 8, Entry 7

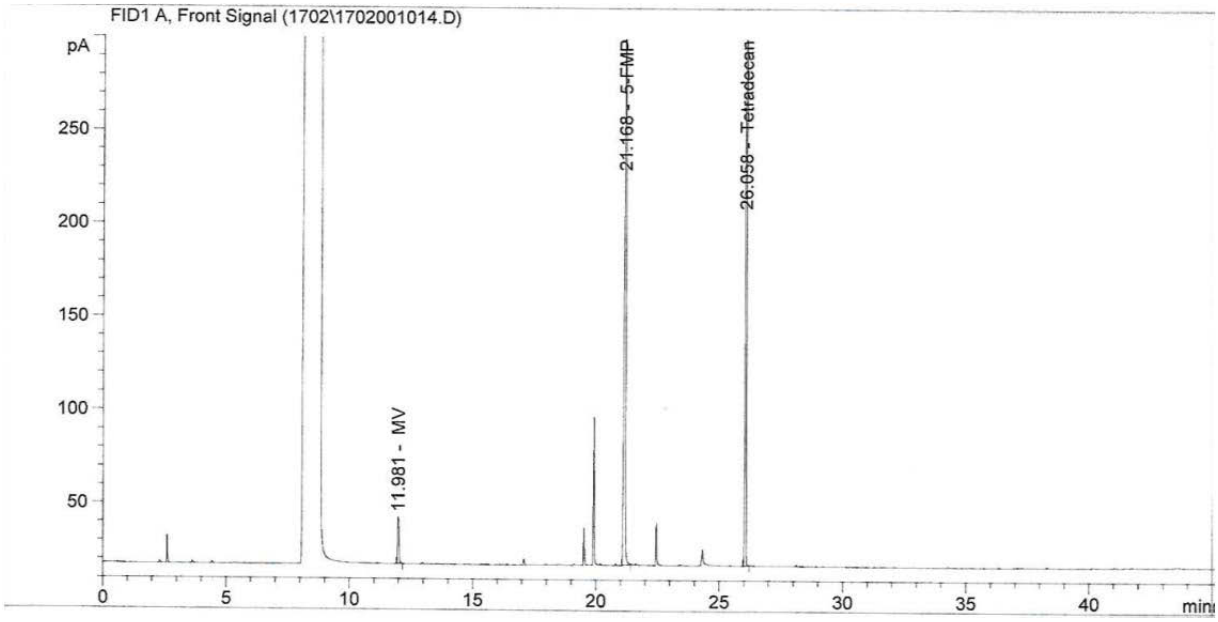

Appendix Fig. 20: Gas chromatogram (GC-FID) of Table 8, Entry 7.

Substance	Retention time [min]	Area
Methyl valerate	12.0	92.19870
Methyl 4-pentenoate	11.2	-
Methyl 3-pentenoate	13.0	-
Methyl 2-pentenoate	14.0	-
Methyl 5-formylvalerate	21.1	1414.18140

Table 8, Entry 8

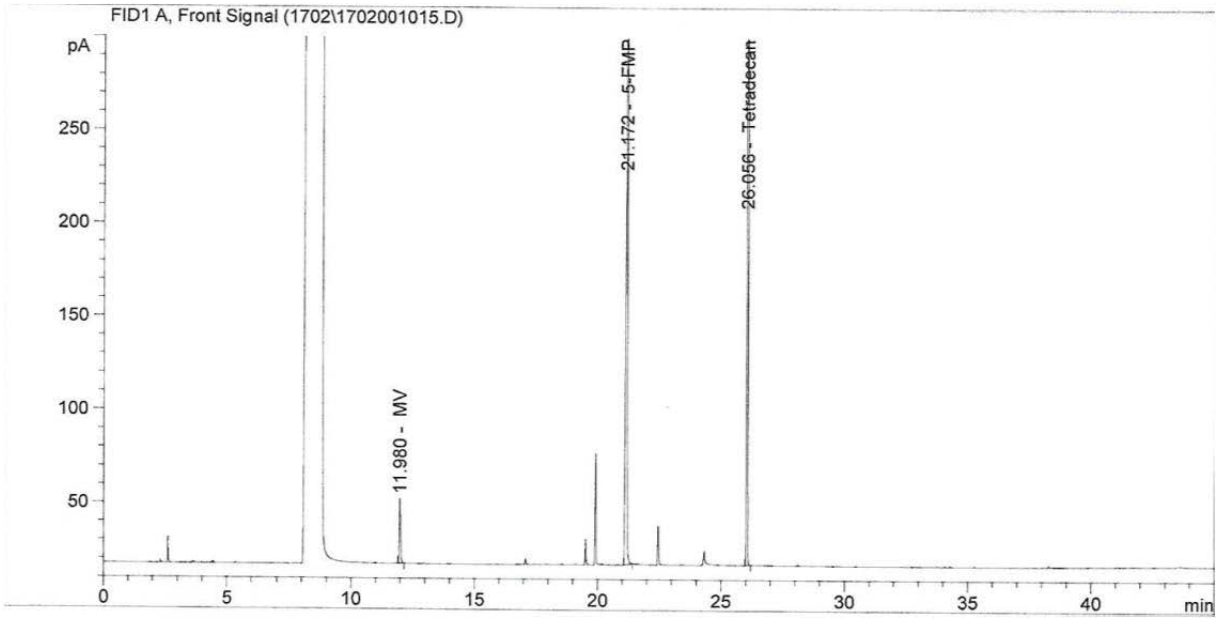

Appendix Fig. 21: Gas chromatogram (GC-FID) of Table 8, Entry 8.

Substance	Retention time [min]	Area
Methyl valerate	12.0	127.22628
Methyl 4-pentenoate	11.2	-
Methyl 3-pentenoate	13.0	-
Methyl 2-pentenoate	14.0	-
Methyl 5-formylvalerate	21.1	1500.22766

Table 8, Entry 9

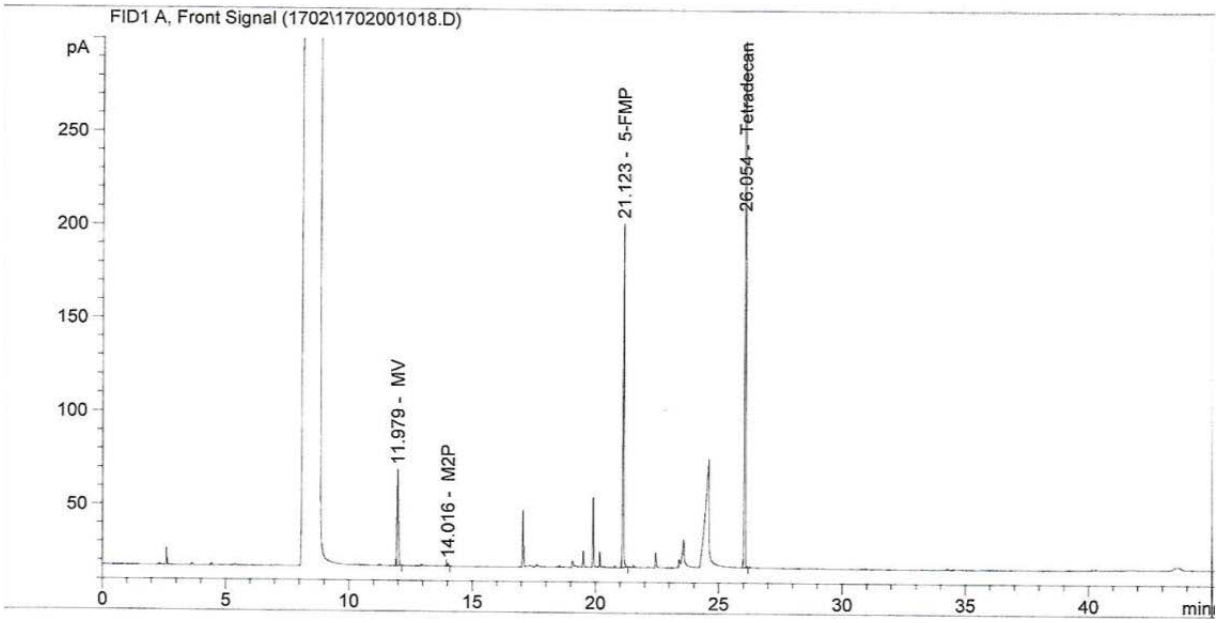

Appendix Fig. 22: Gas chromatogram (GC-FID) of Table 8, Entry 9.

Substance	Retention time [min]	Area
Methyl valerate	12.0	185.51236
Methyl 4-pentenoate	11.2	-
Methyl 3-pentenoate	13.0	-
Methyl 2-pentenoate	14.0	4.53925
Methyl 5-formylvalerate	21.1	490.88638

Table 8, Entry 10

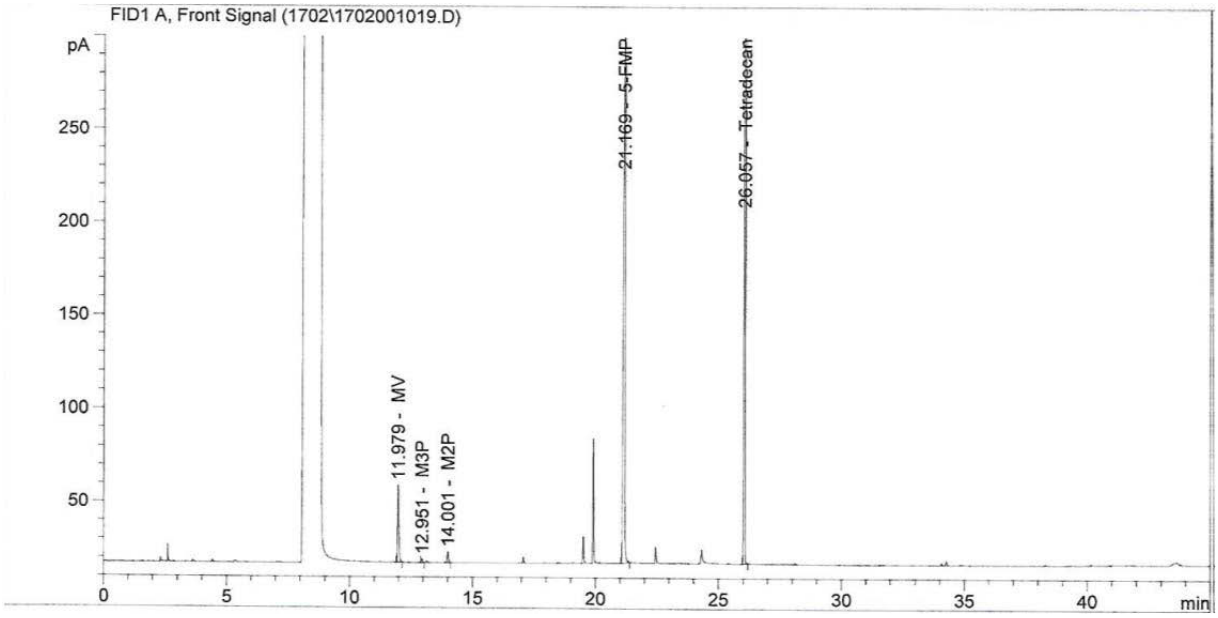

Appendix Fig. 23: Gas chromatogram (GC-FID) of Table 8, Entry 10.

Substance	Retention time [min]	Area
Methyl valerate	12.0	150.54105
Methyl 4-pentenoate	11.2	-
Methyl 3-pentenoate	13.0	5.88986
Methyl 2-pentenoate	14.0	17.32132
Methyl 5-formylvalerate	21.1	1442.29626

A.1.4. Optimisation of reaction conditions for the homogeneous hydroformylation of methyl pentenoates with a BiphePhos-modified Rh(I)-catalyst

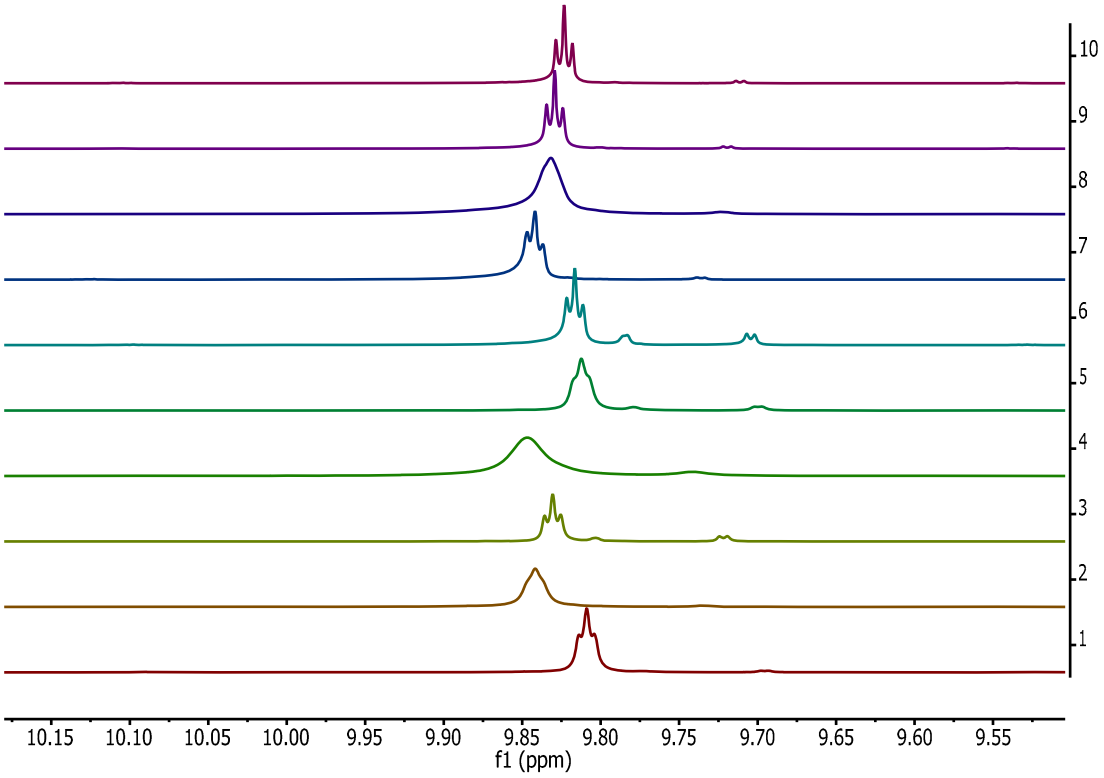

Appendix Fig. 24: Stacked ^{1}H NMR spectra of the product mixtures of table 9.

Table 9, Entry 1

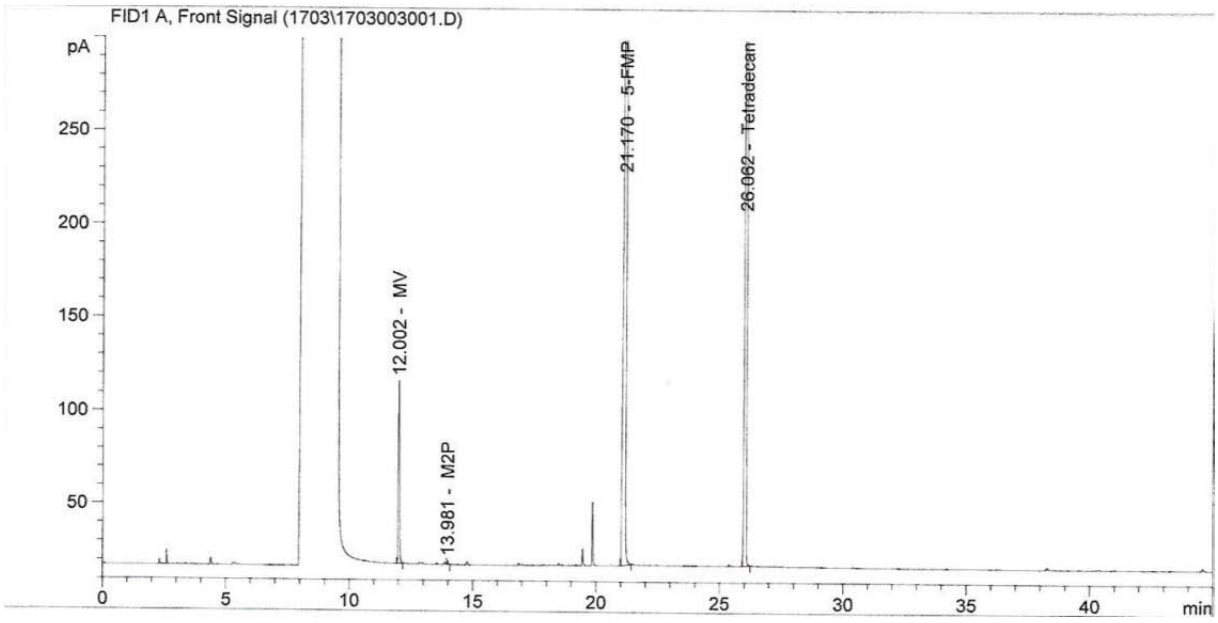

Appendix Fig. 25: Gas chromatogram (GC-FID) of Table 9, Entry 1.

Substance	Retention time [min]	Area
Methyl valerate	12.0	341.62698
Methyl 4-pentenoate	11.2	-
Methyl 3-pentenoate	13.0	-
Methyl 2-pentenoate	14.0	5.96534
Methyl 5-formylvalerate	21.2	3580.38867

Table 9, Entry 2

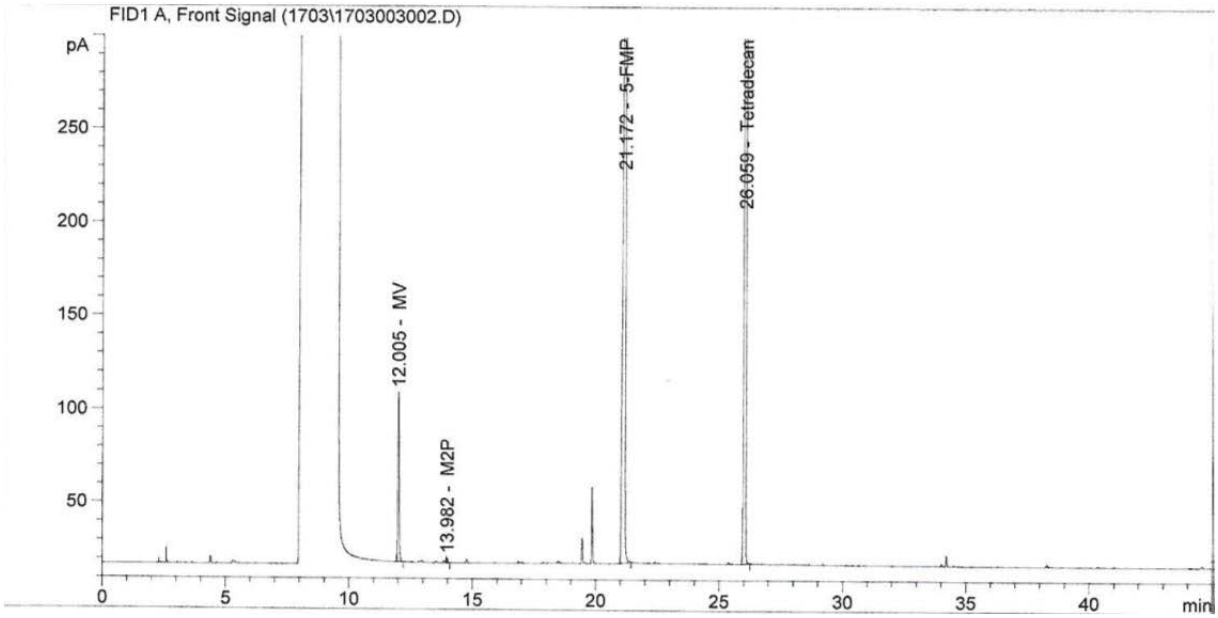

Appendix Fig. 26: Gas chromatogram (GC-FID) of Table 9, Entry 2.

Substance	Retention time [min]	Area
Methyl valerate	12.0	316.49695
Methyl 4-pentenoate	11.2	-
Methyl 3-pentenoate	13.0	-
Methyl 2-pentenoate	14.0	6.94438
Methyl 5-formylvalerate	21.2	3652.43091

Table 9, Entry 3

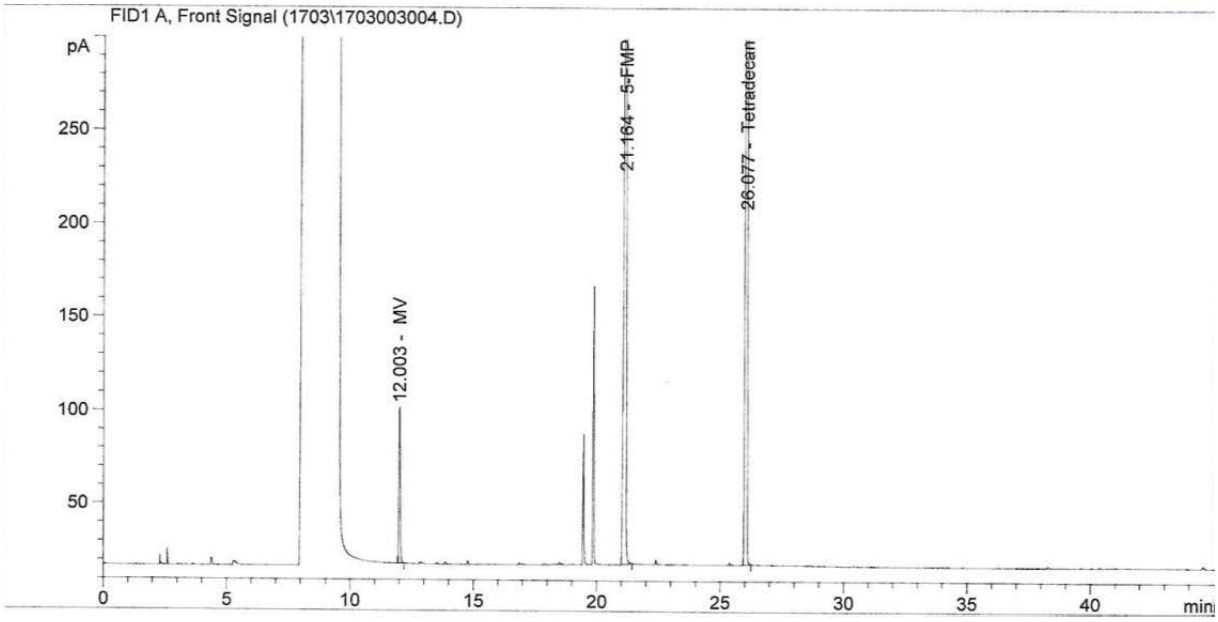

Appendix Fig. 27: Gas chromatogram (GC-FID) of Table 9, Entry 3.

Substance	Retention time [min]	Area
Methyl valerate	12.0	290.56848
Methyl 4-pentenoate	11.2	-
Methyl 3-pentenoate	13.0	-
Methyl 2-pentenoate	14.0	-
Methyl 5-formylvalerate	21.2	3367.05273

Table 9, Entry 4

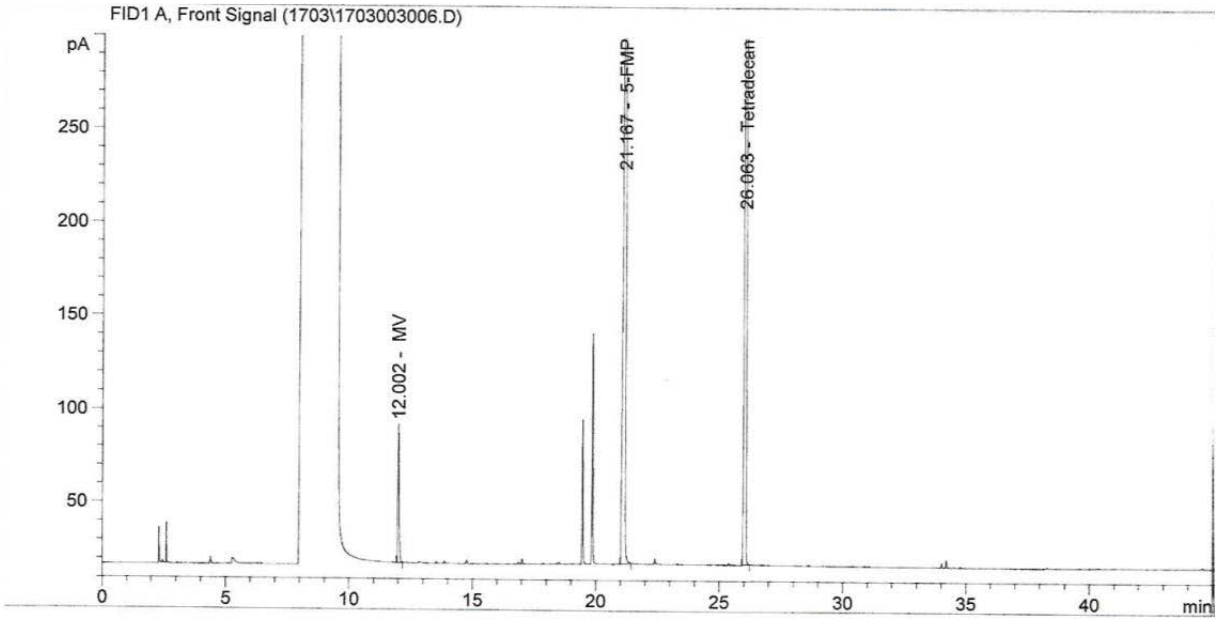

Appendix Fig. 28: Gas chromatogram (GC-FID) of Table 9, Entry 4.

Substance	Retention time [min]	Area
Methyl valerate	12.0	256.08514
Methyl 4-pentenoate	11.2	-
Methyl 3-pentenoate	13.0	-
Methyl 2-pentenoate	14.0	-
Methyl 5-formylvalerate	21.2	3444.64429

Table 9, Entry 5

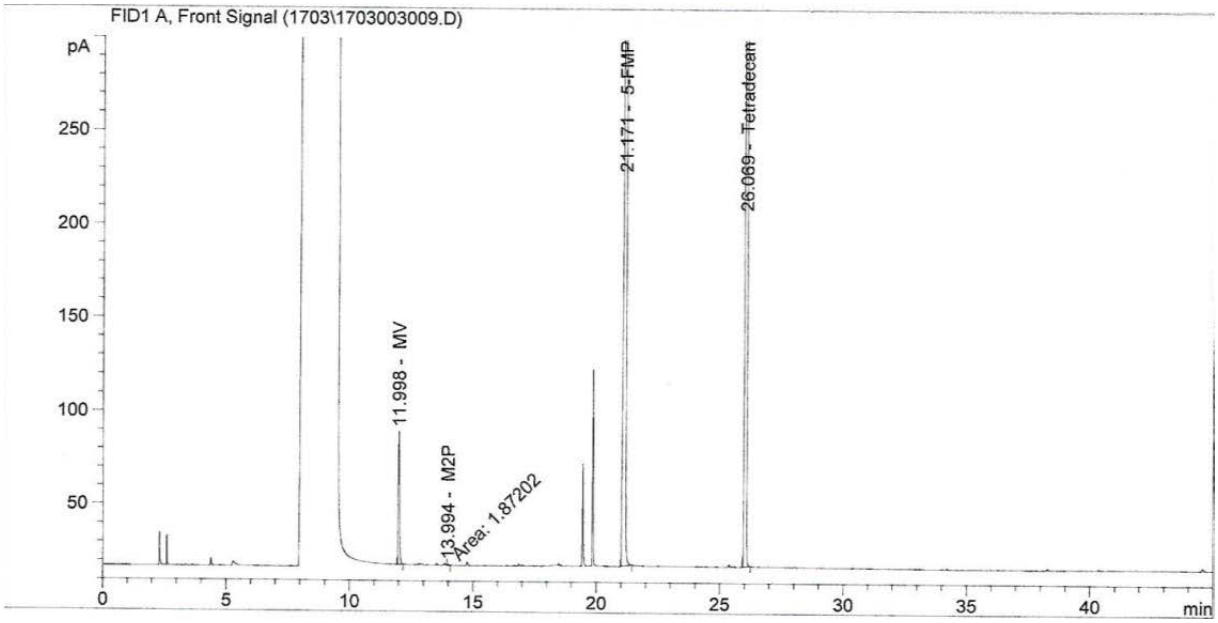

Appendix Fig. 29: Gas chromatogram (GC-FID) of Table 9, Entry 5.

Substance	Retention time [min]	Area
Methyl valerate	12.0	245.43236
Methyl 4-pentenoate	11.2	-
Methyl 3-pentenoate	13.0	-
Methyl 2-pentenoate	14.0	1.87202
Methyl 5-formylvalerate	21.2	3638.69580

Table 9, Entry 6

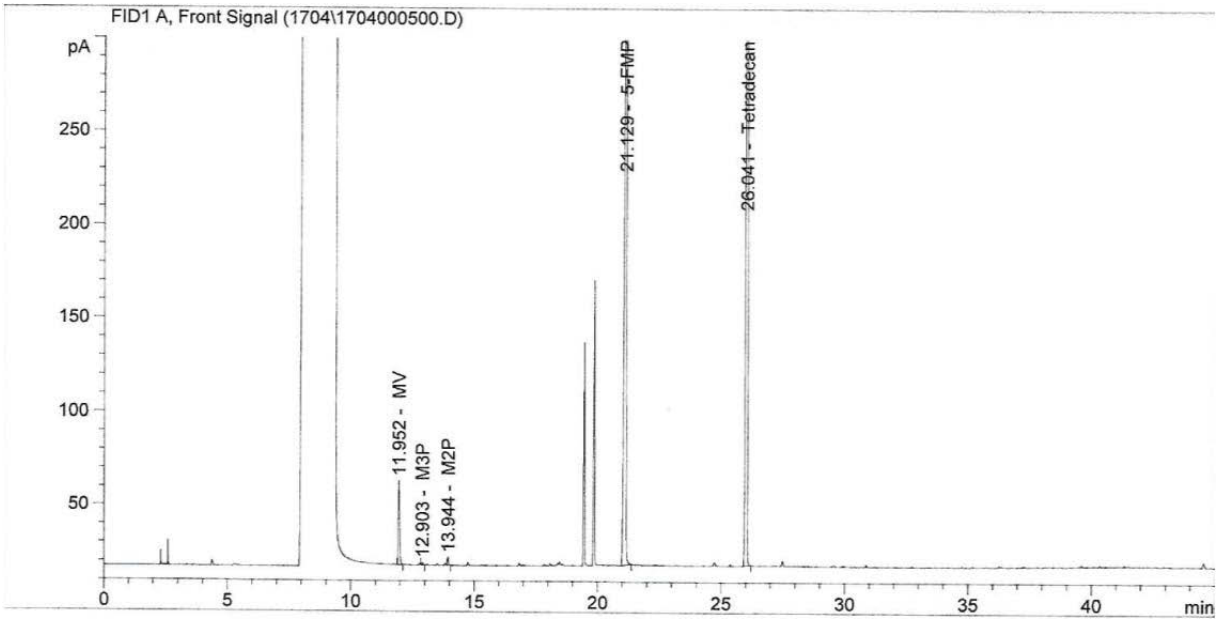

Appendix Fig. 30: Gas chromatogram (GC-FID) of Table 9, Entry 6.

Substance	Retention time [min]	Area
Methyl valerate	12.0	156.78535
Methyl 4-pentenoate	11.2	-
Methyl 3-pentenoate	13.0	4.65905
Methyl 2-pentenoate	14.0	12.18255
Methyl 5-formylvalerate	21.2	2562.40381

Table 9, Entry 7

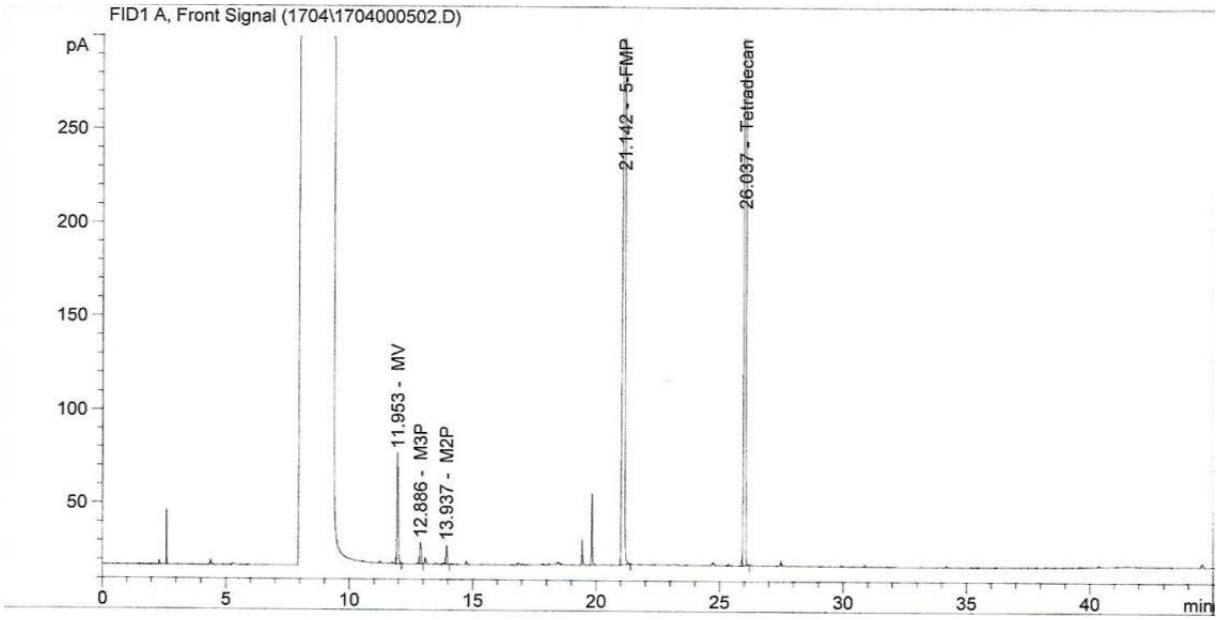

Appendix Fig. 31: Gas chromatogram (GC-FID) of Table 9, Entry 7.

Substance	Retention time [min]	Area
Methyl valerate	12.0	205.25499
Methyl 4-pentenoate	11.2	-
Methyl 3-pentenoate	13.0	36.88977
Methyl 2-pentenoate	14.0	29.30729
Methyl 5-formylvalerate	21.2	3119.69263

Table 9, Entry 8

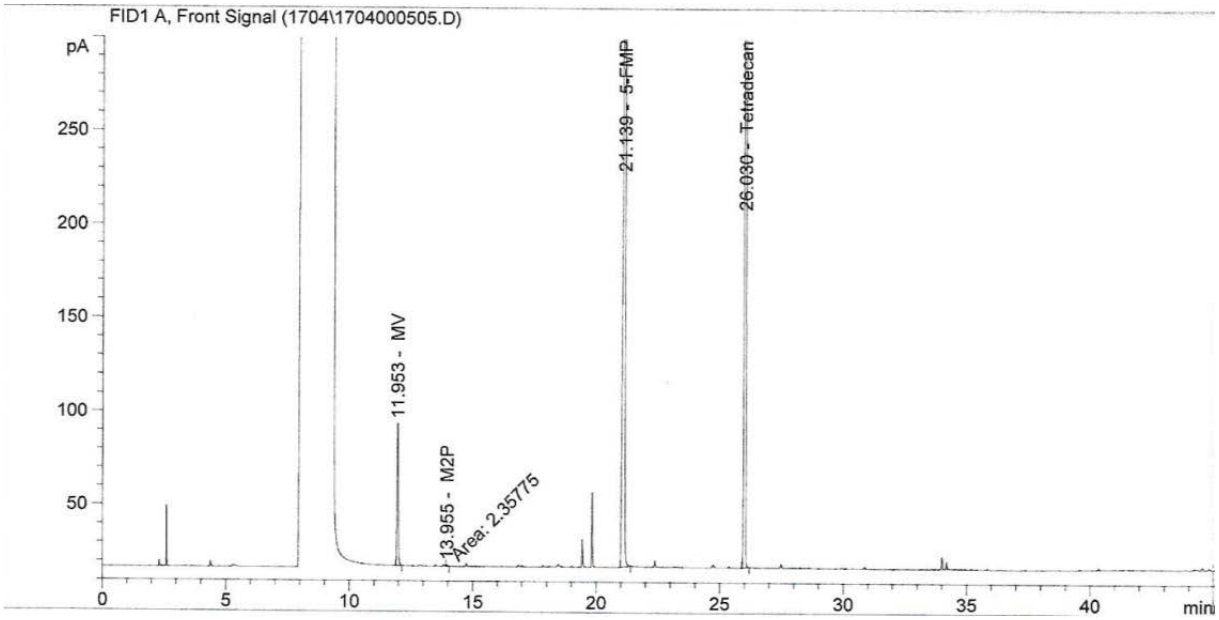

Appendix Fig. 32: Gas chromatogram (GC-FID) of Table 9, Entry 8.

Substance	Retention time [min]	Area
Methyl valerate	12.0	267.54190
Methyl 4-pentenoate	11.2	-
Methyl 3-pentenoate	13.0	-
Methyl 2-pentenoate	14.0	2.35775
Methyl 5-formylvalerate	21.1	2927.59814

Table 9, Entry 9

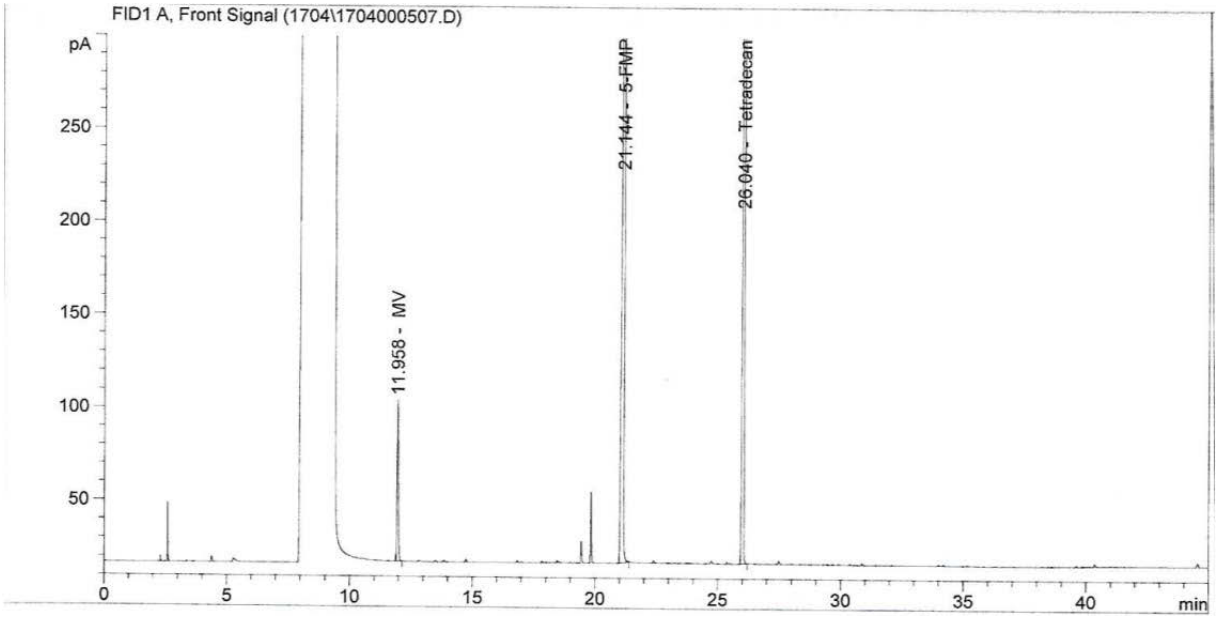

Appendix Fig. 33: Gas chromatogram (GC-FID) of Table 9, Entry 9.

Substance	Retention time [min]	Area
Methyl valerate	12.0	300.61893
Methyl 4-pentenoate	11.2	-
Methyl 3-pentenoate	13.0	-
Methyl 2-pentenoate	14.0	-
Methyl 5-formylvalerate	21.2	3121.18066

Table 9, Entry 10

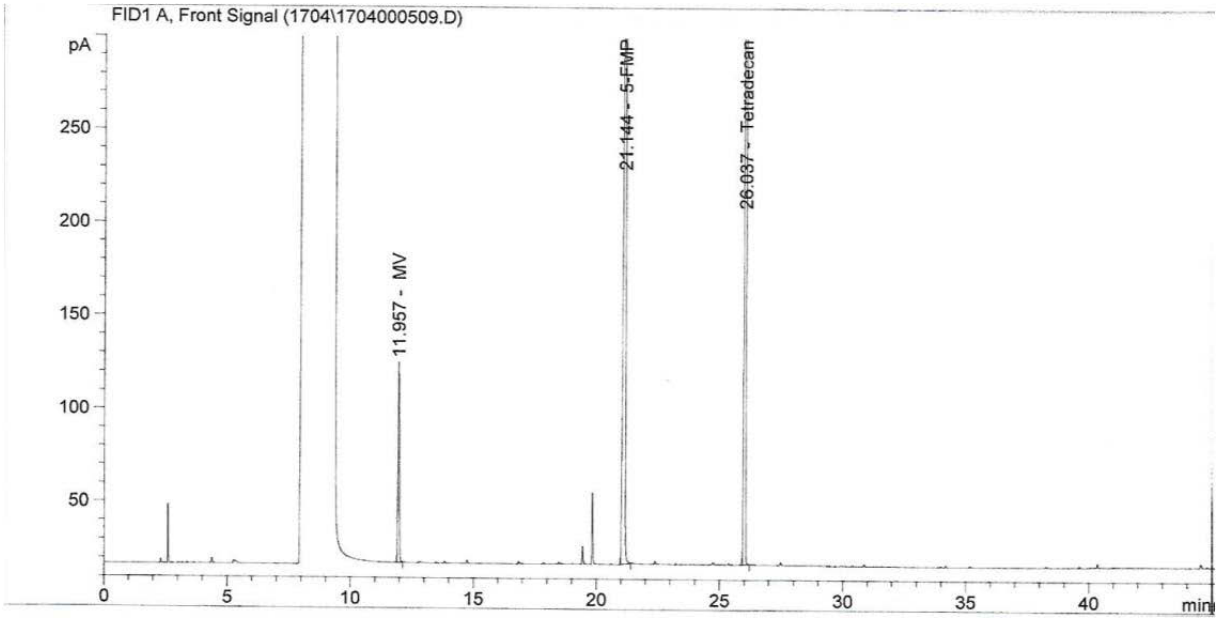

Appendix Fig. 34: Gas chromatogram (GC-FID) of Table 9, Entry 10.

Substance	Retention time [min]	Area
Methyl valerate	12.0	372.86945
Methyl 4-pentenoate	11.2	-
Methyl 3-pentenoate	13.0	-
Methyl 2-pentenoate	14.0	-
Methyl 5-formylvalerate	21.2	3104.51709

A.1.5. Recycling of the BINAS-modified Rh(I)-catalyst in the two-phasic hydro-formylation of methyl pentenoates

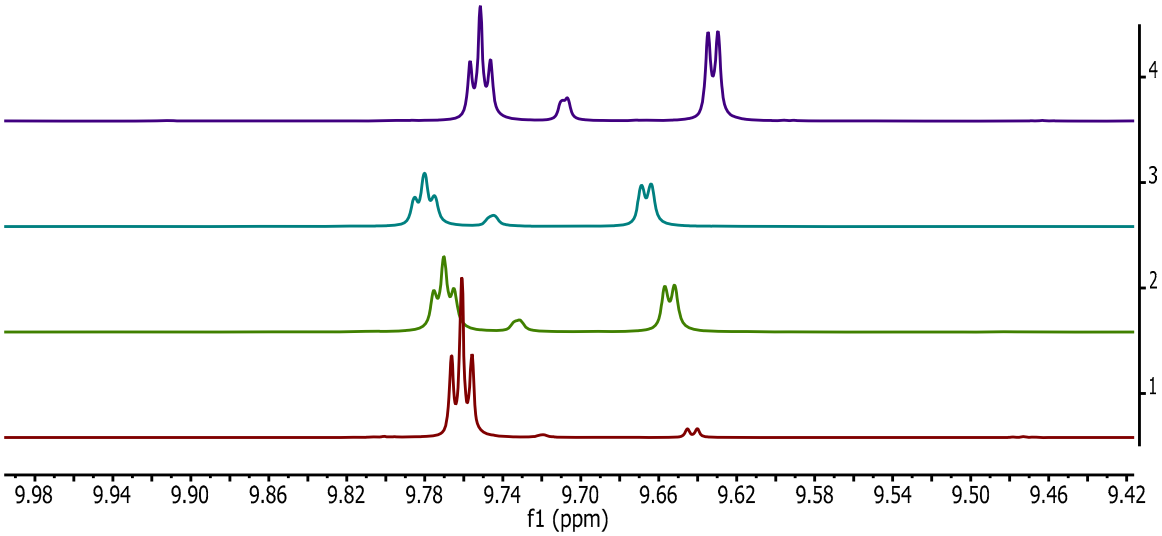

Appendix Fig. 35: Stacked ^{1}H NMR spectra in CD_2Cl_2 at rt of the products mixtures of table 10.

Table 10, Entry 1

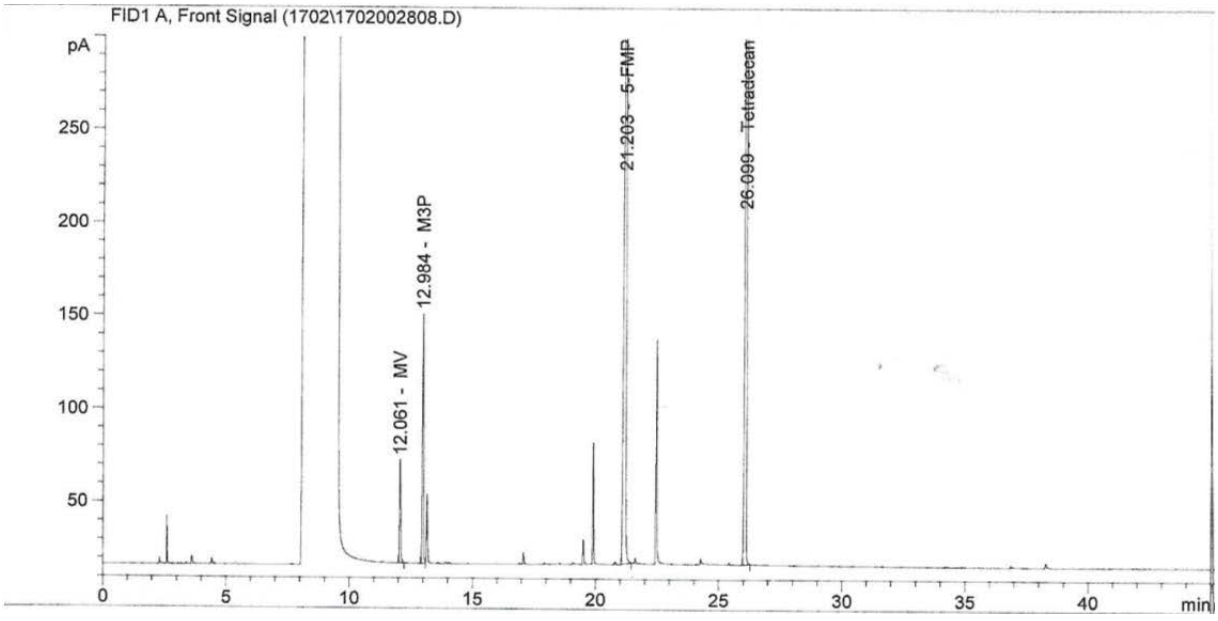

Appendix Fig. 36: Gas chromatogram (GC-FID) of Table 10, Entry 1.

Substance	Retention time [min]	Area
Methyl valerate	12.0	182.30817
Methyl 4-pentenoate	11.2	-
Methyl 3-pentenoate	13.0	-
Methyl 2-pentenoate	14.0	-
Methyl 5-formylvalerate	21.2	2236.65723

Table 10, Entry 2

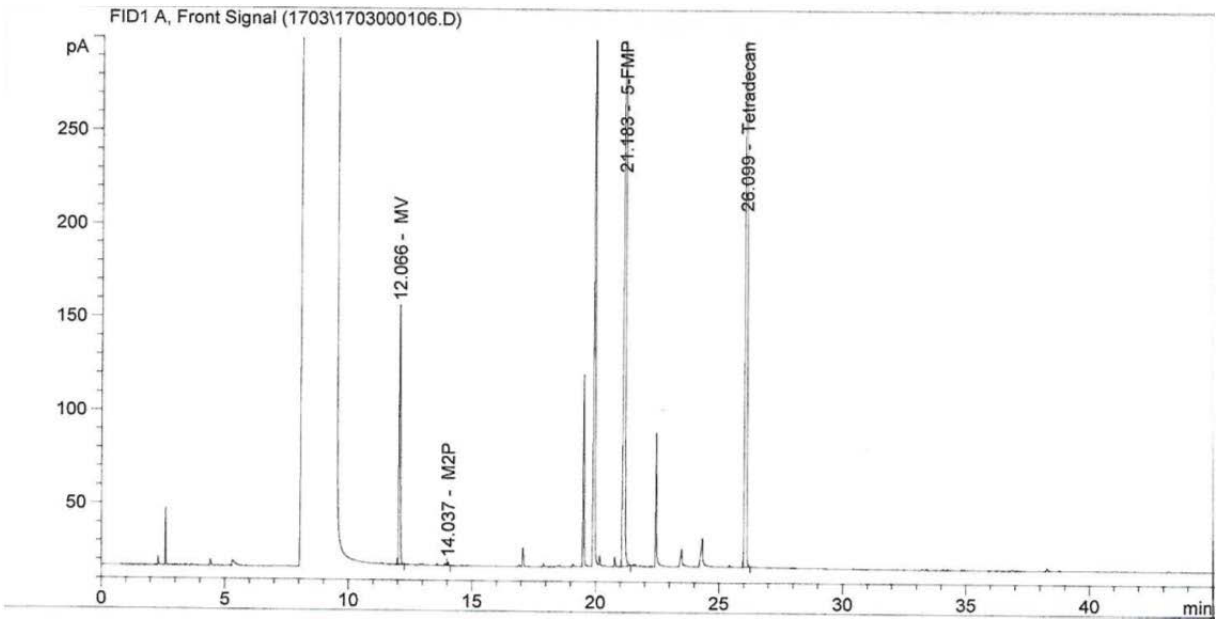

Appendix Fig. 37: Gas chromatogram (GC-FID) of Table 10, Entry 2.

Substance	Retention time [min]	Area
Methyl valerate	12.0	43.95434
Methyl 4-pentenoate	11.2	-
Methyl 3-pentenoate	13.0	-
Methyl 2-pentenoate	14.0	-
Methyl 5-formylvalerate	21.2	543.82300

Table 10, Entry 3

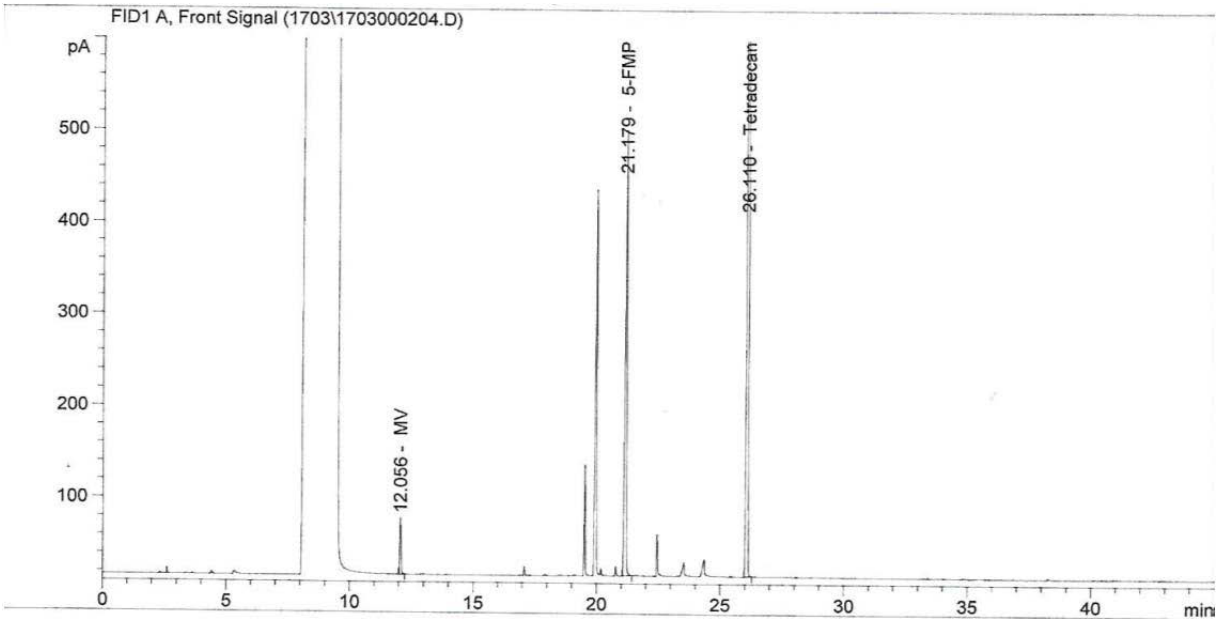

Appendix Fig. 38: Gas chromatogram (GC-FID) of Table 10, Entry 3.

Substance	Retention time [min]	Area
Methyl valerate	12.0	16.50732
Methyl 4-pentenoate	11.2	-
Methyl 3-pentenoate	13.0	-
Methyl 2-pentenoate	14.0	-
Methyl 5-formylvalerate	21.2	171.42970

Table 10, Entry 4

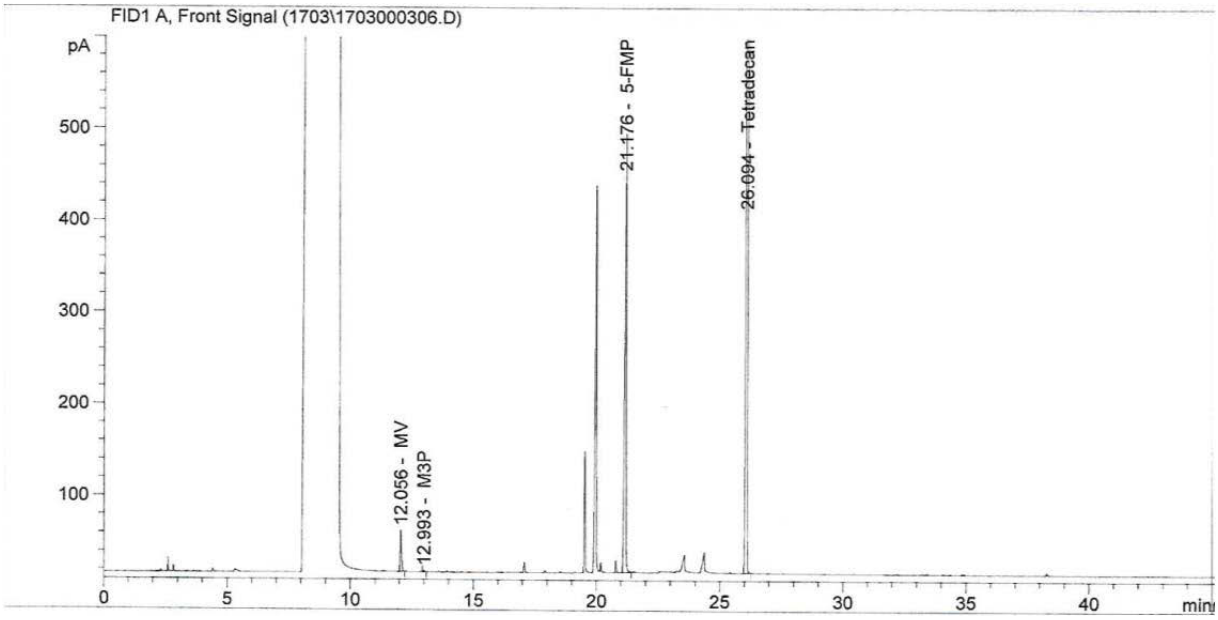

Appendix Fig. 39: Gas chromatogram (GC-FID) of Table 10, Entry 4.

Substance	Retention time [min]	Area
Methyl valerate	12.0	46.60141
Methyl 4-pentenoate	11.2	-
Methyl 3-pentenoate	13.0	22.25898
Methyl 2-pentenoate	14.0	145.06421
Methyl 5-formylvalerate	21.2	728.29700

A.1.5.1. Sample preparation ICP-OES

Sample prepared from	Theoretical amount [mg*L^{-1}]		Found [mg*L^{-1}]	
	Rh	P	Rh	P
Aqueous phase	1.5	50	0.752	1.71
Organic phase	1.5	50	0.152	Not detected

A.1.6. Mechanistic investigations on the Rh catalysed hydroformylation of methyl pentenoates

A.1.6.1. Isomerisation behaviour in the presence of a BiphePhos-modified Rh catalyst

A.1.6.1.1. Isomerisation in the presence of the precatalyst [Rh(BIPHEPHOS)(acac)]

Table 11, Entry 1

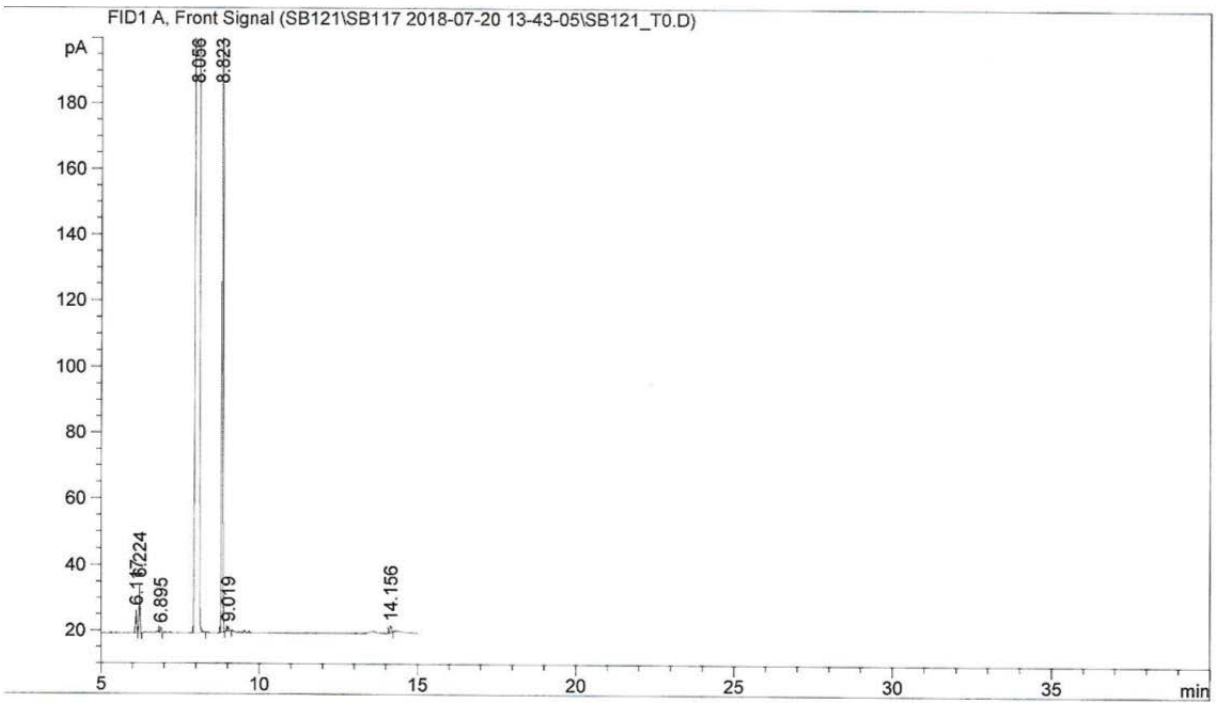

Appendix Fig. 40: Gas chromatogram (GC-FID) of Table 11, Entry 1.

Substance	Configuration	Area	Amount [%]
Methyl 4-pentenoate	-	551.78723	100
Methyl 3-pentenoate	E	-	-
	Z	-	-
Methyl 2-pentenoate	E	-	-
	Z	-	-

Table 11, Entry 2

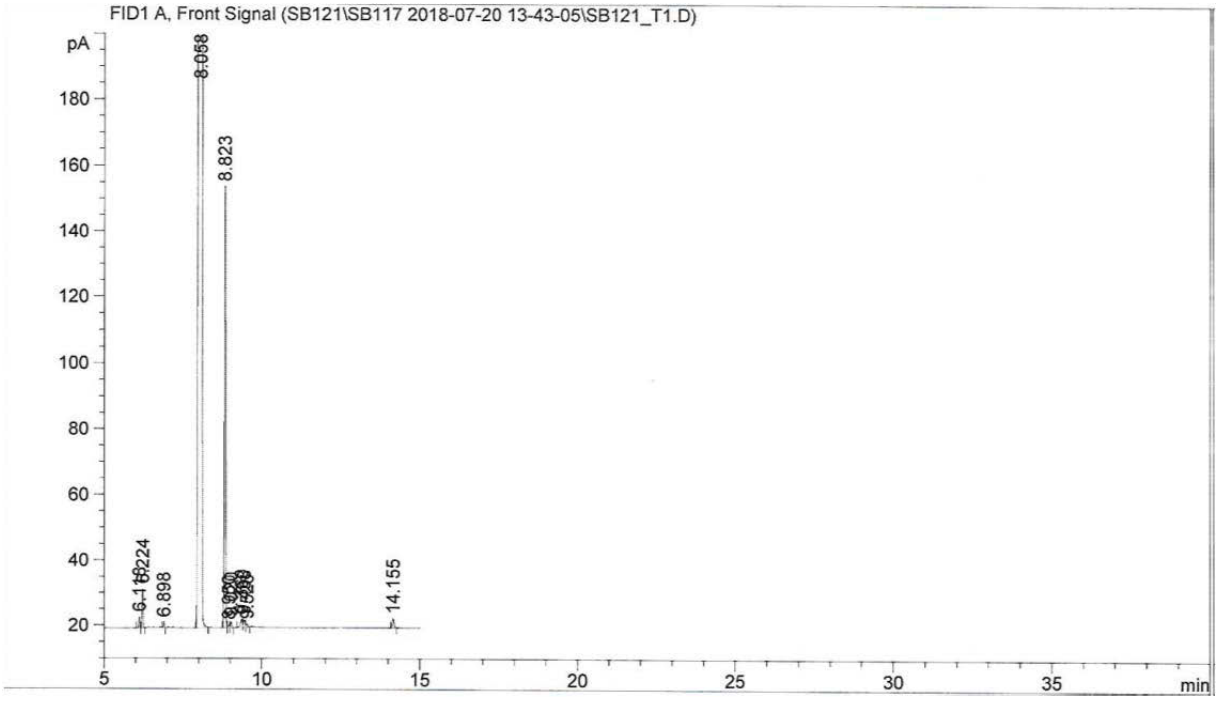

Appendix Fig. 41: Gas chromatogram (GC-FID) of Table 11, Entry 2.

Substance	Configuration	Retention time [min]	Area	Amount [%]
Methyl 4-pentenoate	-	8.8	342.22226	94.7
Methyl 3-pentenoate	E		11.36650	3.1
	Z		7.97241	2.2
Methyl 2-pentenoate	E		-	-
	Z		-	-

Table 11, Entry 3

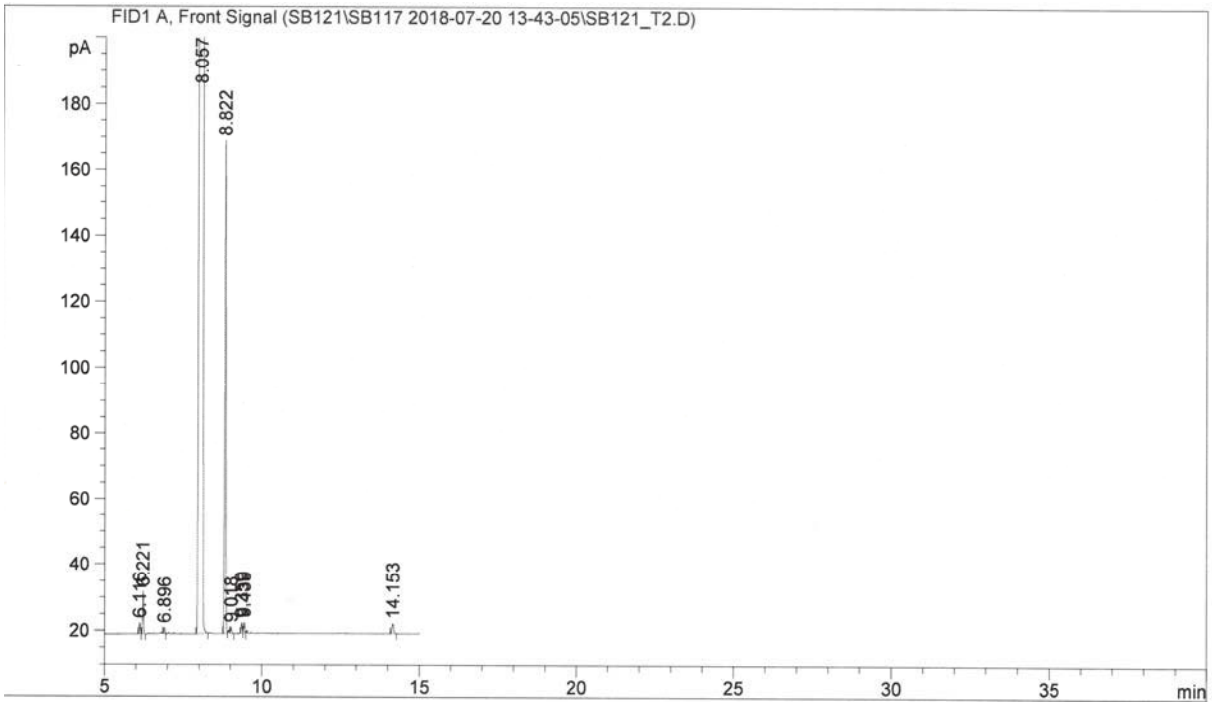

Appendix Fig. 42: Gas chromatogram (GC-FID) of Table 11, Entry 3.

Substance	Configuration	Retention time [min]	Area	Amount [%]
Methyl 4-pentenoate	-	8.8	379.23044	95.9
Methyl 3-pentenoate	E	9.0	7.90380	2.0
	Z	9.4	8.16676	2.1
Methyl 2-pentenoate	E		-	-
	Z		-	-

Table 11, Entry 4

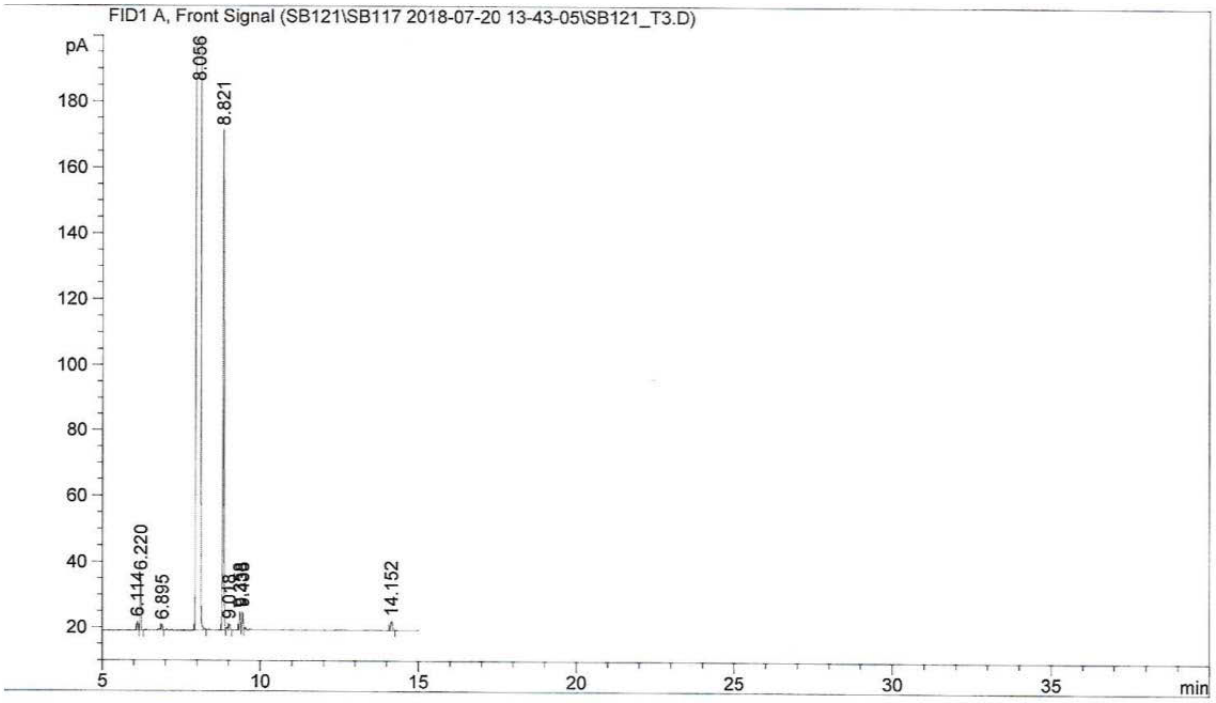

Appendix Fig. 43: Gas chromatogram (GC-FID) of Table 11, Entry 4.

Substance	Configuration	Retention time [min]	Area	Amount [%]
Methyl 4-pentenoate	-	8.8	384.28680	93.3
Methyl 3-pentenoate	E	9.0	13.52419	3.3
	Z	9.4	13.95624	3.4
Methyl 2-pentenoate	E		-	-
	Z		-	-

Table 11, Entry 5

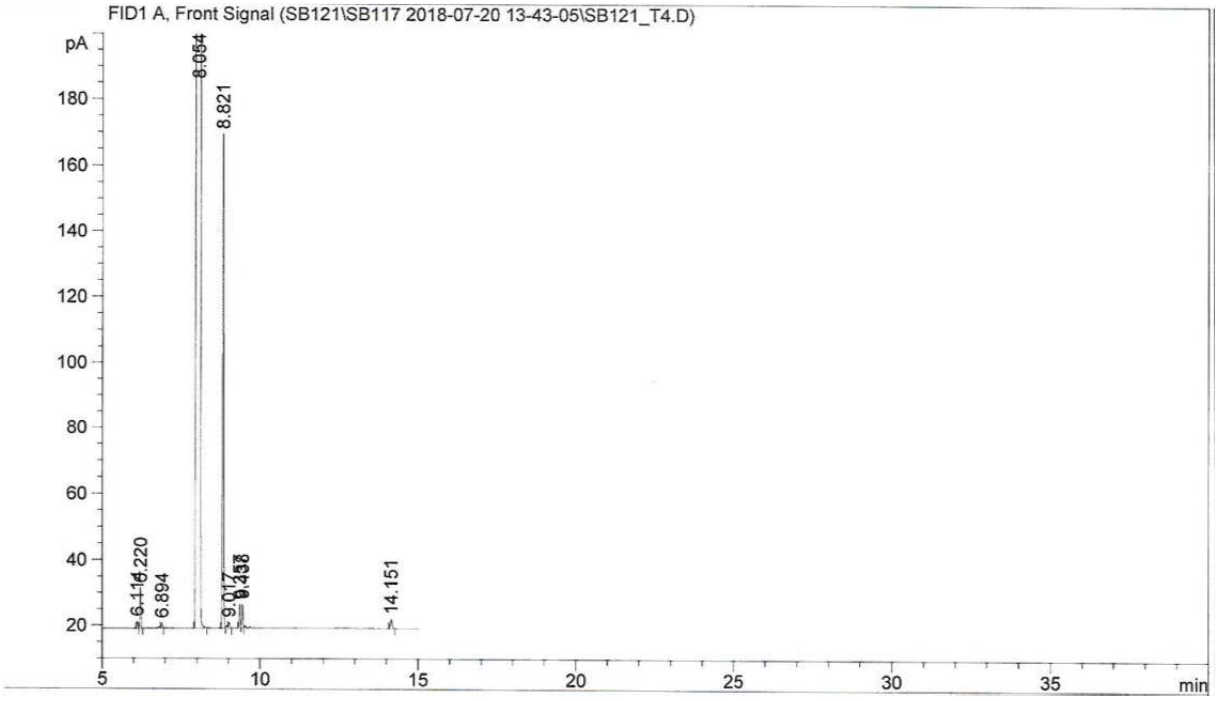

Appendix Fig. 44: Gas chromatogram (GC-FID) of Table 11, Entry 5.

Substance	Configuration	Retention time [min]	Area	Amount [%]
Methyl 4-pentenoate	-	8.8	379.72226	91.2
Methyl 3-pentenoate	E	9.0	18.03593	4.6
	Z	9.4	18.64982	4.5
Methyl 2-pentenoate	E		-	-
	Z		-	-

Table 11, Entry 6

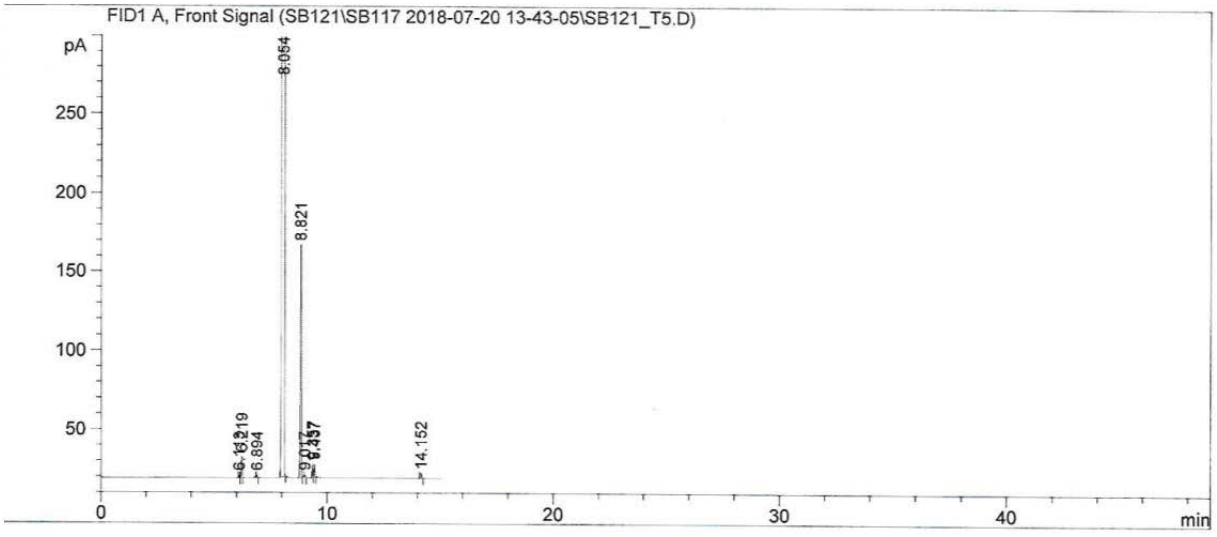

Appendix Fig. 45: Gas chromatogram (GC-FID) of Table 11, Entry 6.

Substance	Configuration	Retention time [min]	Area	Amount [%]
Methyl 4-pentenoate	-	8.8	372.92142	90.4
Methyl 3-pentenoate	E	9.0	20.02941	4.9
	Z	9.4	19.49517	4.7
Methyl 2-pentenoate	E		-	-
	Z		-	-

Table 11, Entry 7

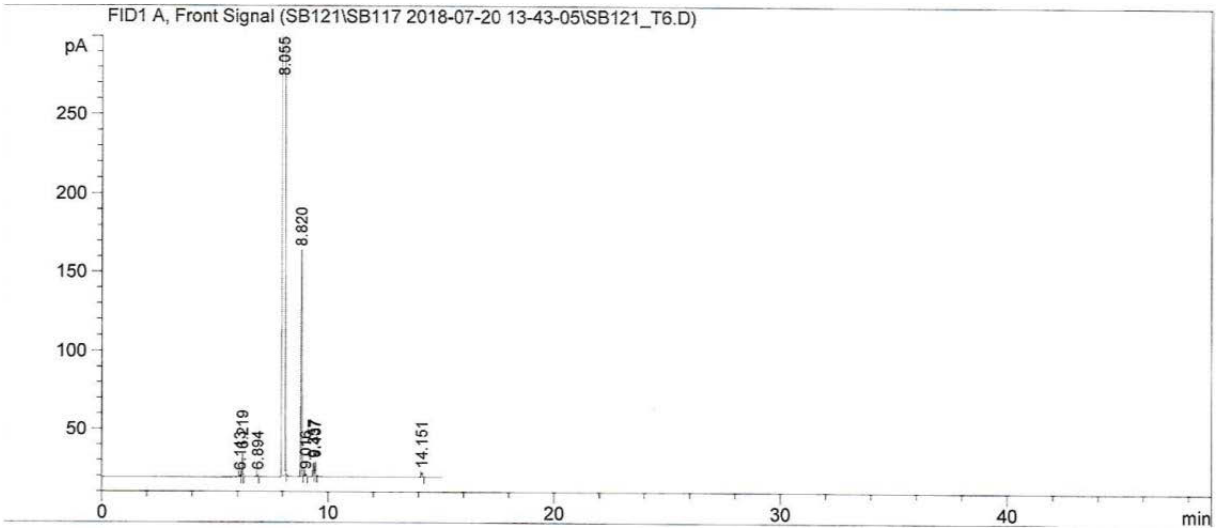

Appendix Fig. 46: Gas chromatogram (GC-FID) of Table 11, Entry 7.

Substance	Configuration	Retention time [min]	Area	Amount [%]
Methyl 4-pentenoate	-	8.8	363.89853	89.4
Methyl 3-pentenoate	E	9.0	21.86732	5.4
	Z	9.4	21.36953	5.2
Methyl 2-pentenoate	E		-	-
	Z		-	-

Table 11, Entry 8

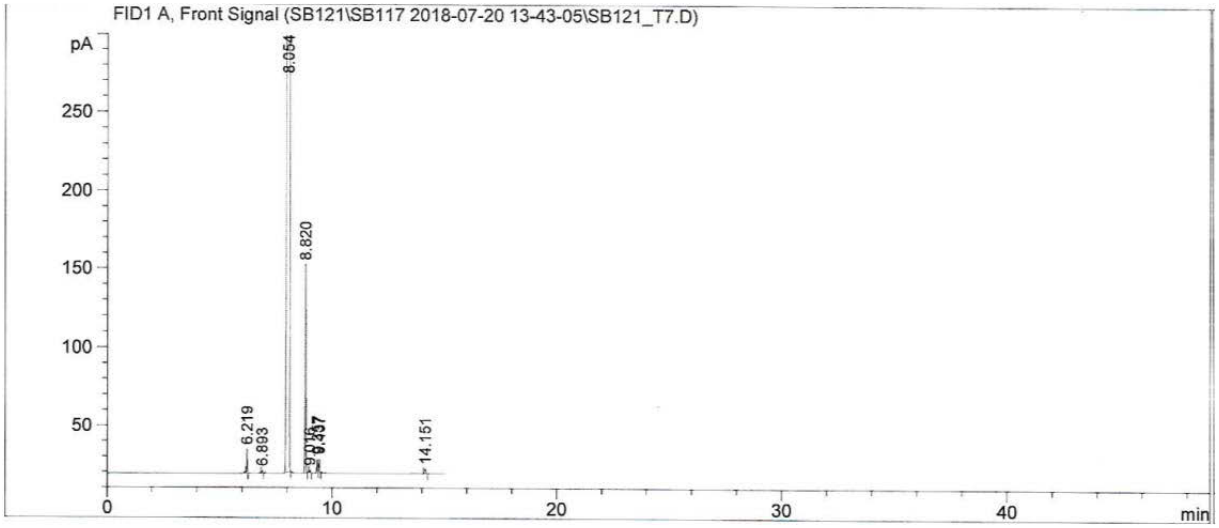

Appendix Fig. 47: Gas chromatogram (GC-FID) of Table 11, Entry 8.

Substance	Configuration	Retention time [min]	Area	Amount [%]
Methyl 4-pentenoate	-	8.8	336.57446	88.7
Methyl 3-pentenoate	E	9.0	21.83034	5.8
	Z	9.4	21.01824	5.5
Methyl 2-pentenoate	E		-	-
	Z		-	-

Table 11, Entry 9

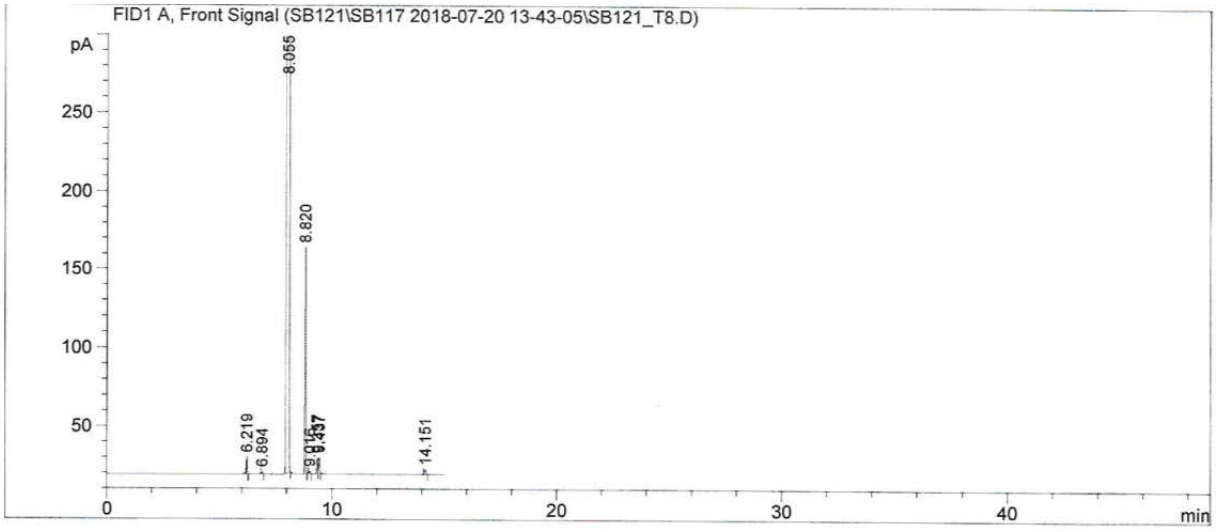

Appendix Fig. 48: Gas chromatogram (GC-FID) of Table 11, Entry 9.

Substance	Configuration	Retention time [min]	Area	Amount [%]
Methyl 4-pentenoate	-	8.8	366.69708	88.0
Methyl 3-pentenoate	E	9.0	25.15307	6.0
	Z	9.4	24.68432	5.9
Methyl 2-pentenoate	E		-	-
	Z		-	-

A.2. Alkoxycarbonylation of isomeric methyl pentenoates

A.2.1. Preliminary experiments

Table 12, Entry 1

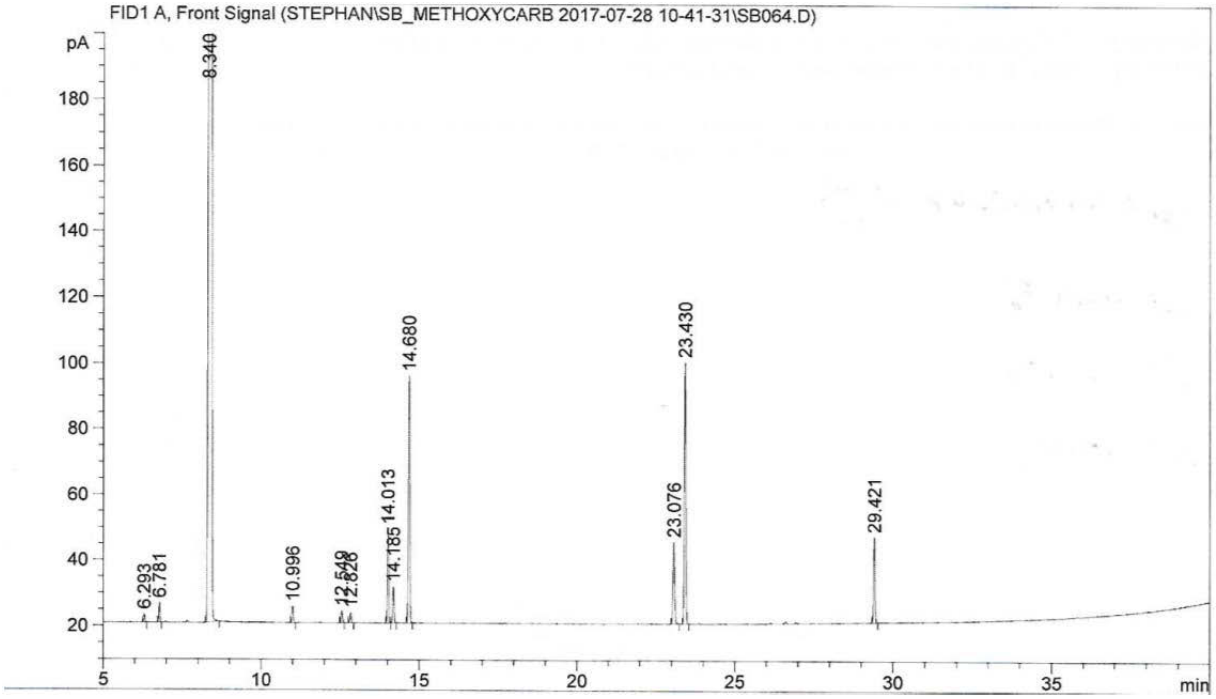

Appendix Fig. 49: Gas chromatogram (GC-FID) of Table 12, Entry 1.

Substance	Retention time [min]	Area
Methyl valerate	-	-
Methyl 4-pentenoate	11.0	9.11247
Methyl 3-pentenoate	14.0	87.71324
Methyl 2-pentenoate	14.7	236.03847
Dimethyl adipate	29.4	80.88873

Table 12, Entry 2

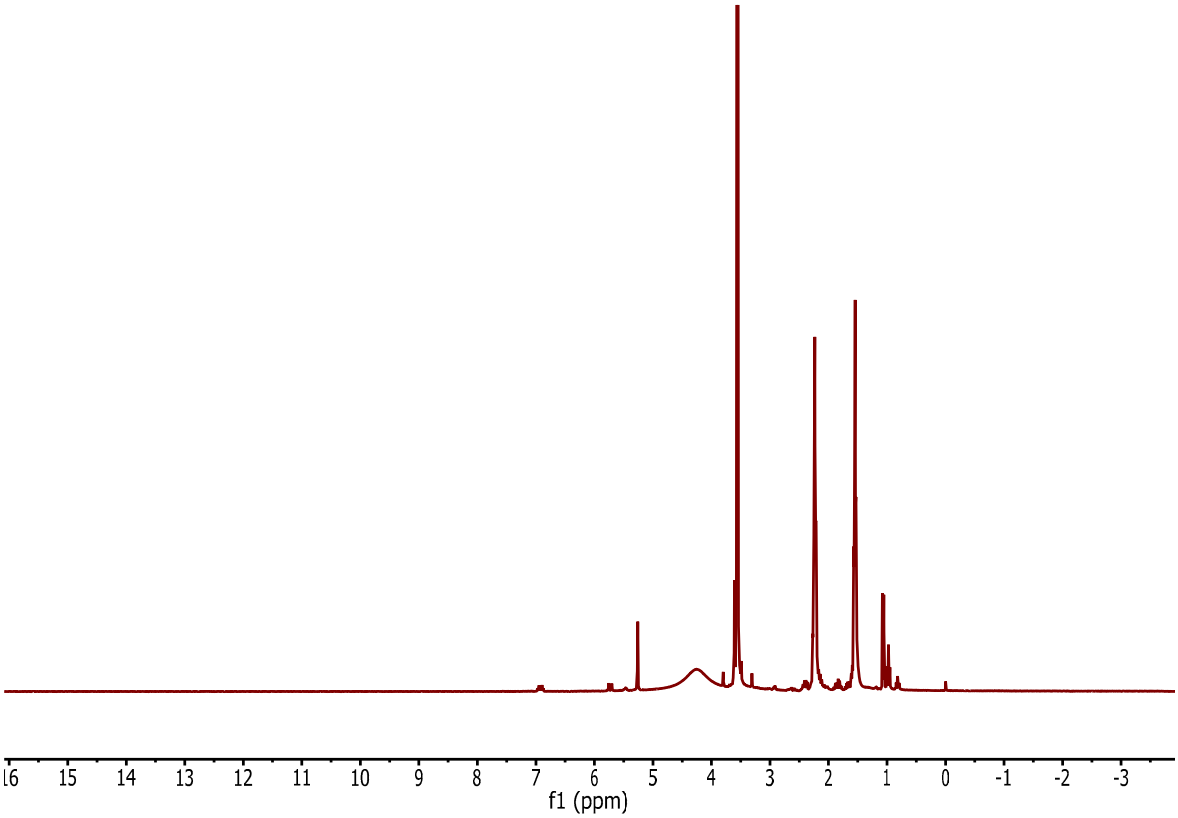

Appendix Fig. 50: ^{1}H NMR in CD_2Cl_2 at rt of the product mixture in table 12, entry 2.

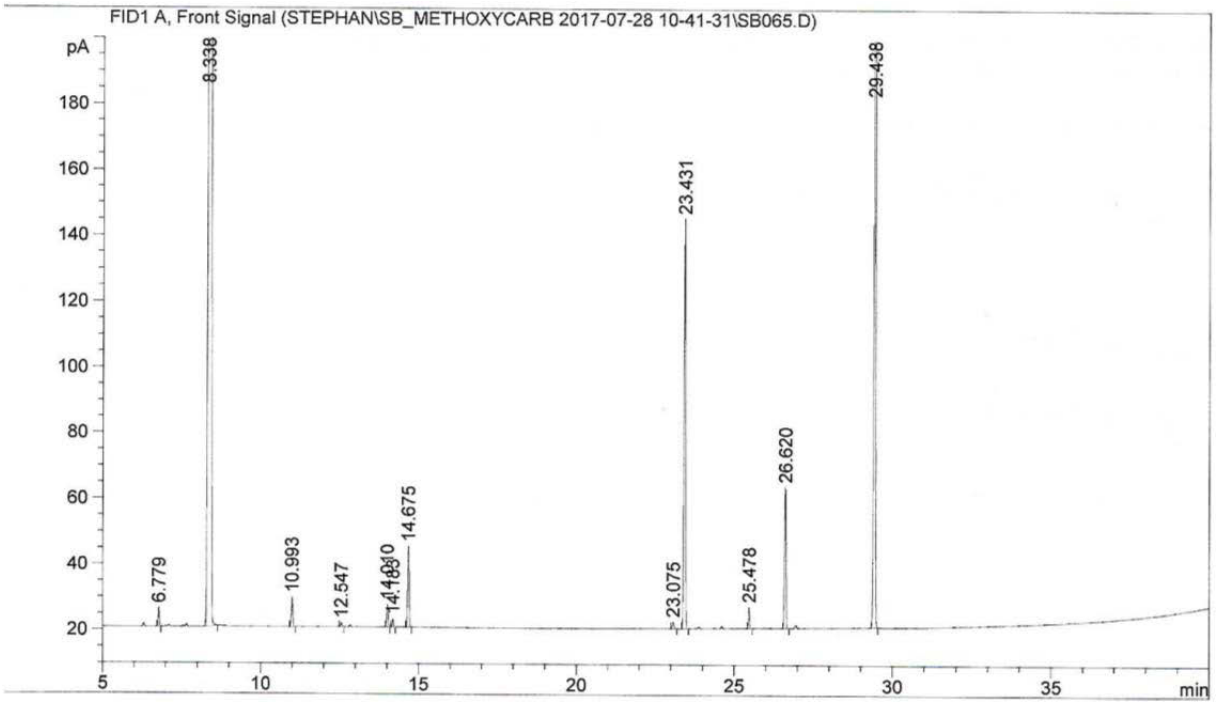

Appendix Fig. 51: Gas chromatogram (GC-FID) of Table 12, Entry 2.

Substance	Retention time [min]	Area
Methyl valerate	-	-
Methyl 4-pentenoate	11.0	3.56940
Methyl 3-pentenoate	14.0	20.88190
Methyl 2-pentenoate	14.7	77.17008
Dimethyl adipate	29.4	818.86993
Dimethyl 5-methylglutarate	26.6	132.30080
Dimethyl 4-ethylsuccinate	-	-

Table 12, Entry 3

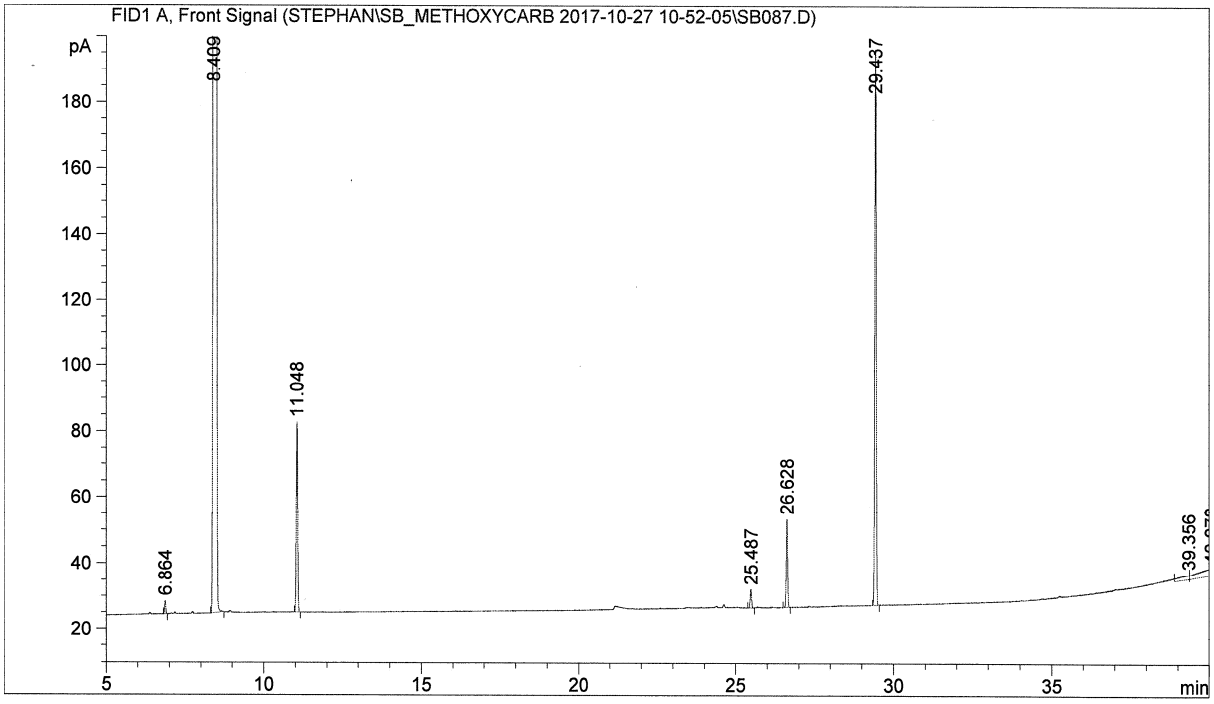

Appendix Fig. 52: Gas chromatogram (GC-FID) of Table 12, Entry 3.

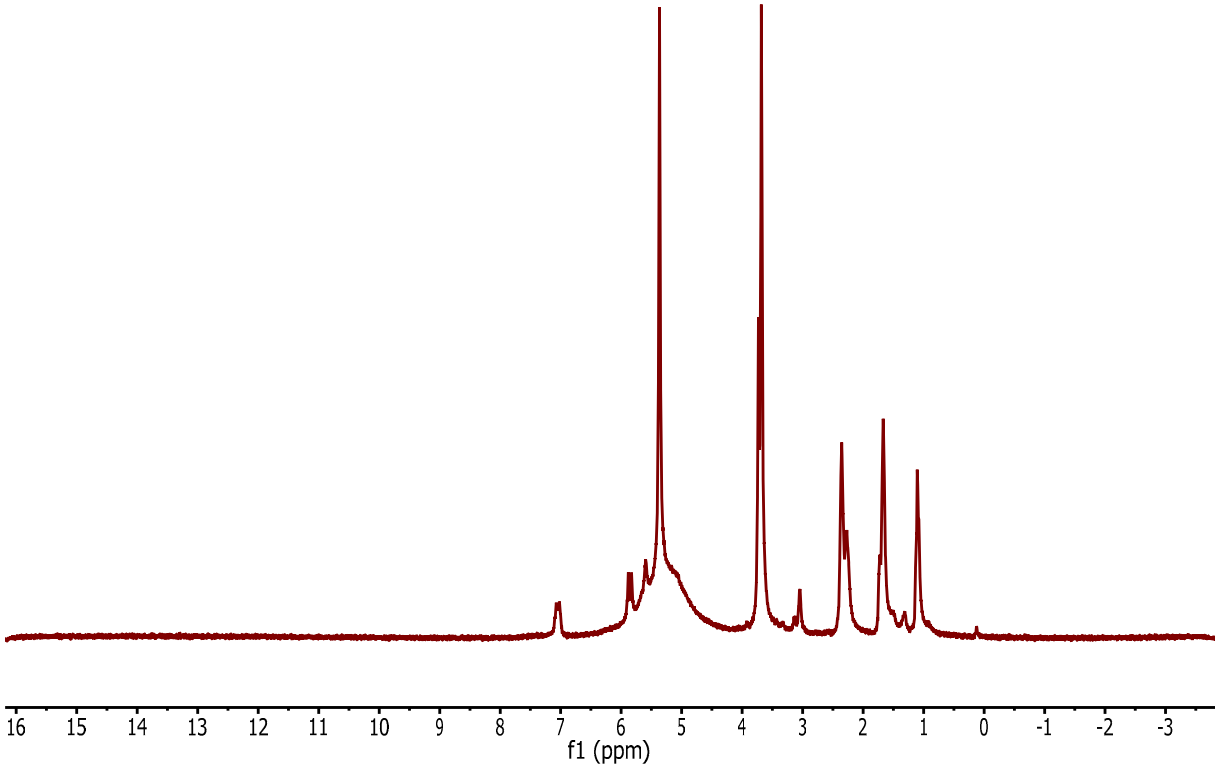

Appendix Fig. 53: ^{1}H NMR in CD_2Cl_2 at rt of the product mixture in table 12, entry 3.

Substance	Retention time [min]	Area
Methyl valerate	-	-
Methyl 4-pentenoate	11.0	-
Methyl 3-pentenoate	14.0	-
Methyl 2-pentenoate	14.7	-
Dimethyl adipate	29.4	539.48730
Dimethyl 5-methylglutarate	26.6	82.285117
Dimethyl 4-ethylsuccinate	-	-

A.2.2. Optimisation of reaction conditions for the catalysis with PyTBPF and PyTBPX

A.2.2.1. PyTBPF

Table 13, Entry 1

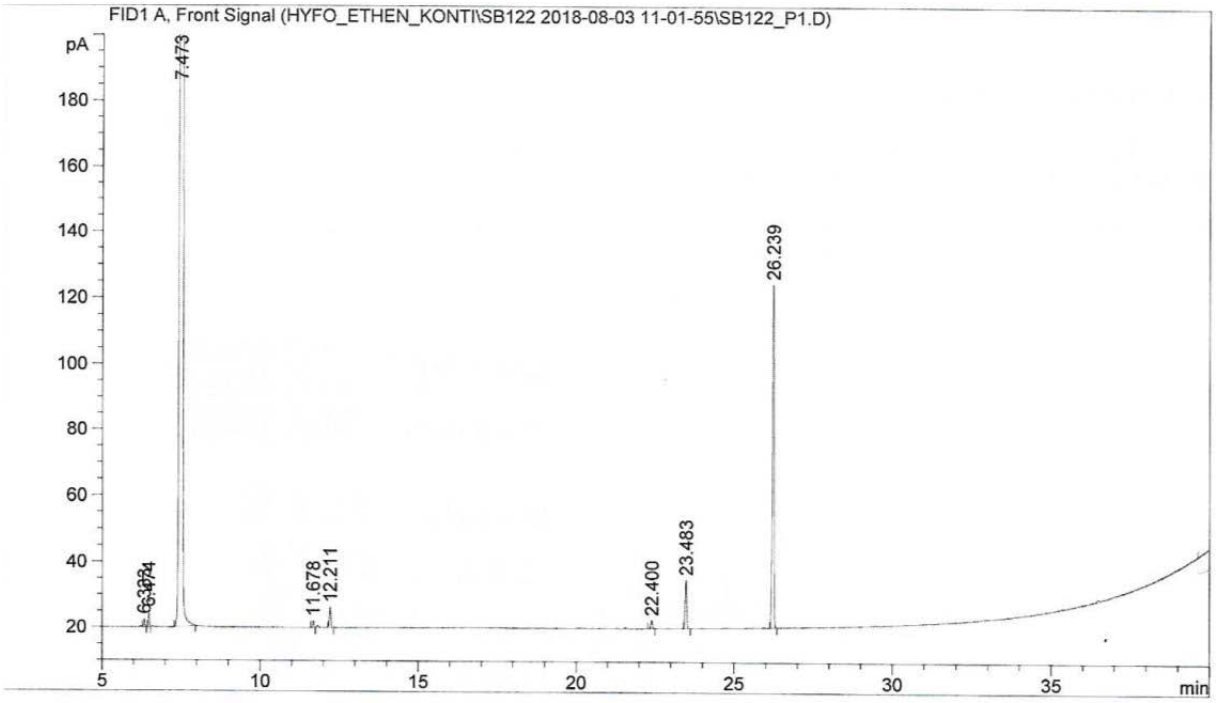

Appendix Fig. 54: Gas chromatogram (GC-FID) of Table 13, Entry 1.

Substance	Retention time [min]	Area
Methyl valerate	11.7	6.57935
Methyl 4-pentenoate	12.2	21.41542
Methyl 3-pentenoate	-	-
Methyl 2-pentenoate	-	-
Dimethyl adipate	26.2	368.34613
Dimethyl 5-methylglutarate	23.5	51.08490
Dimethyl 4-ethylsuccinate	22.4	8.84762

Table 13, Entry 2

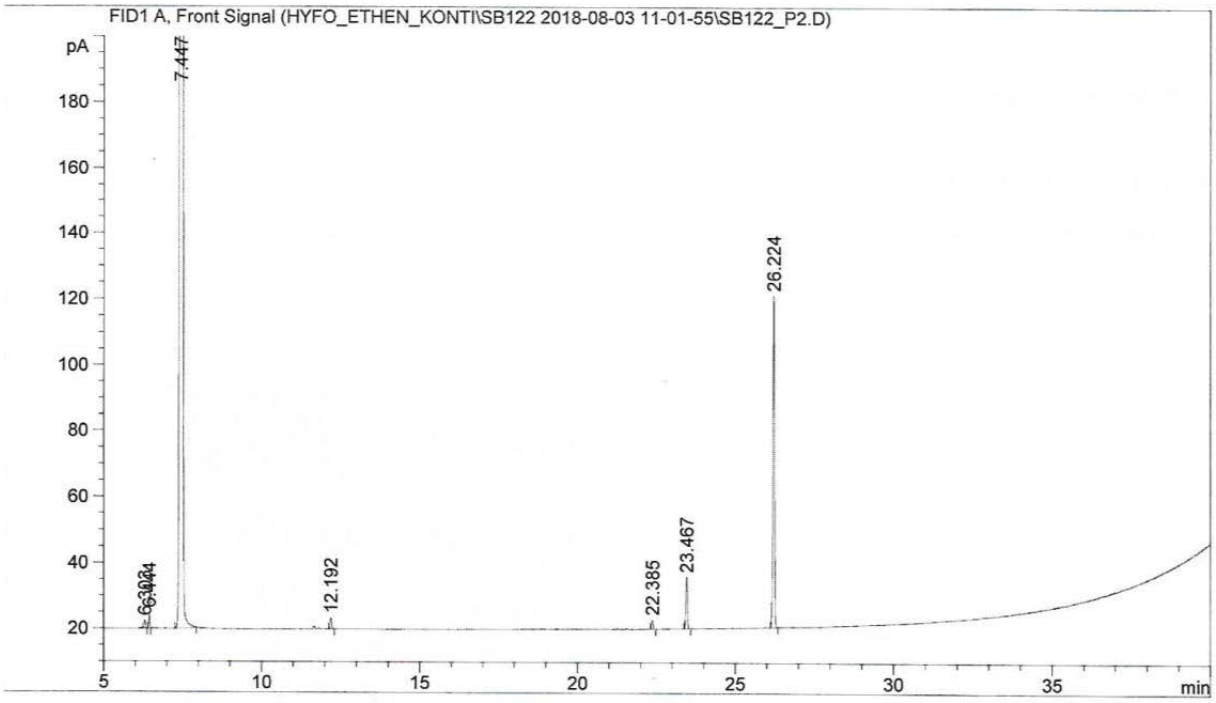

Appendix Fig. 55: Gas chromatogram (GC-FID) of Table 13, Entry 2.

Substance	Retention time [min]	Area
Methyl valerate	11.7	-
Methyl 4-pentenoate	12.2	11.31914
Methyl 3-pentenoate	-	-
Methyl 2-pentenoate	-	-
Dimethyl adipate	26.2	357.39029
Dimethyl 5-methylglutarate	23.5	55.06871
Dimethyl 4-ethylsuccinate	22.4	9.29526

Table 13, Entry 3

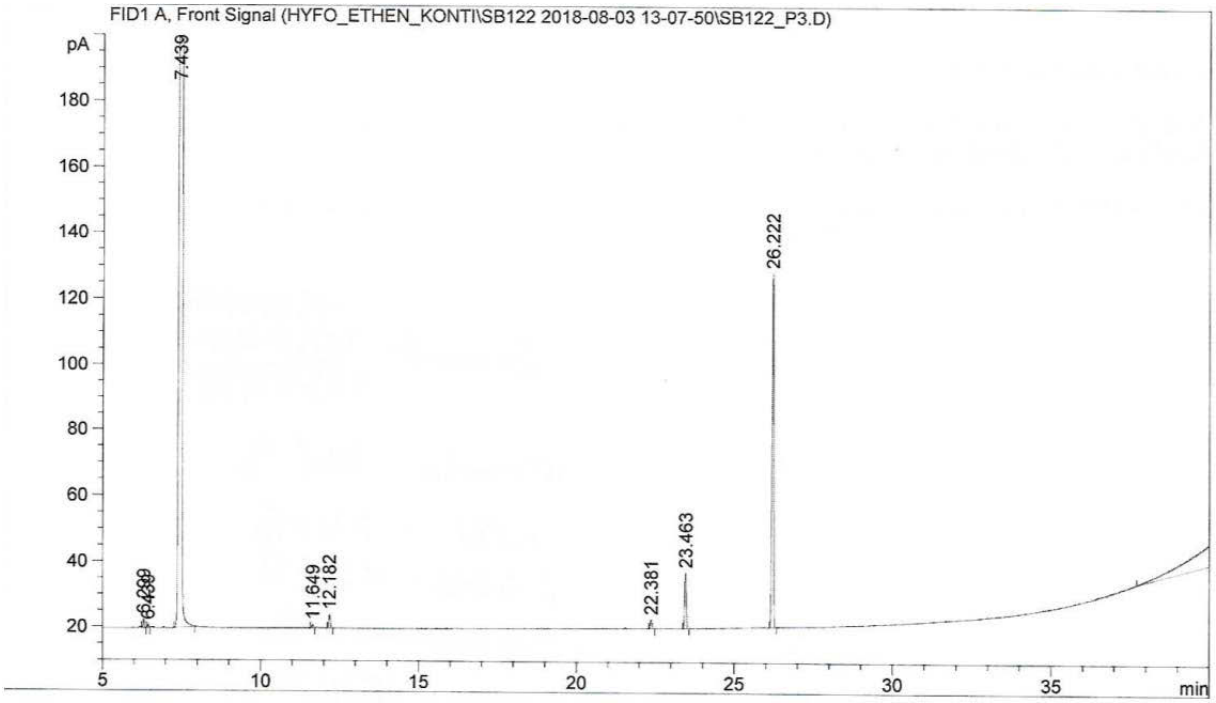

Appendix Fig. 56: Gas chromatogram (GC-FID) of Table 13, Entry 3.

Substance	Retention time [min]	Area
Methyl valerate	11.7	3.40088
Methyl 4-pentenoate	12.2	14.00400
Methyl 3-pentenoate	-	-
Methyl 2-pentenoate	-	-
Dimethyl adipate	26.2	383.51471
Dimethyl 5-methylglutarate	23.5	59.35001
Dimethyl 4-ethylsuccinate	22.4	9.66878

Table 13, Entry 4

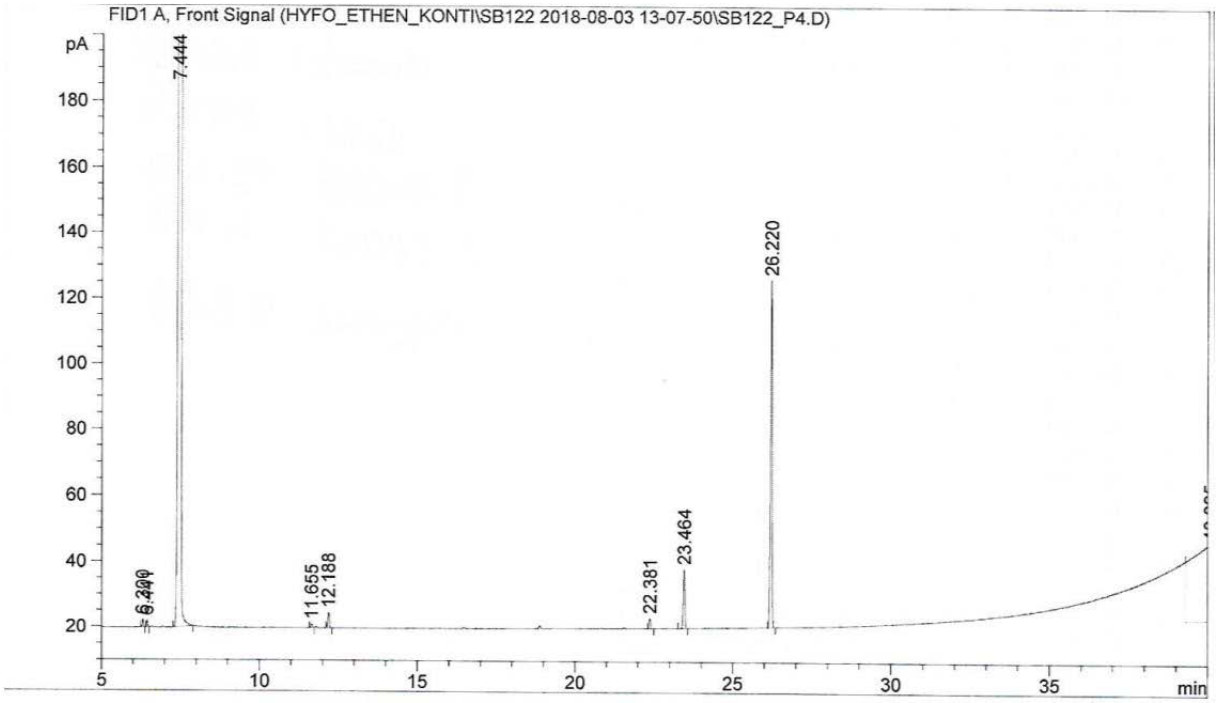

Appendix Fig. 57: Gas chromatogram (GC-FID) of Table 13, Entry 4.

Substance	Retention time [min]	Area
Methyl valerate	11.7	3.51023
Methyl 4-pentenoate	12.2	15.51378
Methyl 3-pentenoate	-	-
Methyl 2-pentenoate	-	-
Dimethyl adipate	26.2	377.35120
Dimethyl 5-methylglutarate	23.5	62.80806
Dimethyl 4-ethylsuccinate	22.4	10.85977

Table 13, Entry 5

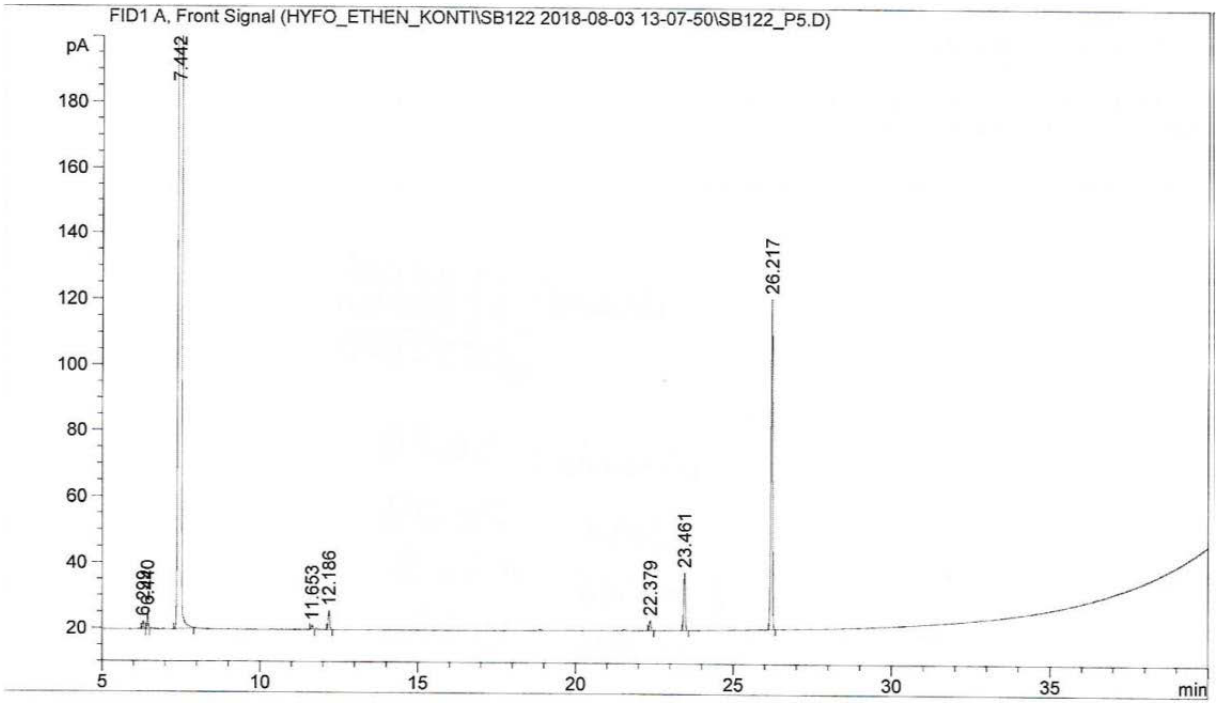

Appendix Fig. 58: Gas chromatogram (GC-FID) of Table 13, Entry 5.

Substance	Retention time [min]	Area
Methyl valerate	11.7	4.30559
Methyl 4-pentenoate	12.2	19.55407
Methyl 3-pentenoate	-	-
Methyl 2-pentenoate	-	-
Dimethyl adipate	26.2	355.09210
Dimethyl 5-methylglutarate	23.5	61.35862
Dimethyl 4-ethylsuccinate	22.4	10.42945

Table 13, Entry 6

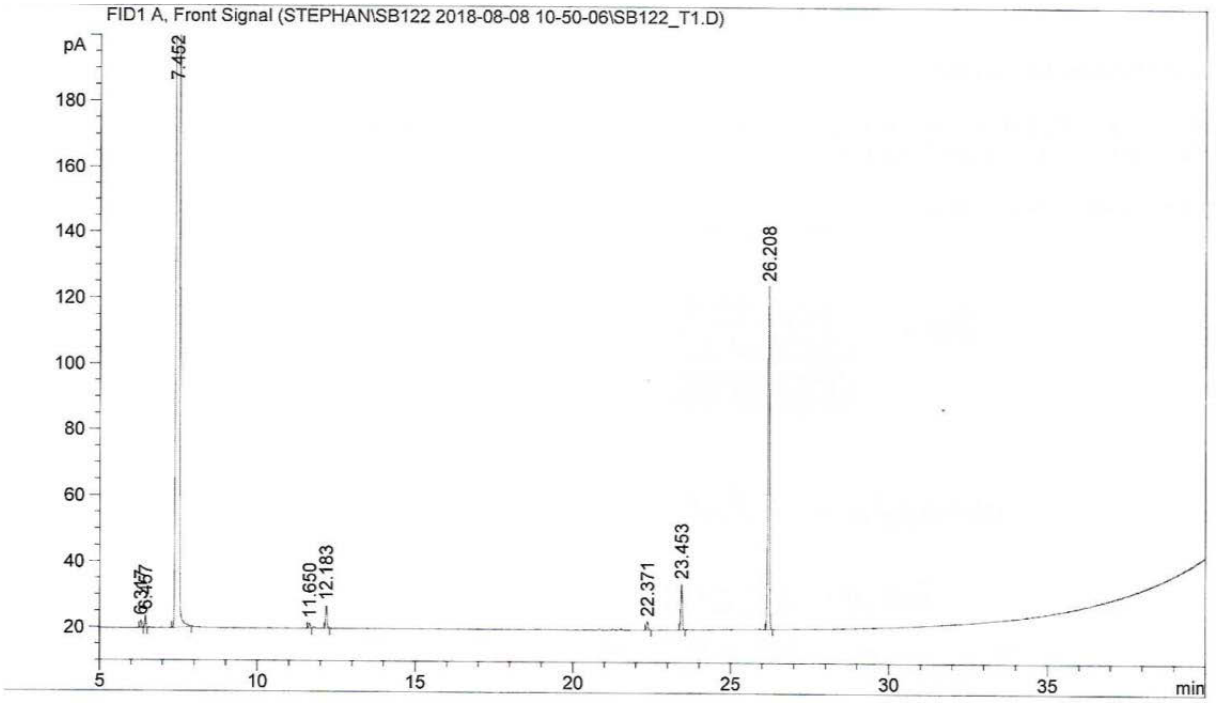

Appendix Fig. 59: Gas chromatogram (GC-FID) of Table 13, Entry 6.

Substance	Retention time [min]	Area
Methyl valerate	11.7	5.20398
Methyl 4-pentenoate	12.2	23.40335
Methyl 3-pentenoate	-	-
Methyl 2-pentenoate	-	-
Dimethyl adipate	26.2	368.17548
Dimethyl 5-methylglutarate	23.5	48.71885
Dimethyl 4-ethylsuccinate	22.4	8.97342

Table 13, Entry 7

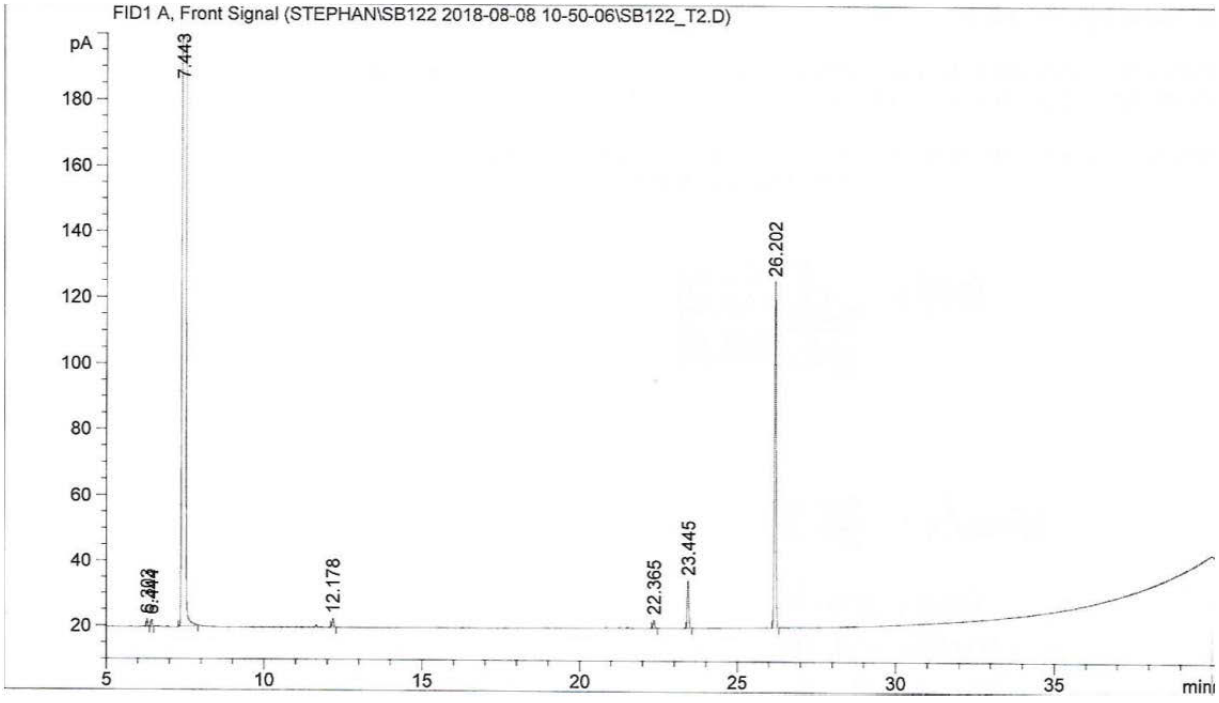

Appendix Fig. 60: Gas chromatogram (GC-FID) of Table 13, Entry 7.

Substance	Retention time [min]	Area
Methyl valerate	11.7	-
Methyl 4-pentenoate	12.2	9.34418
Methyl 3-pentenoate	-	-
Methyl 2-pentenoate	-	-
Dimethyl adipate	26.2	377.23346
Dimethyl 5-methylglutarate	23.5	51.04169
Dimethyl 4-ethylsuccinate	22.4	9.13636

Table 13, Entry 8

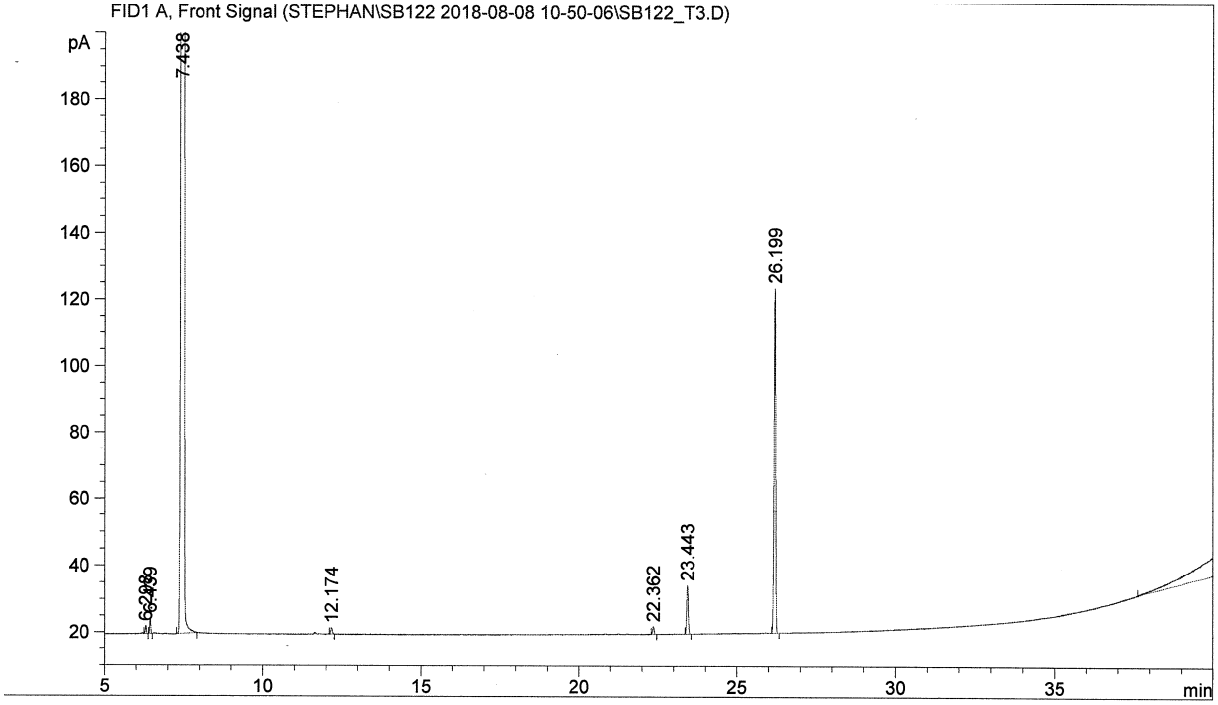

Appendix Fig. 61: Gas chromatogram (GC-FID) of Table 13, Entry 8.

Substance	Retention time [min]	Area
Methyl valerate	11.7	-
Methyl 4-pentenoate	12.2	6.29555
Methyl 3-pentenoate	-	-
Methyl 2-pentenoate	-	-
Dimethyl adipate	26.2	371.44846
Dimethyl 5-methylglutarate	23.5	51.29106
Dimethyl 4-ethylsuccinate	22.4	8.00220

Table 13, Entry 9

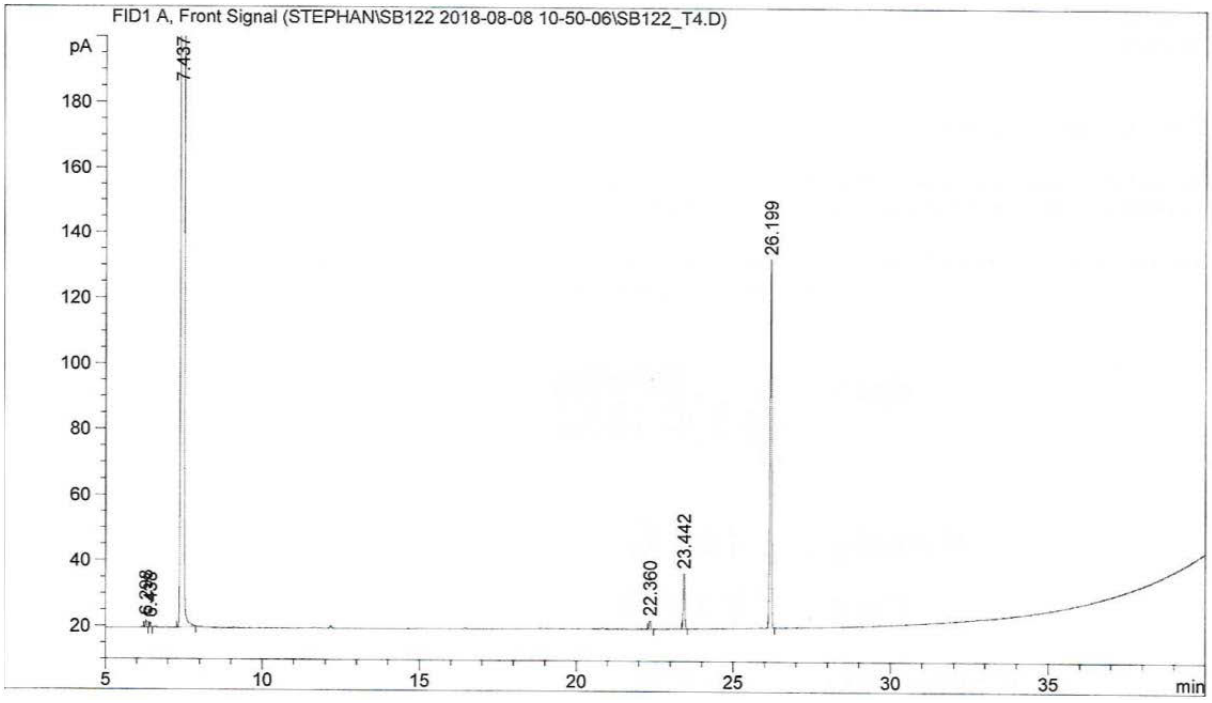

Appendix Fig. 62: Gas chromatogram (GC-FID) of Table 13, Entry 9.

Substance	Retention time [min]	Area
Methyl valerate	11.7	-
Methyl 4-pentenoate	12.2	-
Methyl 3-pentenoate	-	-
Methyl 2-pentenoate	-	-
Dimethyl adipate	26.2	402.04105
Dimethyl 5-methylglutarate	23.5	58.68542
Dimethyl 4-ethylsuccinate	22.4	8.34444

Table 13, Entry 10

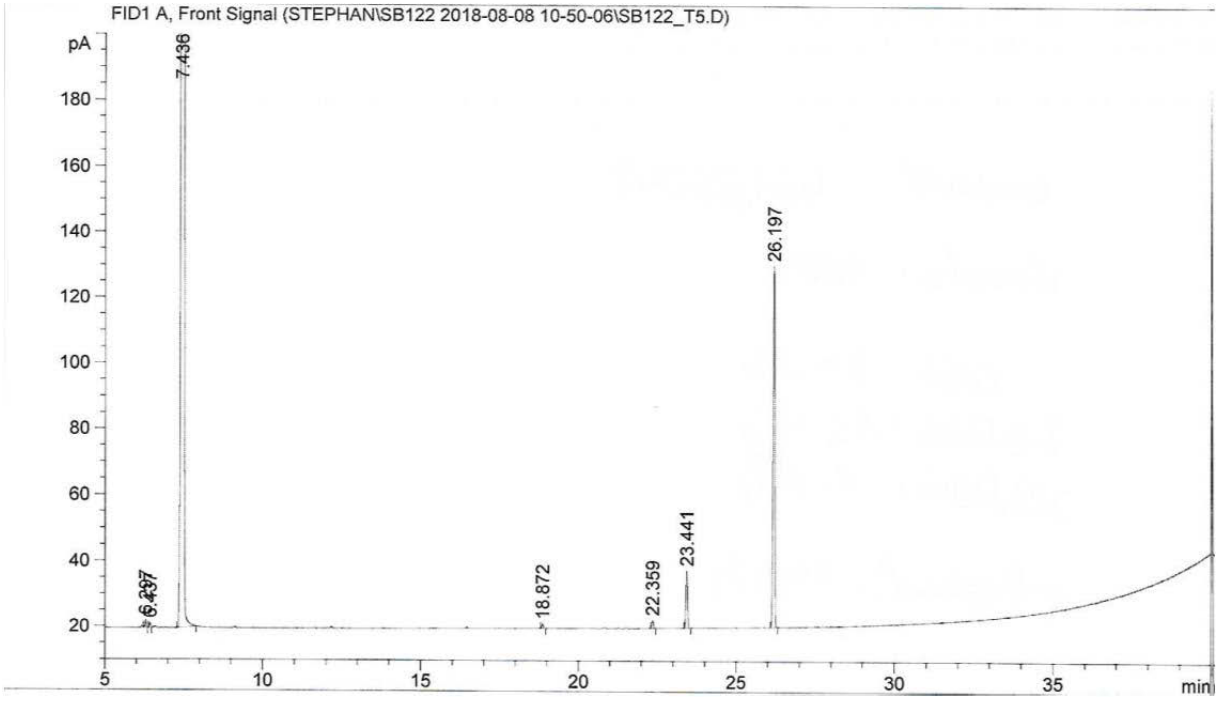

Appendix Fig. 63: Gas chromatogram (GC-FID) of Table 13, Entry 10.

Substance	Retention time [min]	Area
Methyl valerate	11.7	-
Methyl 4-pentenoate	12.2	-
Methyl 3-pentenoate	-	-
Methyl 2-pentenoate	-	-
Dimethyl adipate	26.2	391.90781
Dimethyl 5-methylglutarate	23.5	61.30547
Dimethyl 4-ethylsuccinate	22.4	8.43714

A.2.2.2. PyTBPX

Table 14, Entry 1

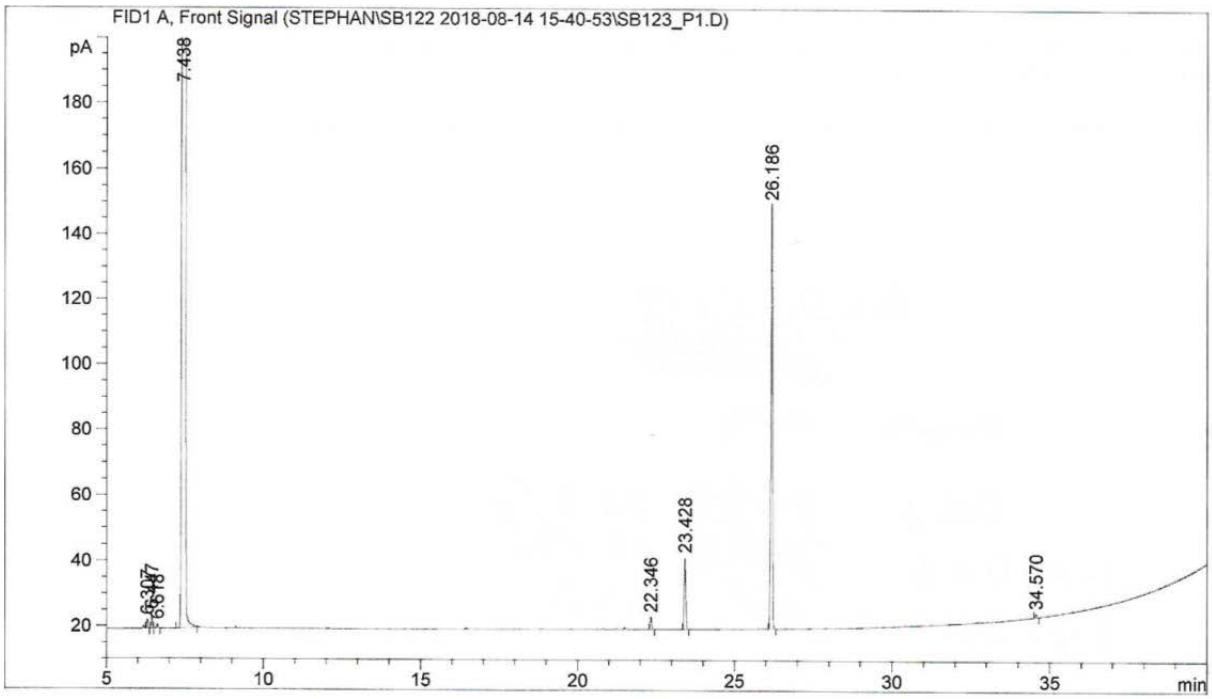

Appendix Fig. 64: Gas chromatogram (GC-FID) of Table 14, Entry 1.

Substance	Retention time [min]	Area
Methyl valerate	11.7	-
Methyl 4-pentenoate	12.2	-
Methyl 3-pentenoate	-	-
Methyl 2-pentenoate	-	-
Dimethyl adipate	26.2	466.7406
Dimethyl 5-methylglutarate	23.5	76.49563
Dimethyl 4-ethylsuccinate	22.4	13.56018

Table 14, Entry 2

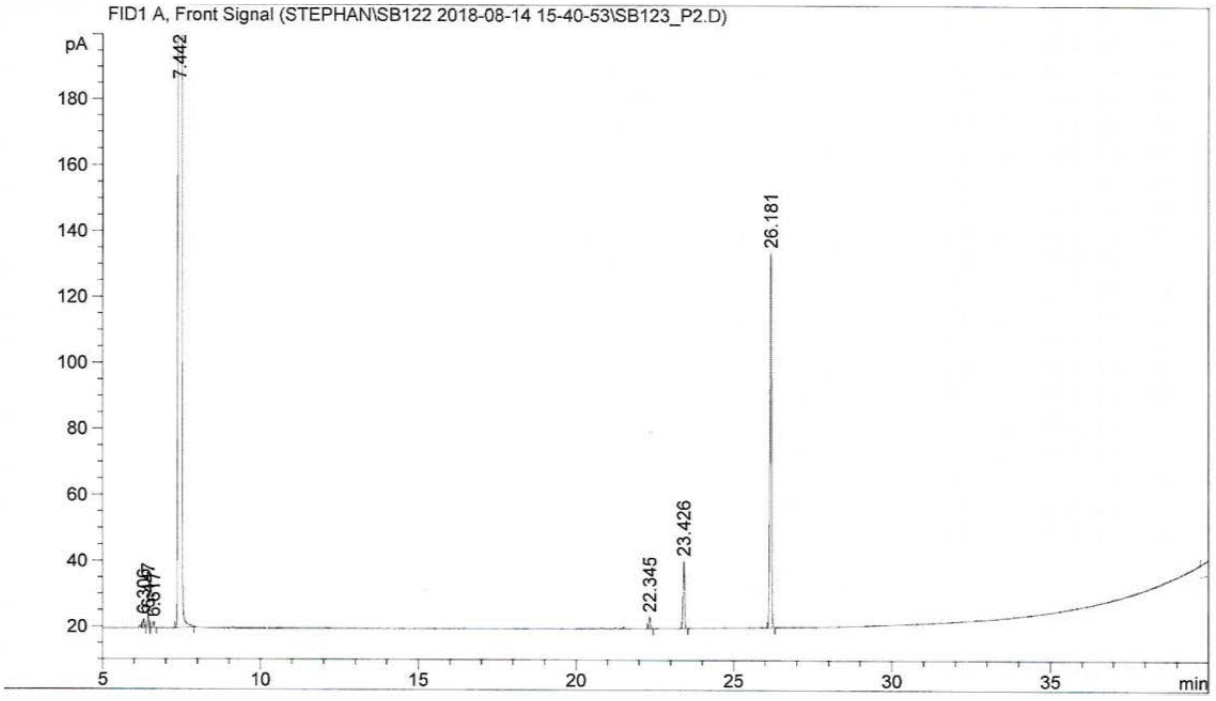

Appendix Fig. 65: Gas chromatogram (GC-FID) of Table 14, Entry 2.

Substance	Retention time [min]	Area
Methyl valerate	11.7	-
Methyl 4-pentenoate	12.2	-
Methyl 3-pentenoate	-	-
Methyl 2-pentenoate	-	-
Dimethyl adipate	26.2	405.80133
Dimethyl 5-methylglutarate	23.5	71.67188
Dimethyl 4-ethylsuccinate	22.4	12.02911

Table 14, Entry 3

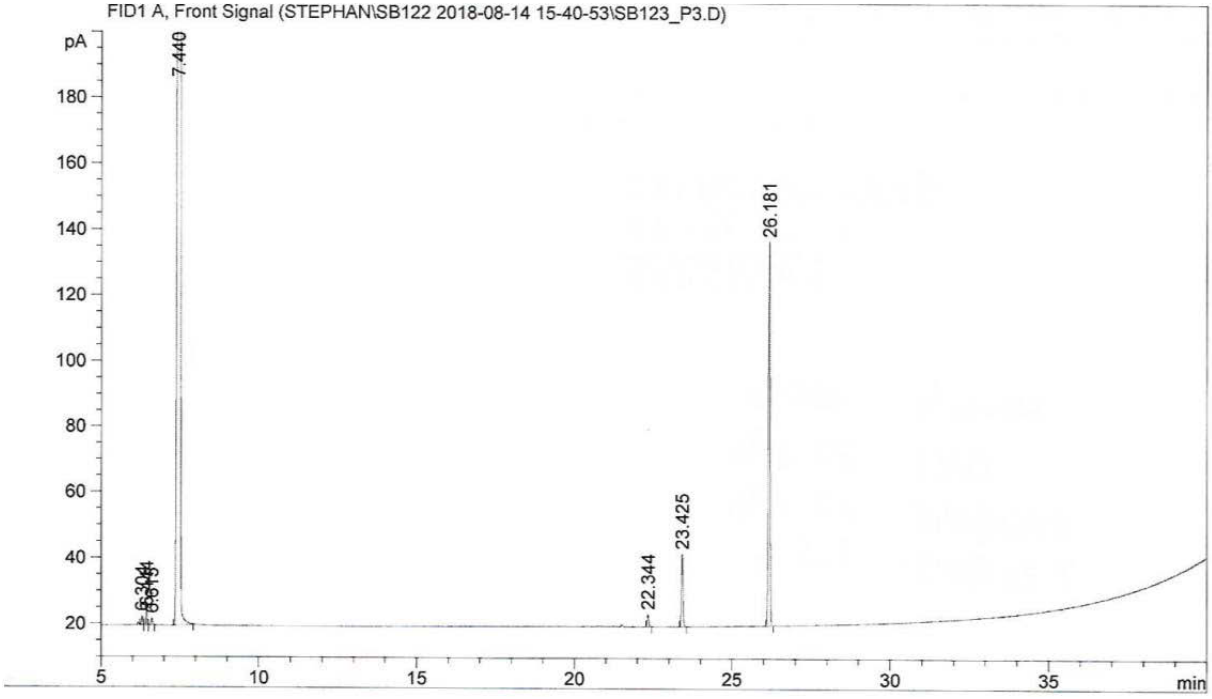

Appendix Fig. 66: Gas chromatogram (GC-FID) of Table 14, Entry 3.

Substance	Retention time [min]	Area
Methyl valerate	11.7	-
Methyl 4-pentenoate	12.2	-
Methyl 3-pentenoate	-	-
Methyl 2-pentenoate	-	-
Dimethyl adipate	26.2	419.32184
Dimethyl 5-methylglutarate	23.5	76.89008
Dimethyl 4-ethylsuccinate	22.4	12.74130

Table 14, Entry 4

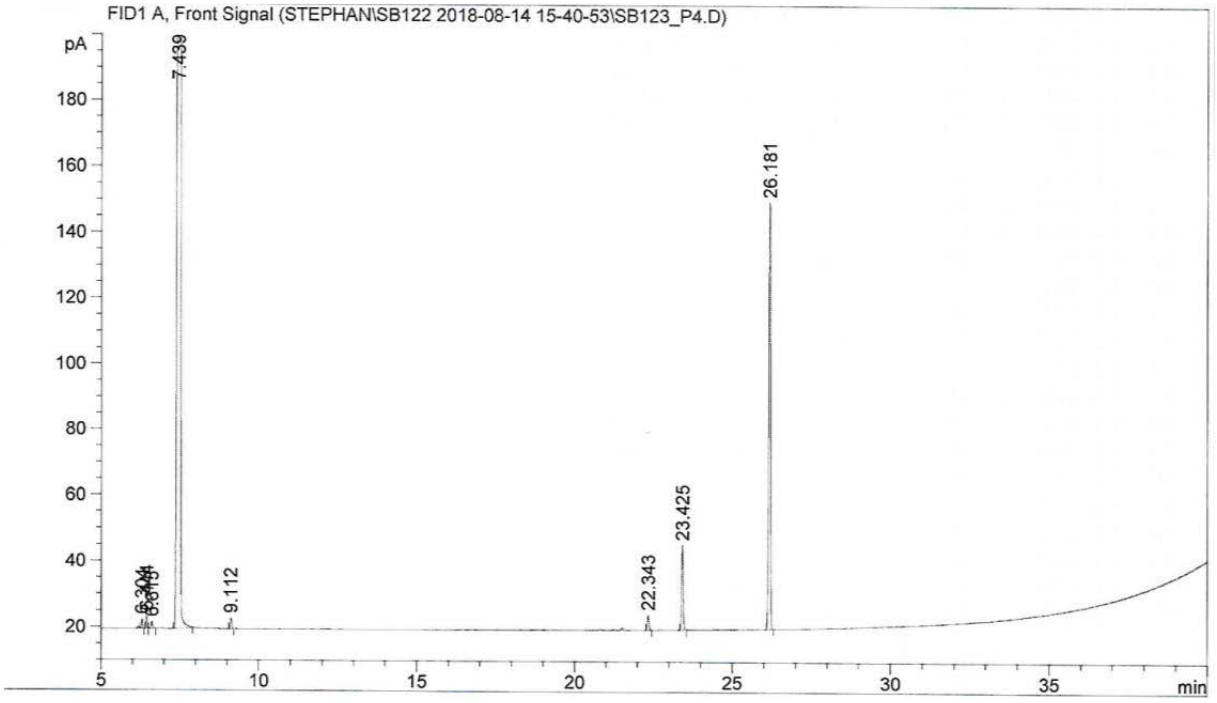

Appendix Fig. 67: Gas chromatogram (GC-FID) of Table 14, Entry 4.

Substance	Retention time [min]	Area
Methyl valerate	11.7	-
Methyl 4-pentenoate	12.2	-
Methyl 3-pentenoate	-	-
Methyl 2-pentenoate	-	-
Dimethyl adipate	26.2	467.59155
Dimethyl 5-methylglutarate	23.5	89.55582
Dimethyl 4-ethylsuccinate	22.4	15.54874

Table 14, Entry 5

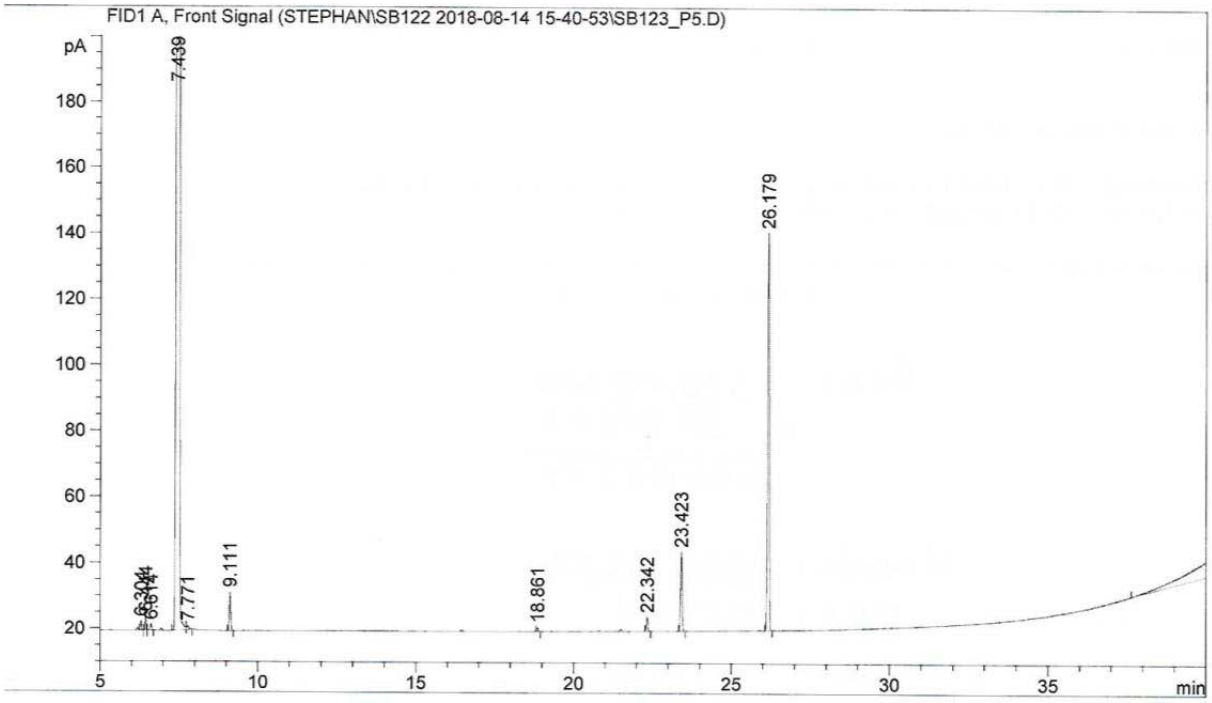

Appendix Fig. 68: Gas chromatogram (GC-FID) of Table 14, Entry 5.

Substance	Retention time [min]	Area
Methyl valerate	11.7	-
Methyl 4-pentenoate	12.2	-
Methyl 3-pentenoate	-	-
Methyl 2-pentenoate	-	-
Dimethyl adipate	26.2	429.34113
Dimethyl 5-methylglutarate	23.5	84.73926
Dimethyl 4-ethylsuccinate	22.4	14.94691

Table 14, Entry 6

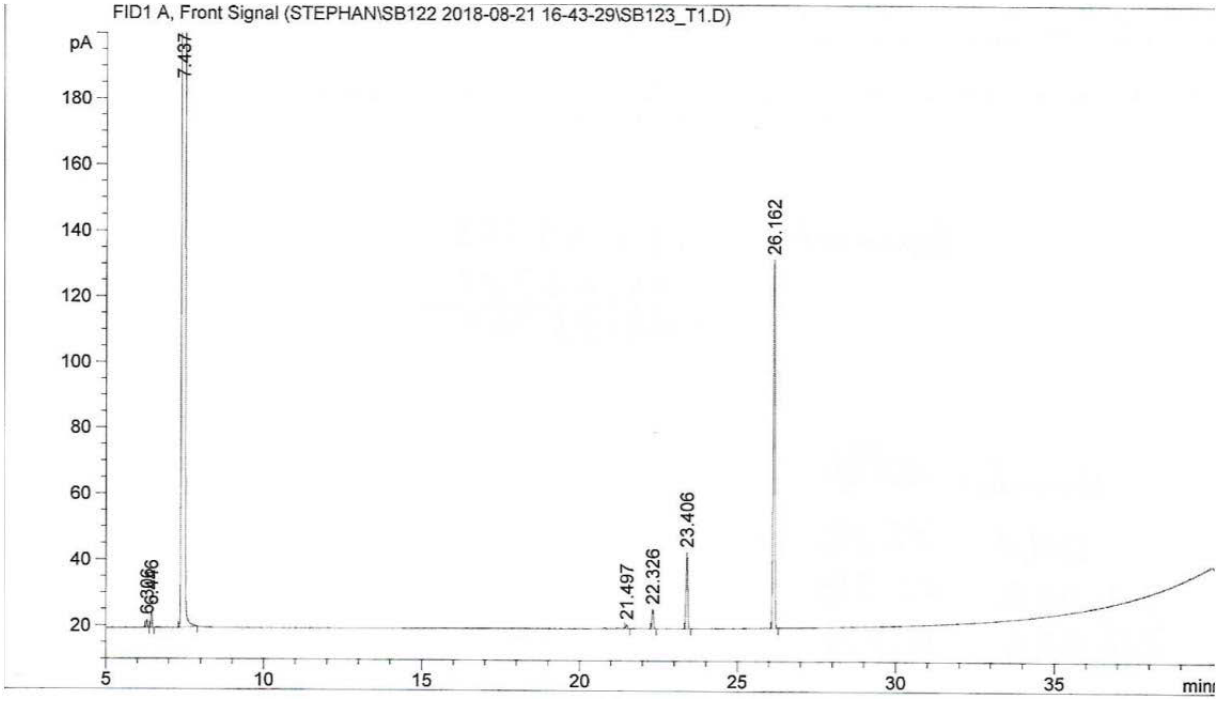

Appendix Fig. 69: Gas chromatogram (GC-FID) of Table 14, Entry 6.

Substance	Retention time [min]	Area
Methyl valerate	11.7	-
Methyl 4-pentenoate	12.2	-
Methyl 3-pentenoate	-	-
Methyl 2-pentenoate	-	-
Dimethyl adipate	26.2	401.09006
Dimethyl 5-methylglutarate	23.5	80.40107
Dimethyl 4-ethylsuccinate	22.4	20.33598

Table 14, Entry 7

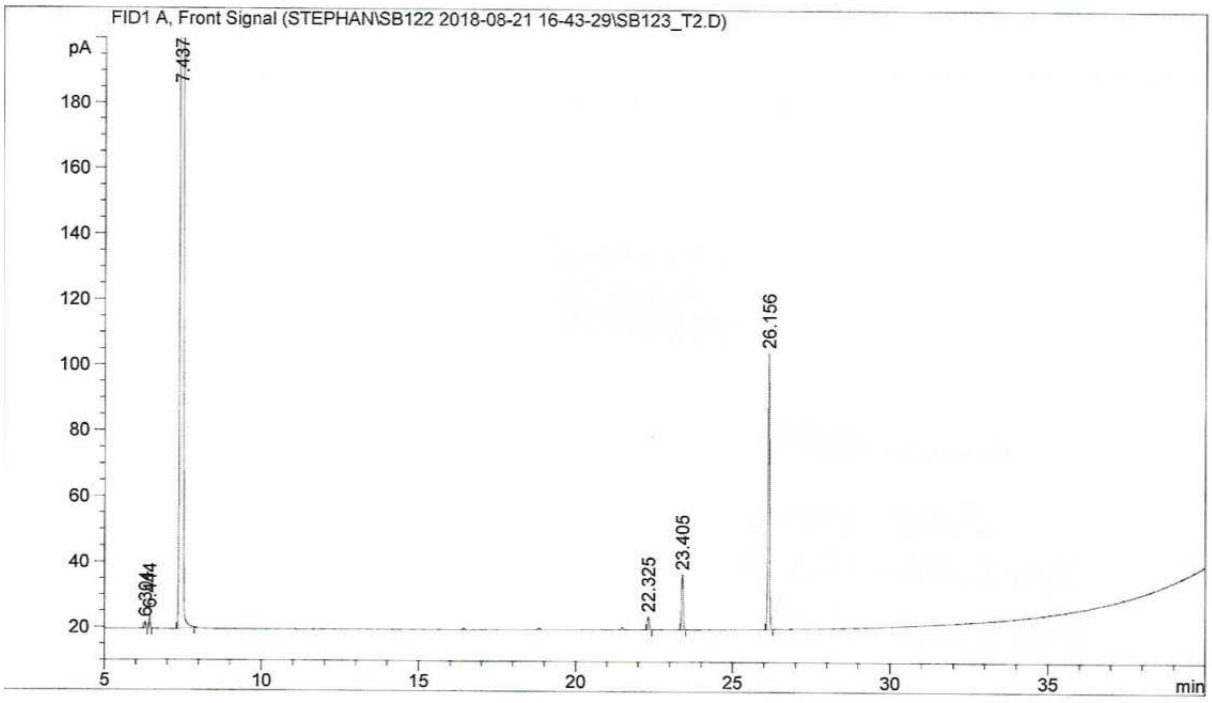

Appendix Fig. 70: Gas chromatogram (GC-FID) of Table 14, Entry 7.

Substance	Retention time [min]	Area
Methyl valerate	11.7	-
Methyl 4-pentenoate	12.2	-
Methyl 3-pentenoate	-	-
Methyl 2-pentenoate	-	-
Dimethyl adipate	26.2	296.50815
Dimethyl 5-methylglutarate	23.5	58.69756
Dimethyl 4-ethylsuccinate	22.4	13.71400

Table 14, Entry 8

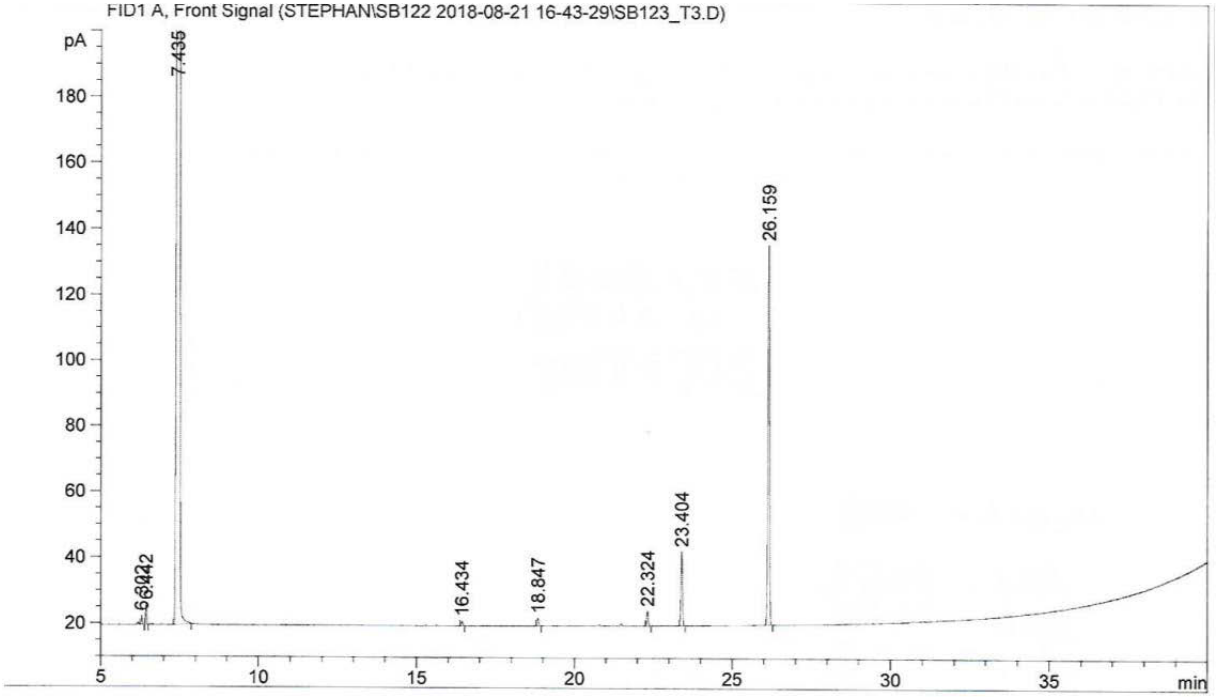

Appendix Fig. 71: Gas chromatogram (GC-FID) of Table 14, Entry 8.

Substance	Retention time [min]	Area
Methyl valerate	11.7	-
Methyl 4-pentenoate	12.2	-
Methyl 3-pentenoate	-	-
Methyl 2-pentenoate	-	-
Dimethyl adipate	26.2	410.26813
Dimethyl 5-methylglutarate	23.5	78.09138
Dimethyl 4-ethylsuccinate	22.4	15.31488

Table 14, Entry 9

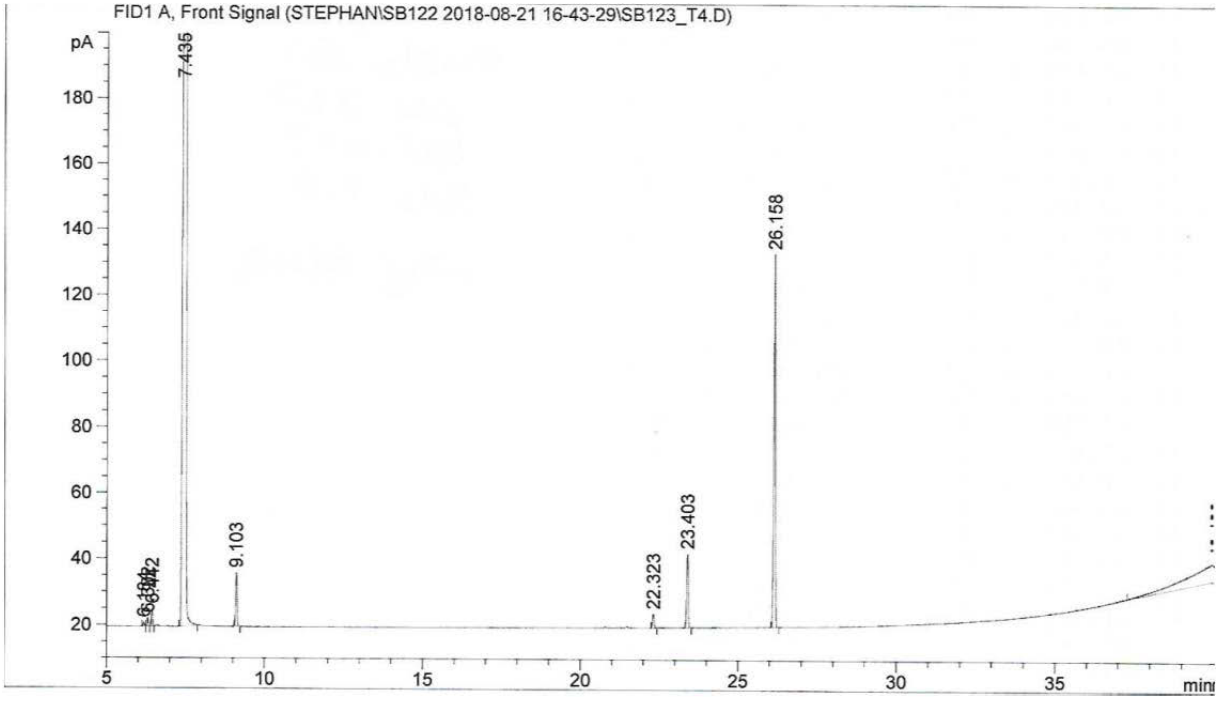

Appendix Fig. 72: Gas chromatogram (GC-FID) of Table 14, Entry 9.

Substance	Retention time [min]	Area
Methyl valerate	11.7	-
Methyl 4-pentenoate	12.2	-
Methyl 3-pentenoate	-	-
Methyl 2-pentenoate	-	-
Dimethyl adipate	26.2	402.62729
Dimethyl 5-methylglutarate	23.5	77.51418
Dimethyl 4-ethylsuccinate	22.4	14.19845

Table 14, Entry 10

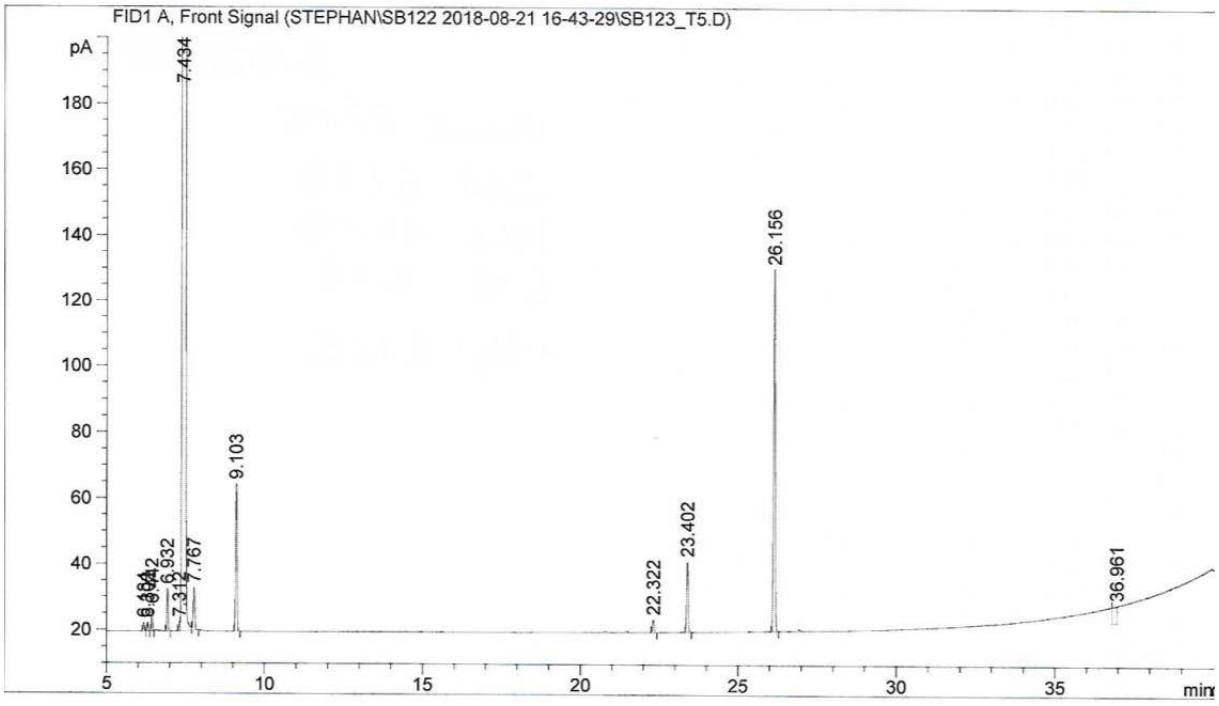

Appendix Fig. 73: Gas chromatogram (GC-FID) of Table 14, Entry 10.

Substance	Retention time [min]	Area
Methyl valerate	11.7	-
Methyl 4-pentenoate	12.2	-
Methyl 3-pentenoate	-	-
Methyl 2-pentenoate	-	-
Dimethyl adipate	26.2	388.06918
Dimethyl 5-methylglutarate	23.5	74.15913
Dimethyl 4-ethylsuccinate	22.4	13.15913

A.2.3. Characterisation and spectroscopic investigations on the catalysts in use

A.2.3.1. Synthesis of [Pd(PyTBPF)Cl]Cl and [Pd(PyTBPX)Cl]Cl

[Pd(PyTBPF)Cl]Cl

^{1}H NMR (300 MHz, dichloromethane-*d*$_2$) δ 8.80 (br. ps. t, J = 7.0 Hz, 2H, Py-H), 8.71 (d, J = 4.5 Hz, 2H Py-H), 7.83 (m, 2H, Py-H), 7.39 (m, 2H, Py-H), 4.45 (br. s, 2H, Cp-H), 4.28 (br. s, 2H, Cp-H), 4.15 (br. s, 2H, Cp-H), 3.98 (br. s, 2H, Cp-H), 1.24 (d, J = 16.3 Hz, 18H, *t*Bu-H). ^{31}P NMR (122 MHz, dichloromethane-*d*$_2$) δ 45.92 (br. s).

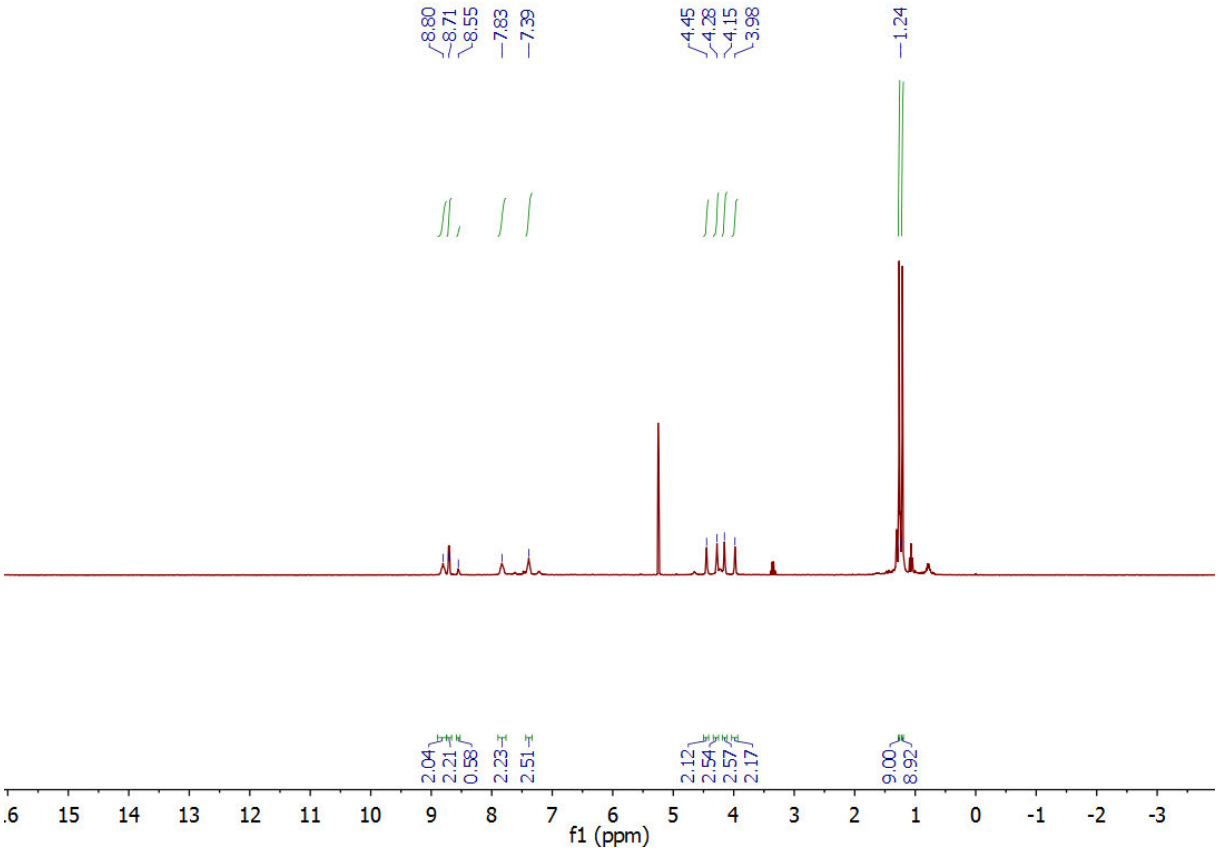

Appendix Fig. 74: ^{1}H NMR of (PyTBPF)PdCl$_2$ in CD$_2$Cl$_2$ at rt and ap.

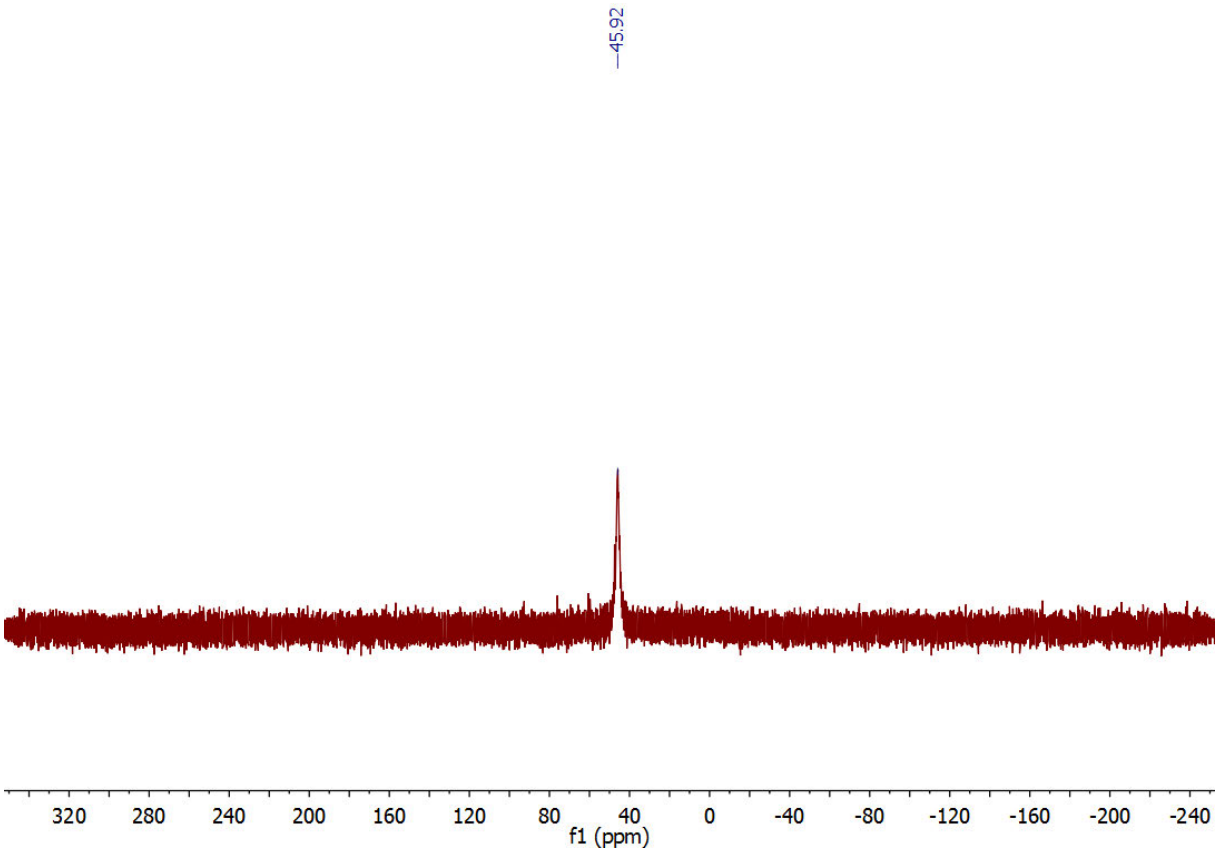

Appendix Fig. 75: ^{31}P NMR of (PyTBPF)$PdCl_2$ in CD_2Cl_2 at rt and ap.

[Pd(PyTBPX)Cl]Cl

^{1}H NMR (300 MHz, dichloromethane-*d*$_2$) δ 8.66 (dm, J = 4.8 Hz, 2H), 8.39 (br. s, 2H), 7.70 (m, 2H), 7.35 (m, 2H), 6.97 (m, 2H), 6.71 (br. s, 2H), 3.72 (br. s, 4H), 1.37 (d, J = 16.6 Hz, 18H). ^{31}P NMR (122 MHz, dichloromethane-*d*$_2$) δ 31.7 ppm (br. s). The purity of the product is 96 % according to the ^{31}P NMR spectrum.

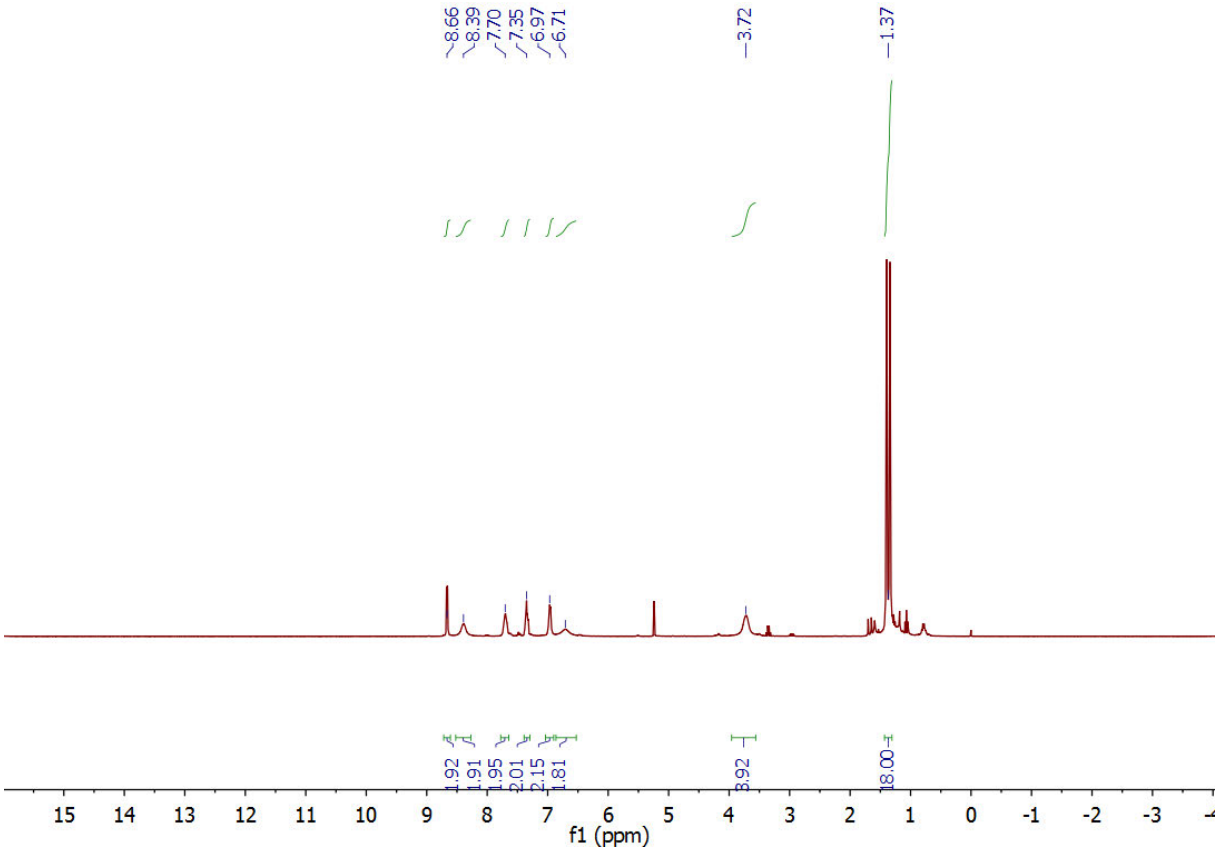

Appendix Fig. 76: ^{1}H NMR of (PyTBPX)PdCl$_2$ in CD$_2$Cl$_2$ at rt and ap.

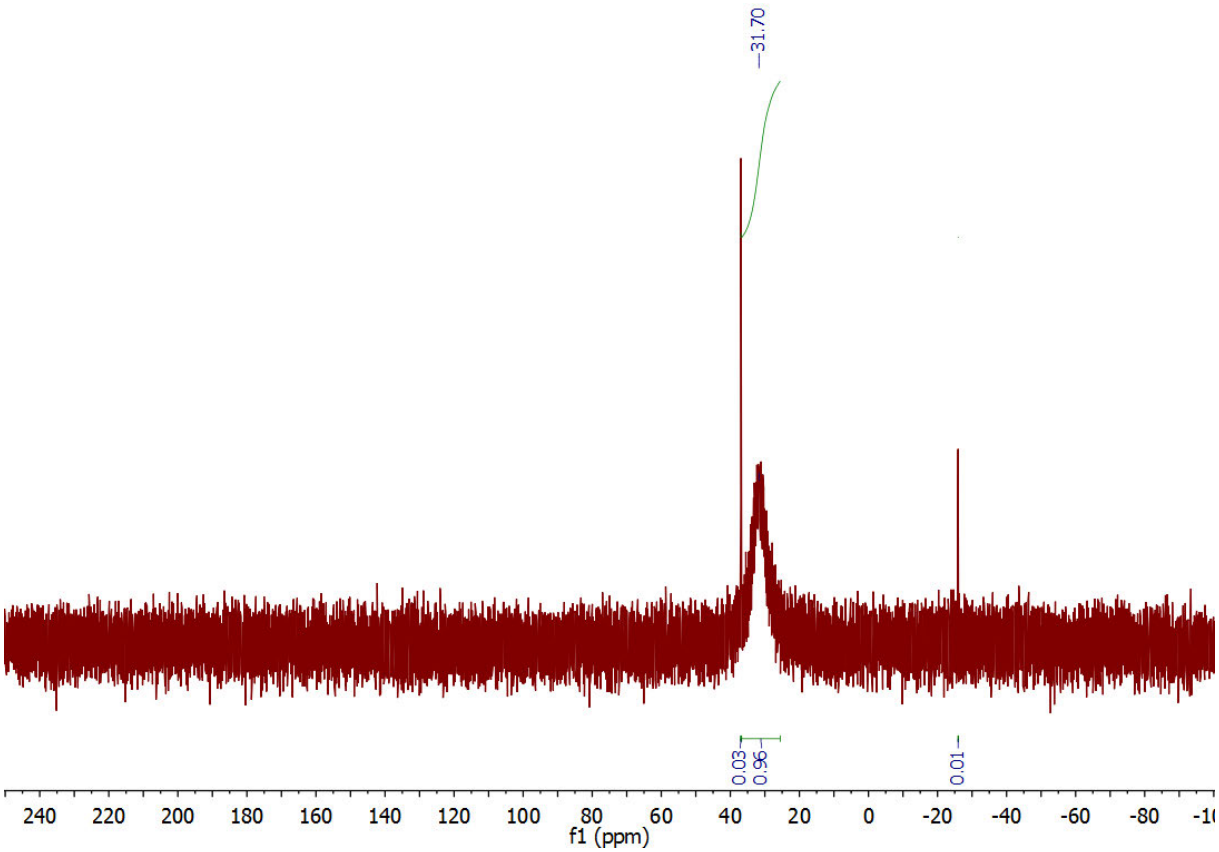

Appendix Fig. 77: ^{31}P NMR of (PyTBPX)$PdCl_2$ in CD_2Cl_2 at rt and ap.

A.2.3.2. H+-free synthesis of [Pd(PyTBPF)OTf]OTf and [Pd(PyTBPX)OTf]OTf starting from [Pd(PyTBPF)Cl]Cl and [Pd(PyTBPX)Cl]Cl

[Pd(PyTBPF)OTf]OTf – Acid free

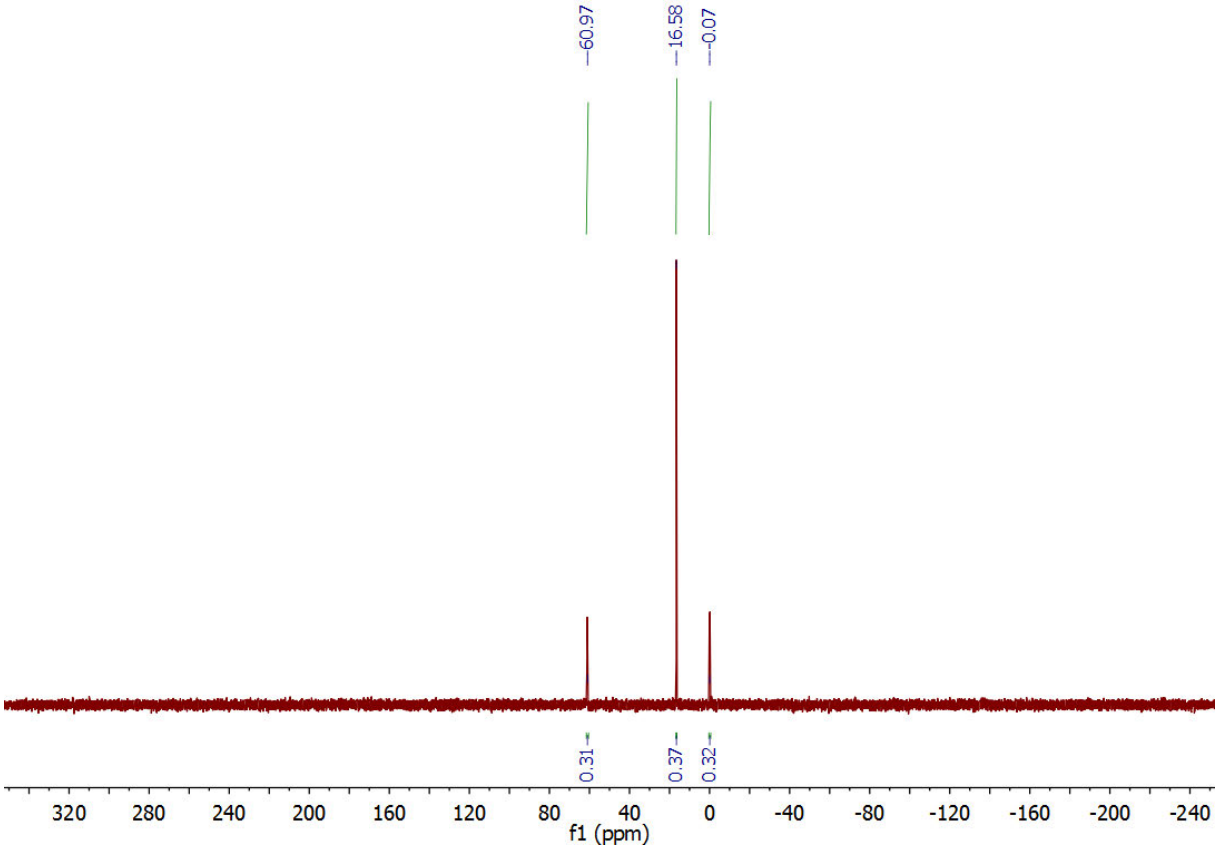

Appendix Fig. 78: ^{31}P NMR of $[(PyTBPF)Pd(CF_3SO_3)]^+(CF_3SO_3)^-$ synthesized without acid in CD_2Cl_2 at rt and ap.

[Pd(PyTBPX)OTf]OTf – Acid free

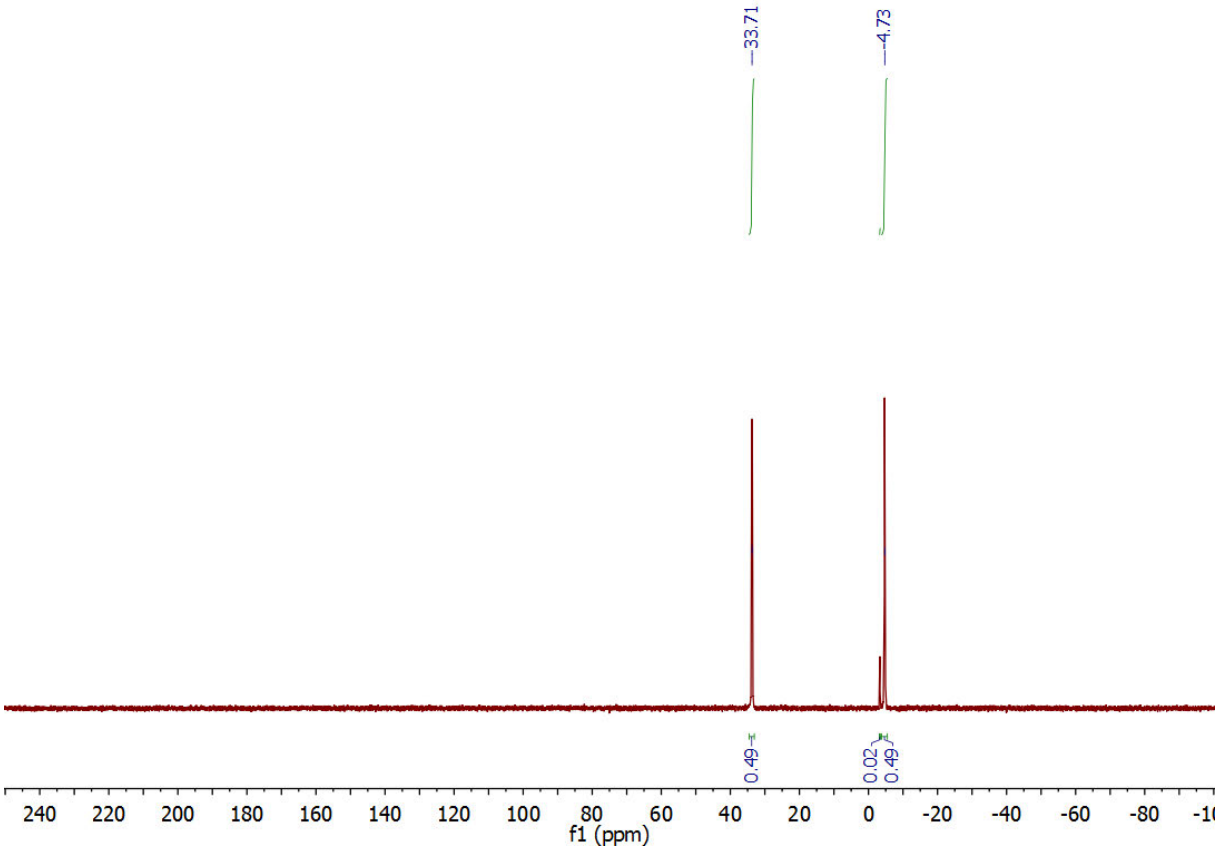

Appendix Fig. 79: ^{31}P NMR of $[(PyTBPX)Pd(CF_3SO_3)]^+(CF_3SO_3)^-$ synthesized without acid in CD_2Cl_2 at rt and ap. Only small amounts of impurities present (~2.0 %).

A.2.3.3. NMR-spectroscopic characterisation of the ligand PyTBPF and PyTBPX

Pytbpf

^1H NMR (300 MHz, dichloromethane-d_2) δ 8.67 (m, 2H), 7.73 (m, 2H), 7.60 (tt, J = 7.6, 2.0 Hz, 2H), 7.20 (m, 2H), 4.50 – 4.43 (m, 2H), 4.09 (m, 2H), 3.82 – 3.75 (m, 4H), 0.85 (d, $^3J_{H,P}$ = 12.4 Hz, 18H). $^{31}P\{^1H\}$ NMR (122 MHz, dichloromethane-d_2) δ 6.95 (s). ^{15}N NMR (40 MHz, dichloromethane-d_2) δ -48.1 (s).

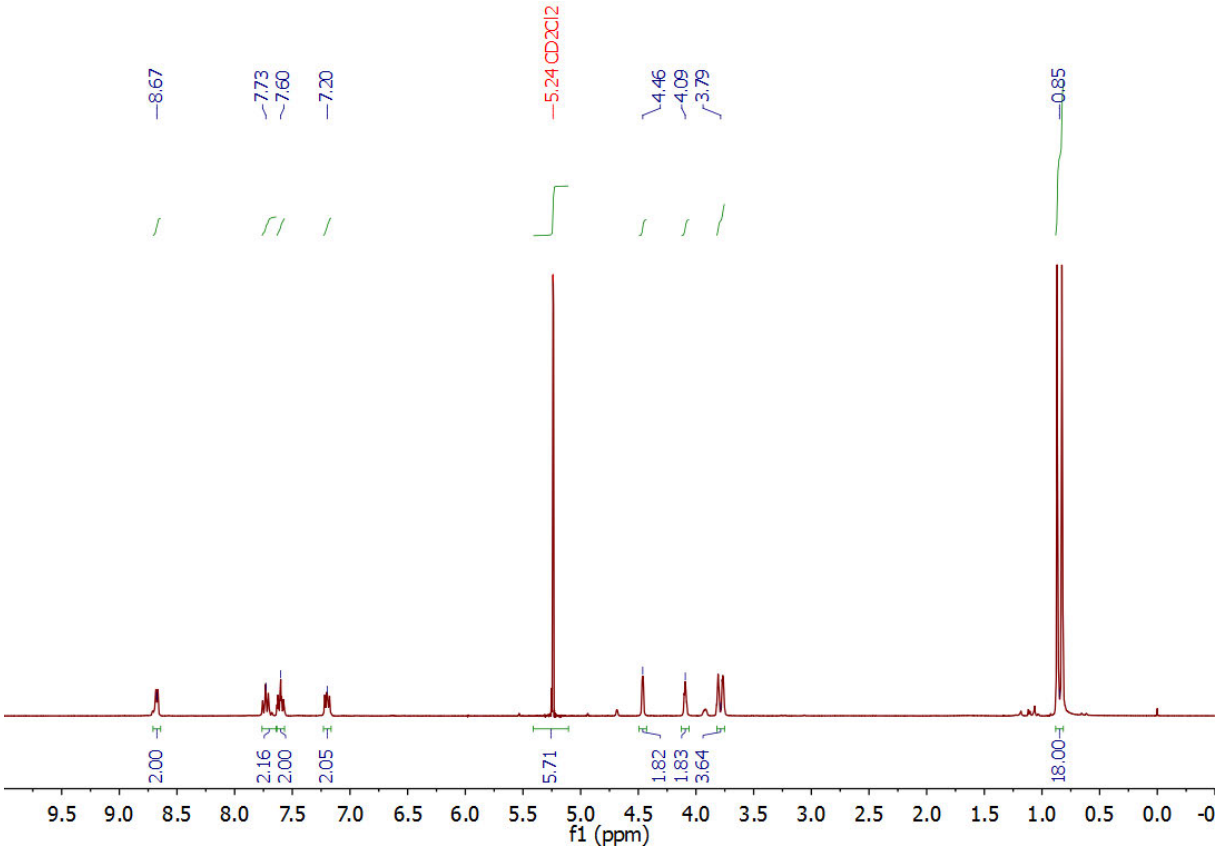

Appendix Fig. 80: ^{1}H *NMR of PyTBPF in* CD_2Cl_2 *at rt and ap.*

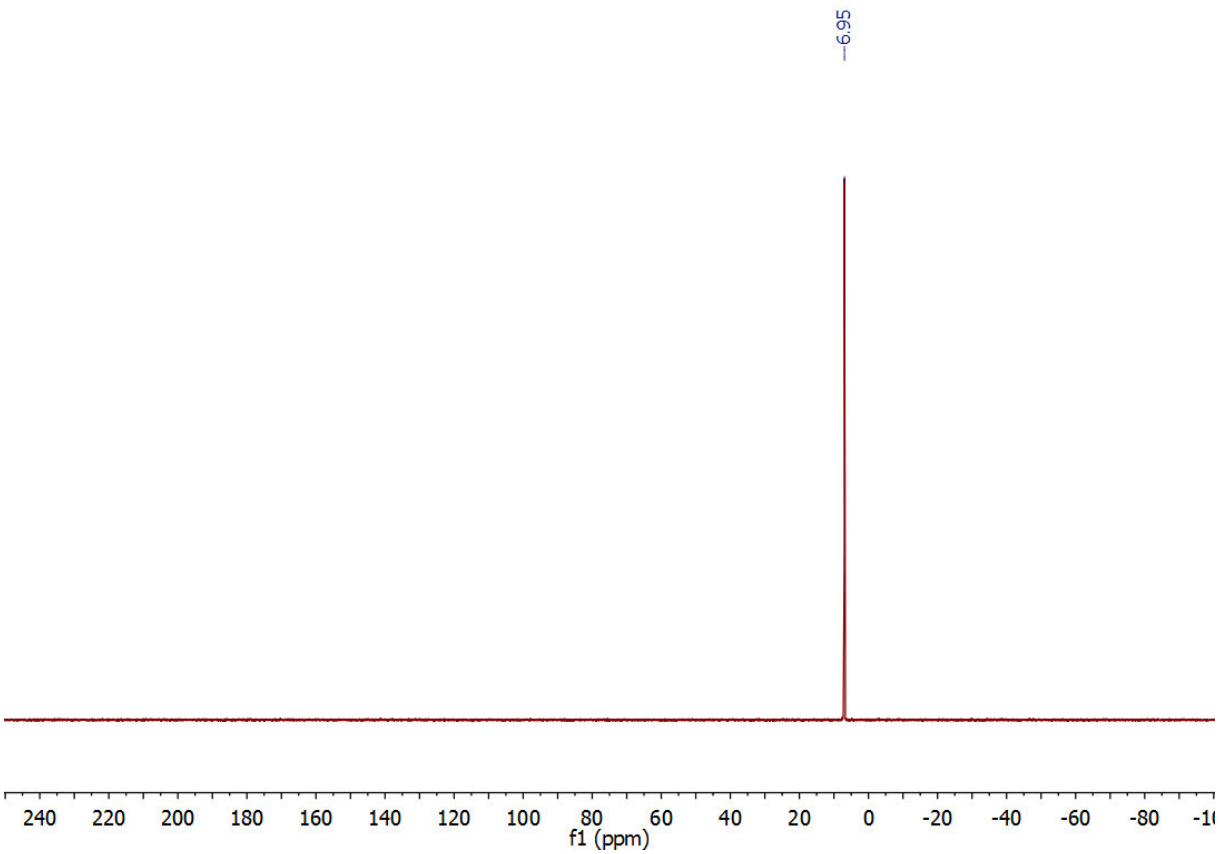

Appendix Fig. 81: ^{31}*P NMR of PyTBPF in* CD_2Cl_2 *at rt and ap.*

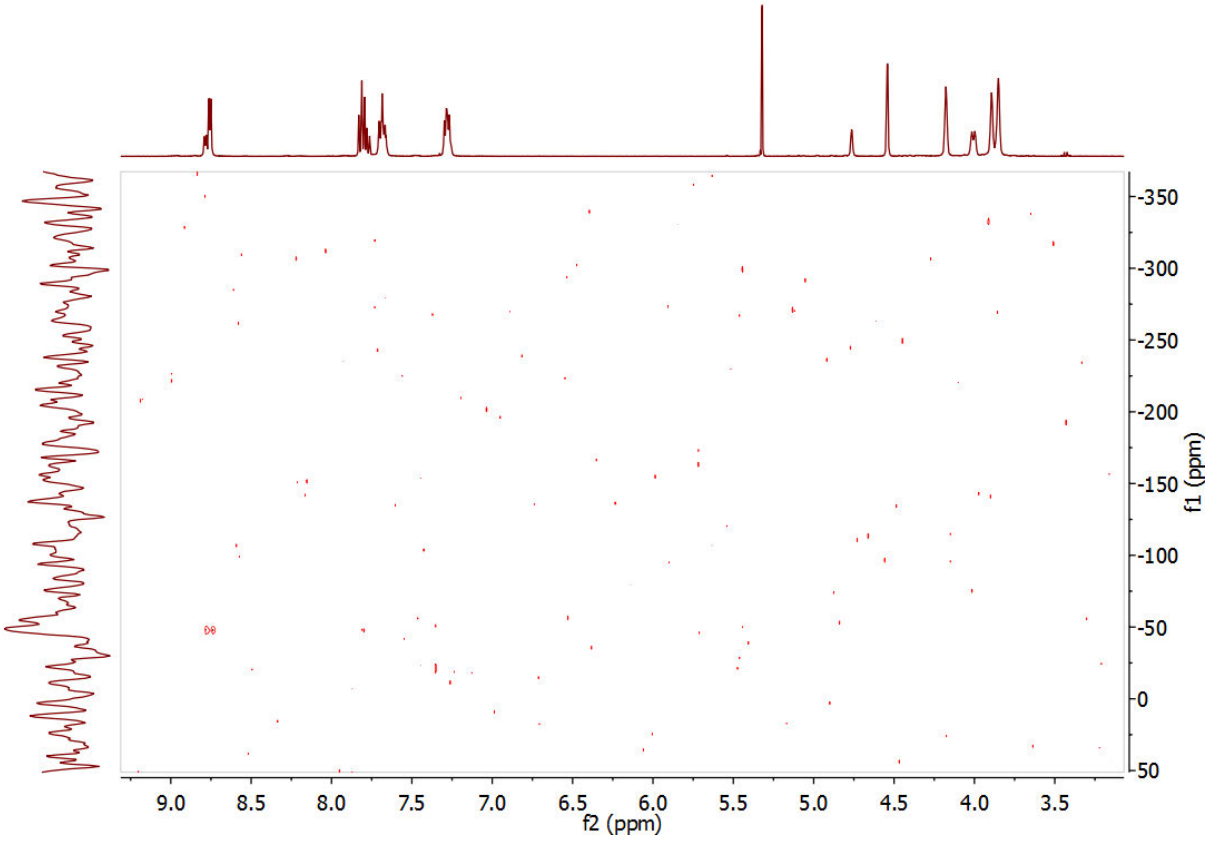

Appendix Fig. 82: $^{1}H/^{15}N$ HMBC NMR of PyTBPF in CD_2Cl_2 at rt.

Pytbpx

^{1}H NMR (300 MHz, methanol-*d*$_4$) δ 8.67 (m, 2H), 7.73 – 7.54 (m, 4H), 7.30 (ddt, J = 7.4, 4.9, 1.6 Hz, 2H), 7.00 – 6.87 (m, 2H), 6.78 – 6.65 (m, 2H), 3.84 (dd, J = 13.8, 4.7 Hz, 2H), 3.39 – 3.27 (m, 2H), 1.10 (d, J = 11.8 Hz, 18H). $^{31}P\{^{1}H\}$ NMR (122 MHz, methanol-*d*$_4$) δ 7.83 (s). ^{15}N NMR (40 MHz, dichloromethane-*d*$_2$) δ -51.6 (s).

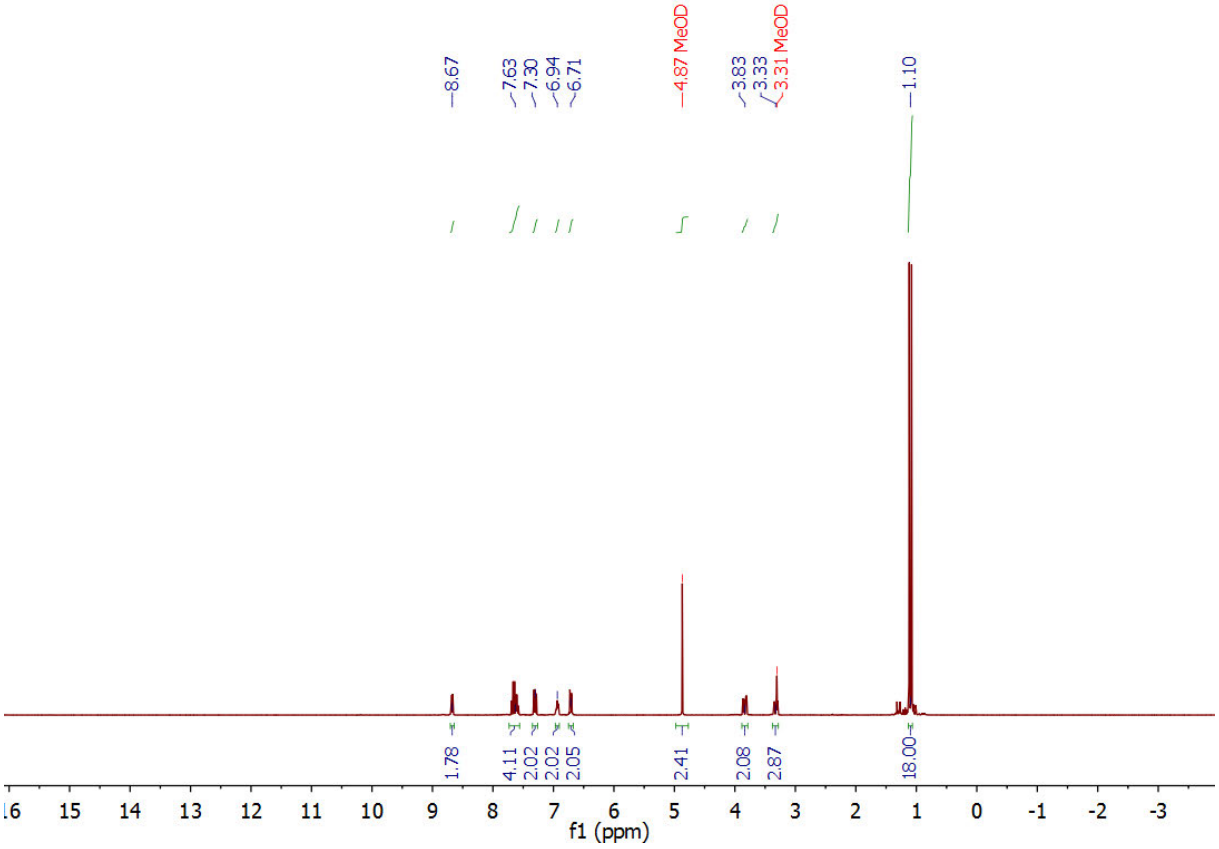

Appendix Fig. 83: ^{1}H NMR of PyTBPX in MeOH-d_4 at rt and ap.

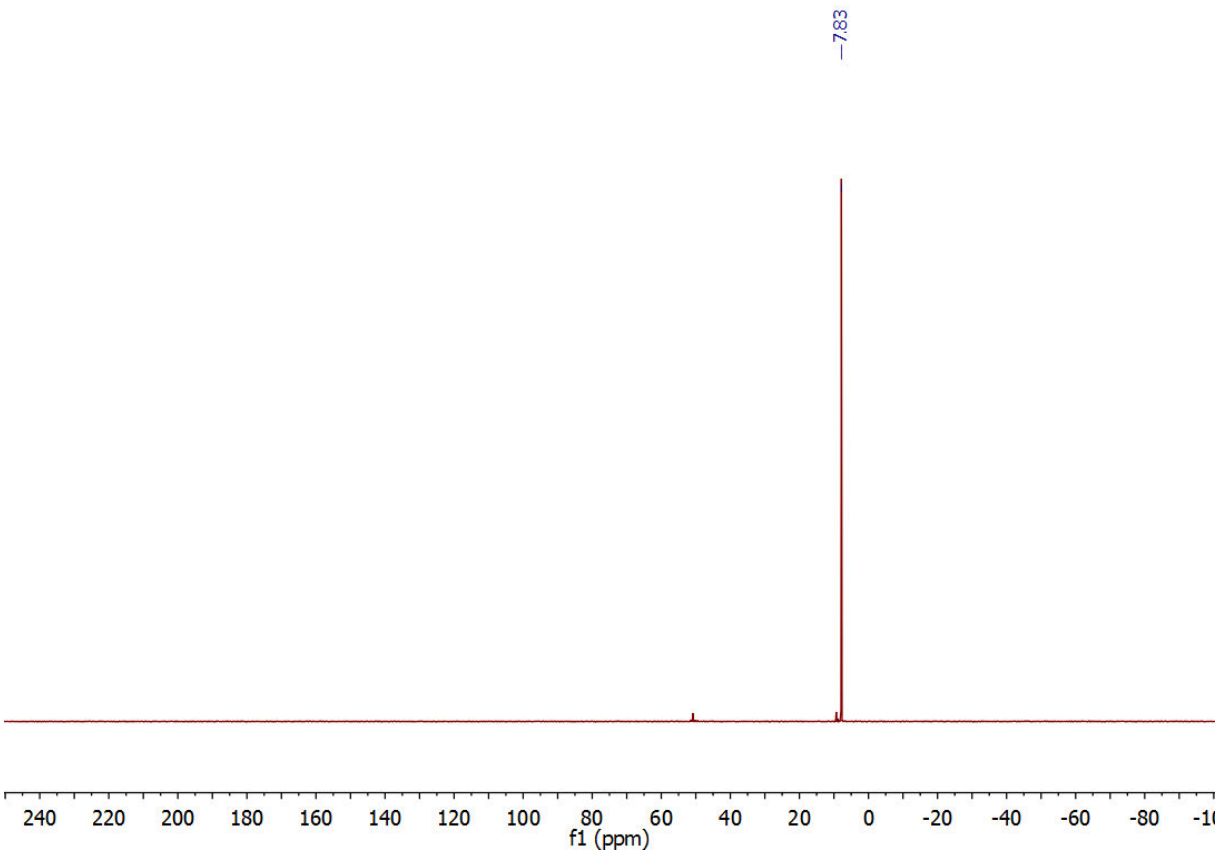

Appendix Fig. 84: ^{31}P NMR of PyTBPX in MeOH-d_4 at rt and ap.

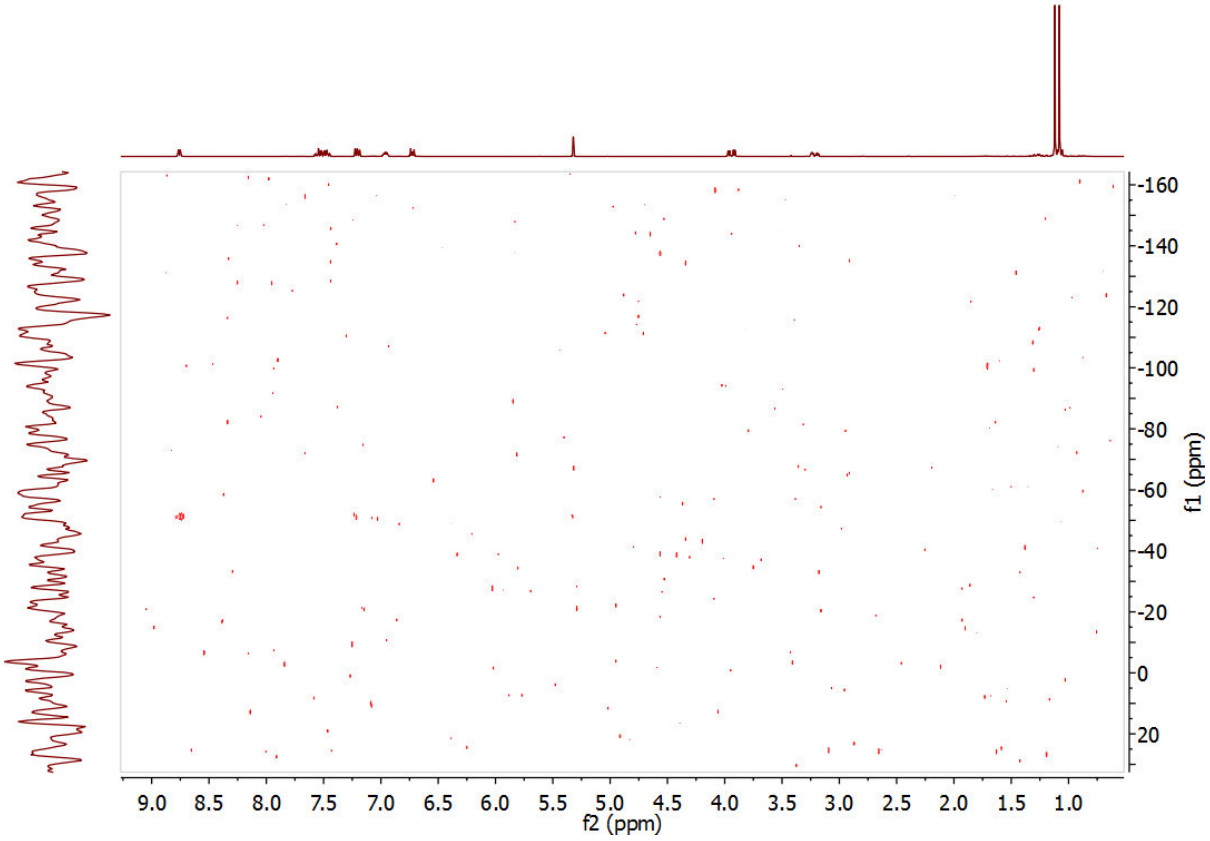

Appendix Fig. 85: $^{1}H/^{15}N$ HMBC NMR of PyTBPX in CD_2Cl_2 at rt.

A.2.3.3.1. Protonation of the ligands with trifluoromethanesulfonic acid

Protonation of BuPox as reference

^{1}H NMR (300 MHz, dichloromethane-*d*2) δ 7.36 – 7.19 (m, 4H, Ar-*H*), 5.7 (dt, $^{1}J_{H,P}$ = 454Hz, $^{3}J_{H,H}$ = 5.6 Hz, 2H, P-*H*), 3.65 (dd, $^{2}J_{H,P}$ = 13.7 Hz, $^{3}J_{H,H}$ = 5.6 Hz, 4H, Ar-C*H*2-P), 1.28 (d, $^{3}J_{H,P}$ = 17.2 Hz, 36H, *t*Bu-*H*). ^{31}P NMR (122 MHz, dichloromethane-*d*2) δ 51.54 (dm, $^{1}J_{H,P}$ = 454 Hz).

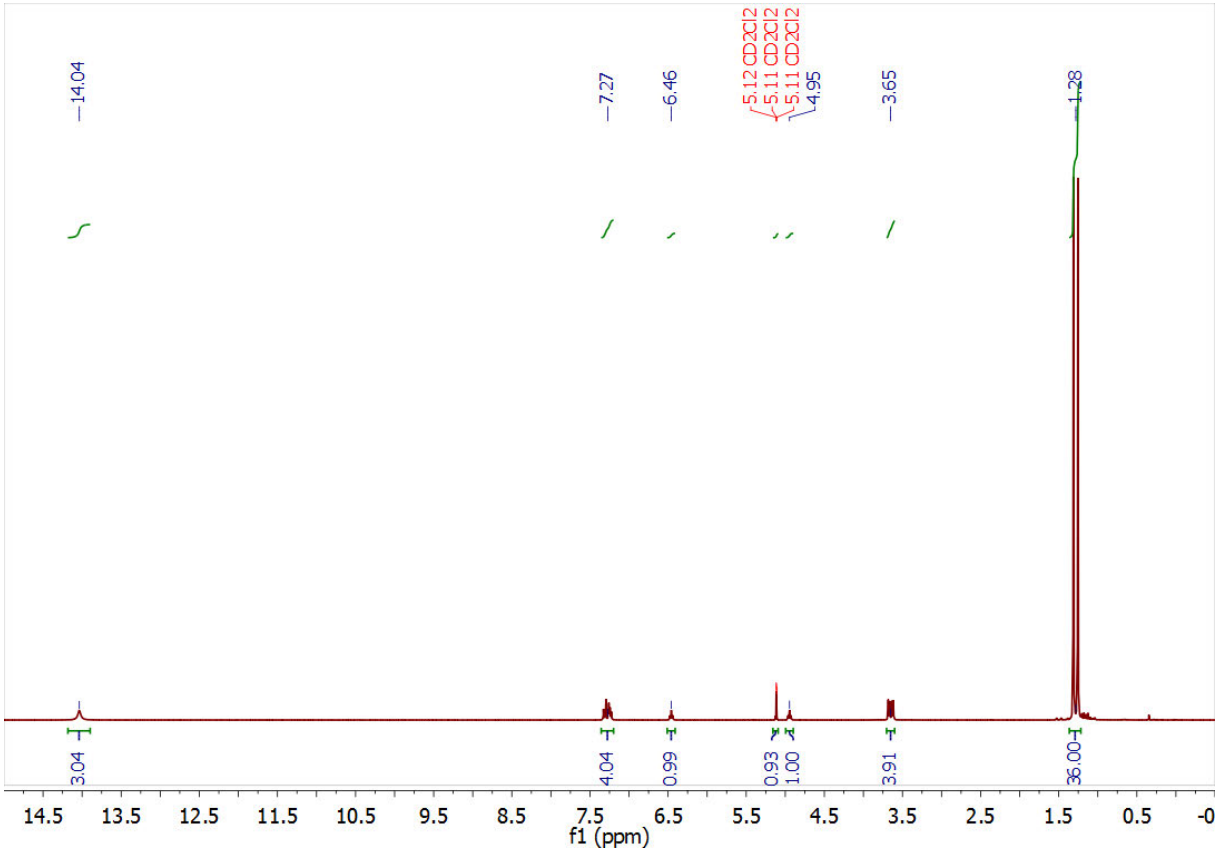

Appendix Fig. 86: ^{1}H NMR of the protonated BuPox ligand in CD_2Cl_2 at rt and ap.

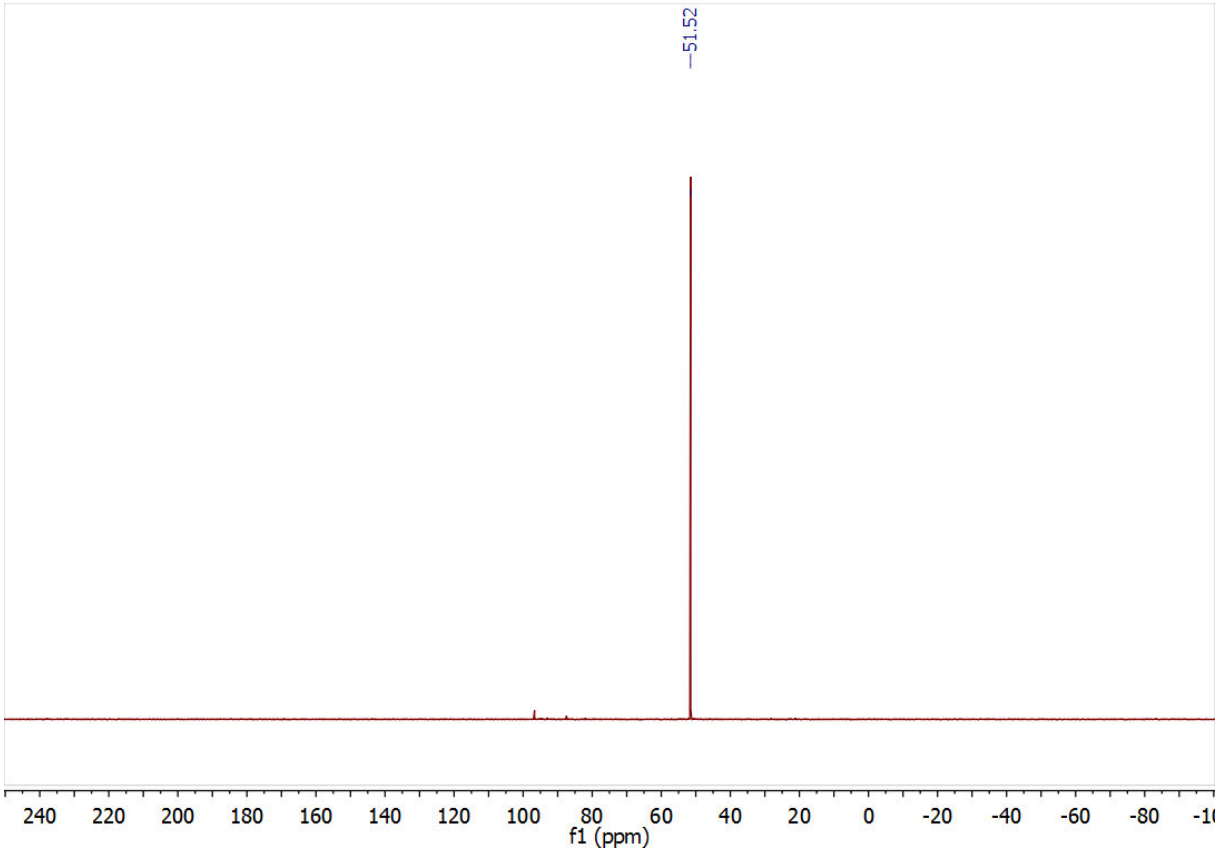

Appendix Fig. 87: $^{31}P\{^{1}H\}$ NMR of the protonated BuPox in CD_2Cl_2 at rt and ap.

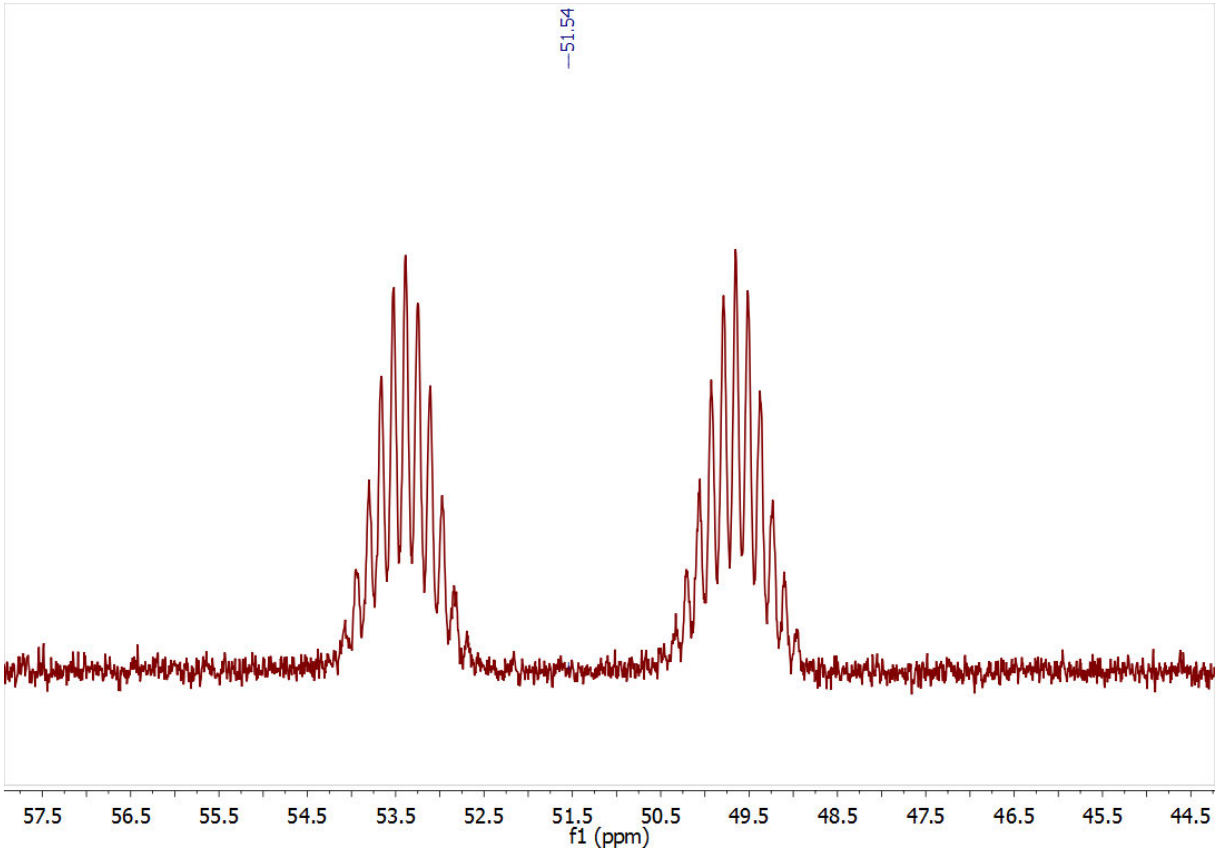

Appendix Fig. 88: Proton coupled ^{31}P NMR of the protonated BuPox Ligand in CD_2Cl_2 at rt and ap. The spectrum is scaled to show the signal of interest only.

PyTBPF

^{1}H NMR (300 MHz, dichloromethane-*d*2) δ 8.83 (m, 2H), 7.98 (t, J = 7.73 Hz, 2H), 7.83 (dd, J = 7.63 Hz, J = 3.87 Hz, 2H), 7.58 (m, 2H), 4.38 (m, 2H), 4.28 (m, 2H), 4.24 (m, 2H), 4.13 (m, 2H), 0.97 (d, $^{3}J_{H,P}$ = 13.76 Hz, 18H). ^{31}P NMR (122 MHz, dichloromethane-*d*2) δ 9.13 (s).

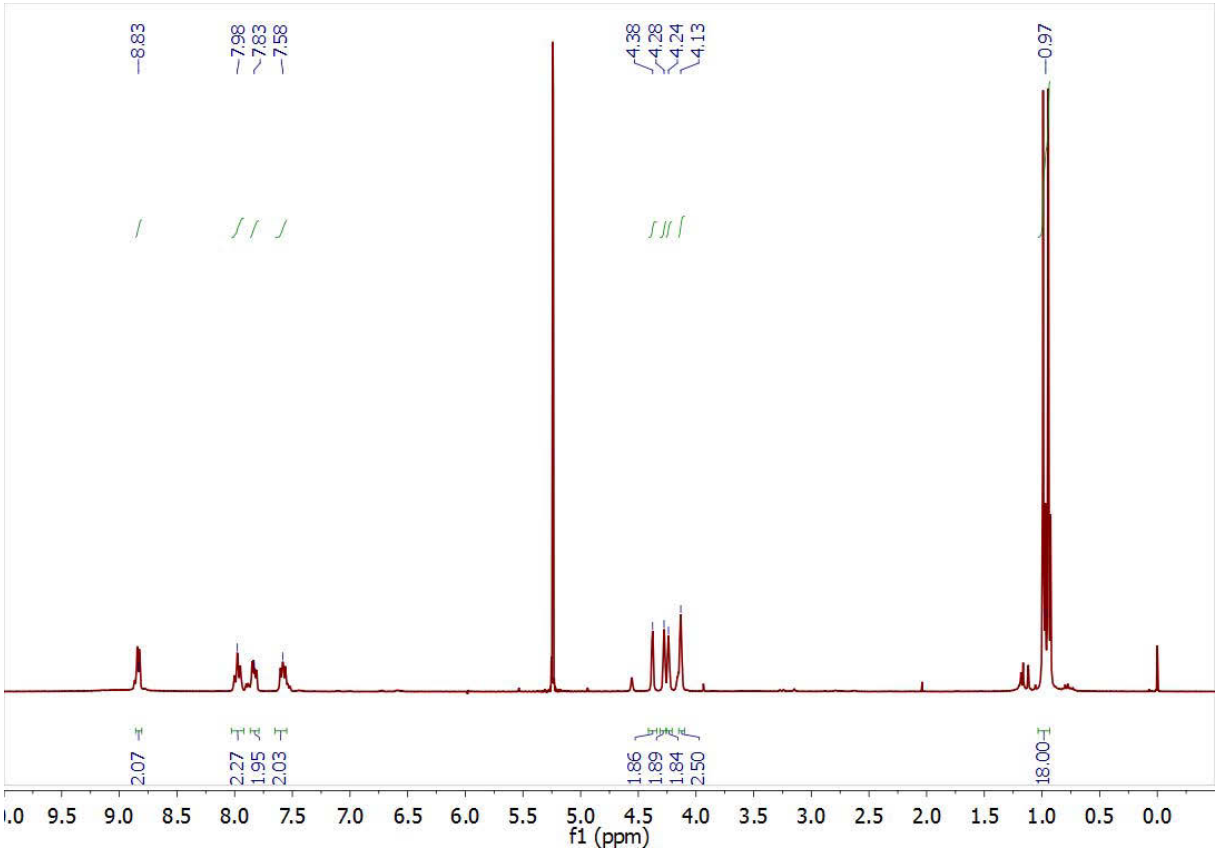

Appendix Fig. 89: ^{1}H NMR of the protonated PyTBPF ligand in CD_2Cl_2 at rt and ap.

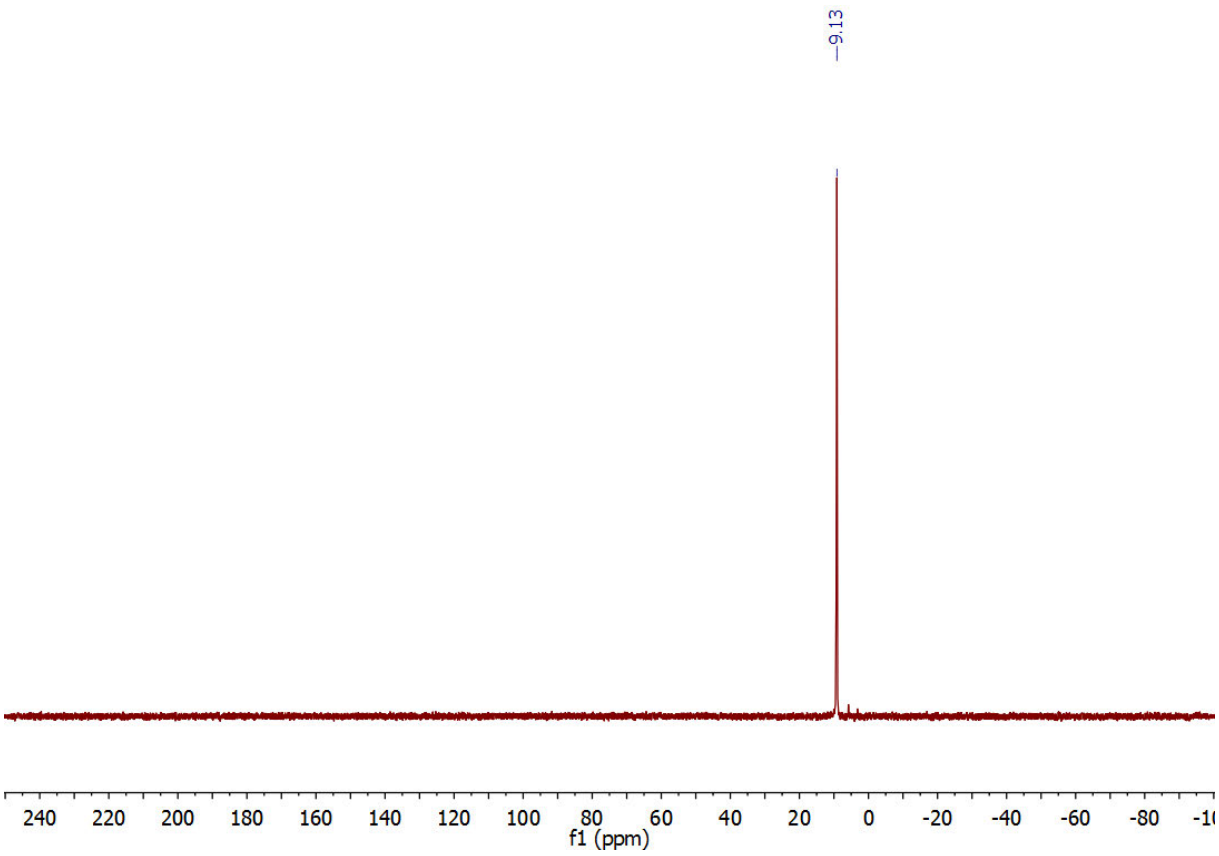

Appendix Fig. 90: $^{31}P\{^{1}H\}$ NMR of the protonated PyTBPF ligand in CD_2Cl_2 at rt and ap.

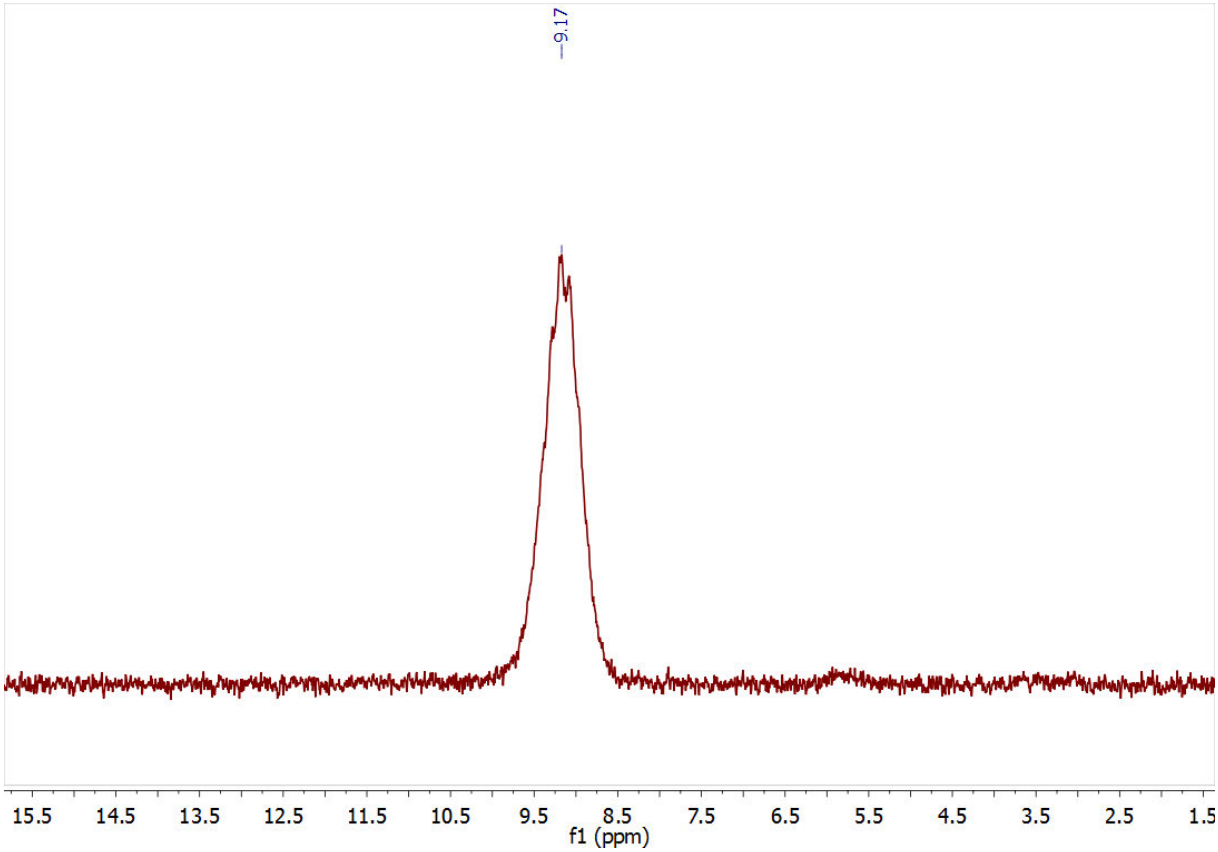

Appendix Fig. 91: ^{31}P NMR of the protonated PyTBPF ligand in CD_2Cl_2 at rt and ap. Only the relevant part of the spectrum is shown.

Pytbpx

^{1}H NMR (300 MHz, dichloromethane-*d*$_2$) δ 8.88 (ddd, $^{3}J_{H,H}$ = 5.6 Hz, $^{4}J_{H,H}$ = 1.7 Hz, $^{5}J_{H,H}$ = 0.7 Hz, 2H), 8.24 (dt, J = 7.8 Hz, J = 1.0 Hz, 2H), 8.05 (d, J = 7.8 Hz, 2H), 7.7 (tm, J = 6.7 Hz, 2H), 7.06 (m, 2H), 6.86 (dd, J = 5.7 Hz, J = 3.4 Hz, 2H), 3.75 (ddd, $^{2}J_{H,H}$ = 14.7 Hz, J = 3.1 Hz, J = 2.3 Hz, 2H), 3.37 (dd, $^{2}J_{H,H}$ = 14.9 Hz, J = 3.1 Hz, 2H), 1.08 (d, $^{3}J_{H,P}$ = 13.2 Hz, 18 H). ^{31}P NMR (122 MHz, dichloromethane-*d*$_2$) δ 8.10 (s).

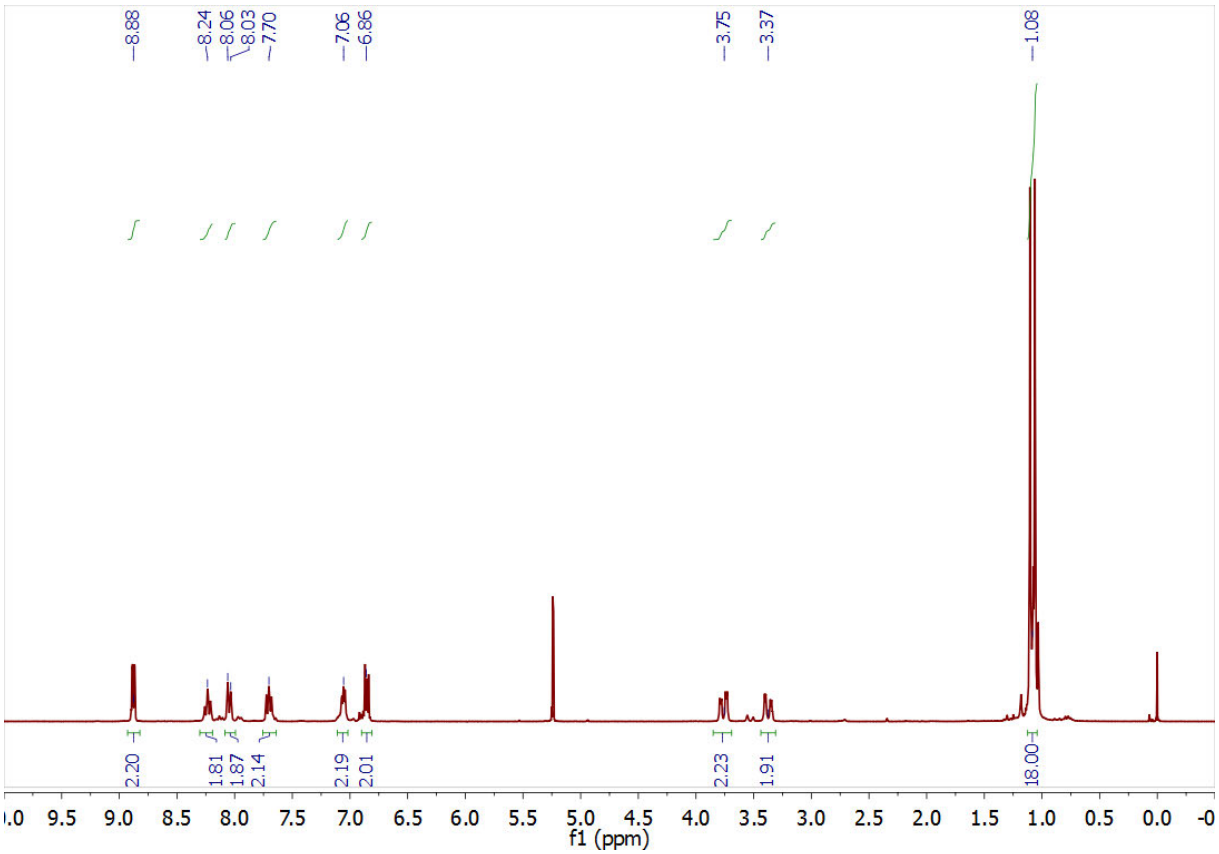

Appendix Fig. 92: ^{1}H NMR of the protonated PyTBPX ligand in CD_2Cl_2 at rt and ap.

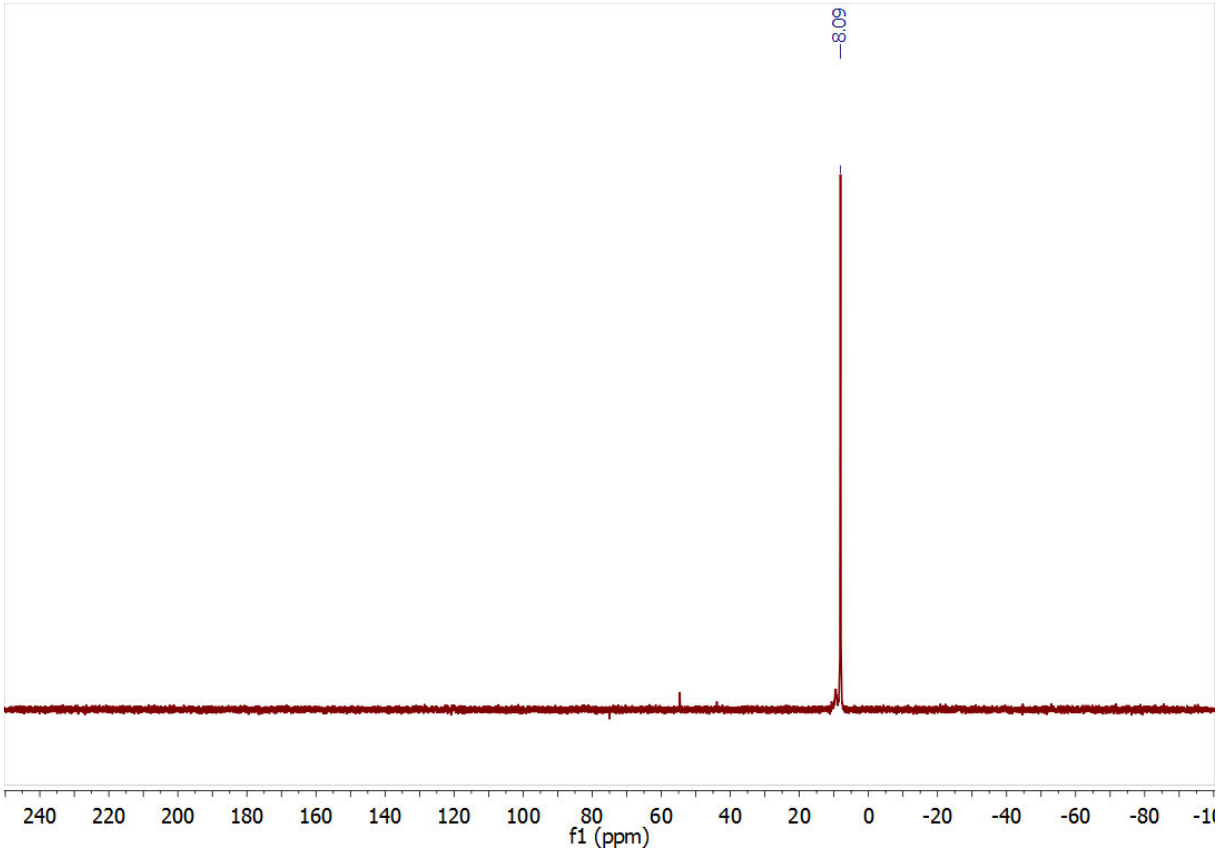

Appendix Fig. 93: $^{31}P\{^{1}H\}$ NMR of the protonated PyTBPX ligand in CD_2Cl_2 at rt and ap.

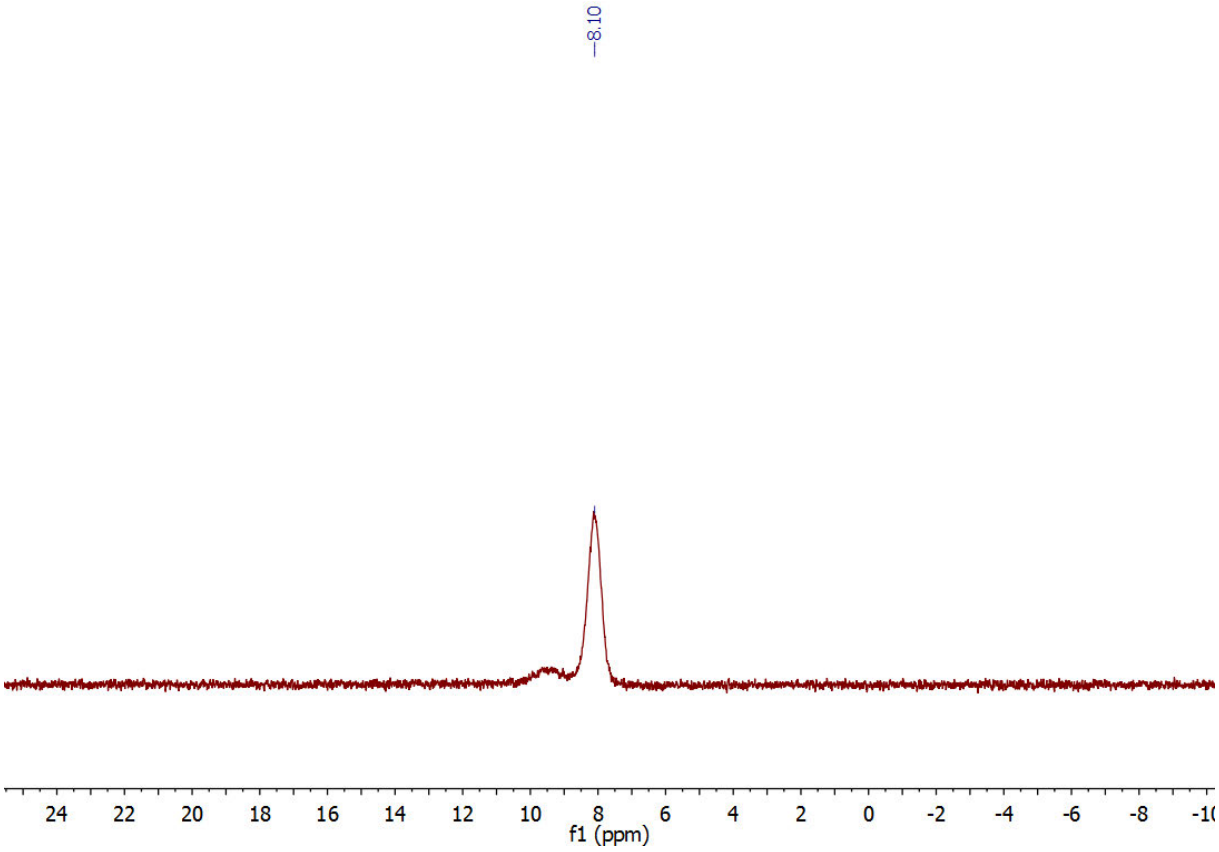

Appendix Fig. 94: Proton coupled ^{31}P NMR of the protonated PyTBPX ligand in CD_2Cl_2 at rt and ap.

A.2.3.4. NMR-spectroscopic characterisation of the complexes Pd(L)dba and [Pd(L)OTf]OTf

Pd(PyTBPF)dba

^{31}P NMR (122 MHz, dichloromethane-*d*$_2$) δ 39.6 (s), 35.4 (s).

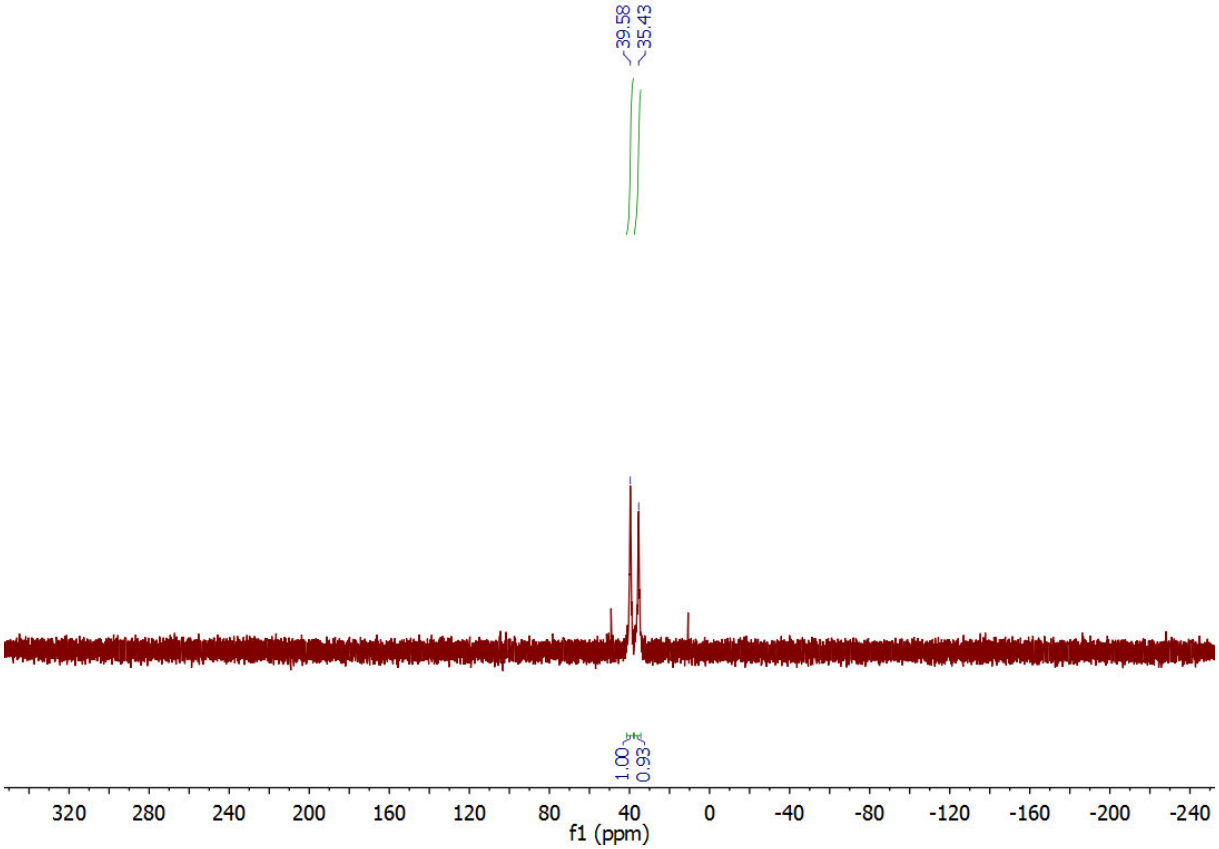

Appendix Fig. 95: ^{31}P NMR of Pd(PyTBPF)dba in CD_2Cl_2 at rt

[Pd(PyTBPF)OTf]OTf

^{31}P NMR (122 MHz, dichloromethane-d_2) δ 59.82 (d, $^{2}J_{P,P}$ = 28.3 Hz, 1P), -1.52 (d, $^{2}J_{P,P}$ = 28.3 Hz, 1P).

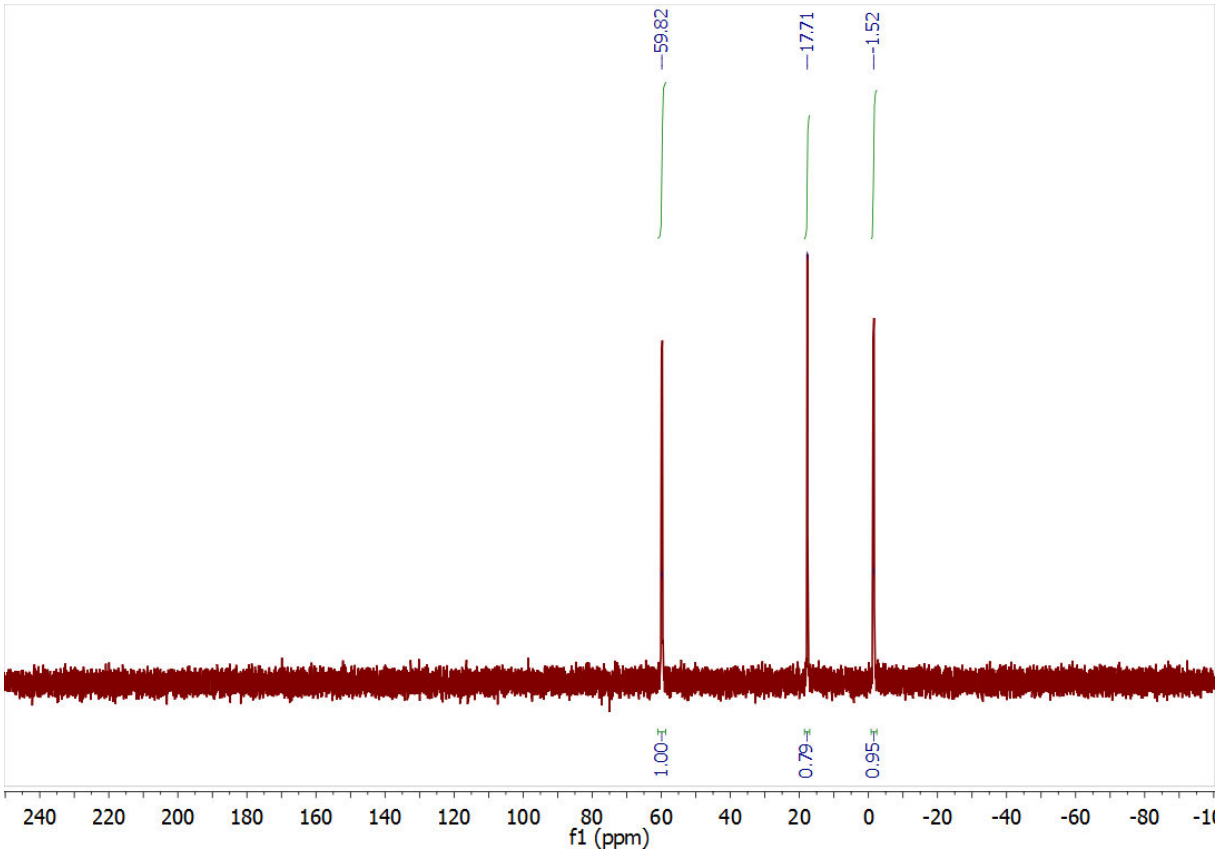

Appendix Fig. 96: ^{31}P NMR of [(PyTBPF)Pd(CF$_3$SO$_3$)]$^+$(CF$_3$SO$_3$)$^-$ in CD$_2$Cl$_2$ at rt and ap.

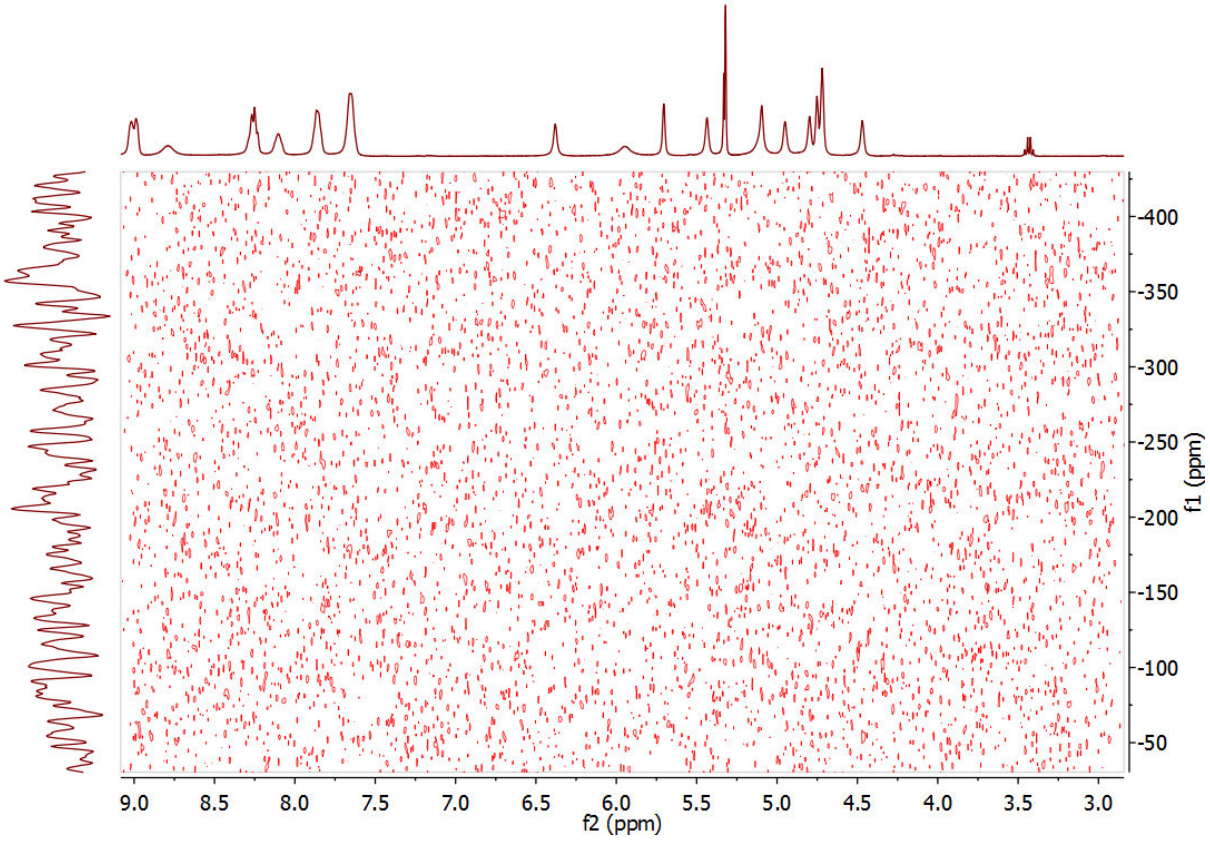

Appendix Fig. 97: $^{1}H/^{15}N$-HMBC NMR spectrum of [Pd(PyTBPF)OTf]OTf in CD_2Cl_2 at rt. No signals assignable to a Py-N are visible.

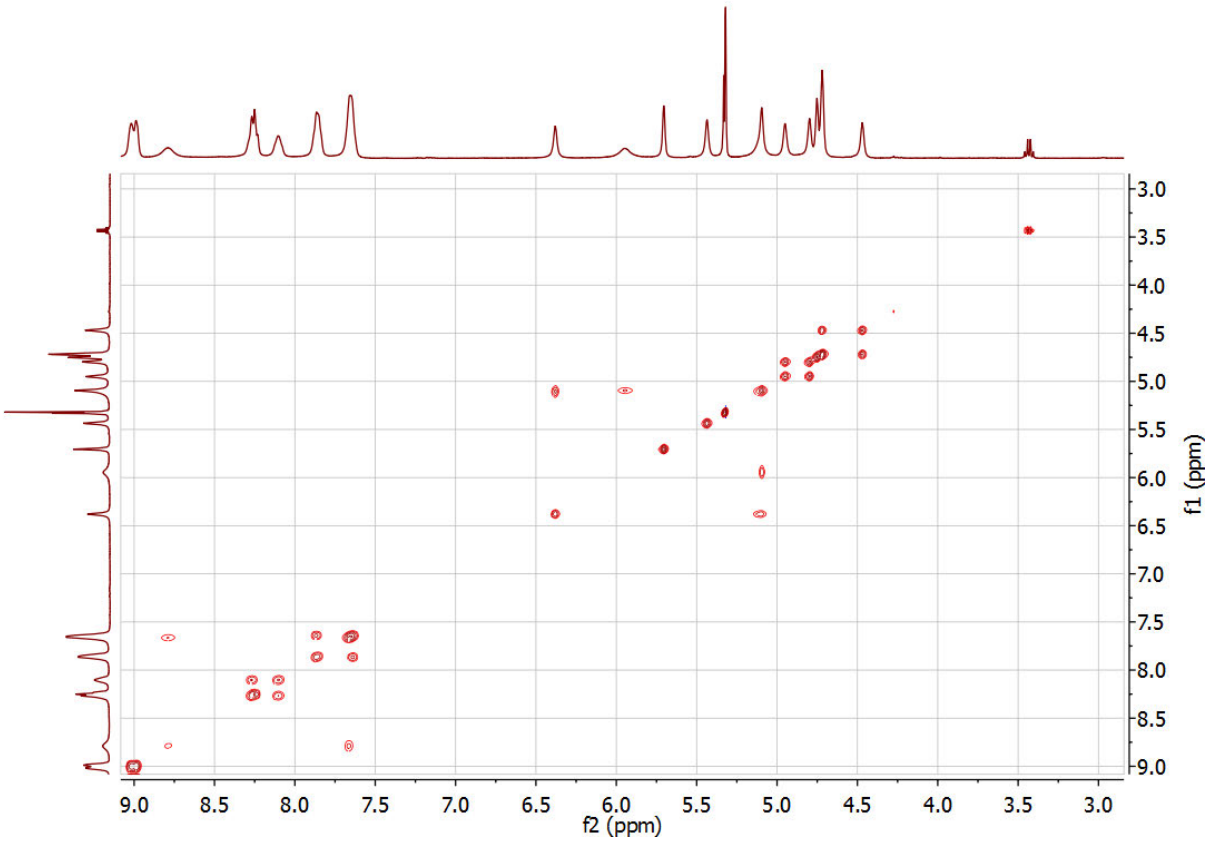

Appendix Fig. 98: ^{1}H NOESY NMR of [Pd(PyTBPF)OTf]OTf in CD_2Cl_2 at rt. Short spin evolution times were picked to show spin correlations due to chemical exchange rather than spatial correlations. For clarity, the tBu signals are not included in this spectrum.

Pd(PyTBPX)dba

^{31}P NMR (122 MHz, dichloromethane-*d*$_2$) δ 46.6 (s), 44.8 (s).

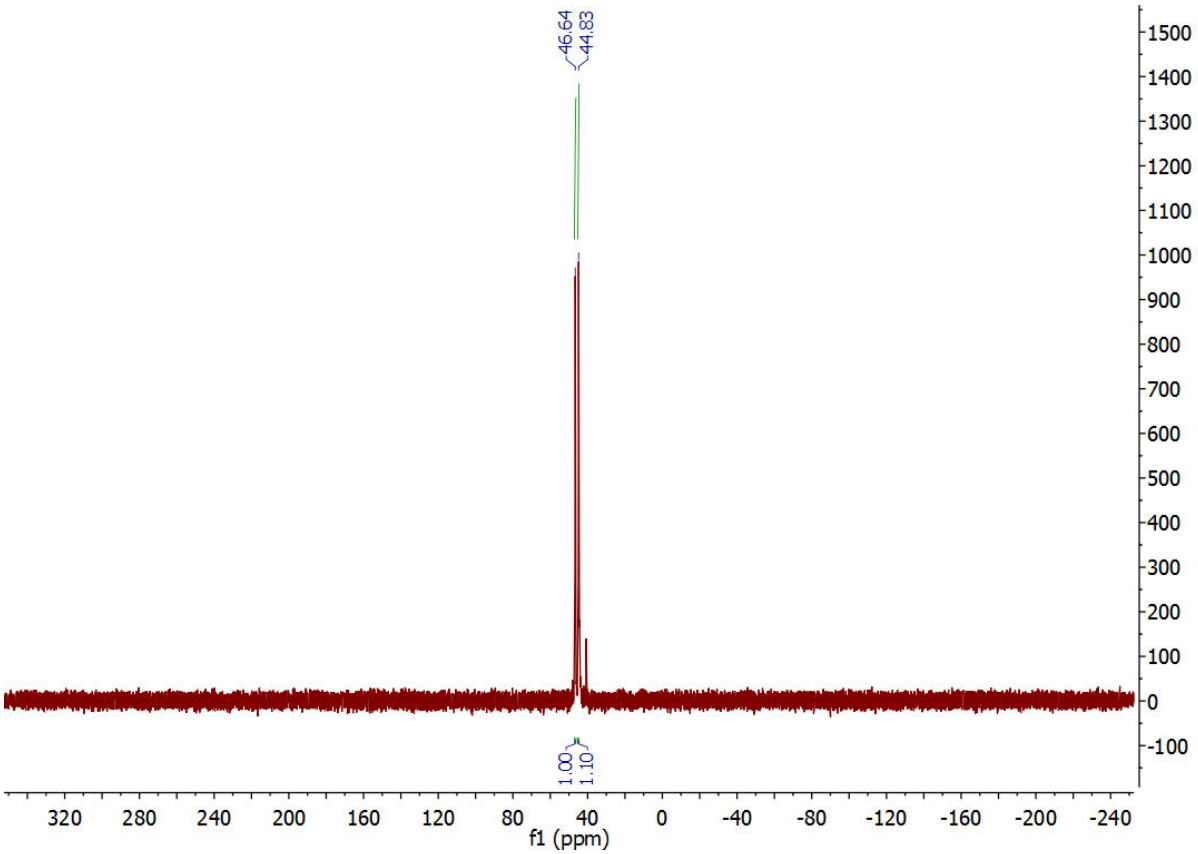

Appendix Fig. 99: ^{31}P NMR of Pd(PyTBPX)dba in CD_2Cl_2 at rt.

[Pd(PyTBPX)OTf]OTf

^{1}H NMR (300 MHz, dichloromethane-*d*$_2$) δ 9.00 – 8.93 (m, 1H, Py^{1}-*H*), 8.86 (d, J = 4.2 Hz, 1H, Py^{2}-*H*), 8.67 Hz (t, J = 6.5 Hz, 1H, Py^{1}-*H*), 8.50 (t, J = 6.8 Hz, 1H, Py^{2}-*H*), 8.30 (t, J = 7.7 Hz, 1H, Py^{1}-*H*), 8.10 – 8.02 (m, 1H, Py^{2}-*H*), 7.77 (t, J = 6.8 Hz, 1H, Py^{1}-*H*), 7.64 – 7.58 (m, 1H, Py^{2}-*H*), 7.55 (d, J = 7 Hz, 1H, Xy-*H*), 7.46 – 7.36 (m, 2H, Xy-*H*), 7.29 (t, J = 7.3 Hz, 1H, Xy-*H*), 4.40 (t, J = 16.1 Hz, 2H, Ar-C*H*^{a}H^{b}-P), 3.69 (dd, J = 15.2 Hz, J = 7.0 Hz, 1H, Ar-CH^{a}*H*^{b}-P), 3.57 (t, J = 13.2 Hz, 1H, Ar-CH^{a}*H*^{b}-P), 1.34 (d, J = 17.5 Hz, 9H, *t*Bu^{1}-*H*), 1.05 (d, J = 19.4 Hz, 9H, *t*Bu^{2}-*H*). ^{31}P NMR (122 MHz, dichloromethane-*d*$_2$) δ 33.50 (d, $^{2}J_{P,P}$ = 11.8 Hz, 1P), -5.04 (d, $^{2}J_{P,P}$ = 11.8 Hz, 1P).

In the ^{1}H NMR spectrum multiple impurities are visible. These impurities are: Diethylether (at δ 3.43 (q, 2H), 1.15 (t, 3H)) and 1,4-benzoquinone (at δ 6.67 (s)). The ratio of complex:BQ:Diethylether is ca. 4:1:1.

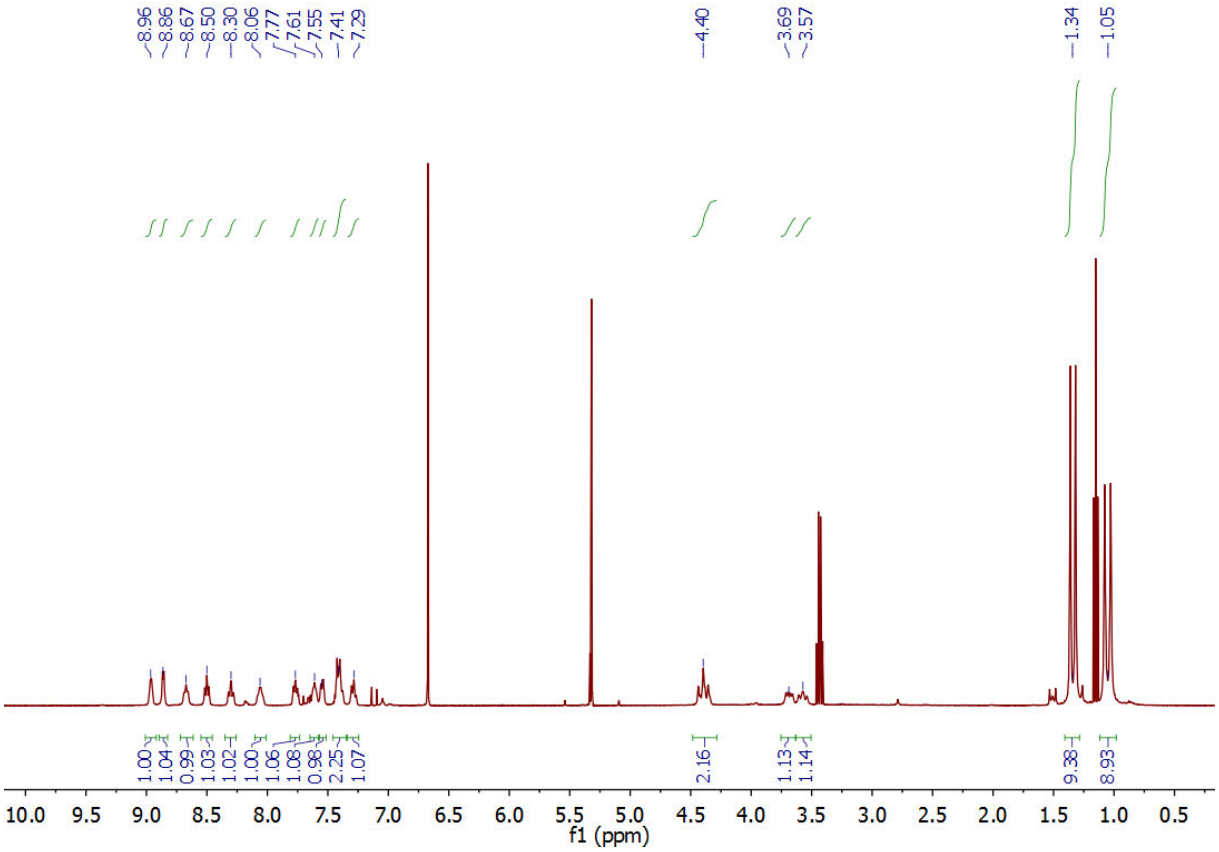

Appendix Fig. 100: ^{1}H NMR of $[(PyTBPX)Pd(CF_3SO_3)]^{+}(CF_3SO_3)^{-}$ in DCM-d_2. Impurities are diethylether and benzoquinone.

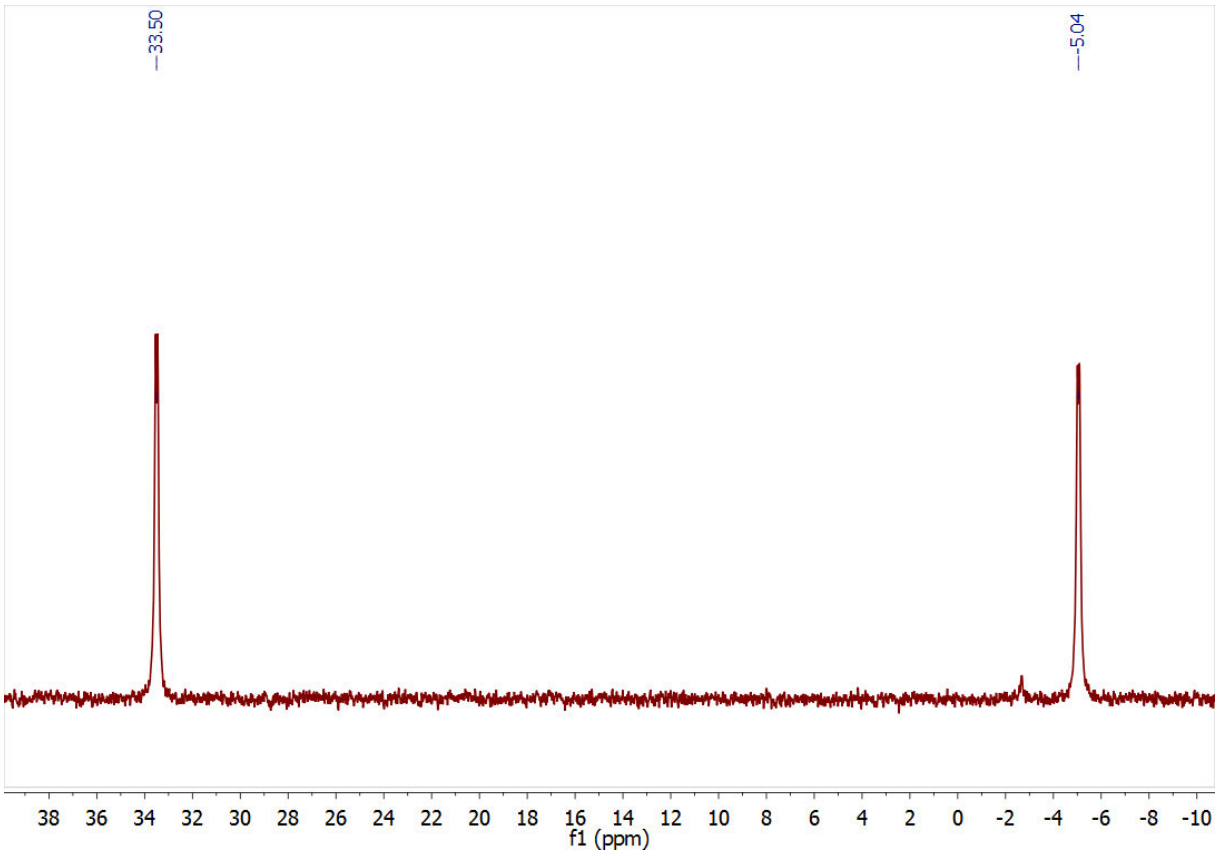

Appendix Fig. 101: ^{31}P NMR of $[(PyTBPX)Pd(CF_3SO_3)]^+(CF_3SO_3)^-$ in CD_2Cl_2 at rt and ap.

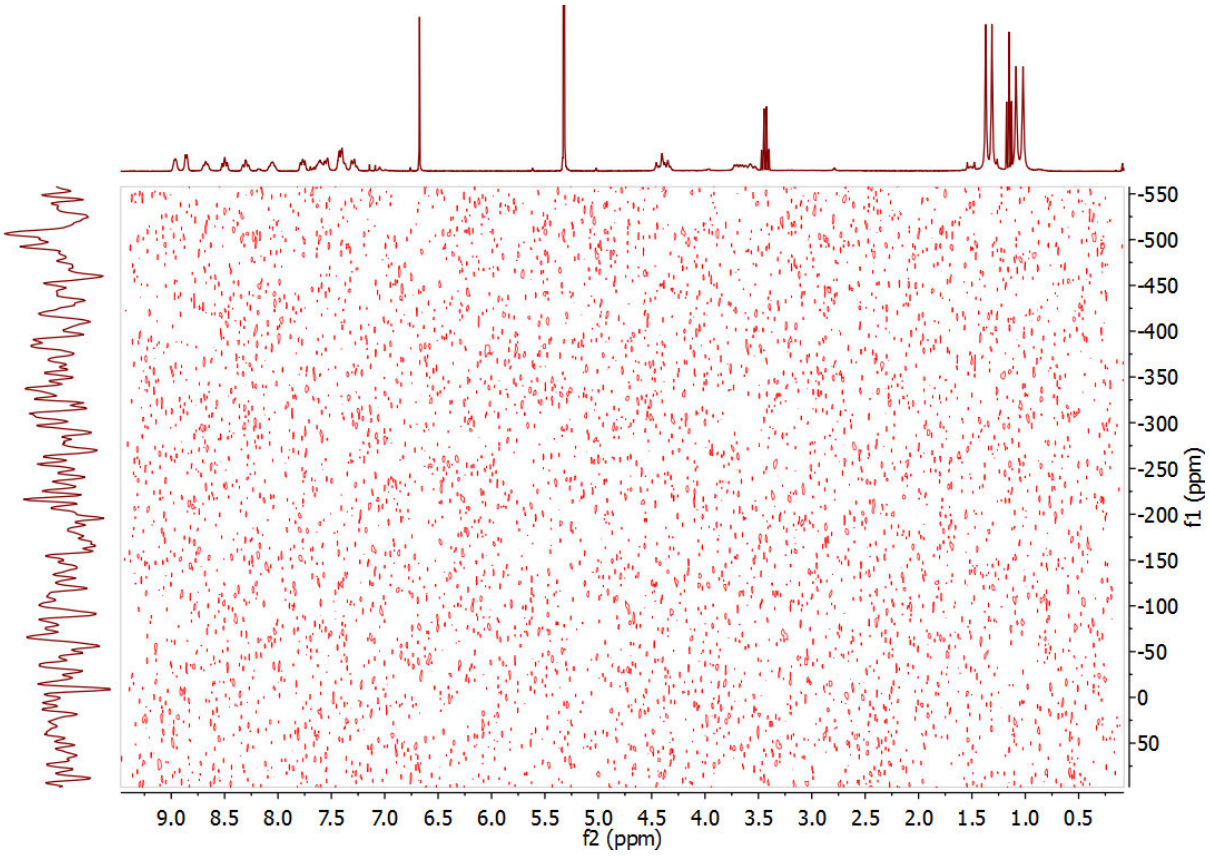

Appendix Fig. 102: $^{1}H/^{15}N$-HMBC NMR spectrum of [Pd(PyTBPX)OTf]OTf in CD_2Cl_2 at rt. No signals assignable to a Py-N are visible.

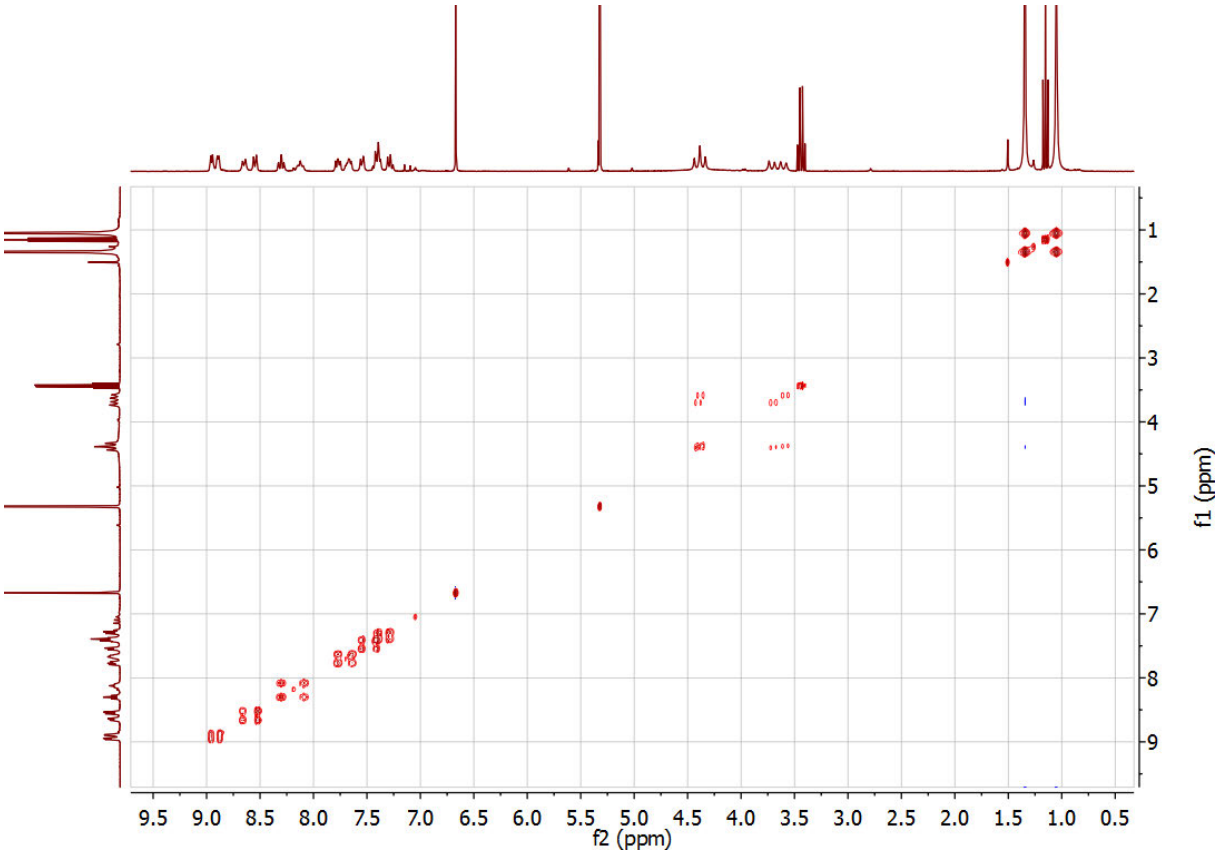

Appendix Fig. 103: ^{1}H NOESY NMR of [Pd(PyTBPX)OTf]OTf in CD_2Cl_2 at rt. Short spin evolution times were picked to show spin correlations due to chemical exchange rather than spatial correlations.

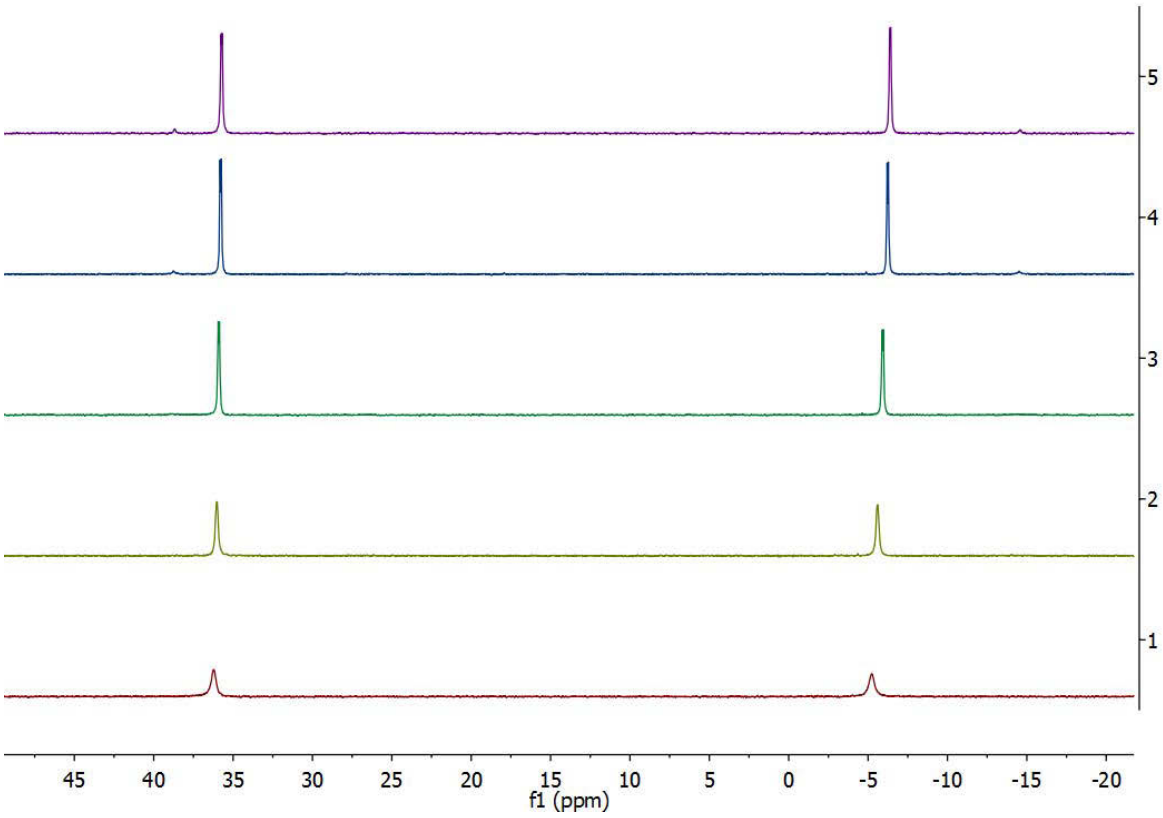

Appendix Fig. 104: low temperature ^{31}P NMR spectra of [Pd(PyTBPX)OTf]OTf in MeOH-d_4. (1) control experiment at 293 K; (2) 273 K; (3) 253 K; (4) 233 K; (5) 223 K.

A.2.3.5. In situ synthesis of the suspected resting states [Pd(L)OTf]OTf or [Pd(L)OTs]OTs starting from different precursors

[Pd(PyTBPF)OTf]OTf

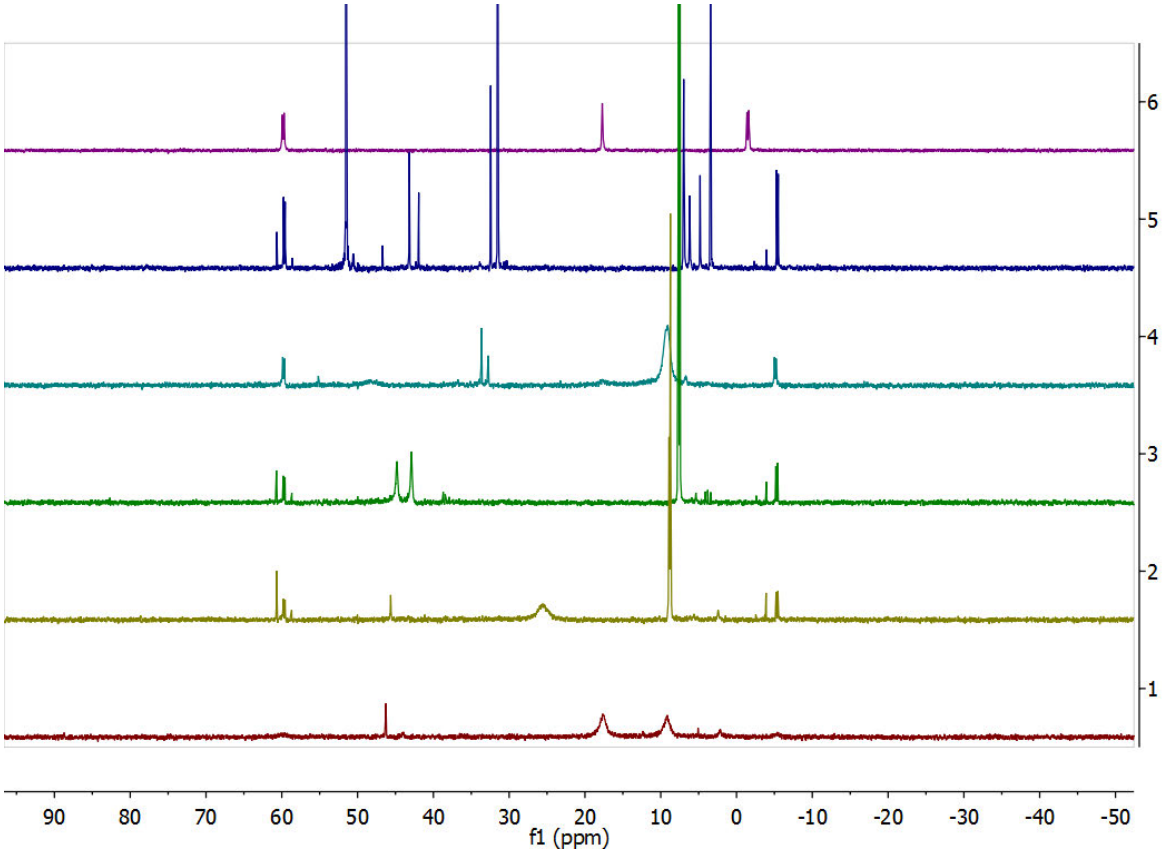

Appendix Fig. 105: $^{31}P\{^{1}H\}$ NMR spectra of the in situ formation of $[(PyTBPF)Pd(CF_3SO_3)]^+(CF_3SO_3)^-$ starting from different Pd precursors in CD_2Cl_2. (1) $Pd_2(dba)_3$ (2) $Pd(OAc)_2$ (3) $Pd(dba)_2$ (4) $PdCl_2$ (5) $Pd(acac)_2$ (6) Pure complex.

[Pd(PyTBPX)OTf]OTf

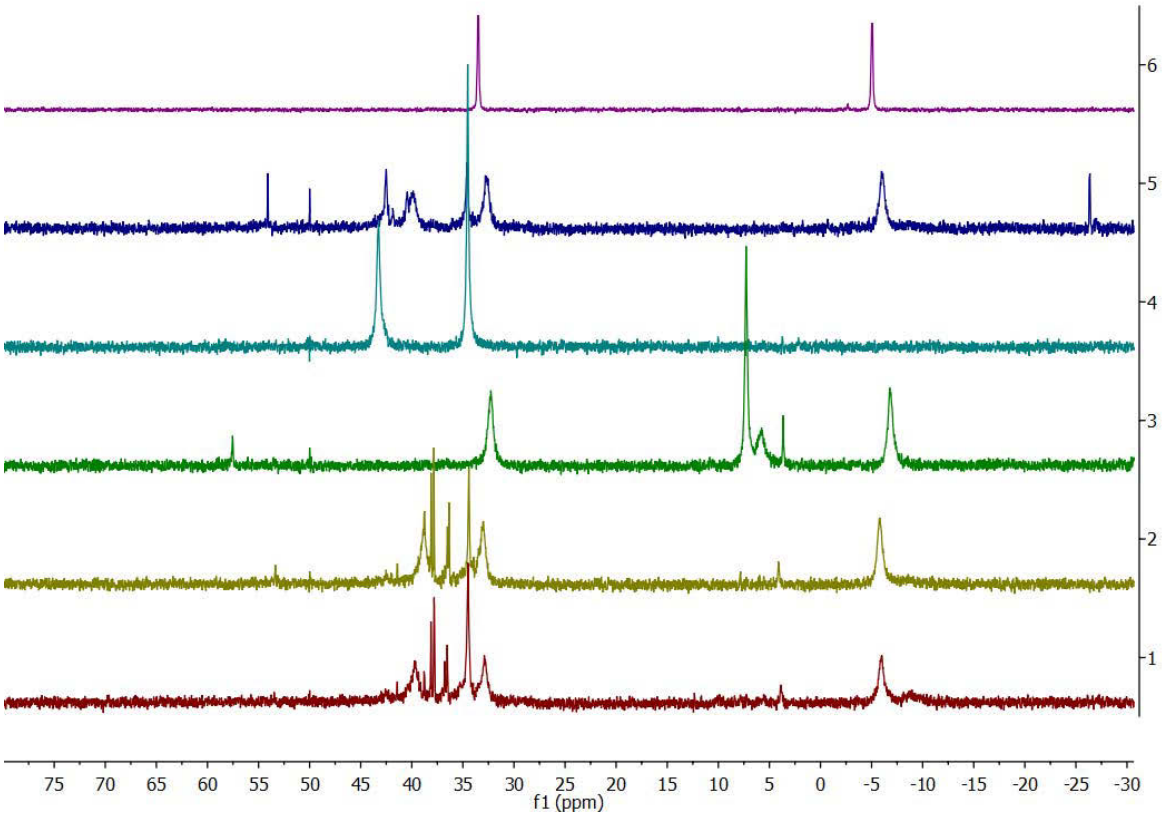

Appendix Fig. 106: $^{31}P\{^{1}H\}$ NMR spectra of the in situ formation of $[(L3)Pd(CF_3SO_3)]^+(CF_3SO_3)^-$ starting from different Pd precursors in CD_2Cl_2. (1) $Pd(dba)_2$ (2) $Pd_2(dba)_3$ (3) $Pd(acac)_2$ (4) $PdCl_2$ (5) $Pd(OAc)_2$ (6) Pure complex.

A.2.3.6. Hydride species

[Pd(BuPox)(H)OTf]

^{1}H NMR (300 MHz, methanol-d_4) δ -10.71 (dd, $^{2}J_{H,P}$(*trans*) = 182.6 Hz, $^{2}J_{H,P}$(*cis*) = 21.7 Hz). ^{31}P NMR (122 MHz, methanol-d_4) δ 75.62 (d, $^{2}J_{P,P}$ = 17.1 Hz), 23.90 (dd, $^{2}J_{P,H}$(trans) = 182.6 Hz, $^{2}J_{P,P}$ = 17.1 Hz, $^{3}J_{P,H}$ = 4.5 Hz).

Cis-P,H-coupling not resolved in ^{31}P NMR.

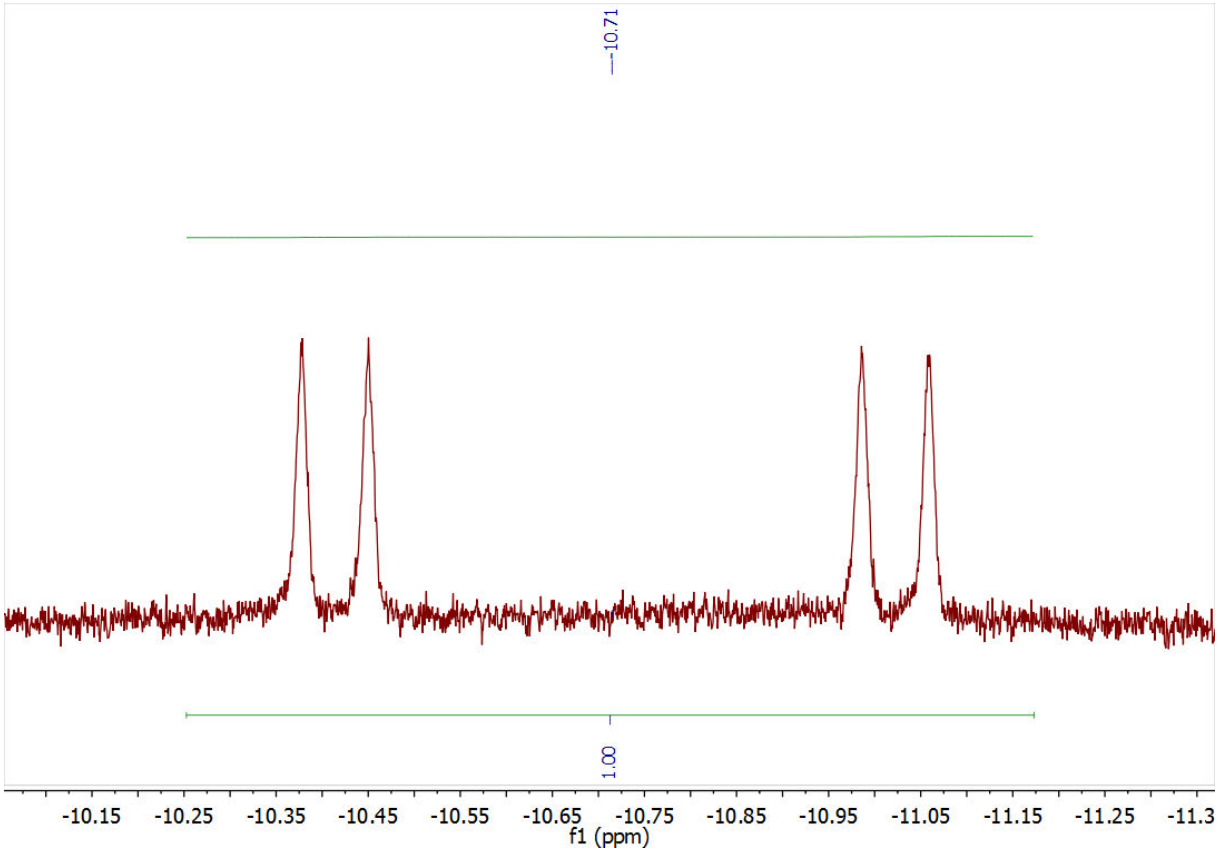

Appendix Fig. 107: ^{1}H NMR spectrum of [(L3)PdH(OTf)] in MeOH-d_4 at rt and ap. Only the hydride signal is displayed.

A.3. Hydroaminomethylation of methyl pentenoates

Table 15, Entry 1

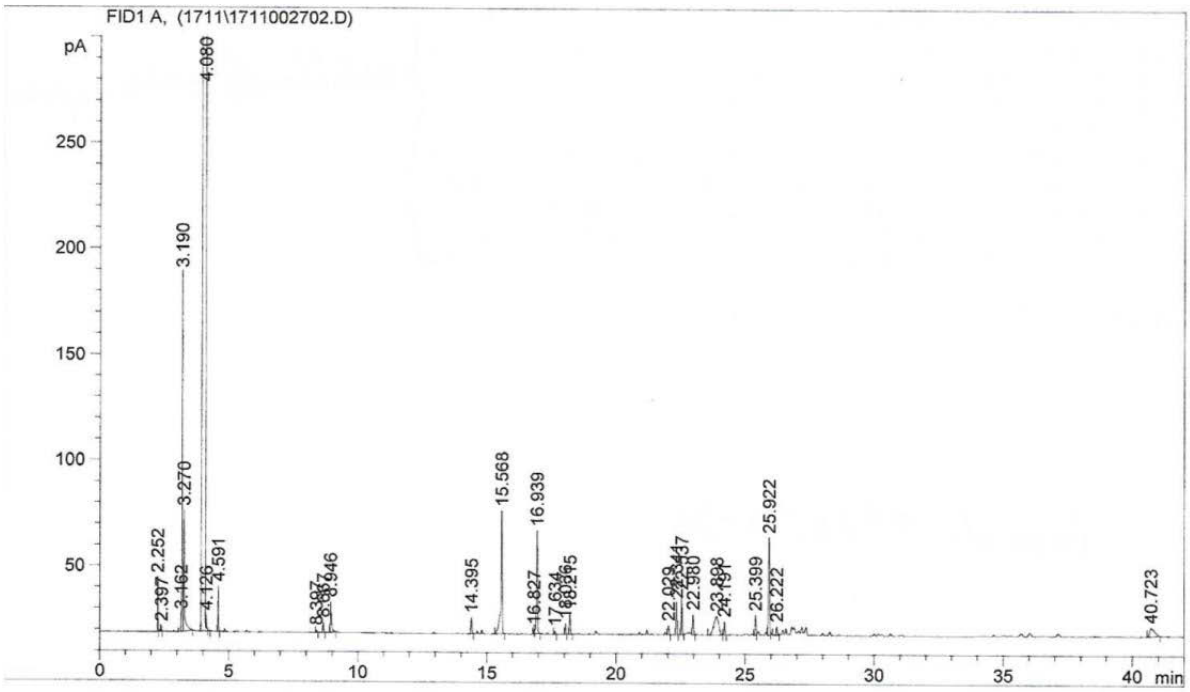

Appendix Fig. 108: Gas chromatogram (GC-FID) of Table 15, Entry 1.

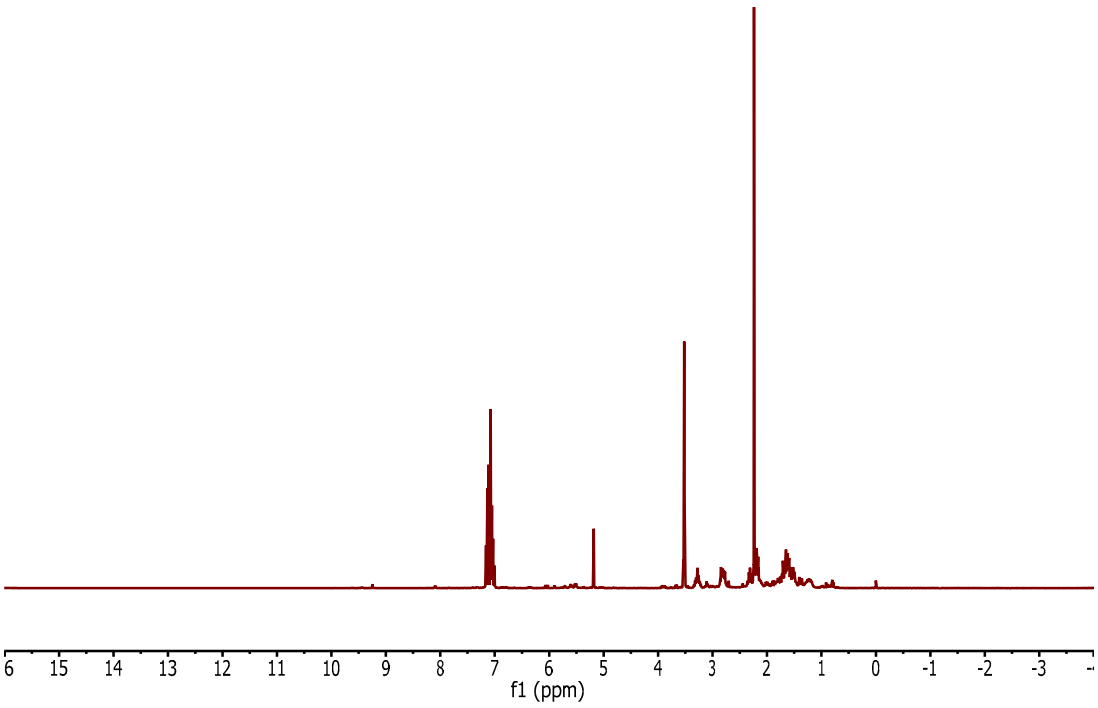

Appendix Fig. 109: ^1H NMR in CD_2Cl_2 at rt of the product mixture in table 15, entry 1.

Substance	Retention time [min]	Area
Methyl valerate	3.2	240.45351
Methyl 4-pentenoate	8.4	2.62184
Methyl 3-pentenoate	8.7	8.89921
Methyl 2-pentenoate	8.9	41.32205
Enamine	14.4, 16.9	155.52165
Amines (regioselectivity could not be determined)	15.6, 18.2	232.76143

Table 15, Entry 2

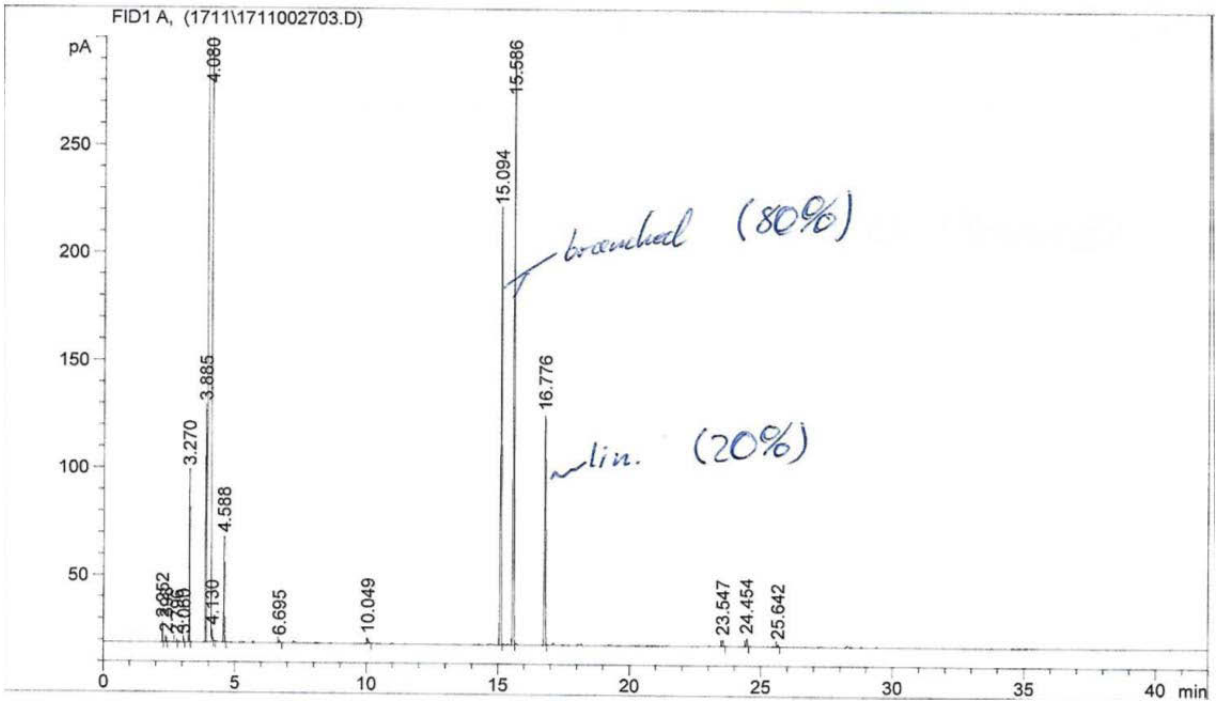

Appendix Fig. 110: Gas chromatogram (GC-FID) of Table 15, Entry 2.

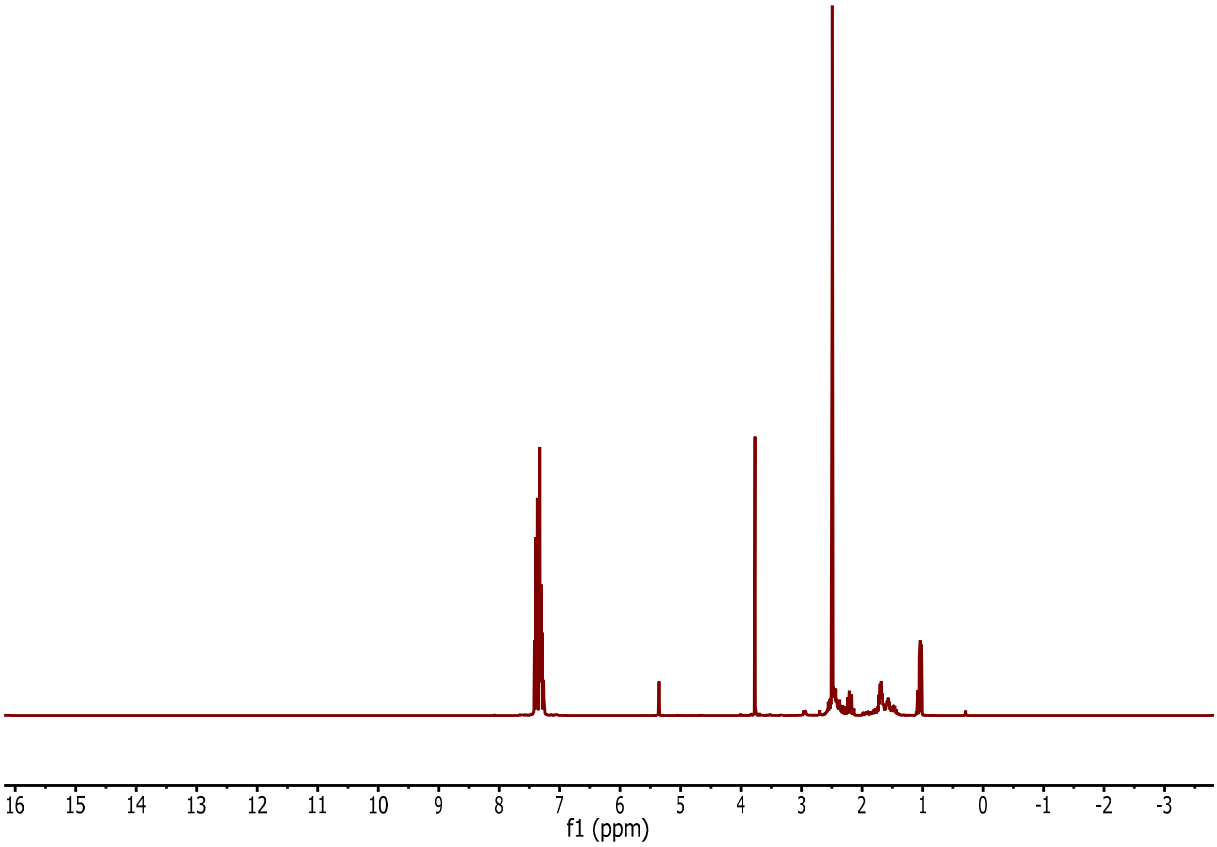

Appendix Fig. 111: ^{1}H NMR in CD_2Cl_2 at rt of the product mixture in table 15, entry 1.

Substance	Retention time [min]	Area
Methyl valerate	3.3	97.94743
Methyl 4-pentenoate	-	-
Methyl 3-pentenoate	-	-
Methyl 2-pentenoate	-	-
Enamine, linear	-	-
Enamine. Branched	-	-
Amine, linear	16.8	294.70255
Amine, branched	15.1, 15.6	1156,20294

Table 15, Entry 3

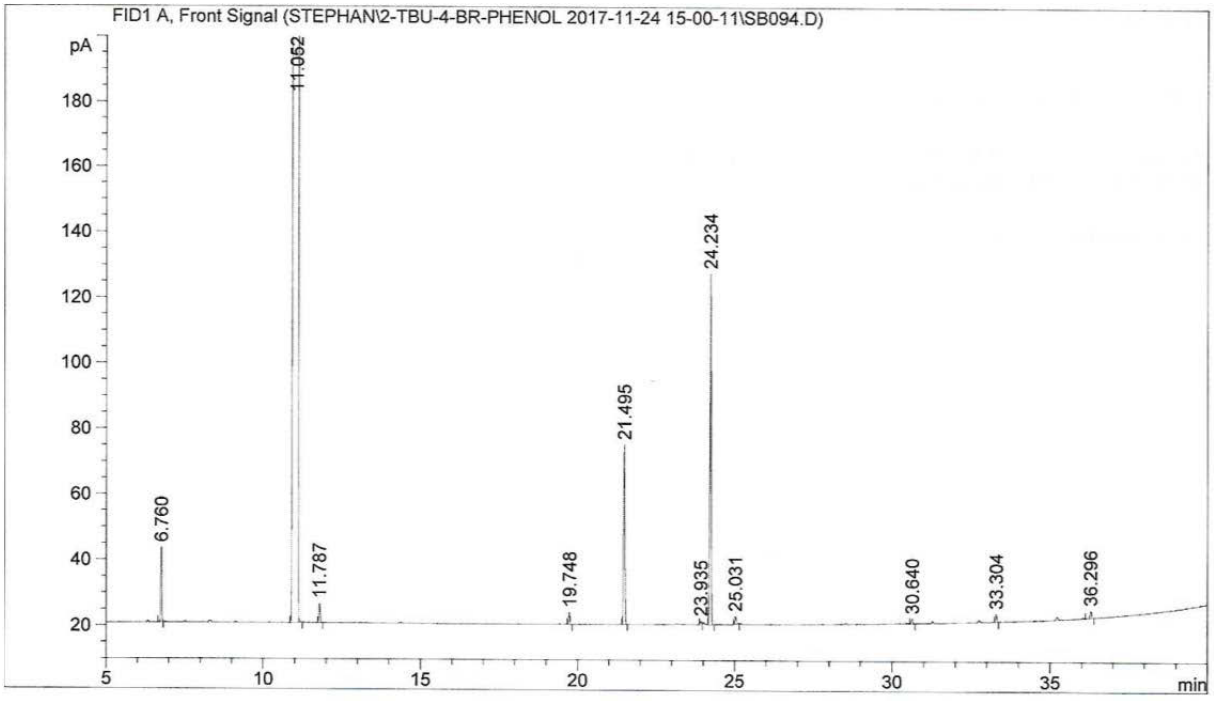

Appendix Fig. 112: Gas chromatogram (GC-FID) of Table 15, Entry 3.

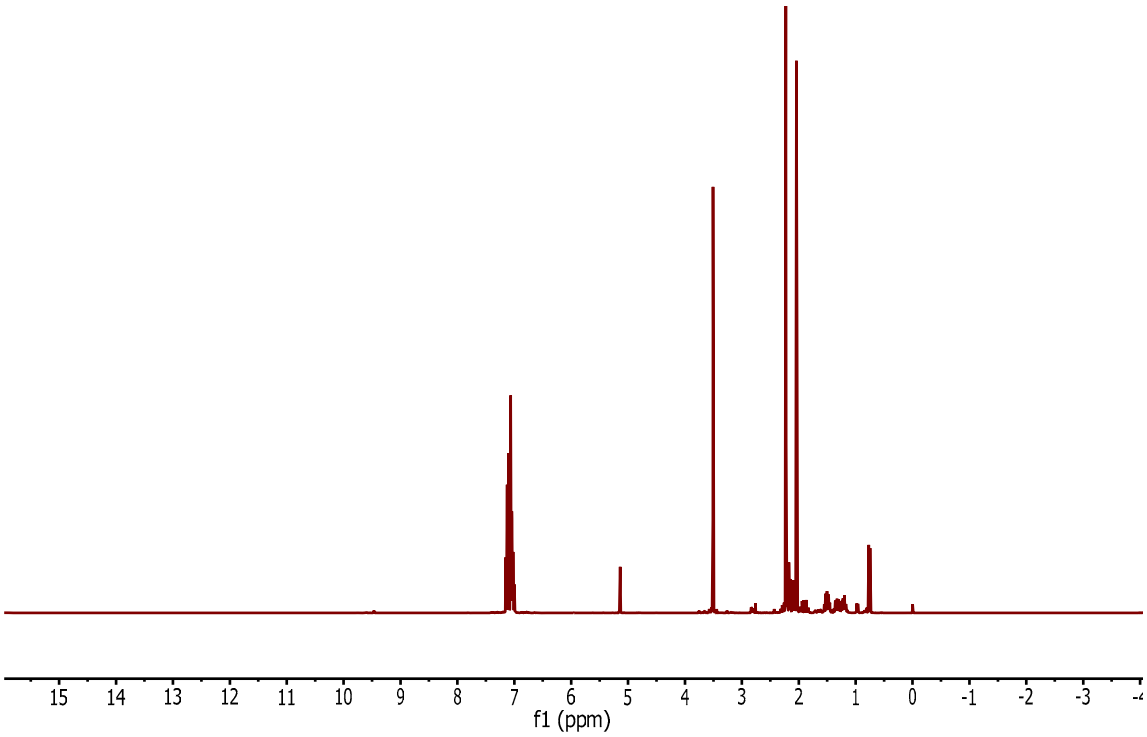

Appendix Fig. 113: ^{1}H NMR in CD_2Cl_2 at rt of the product mixture in table 15, entry 3.

Substance	Retention time [min]	Area
Methyl valerate	3.3	28.27562
Methyl 4-pentenoate	-	-
Methyl 3-pentenoate	11.8	19.34547
Methyl 2-pentenoate	-	-
Enamine, linear	-	-
Enamine. Branched	-	-
Amine, linear	24.234	544.48267
Amine, branched	21.495, 19.748	278.52560

Table 16, Entry 1

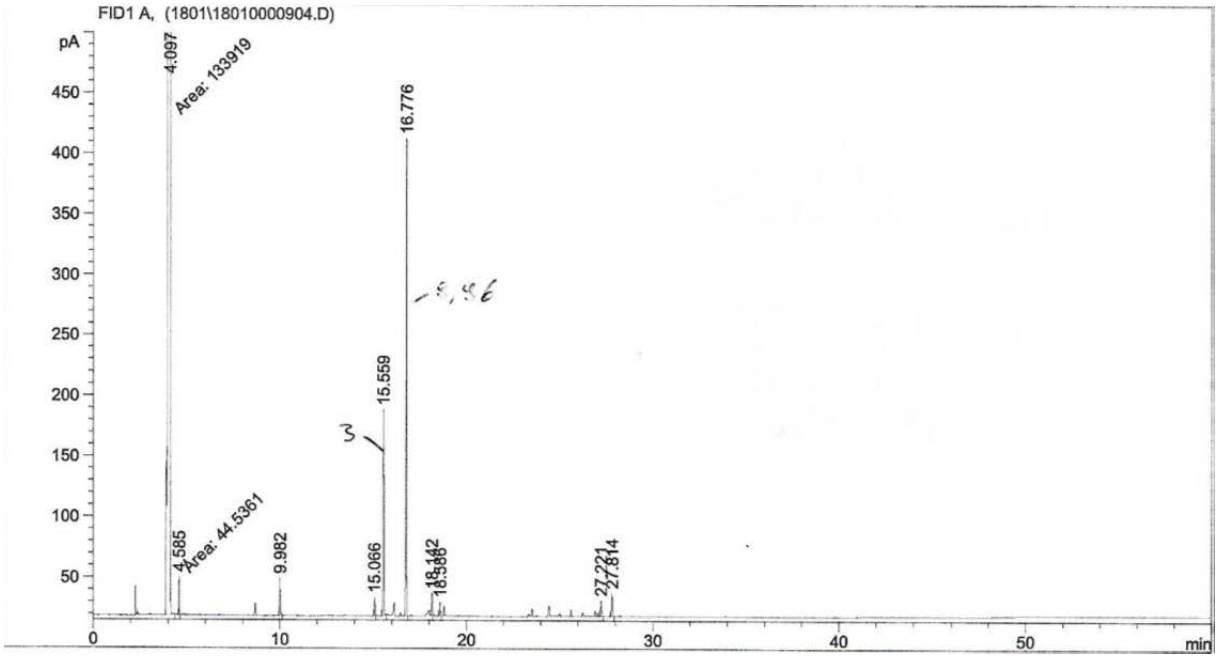

Appendix Fig. 114: Gas chromatogram (GC-FID) of Table 16, Entry 1.

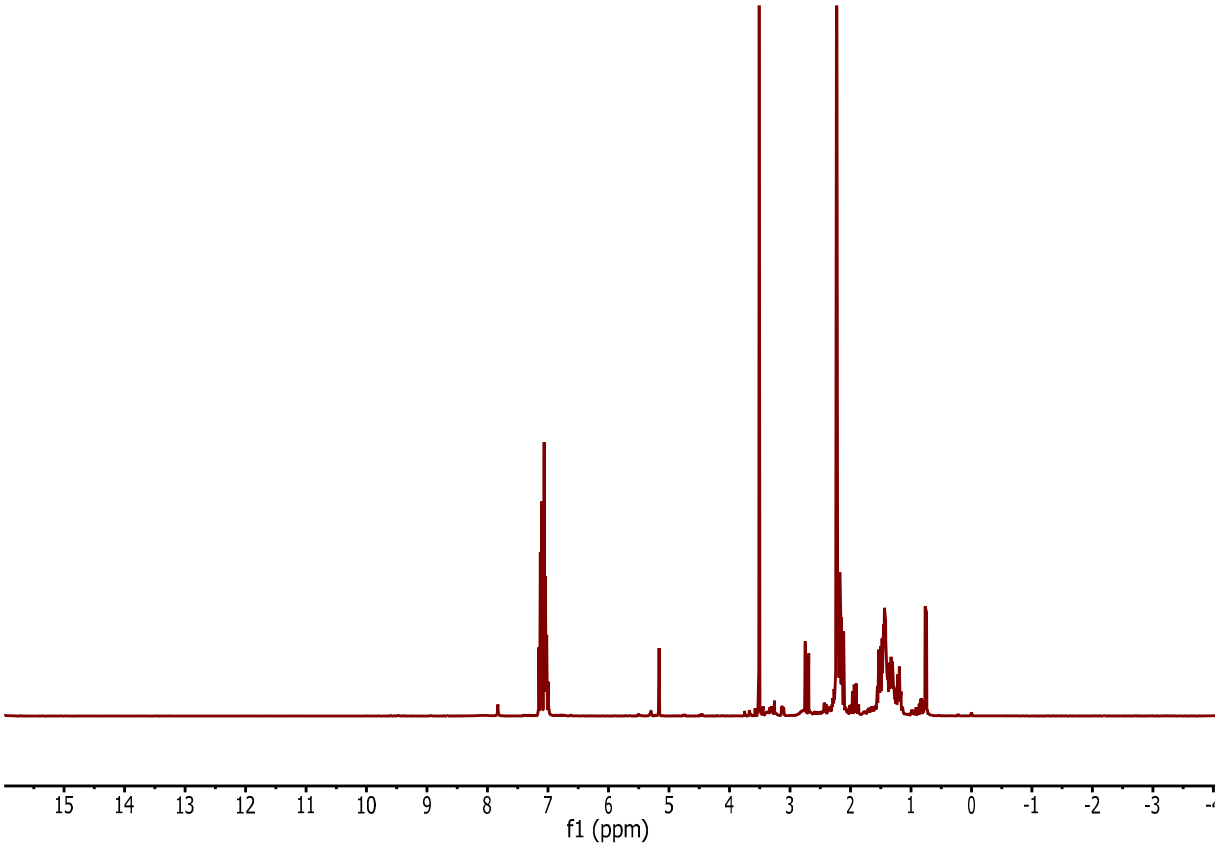

Appendix Fig. 115: ^{1}H NMR in CD_2Cl_2 at rt of the product mixture in table 16, entry 1.

Substance	Retention time [min]	Area
Methyl valerate	4.6	44.53608
Methyl 4-pentenoate	-	-
Methyl 3-pentenoate	-	-
Methyl 2-pentenoate	-	-
Enamine, linear	-	-
Enamine. Branched	-	-
Amine, linear	16.8	1030.48206
Amine, branched	15.6	456.03540
Side products	Other peaks combined	256.90946

Table 16, Entry 2

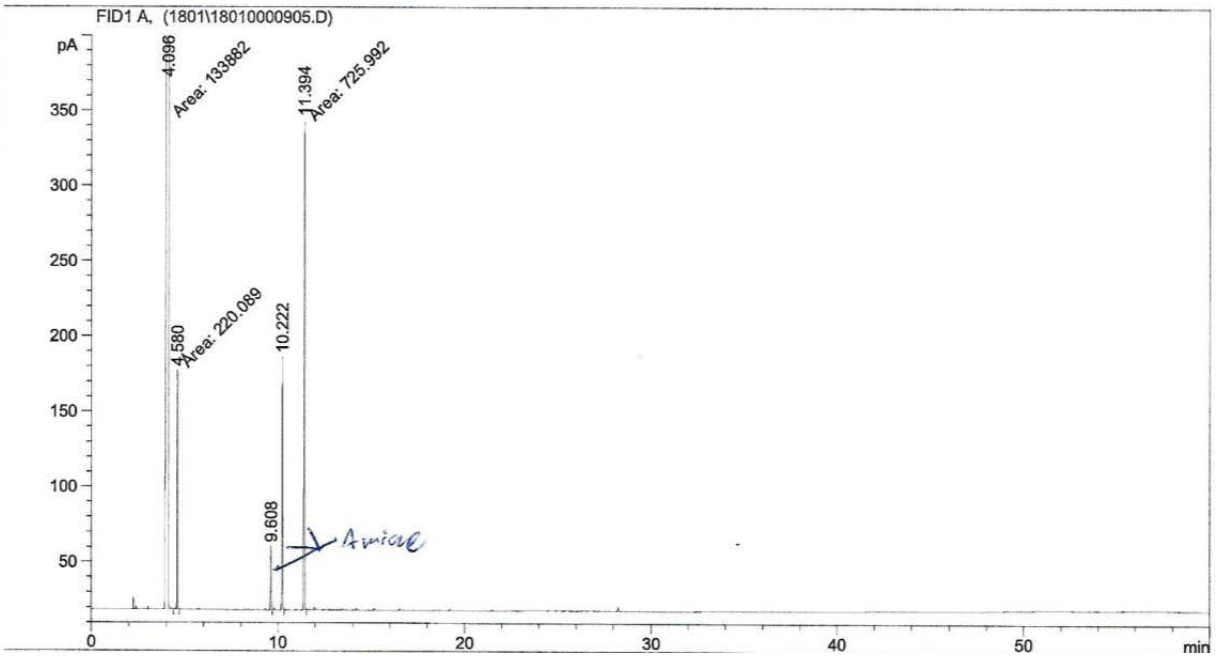

Appendix Fig. 116: Gas chromatogram (GC-FID) of Table 16, Entry 2.

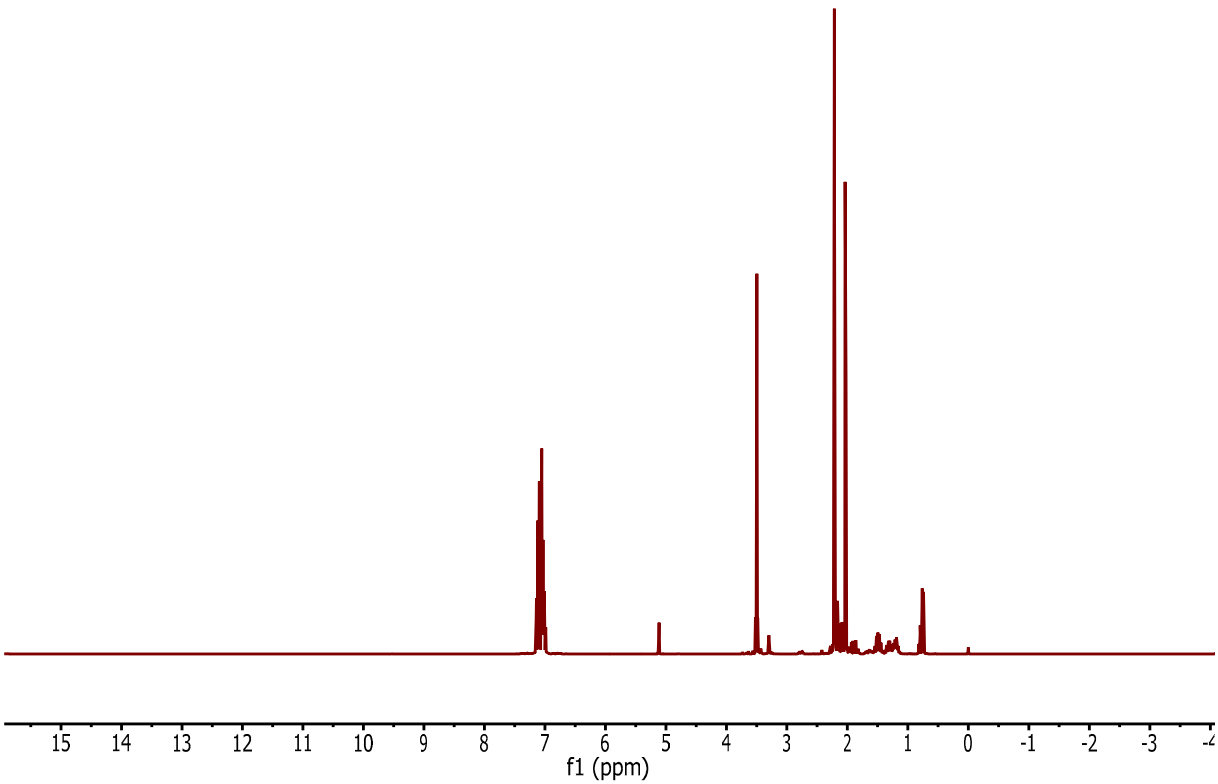

Appendix Fig. 117: ^{1}H NMR in CD_2Cl_2 at rt of the product mixture in table 16, entry 2.

Substance	Retention time [min]	Area
Methyl valerate	4.6	220.08916
Methyl 4-pentenoate	-	-
Methyl 3-pentenoate	-	-
Methyl 2-pentenoate	-	-
Enamine, linear	-	-
Enamine. Branched	-	-
Amine, linear	11.4	725.99200
Amine, branched	9.6, 10.2	460.44387

Table 16, Entry 3

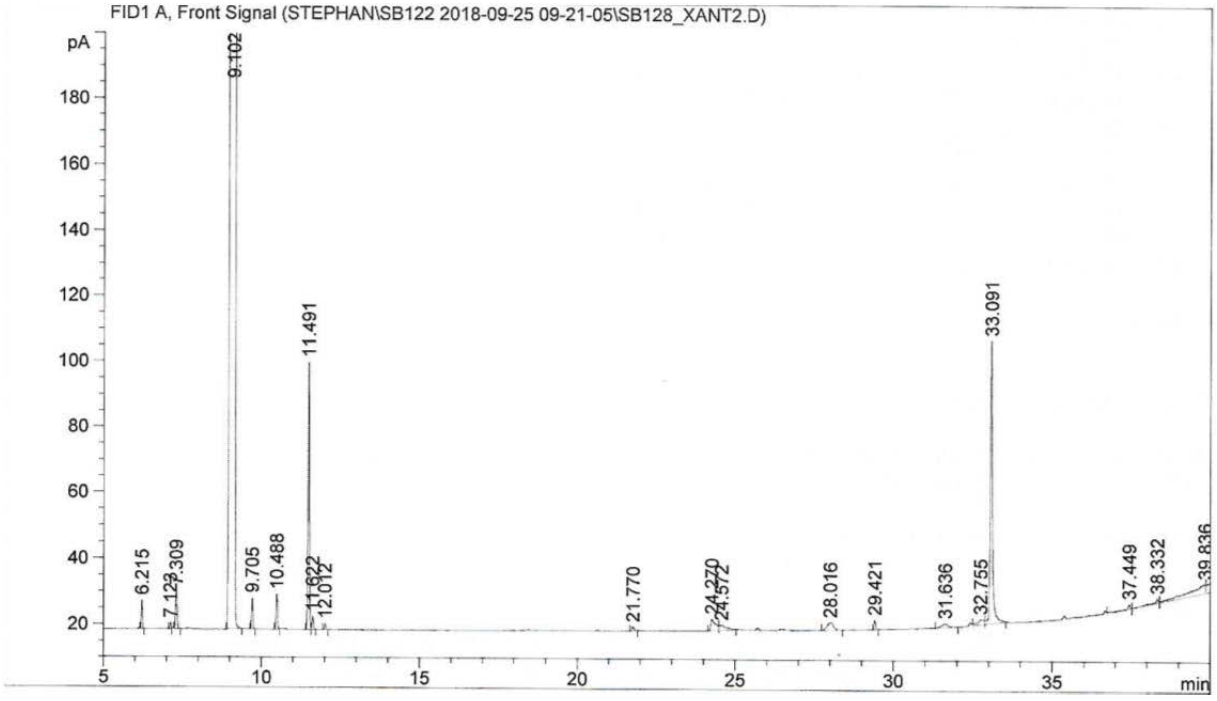

Appendix Fig. 118: Gas chromatogram (GC-FID) of Table 16, Entry 3.

Substance	Retention time [min]	Area
Methyl valerate	9.7	28.43776
Methyl 4-pentenoate	-	-
Methyl 3-pentenoate	10.5	33.66841
Methyl 2-pentenoate	11.5	262.09088
Enamine, linear	-	-
Enamine. Branched	-	-
Amine, linear	33.1	413.72620
Amine, branched	32.8	69.68083

Table 16, Entry 4

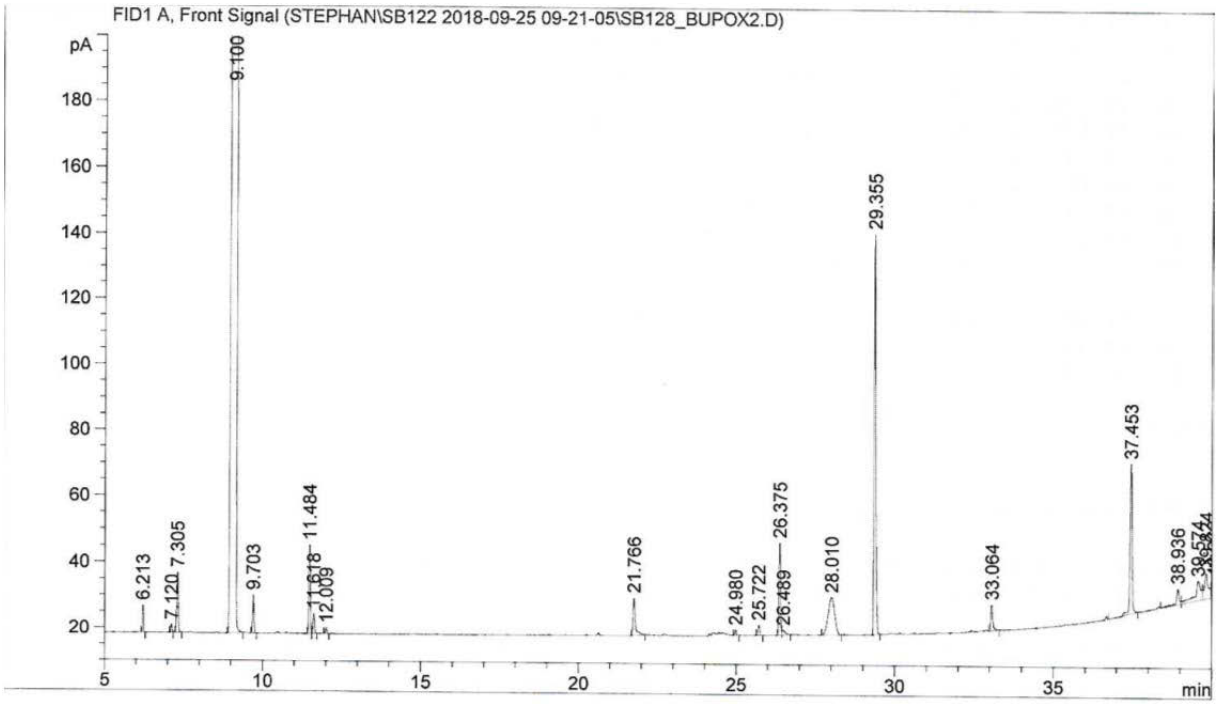

Appendix Fig. 119: Gas chromatogram (GC-FID) of Table 16, Entry 4.

Substance	Retention time [min]	Area
Methyl valerate	9.7	34.88511
Methyl 4-pentenoate	-	-
Methyl 3-pentenoate	10.5	85.93762
Methyl 2-pentenoate	11.5	19.73649
Enamine, linear	-	-
Enamine. Branched	-	-
Amine, linear	29.4	445.60114
Amine, branched	26.4, 28.0	261,16686

Table 16, Entry 5

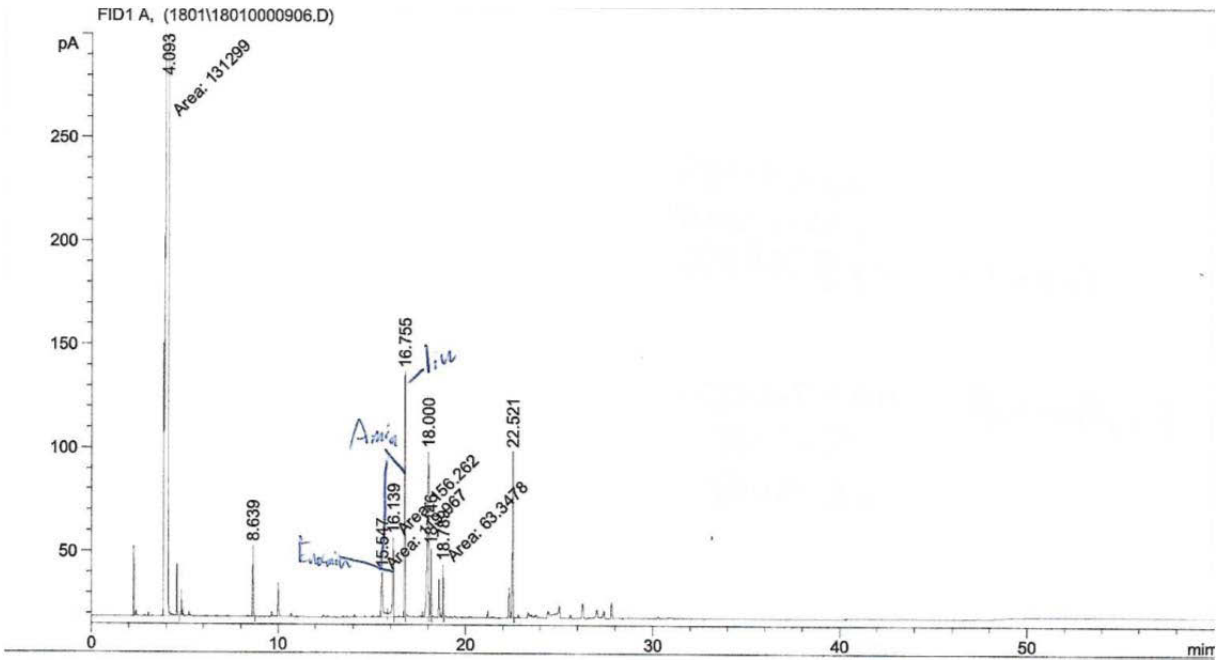

Appendix Fig. 120: Gas chromatogram (GC-FID) of Table 16, Entry 5.

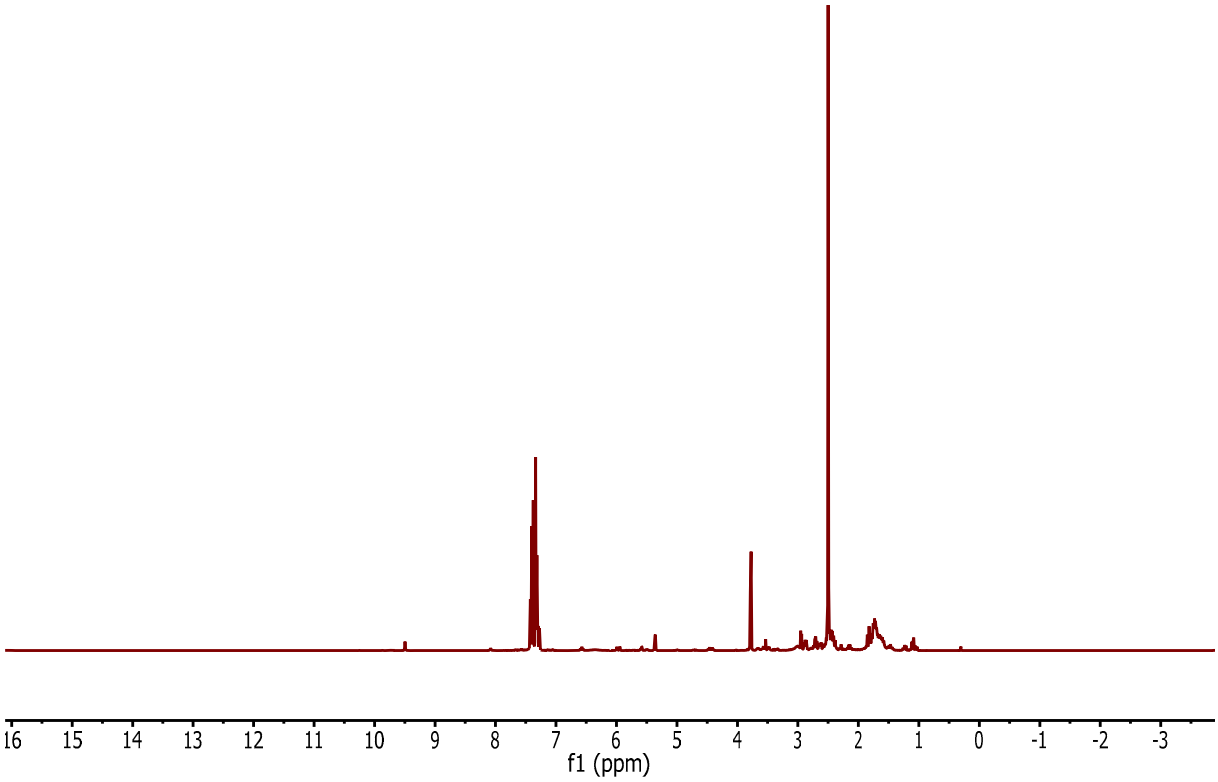

Appendix Fig. 121: ^{1}H NMR in CD_2Cl_2 at rt of the product mixture in table 16, entry 5.

Substance	Retention time [min]	Area
Methyl valerate	-	-
Methyl 4-pentenoate	-	-
Methyl 3-pentenoate	-	-
Methyl 2-pentenoate	8.6	72.33182
Enamine, linear	-	-
Enamine. Branched	16.1	156.26230
Amine, linear	16.8	295.15521
Amine, branched	15.5	119.96657
Side products	Other combined peaks	650.93384

Table 16, Entry 6

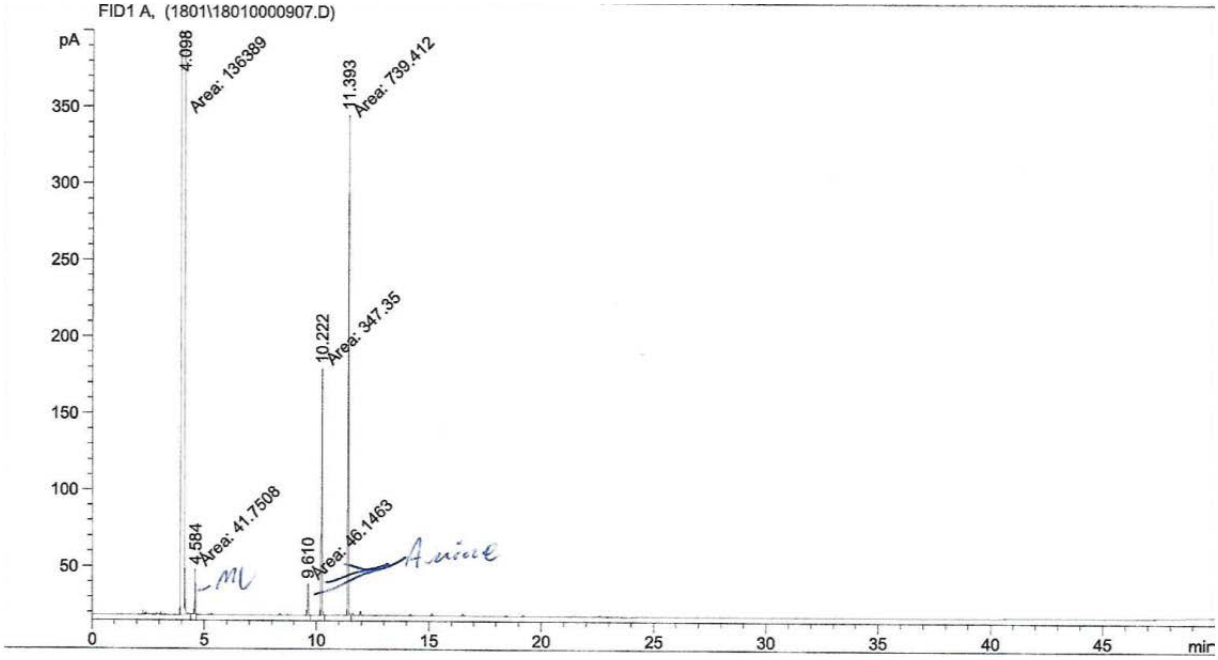

Appendix Fig. 122: Gas chromatogram (GC-FID) of Table 16, Entry 6.

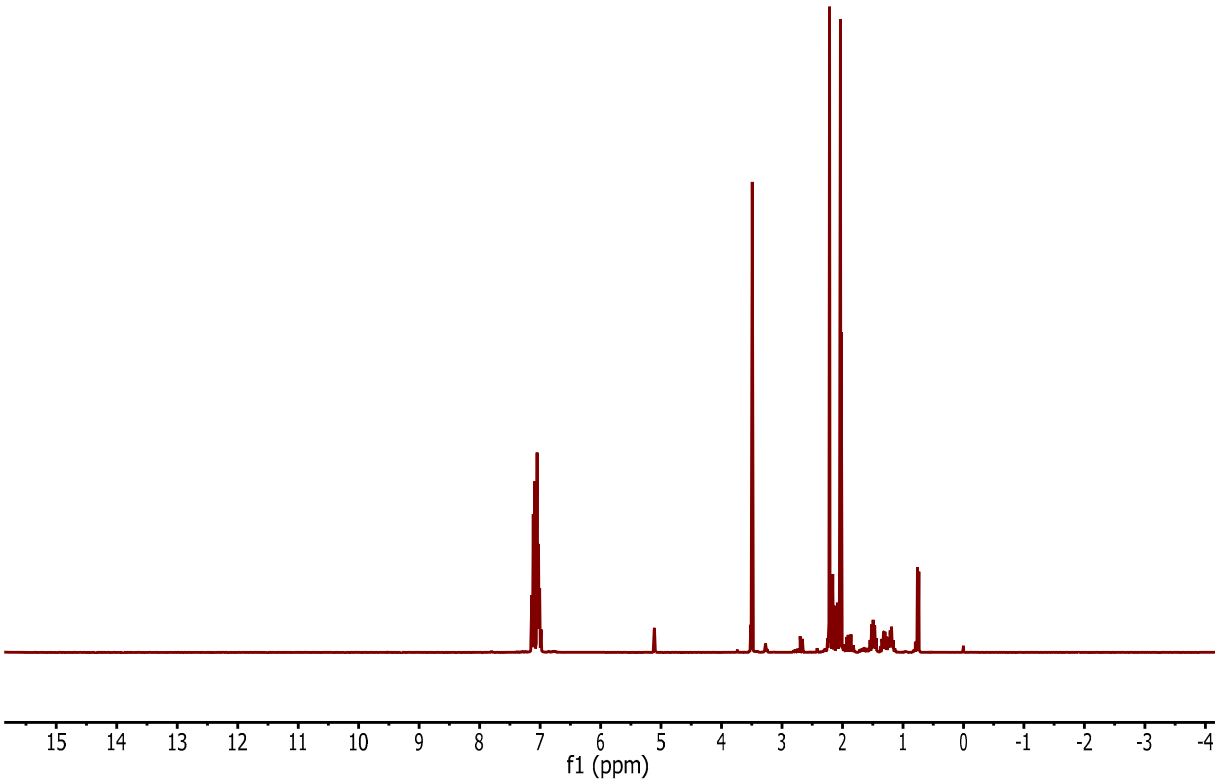

Appendix Fig. 123: ^{1}H NMR in CD_2Cl_2 at rt of the product mixture in table 16, entry 6.

Substance	Retention time [min]	Area
Methyl valerate	4.6	41.75081
Methyl 4-pentenoate	-	-
Methyl 3-pentenoate	-	-
Methyl 2-pentenoate	-	-
Enamine, linear	-	-
Enamine. Branched	-	-
Amine, linear	11.4	739.41235
Amine, branched	10.2	393.49666
Side products	9.6	650.93384

Table 17

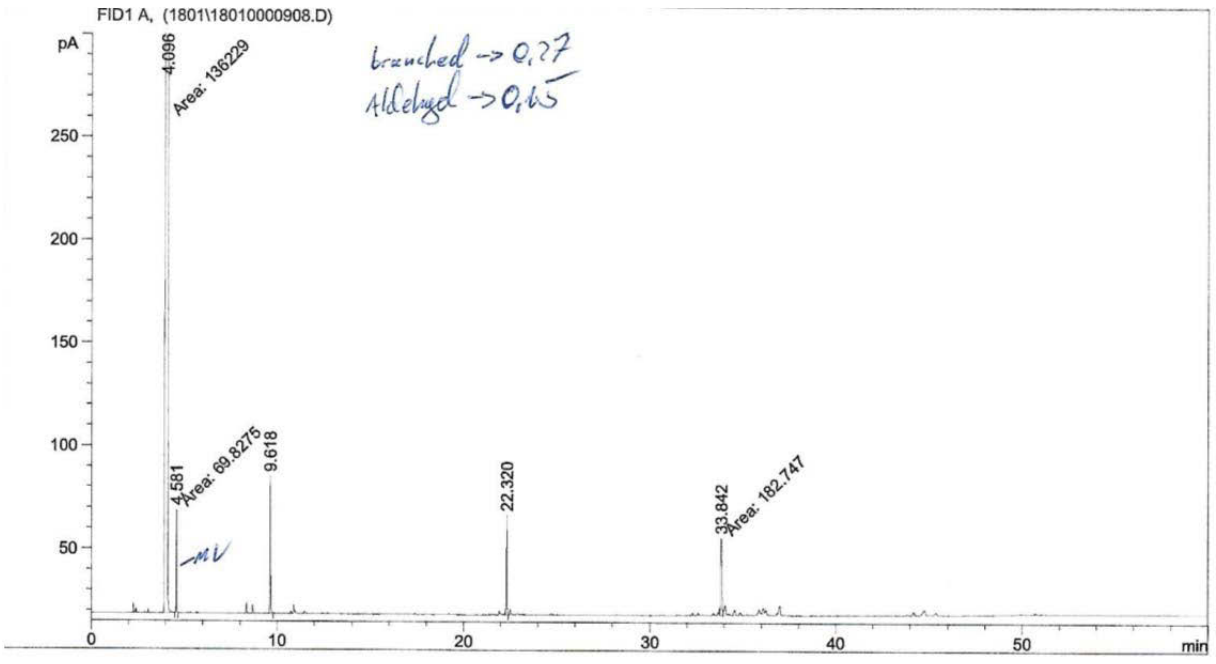

Appendix Fig. 124: Gas chromatogram (GC-FID) of Table 17.

Substance	Retention time [min]	Area
Methyl valerate	4.6	69.82750
Methyl 4-pentenoate	-	-
Methyl 3-pentenoate	-	-
Methyl 2-pentenoate	-	-
Enamines	-	-
Primary amines	9.6	142.16266
Secondary amines	22.3	126.32002
Tertiary amines	33.8	182.74652

Ligand	Amin	Einwaagen [g]				
		M4P	M3P	$Rh(CO)_2acac$	Ligand	Amin
Biphephos	Pyrrolidin	0.147	0	(0.118 mL stock solution)	0.0044	0.129
	Piperidin	0.151	0	See above	0.0045	0.191
		0.147	0.016	See above	0.0045	0.195
	DMA	0.148	0	See above	0.0045	0.262
	(aq., 40 w.-%)	0.146	0.017	See above	0.0046	0.258
	aq. NH_3	0.148	0.011	See above	0.0045	0.140
Xantphos	Piperidin	0.147	0.017	See above		0.195
Bupox	Piperidin	0.147	0.016	See above		0.195
SK-35	Piperidin	0.153	0.028	See above	0.0035	0.197
	DMA	0.143	0.024	See above	0.0035	0.256

A.4. Hydroformylation of unusual substrates

A.4.1. Hydroformylation of 1,2,4-trivinylcyclohexane

Table 19, Entry 1

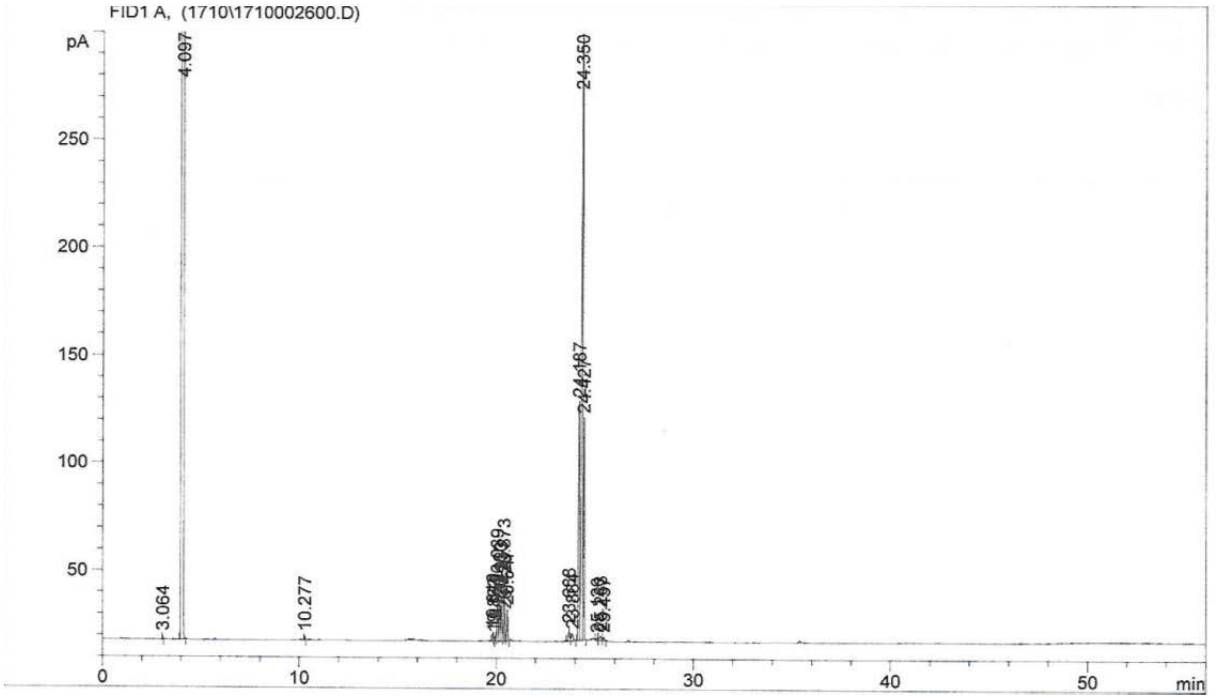

Appendix Fig. 125: Gas chromatogram (GC-FID) of Table 19, Entry 1.

Substance	Retention times [min]	Area
1,2,4-Trivinylcyclohexane	-	-
Monoaldehydes	10.0-11.0	traces
Dialdehydes	19.5-20.5	372.69441
Trialdehydes	23.5-24.5	1985.53167
Side products	-	-

Table 19, Entry 2

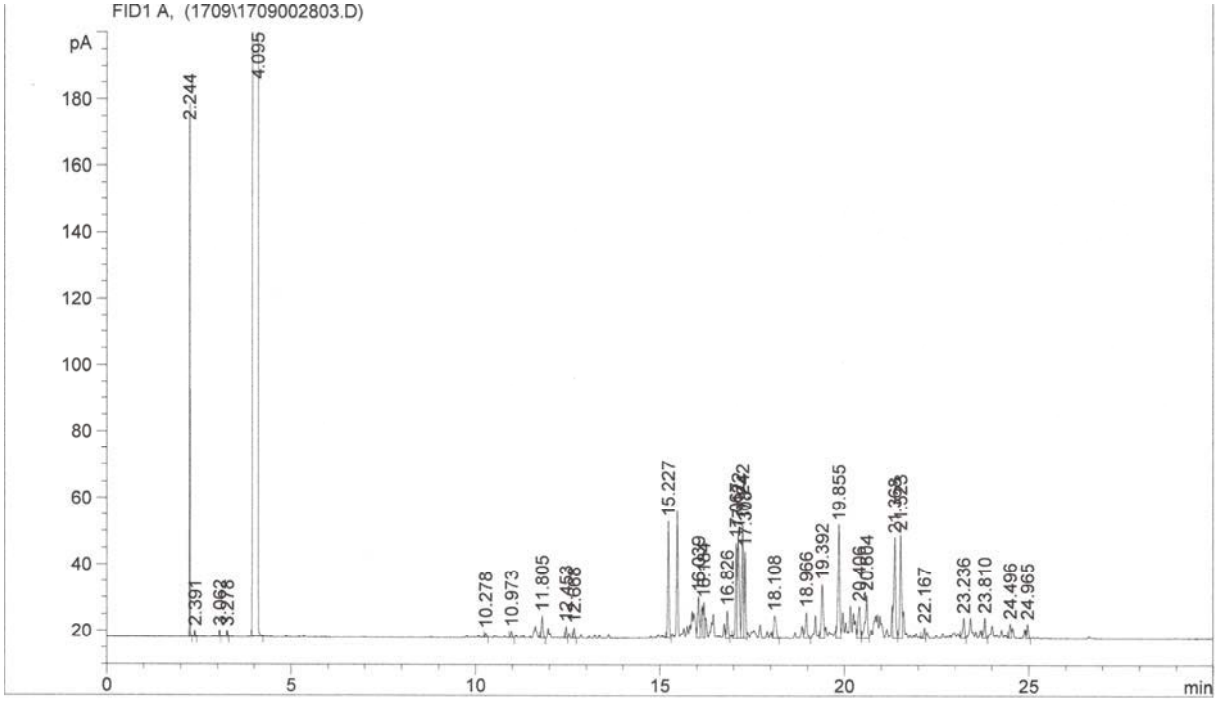

Appendix Fig. 126: Gas chromatogram (GC-FID) of Table 19, Entry 2.

Substance	Retention time [min]	Area
1,2,4-Trivinylcyclohexane	-	-
Monoaldehydes	10.0-13.0	34.02066
Dialdehydes	19.5-21.5	402.86671
Trialdehydes	23.0-25.0	65.22399

A.4.1.1. Rh catalysed hydroaminomethylation of 1,2,4-trivinylcyclohexane

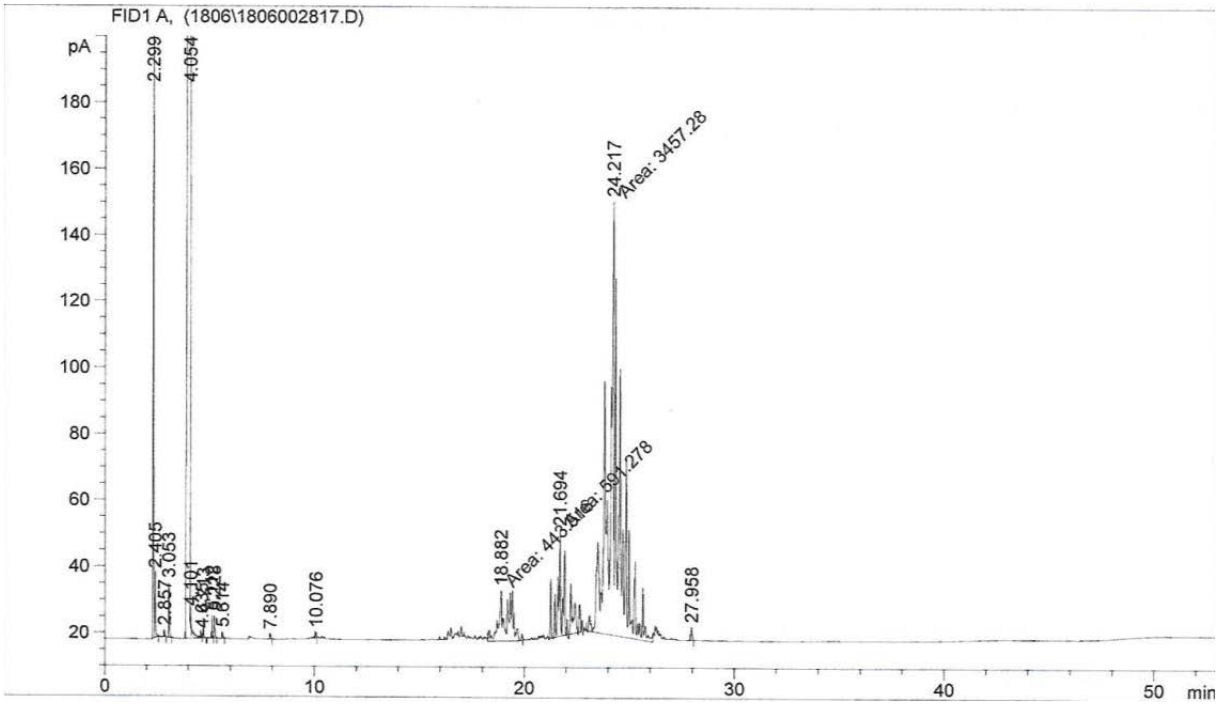

Appendix Fig. 127: Rhodium catalysed HAM of TVCH.

A.4.1.2. Synthesis of a triphosphite derived from 1,2,4-tris(3-hydroxopropyl)cyclohexane

A.4.1.2.1. Synthesis of bis(2,4-di-tert-butylphenyl)phosphorochloridite

^{1}H NMR (300 MHz, Methylene Chloride-d_2) δ 7.50 (d, J = 2.5 Hz, 2H), 7.37 (dd, J = 8.4, 1.4 Hz, 2H), 7.27 (dd, J = 8.4, 2.5 Hz, 2H), 1.49 (s, 18H), 1.38 (s, 18H). ^{31}P NMR (122 MHz, Methylene Chloride-d_2) δ 160.86 (s).

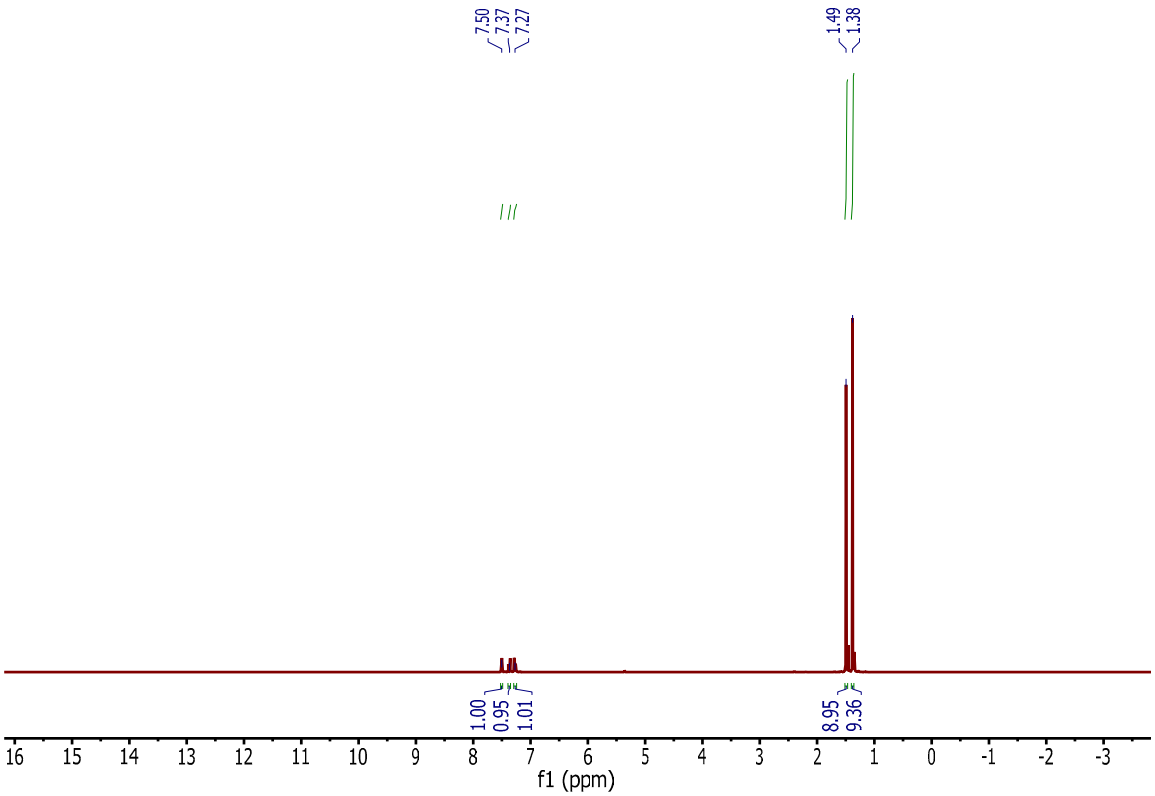

Appendix Fig. 128: ^{1}H NMR of the phosphorochloridte in CD_2Cl_2 at rt.

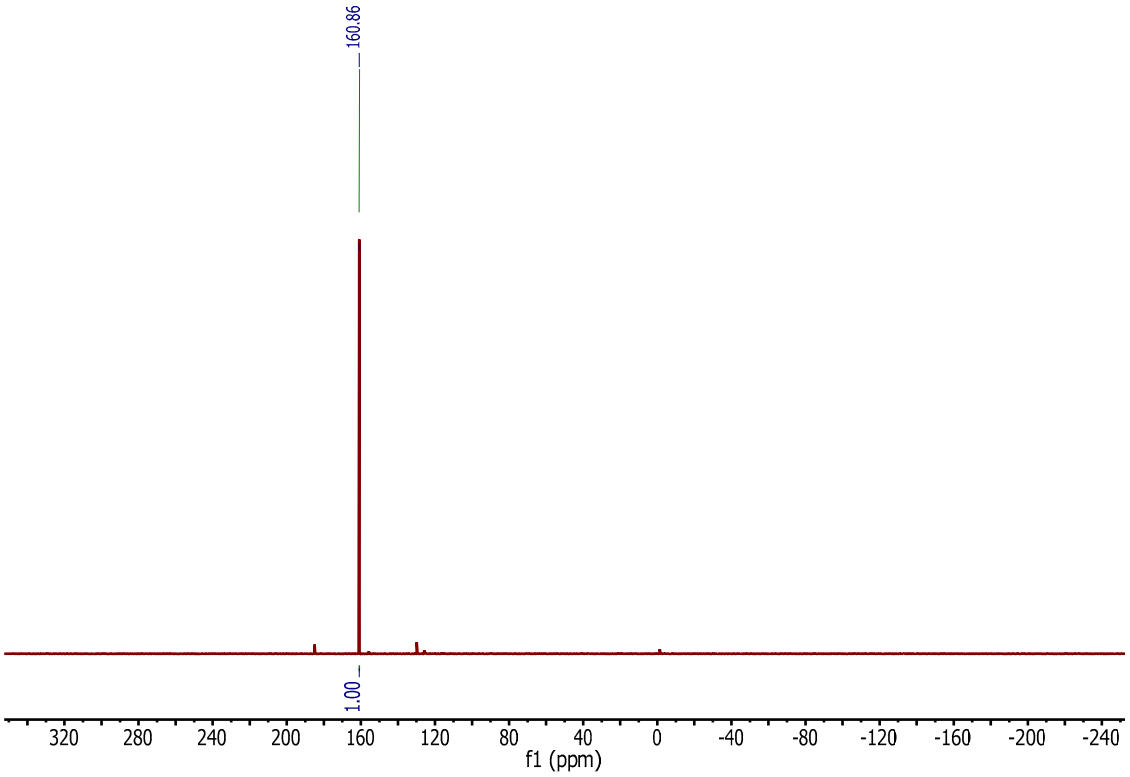

Appendix Fig. 129: ^{31}P NMR of the phosphorochloridite in CD_2Cl_2 at rt.

A.4.1.2.2. Synthesis of the triphosphites starting from 1,2,4-tris(3-hydroxopropyl)cyclohexane

^{1}H NMR (300 MHz, Methylene Chloride-d_2) δ 7.40 (m, 6 H), 7.14 (s, 12 H), 4.12 (m, 6 H), 1.63 (m, 9 H), 1.45 (m, 54H), 1.31 (m, 54H), 1.15 (m, 6 H). ^{31}P NMR (162 MHz, Methylene Chloride-d_2) δ 131.78 – 123.15 (m).

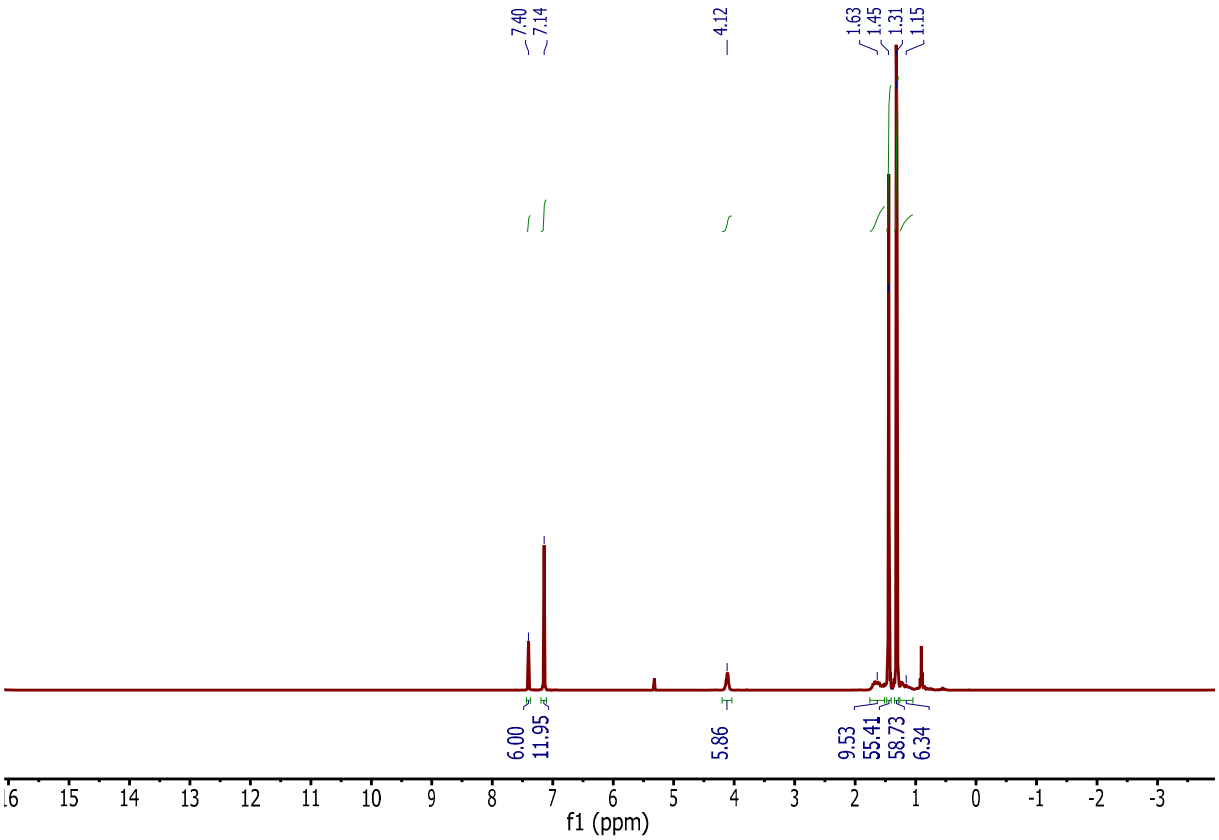

Appendix Fig. 130: ^{1}H NMR of SB111 in CD_2Cl_2 at rt.

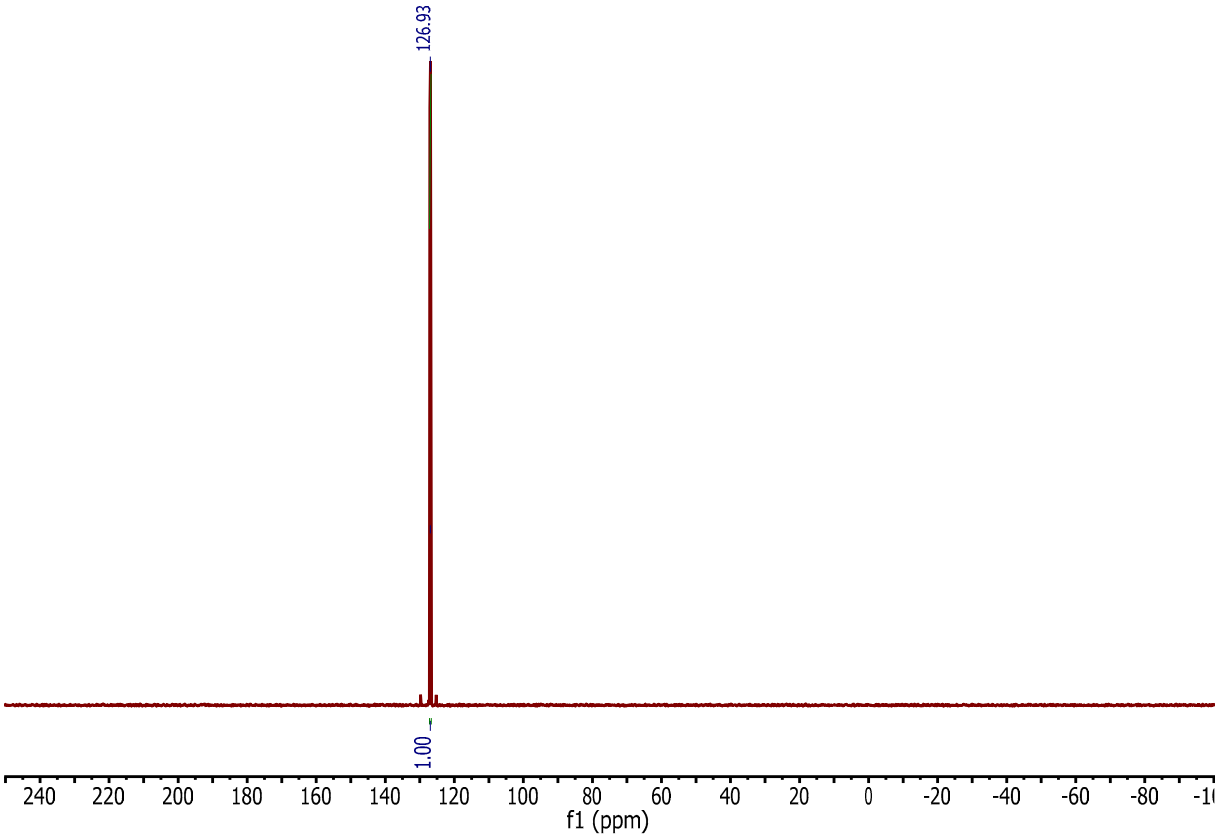

Appendix Fig. 131: ^{31}P NMR of SB111 in CD_2Cl_2 at rt.

A.4.1.2.3. Trial of the synthesised triphosphites in the Rh catalysed hydroformylation

Table 20, Entry 1

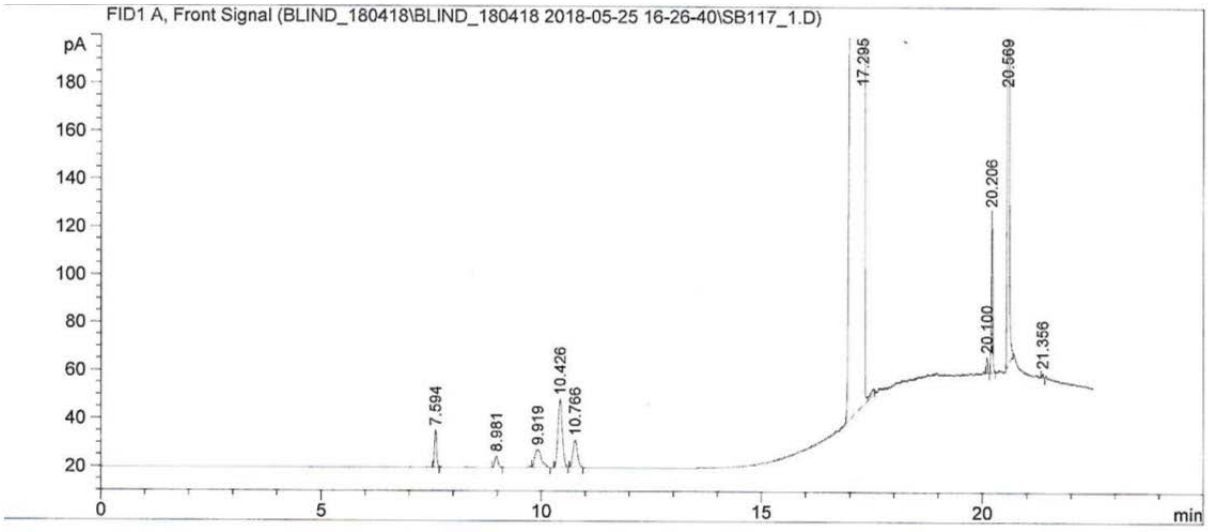

Appendix Fig. 132: Gas chromatogram (GC-FID) of Table 20, Entry 1.

Substance	Retention time [min]	Area
Octene, different isomers	7.5-10.8	425.78719
Nonanal	20.6	1726.39001
Aldehydes, branched	20.1, 20.2, 21.4	147.07728

Table 20, Entry 2

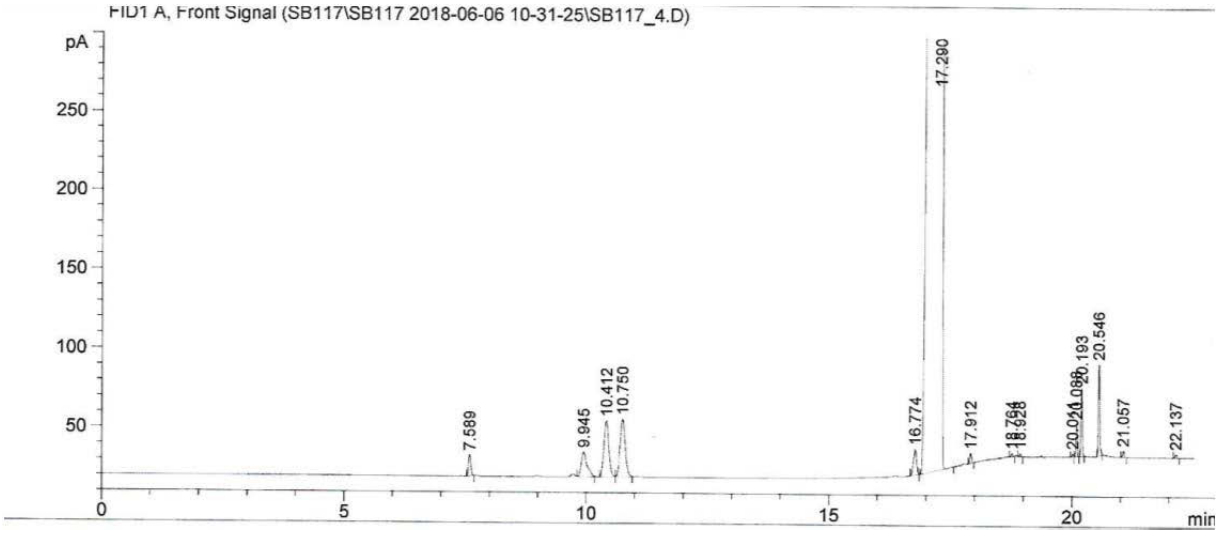

Appendix Fig. 133: Gas chromatogram (GC-FID) of Table 20, Entry 2.

Substance	Retention time [min]	Area
Octene, different isomers	7.5-10.8	756.14317
Nonanal	20.6	118.93311
Aldehydes, branched	20.1, 20.2,.21.4	123.86169
Side products	All other peaks	42.65378

Table 20, Entry 3

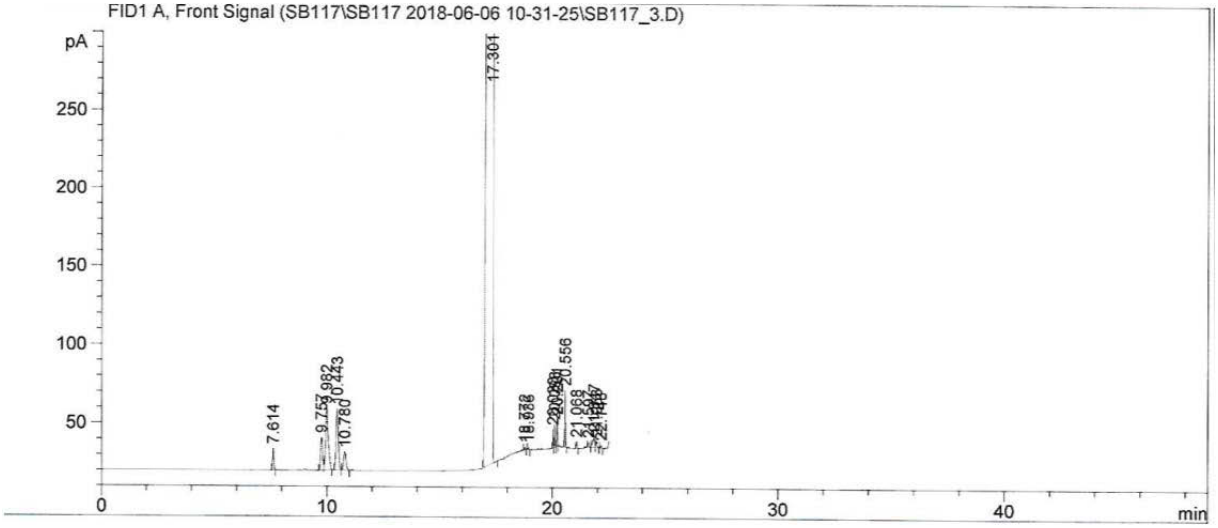

Appendix Fig. 134: Gas chromatogram (GC-FID) of Table 20, Entry 3.

Substance	Retention time [min]	Area
Octene, different isomers	7.5-10.8	863.80919
Nonanal	20.6	73.36377
Aldehydes, branched	20.1, 20.2,.21.4	93.48969
Side products	All other peaks	85.86129

Table 20, Entry 4

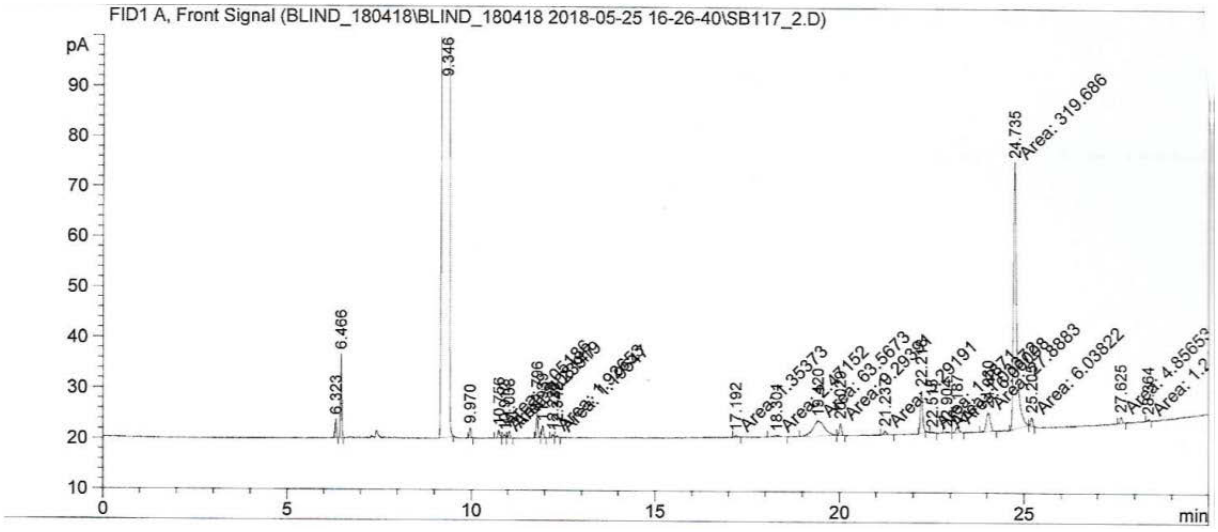

Appendix Fig. 135: Gas chromatogram (GC-FID) of Table 20, Entry 4.

Substance	Retention time [min]	Area
Methyl valerate	10.0	5.96930
Methyl 4-pentenoate	10.8	5.05186
Methyl 3-pentenoate	11.0	6.27066
Methyl 2-pentenoate	11.8	24.14089
Methyl 5-formylvalerate	24.7	319.68561
Methyl 4-formylvalerate	24.0	27.88828
Methyl 3-formylvalerate	-	-

Table 20, Entry 5

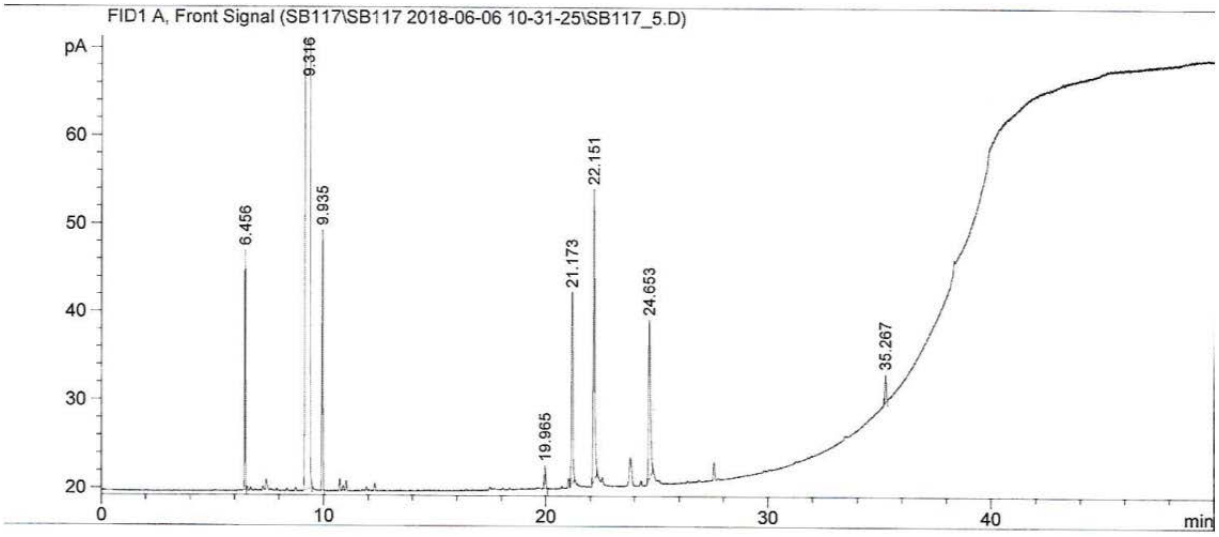

Appendix Fig. 136: Gas chromatogram (GC-FID) of Table 20, Entry 5.

Substance	Retention time [min]	Area
Methyl valerate	9.9	90.64935
Methyl 4-pentenoate	-	-
Methyl 3-pentenoate	-	-
Methyl 2-pentenoate	-	-
Methyl 5-formylvalerate	24.7	98.21521
Methyl 4-formylvalerate	22.2	148.44739
Methyl 3-formylvalerate	21.2	85.82200

Table 20, Entry 6

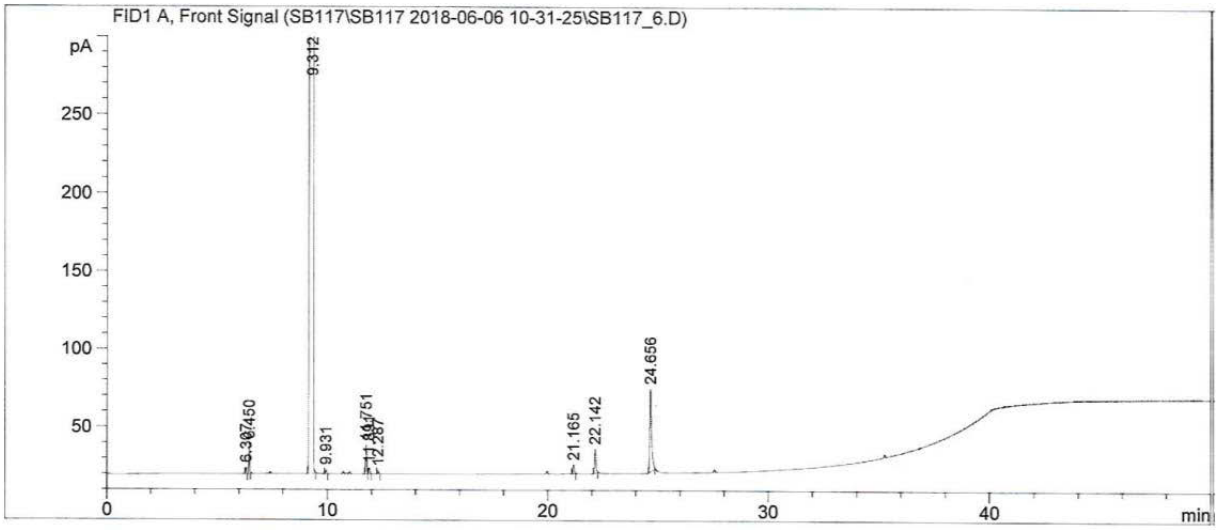

Appendix Fig. 137: Gas chromatogram (GC-FID) of Table 20, Entry 6.

Substance	Retention time [min]	Area
Methyl valerate	9.9	8.28672
Methyl 4-pentenoate	11.8	60.74820
Methyl 3-pentenoate	11.9	14.76285
Methyl 2-pentenoate	12.3	7.12904
Methyl 5-formylvalerate	24.7	301.72928
Methyl 4-formylvalerate	22.1	66.72614
Methyl 3-formylvalerate	21.2	22.66245

Table 20, Entry 7

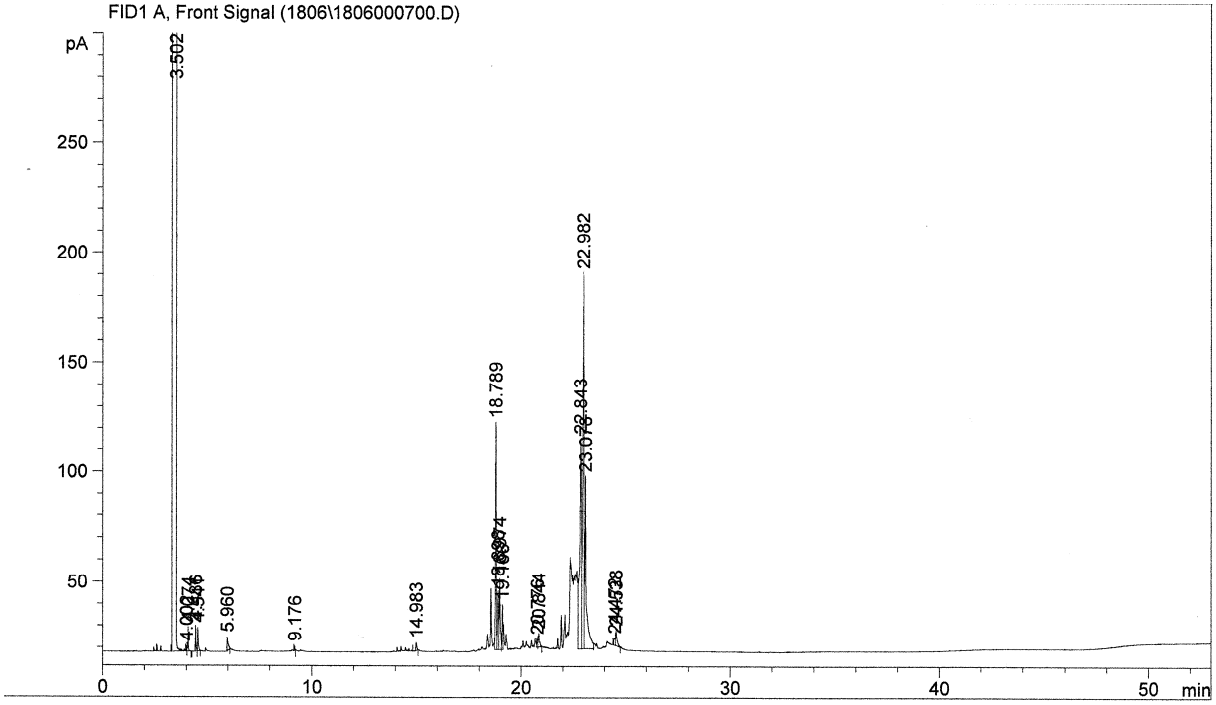

Appendix Fig. 138: Gas chromatogram (GC-FID) of Table 20, Entry 7.

Substance	Retention time [min]	Area
1,2,4-Trivinylcyclohexane	4.0-6.0	85.07731
Monoaldehydes	9.0-10.0	traces
Dialdehydes	18.5-19.5	597.66502
Trialdehydes	22.5-23.2	1710,45041

Ligand	Substrate	m_{Ligand} [mg]	$m_{Substrate}$ [g]	C [%]	$Y_{Aldehyde}$ [%]	S_{linear} [%]
SB111	1-Octen	9.0	0.1605	82	82	93
	2-Octen	9.0	0.1605	24	23	51
	n-Octen (mixture, technical)	9.0	0.1605	16	15	50
	M4P	9.0	0.1465	100	96	90
	M3P	9.0	0.1465	100	79	30
	M4P/M3P (9:1)	9.0	0.1465	83	81	76
	TVCH	9.0	0.2320	97	71	-